Viral gene transfer systems for cancer immunotherapy:

semireplication-competent VSV and receptor-targeted AAV for the delivery of immunomodulatory proteins

vom Fachbereich Biologie der Technischen Universität Darmstadt

zur Erlangung des akademischen Grades

eines Doctor rerum naturalium

Dissertation von

Diplom Biochemikerin Johanna Reul

aus Mainz

1. Referentin: Prof. Dr. Beatrix Süß
2. Referent: Prof. Dr. Gerhard Thiel
3. Referent: Prof. Dr. Christian Buchholz

Darmstadt 2018

Reul, Johanna: Viral gene transfer systems for cancer immunotherapy: semireplication-competent VSV and receptor-targeted AAV for the delivery of immunomodulatory proteins
Darmstadt, Technische Universität Darmstadt,
Jahr der Veröffentlichung der Dissertation auf TUprints: 2019
URN: urn:nbn:de:tuda-tuprints-83320
Tag der mündlichen Prüfung: 24.01.2018

Die vorliegende Arbeit wurde unter der Leitung von Prof. Dr. Christian Buchholz in der Arbeitsgruppe „Molekulare Biotechnologie und Gentherapie“ am Paul-Ehrlich-Institut in Langen angefertigt.

Die Betreuung seitens der Technischen Universität Darmstadt erfolgte durch Prof. Dr. Beatrix Süß vom Fachbereich Biologie.

Summary

In recent years, immunotherapy approaches for the treatment of cancer have been intensively investigated and substantial benefit observed in clinical trials has led to the marketing authorization of various immunotherapeutic drugs including monoclonal antibodies and cytokine-based therapies. Even though, several studies demonstrated effectivity of cancer immunotherapy, improvement is still required to address issues such as efficacy and safety. Development of suitable delivery systems might contribute to the improvement of immunotherapeutic approaches for cancer, whereby one strategy involves the application of viral vectors. For this purpose, viruses can be used in two ways: Either as replication-deficient viral vectors that solely deliver the therapeutic gene of interest or as replication-competent oncolytic viruses that directly kill tumor cells and are additionally engineered to encode immunomodulatory transgenes. The latter strategy was addressed in the first part of the thesis which aimed at combining the oncolytic activity of semireplication-competent vesicular stomatitis virus (srVSV) with the viral-mediated expression of immunotherapeutic transgenes in order to induce a long-lasting antitumor immune response. The second part of the thesis intended to generate and characterize replication-deficient, receptor-targeted adeno-associated viral (AAV) vectors for the tumor-specific delivery of immune checkpoint inhibitors.

The srVSV system is based on two *trans*-complementing, propagation-deficient VSV vectors, VSVΔG and VSVΔL. Both vectors were armed with the immunostimulatory transgenes granulocyte-macrophage colony-stimulating factor (GM-CSF), FMS-like tyrosine kinase 3 ligand (Flt3L), B7 and the tumor-associated antigens Her2/neu as well as CTLA4-Her2/neu to enhance srVSV-mediated antitumor immune responses. After insertion of the immunotherapeutic transgenes into the VSVΔG as well as VSVΔL vector genomes, all recombinant vectors were successfully generated *de novo* and analyses confirmed srVSV-mediated transgene expression *in vitro.* As VSV is exquisitely sensitive to type I interferon (IFN)-induced antiviral responses, different murine tumor cell lines were analyzed for their IFN sensitivity to identify a suitable VSV-permissive syngeneic tumor mouse model for the preclinical studies. The murine colon cancer cell line MC38 was identified as a potentially appropriate tumor model since MC38 cells were productively infectable even when pretreated with high doses of IFNα. First preclinical data showed the capability of transgene-armed as well as control srVSV to induce an antitumor immune response in the MC38 tumor model eventually leading to cure in some animals. However, the *in vivo* data showed only a marginally improved therapeutic

efficacy of transgene-armed versus control srVSV. Accordingly, more preclinical studies are required to clarify whether arming of srVSV with immunomodulatory payload indeed improves srVSV therapy efficacy.

Monoclonal antibodies directed against immune checkpoints, such as programmed cell death protein-1 (PD-1) and its ligand PD-L1, have shown promising results for the treatment of certain cancer types eventually leading to the marketing authorization of several products. However, drawbacks of this therapy include lack of efficacy in some patients and treatment-related toxicity. Probably the systemic administration of these antibodies does not only promote the activation of immune responses in the tumor microenvironment but also in healthy tissue. Therefore, this project aimed at the specific delivery of immune checkpoint inhibitors precisely to sites of tumor growth. To this end, Her2/neu-targeted AAV (Her2-AAV) vectors were equipped with the coding sequence of PD-1- or PD-L1-specific inhibitors. *In vitro* analyses showed that the inhibitors were readily detectable in the supernatant of AAV-transduced tumor cells. Furthermore, AAV-encoded αPD-1 as well as αPD-L1 specifically bound their target antigens. *In vivo* imaging analyses revealed that Her2-AAV successfully targeted tumor cells upon systemic injection into immunocompetent BALB/c mice bearing subcutaneously growing Her2/neu-positive RENCA tumors, while non-targeted AAV2 transduced mainly liver. Finally, *in vivo* delivery of AAV-encoded αPD-1 was assessed in the aforementioned mouse model. Mice injected with AAV2 showed the highest αPD-1 levels in the liver. In contrast, Her2-AAV successfully redirected the immune checkpoint inhibitor from liver to Her2/neu-positive tumor tissue upon systemic injection. In conclusion, this study is a proof of concept that tumor-targeted AAV vectors can be used for the delivery of immune checkpoint inhibitors to the site of tumor growth. It will pave the way for further investigations addressing toxicity and efficacy of vector-mediated compared to systemic immune checkpoint modulation.

Zusammenfassung

Immuntherapeutische Ansätze stehen derzeit im Fokus der Forschung zur Behandlung von Krebserkrankungen und vielversprechende klinische Studien führten zur Markteinführung verschiedener Immuntherapeutika, einschließlich monoklonaler Antikörper und Zytokin-basierter Therapien. Um die Wirksamkeit und Sicherheit immuntherapeutischer Therapien zu verbessern, könnten virale Gentransfersysteme geeignete Instrumente darstellen. In diesem Zusammenhang ist der Einsatz von Viren auf zwei Arten denkbar: Entweder als replikationsdefiziente virale Vektoren, die ausschließlich für das therapeutische Gen kodieren oder als replikationskompetente onkolytische Viren, die nicht nur mit zusätzlichen immuntherapeutischen Genen ausgestattet sind, sondern Tumorzellen auch direkt lysieren können. Die letztgenannte Strategie wurde im ersten Teil dieser Arbeit verfolgt. Ziel war es die onkolytische Aktivität von semi-replikationskompetentem Virus der vesikulären Stomatitis (srVSV) mit der Expression von viral-kodierten immuntherapeutischen Transgenen zu kombinieren, um eine lang anhaltende antitumorale Immunantwort zu induzieren. Im zweiten Teil dieser Arbeit steht die Entwicklung von replikations-defizienten, zielgerichteten Adeno-assoziierten viralen (AAV) Vektoren für den tumorspezifischen Transfer von Immuncheckpoint-Inhibitoren im Fokus.

Das srVSV-System basiert auf zwei sich in *trans* komplementierenden, propagations-defizienten Vektoren, VSVΔG und VSVΔL. Zur Steigerung der antitumoralen Wirksamkeit wurden beide Vektoren mit den immuntherapeutischen Transgenen *granulocyte-macrophage colony-stimulating factor* (GM-CSF), *FMS-like tyrosine kinase 3 ligand* (Flt3L), B7 und dem tumorassoziierten Antigen Her2/neu sowie CTLA4-Her2/neu ausgestattet. Nach erfolgter Insertion der Transgene in das Genom der VSV Deletionsmutanten wurden die rekombinanten Vektoren erfolgreich hergestellt und die Expression der von srVSV kodierten Transgene wurde *in vitro* nachgewiesen. Da VSV sensitiv gegenüber Typ I Interferon (IFN)-induzierten antiviralen Immunantworten ist, wurde zur Identifikation eines geeigneten Tumormodells für die präklinischen Studien, die Sensitivität verschiedener muriner Tumorzelllinien gegenüber IFNα untersucht. Die Darmkrebszelllinie MC38 wurde als potenziell geeignetes Tumormodell identifiziert, da sie auch nach Vorbehandlung mit hohen IFNα Konzentrationen noch infizierbar war. Erste präklinische Untersuchungen zeigten, dass sowohl srVSV, welches mit immunstimulierenden Transgenen armiert war, als auch nicht-armiertes srVSV eine antitumorale Immunantwort im MC38 Tumormodell induzieren konnten. Hierbei

zeigten die mit immunstimulatorischen Transgen-armierten srVSV lediglich eine geringfügige Steigerung der therapeutischen Wirksamkeit im Vergleich zu der nicht-armierten srVSV-Kontrollgruppe. Daher sind weitere präklinische Studien notwendig, um endgültig zu klären, ob der Einbau der gewählten immuntherapeutischen Transgene die antitumorale Wirksamkeit von srVSV steigern kann.

Monoklonale Antikörper, welche gegen Immuncheckpoints wie *programmed cell death protein-1* (PD-1) oder seinen Liganden PD-L1 gerichtet sind, haben vielversprechende Behandlungsergebnisse bei fortgeschrittenen Krebserkrankungen erzielt, was zur Markteinführung verschiedener sogenannter Immuncheckpoint-Inhibitoren führte. Jedoch spricht nicht jeder Patient auf die Behandlung an und zudem können als Nebenwirkung schwerwiegende Autoimmunreaktionen auftreten. Vermutlich begünstigt die systemische Applikation der Antikörper nicht nur eine Stimulation des Immunsystems im Tumorgewebe, sondern auch in gesunden Organen. Daher wurden in dieser Arbeit zielgerichtete AAV-Vektoren für den tumorspezifischen Transfer von Immuncheckpoint-Inhibitoren entwickelt. Hierfür wurden AAV-Vektoren verwendet, die über die Bindung an den Rezeptor Her2/neu, welcher auf vielen Tumorentitäten hochreguliert wird, den Gentransfer vermitteln (Her2-AAV). Diese Vektoren wurden mit der kodierenden Sequenz für PD-1- oder PD-L1-spezifische Inhibitoren ausgestattet. *In vitro* Untersuchungen bestätigten die AAV-vermittelte Expression der Immuncheckpoint-Inhibitoren sowie deren spezifischen Anbindung an ihr Zielantigen PD-1 oder PD-L1. *In vivo Imaging* Analysen zeigten, dass Her2-AAV nach systemischer Applikation in immunkompetenten BALB/c Mäusen mit subkutan wachsenden HER2/neu-positiven RENCA Tumoren einen präzisen Gentransfer in das Tumorgewebe vermittelte, wohingegen ungerichtete AAV2-Vektoren einen Gentransfer in die Leber vermittelten. Zuletzt wurde die AAV-vermittelte Expression von αPD-1 in dem zuvor genannten Tumormodell untersucht. Die systemische Applikation von Her2-AAV führte zu erhöhten αPD-1 Werten im Tumor verglichen zu den Werten in der Leber. Im Gegensatz dazu wiesen die mit AAV2 behandelten Mäuse höhere αPD-1 Werte in der Leber auf. Zusammenfassend zeigt die vorliegende Arbeit, dass sich Her2-AAV für den tumor-gerichteten Transfer von Immuncheckpoint-Inhibitoren eignet. Die in dieser Arbeit entwickelten AAV-Vektoren liefern die Grundlage, auf der weiterführende Studien durchgeführt werden können, um letztendlich die Sicherheit und Wirksamkeit von Vektor-vermittelter mit systemischer Immuncheckpoint-Blockade vergleichen zu können.

Table of contents

Summary ..... **I**

Zusammenfassung ..... **III**

Table of contents ..... **V**

1 Introduction **1**

1.1 Cancer immunotherapy **1**

1.1.1 Cytokines 2

1.1.2 Cancer vaccines 2

1.1.3 Adoptive cell transfer 3

1.1.4 Immune checkpoint inhibitors 4

1.1.5 Oncolytic immunotherapy 8

1.2 Vesicular stomatitis virus **10**

1.2.1 VSV biology 10

1.2.2 VSV – an oncolytic virus 12

1.3 Adeno-associated virus **15**

1.3.1 AAV-based gene transfer vectors 16

1.3.2 Surface engineering of AAV vectors 17

1.4 Objectives **19**

2 Material and Methods **21**

2.1 Material **21**

2.1.1 Reagents, chemicals, recombinant proteins and cytokines 21

2.1.2 Commercially available kits 22

2.1.3 Enzymes 23

2.1.4 Buffers 23

2.1.5 Antibodies 24

2.1.6 Oligonucleotides 25

2.1.7 Plasmids 26

2.1.8 Bacterial & eukaryotic cells 29

2.1.9 Viruses 30

2.2 Molecular biology **30**

2.2.1 Transformation of chemically competent bacteria 30

2.2.2 Plasmid preparation 31

2.2.3 Restriction of DNA 32

2.2.4 Agarose gel electrophoresis 32

2.2.5 Dephosphorylation and ligation of DNA 33
2.2.6 Polymerase chain reaction 33
2.2.7 DNA sequencing 34
2.2.8 Quantitative polymerase chain reaction 35
2.3 Protein biochemical methods 35
2.3.1 Determination of protein concentrations 35
2.3.2 SDS-polyacrylamide gel electrophoresis 36
2.3.3 Coomassie staining of SDS-PAGE 37
2.3.4 Western blot analysis 37
2.3.5 Enzyme-linked immunosorbent assay 38
2.3.6 Protein affinity tag purification from cell culture supernatant 40
2.4 Cell culture and virological methods 40
2.4.1 Cultivation of eukaryotic cell lines 40
2.4.2 Freezing and thawing of cells 41
2.4.3 Transfection of BHK-21 cells 41
2.4.4 Production of recombinant αPD-1 and αPD-L1 42
2.4.5 VSV rescue 42
2.4.6 Plaque purification of VSV and preparation of virus stocks 43
2.4.7 Determination of the 50 % tissue culture infective dose 45
2.4.8 Infection 45
2.4.9 Cell viability assay 46
2.4.10 AAV vector production and concentration 46
2.4.11 Transduction 47
2.4.12 Generation of stably transgenic cell lines 48
2.4.13 Flow cytometry 48
2.4.14 ELISpot 49
2.5 Experimental mouse work 50
2.5.1 Injection of tumor cells 50
2.5.2 Injection of vector particles 50
2.5.3 Blood sampling 51
2.5.4 *In vivo* Imaging 51
2.5.5 Isolation and cultivation of splenocytes from mice 51
2.5.6 Preparation of mouse organ lysates 52
3 Results 53
3.1 Development of semireplication-competent VSV as a novel vector system for oncolytic immunotherapy 53

3.1.1 Incorporation of immunotherapeutic transgenes into VSV vector genomes 53
3.1.2 *De novo* generation of srVSV 58
3.1.3 Analyzing srVSV-mediated expression of immunostimulatory proteins 63
3.1.4 Sensitivity of murine tumor cell lines to the antiviral effects of type I IFN 67
3.1.5 Generation and characterization of srVSV for the *in vivo* studies 71
3.1.6 Analyzing therapeutic efficacy of srVSV equipped with immunotherapeutic transgenes *in vivo* 75
3.1.7 Evaluating viral dose on therapy efficacy 78
3.2 Towards tumor-targeted delivery of immune checkpoint inhibitors by receptor-targeted AAV 82
3.2.1 Generation and characterization of AAV encoding αPD-1 and αPD-L1 82
3.2.2 AAV-mediated expression of αPD-1 and αPD-L1 86
3.2.3 Establishing an ELISA for the detection of αPD-1 and αPD-L1 87
3.2.4 Quantification of AAV-encoded αPD-1 and αPD-L1 89
3.2.5 Functionality of AAV-encoded αPD-L1 91
3.2.6 Functionality of AAV-encoded αPD-1 93
3.2.7 Detection of *in vivo* delivered immune checkpoint inhibitors 96
3.2.8 Her2-AAV tumor-targeting in immunocompetent mice 98
3.2.9 Tumor-targeted delivery of αPD-1 by Her2-AAV 101
4 Discussion 103
4.1 Arming VSV with immunotherapeutic transgenes 103
4.1.1 Mechanisms of action of the incorporated immunotherapeutic transgenes 104
4.1.2 Therapeutic efficacy of srVSV armed with immunotherapeutic cargo 106
4.2 Oncolytic immunotherapy requires a balance between antitumor and antiviral immune responses 107
4.2.1 Type I IFN-induced antiviral immune responses 108
4.2.2 Humoral immune responses 110
4.2.3 Antiviral immune responses may interfere with srVSV-mediated expression of immunomodulatory proteins 111
4.2.4 Possible strategies to improve srVSV therapy 112
4.3 Local delivery of immune checkpoint inhibitors 112
4.3.1 Delivery of antibodies and antibody-like molecules by AAV vectors 114
4.3.2 Further strategies to achieve local delivery of immune checkpoint inhibitors 119
5 References 125
6 Abbreviations 147

7 Curriculum Vitae 151

8 Publications 152

9 Danksagung 154

10 Ehrenwörtliche Erklärung 155

1 Introduction

1.1 Cancer immunotherapy

Immunotherapy represents a promising treatment modality for different cancer types relying on harnessing the immune system to combat the malignancy. Already in 1909 Paul Ehrlich hypothesized that the immune system is able to suppress tumor development (Ichim, 2005; Ehrlich, 1909). Later on the theory of immunosurveillance was postulated, a concept describing the ability of the immune system to recognize and destroy the vast majority of tumor cells during initial transformation (Zitvogel et al, 2006; Thomas, 1982).

The mechanisms required to induce a cellular antitumor immune response are comparable to host immune responses to infections. The immune system potentially recognizes tumor cells due to their expression of 'neo-antigens' arising through genetic alterations and epigenetic changes (Melero et al, 2014; Gubin et al, 2015; Alexandrov et al, 2013). These tumor antigens, being released by dying tumor cells for instance, are captured by antigen-presenting cells (APCs). Here, dendritic cells (DCs) are the key APCs that are responsible to stimulate antitumor immune responses (Mellman et al, 2011; Melief, 2008). Upon the encounter of the antigen in combination with a suitable maturation signal, DCs migrate to secondary lymphoid organs where they present the processed antigens to T cells in order to elicit a protective T cell response (Mellman et al, 2011). In particular, cytotoxic $CD8^+$ T cells that can directly lyse cancer cells and produce inflammatory cytokines, such as interferon γ (IFNγ), are assumed to be crucial for antitumor immunity. However, also helper $CD4^+$ T cells are claimed to play an important role during antitumor immune responses as they stimulate the function of $CD8^+$ T cells and also produce inflammatory cytokines (Pardoll, 2002; Toes et al, 1999). Finally, cancer-specific T cells migrate to the tumor site to directly mediate tumor cell killing by apoptosis (Mellman et al, 2011).

However, cancer cells can acquire different strategies during carcinogenesis to evade immune recognition resulting from the selective pressure by the immune system. Cancer cells are capable to escape immunosurveillance by outgrowth of malignant cells with reduced antigenicity and immunogenicity (Beatty & Gladney, 2015). Loss of antigenicity of malignant cells can be induced by defects in antigen processing and presentation, for instance due to downregulation of major histocompatibility complex (MHC) molecules (So et al, 2005; Zitvogel et al, 2006). Upregulation of immunosuppressive molecules such

as programmed cell death ligand-1 (PD-L1) on the surface of tumor cells can further inhibit intratumoral T cell activity (Pardoll, 2012). Secretion of immunosuppressive cytokines such as transforming growth factor β (TGF-β) additionally reduces the immunogenicity of the malignancy by inhibiting cytotoxic T cells and DCs while stimulating differentiation of immunosuppressive regulatory T cells (T_{reg} cells) (Thomas & Massagué, 2005; Melero et al, 2014; Beatty & Gladney, 2015; Sisirak et al, 2013; Gray et al, 1994; Chen et al, 2003). Another described mechanism for tumor cell immune escape is the recruitment of suppressive immune cells such as T_{reg} cells and myeloid-derived suppressor cells which orchestrate a tumor microenvironment provoking an inhibition of the antitumor immune response (Curiel et al, 2004; Viguier et al, 2004; Melero et al, 2014; Nagaraj & Gabrilovich, 2008; Srivastava et al, 2012).
Different strategies have been developed to break cancer immune tolerance including non-specific stimulation of the immune system by cytokines, cancer vaccines, adoptive cell transfer therapy, monoclonal antibodies (mAbs) modulating immune checkpoint pathways and oncolytic viruses.

1.1.1 Cytokines

Cancer immunotherapeutic approaches started with cytokine therapies using IFNα and interleukin 2 (IL-2) being approved by the Food and Drug Administration (FDA) for tumor therapy in the 1990s (Jiang & Zhou, 2015; Lee & Margolin, 2011). Multiple mechanisms eliciting antitumor effects are described for IFNα including antiproliferative as well as antiangiogenic activities and the induction of MHC class I expression on tumor cells which enhances recognition by the immune system (Ferrantini et al, 2007). The mechanism underlying the antitumor effects of IL-2 is not fully understood but it is supposed to be based on its ability to induce activation and proliferation of T cells and natural killer (NK) cells among others (Skrombolas & Frelinger, 2014). However, even though cytokine therapy can induce durable complete tumor remissions in few cases, treatment is often associated with toxicities (Jiang & Zhou, 2015).

1.1.2 Cancer vaccines

Another approach in cancer immunotherapy are therapeutic cancer vaccines specifically stimulating the natural immune response against cancer to treat an existing malignancy and to induce a long-lasting antitumor immunity (Jiang & Zhou, 2015; Baxevanis et al,

2009). Most approaches rely on using tumor antigens, the so-called tumor-associated antigens (TAAs), which can be divided into shared and unique TAAs. Shared TAAs include cancer-testis antigens, differentiation antigens and antigens that are overexpressed on cancer cells. Unique TAAs arise through somatic point mutations induced by physical or chemical carcinogens (Tagliamonte et al, 2014). A commonly targeted shared TAA in cancer therapy is Her2/neu, a receptor tyrosine kinase which is overexpressed in various human malignancies such as breast, ovarian as well as gastric carcinomas and has been associated with poor prognosis (Slamon et al, 1989; Klapper et al, 2000; Roth et al, 2005). Tumor antigens for vaccination can be administered by viral vectors, peptides or recombinant proteins with an appropriate adjuvant, DNA or antigen-loaded DCs (Larocca & Schlom, 2011; van der Burg et al, 2006; Herrada et al, 2012; Palucka & Banchereau, 2013). In 2010, sipuleucel-T, a DC-based cancer vaccine, was approved by the FDA for the treatment of advanced prostate cancer. Sipuleucel-T is a cellular product based on autologous peripheral blood mononuclear cells (PBMCs) that are incubated *ex vivo* with a fusion protein composed of the prostate-cancer antigen prostatic acid phosphatase (PAP) and the DC growth and differentiation factor granulocyte-macrophage colony-stimulating factor (GM-CSF). Matured antigen-loaded DCs are re-infused into the patient to elicit an antitumor immune response (Farkona et al, 2016). Clinical studies revealed a 4.1 month improvement in median survival of sipuleucel-T treated patients compared to the placebo group (Kantoff et al, 2010).

1.1.3 Adoptive cell transfer

Adoptive cell transfer (ACT) is another promising strategy in cancer immunotherapy utilizing antitumor properties of T cells to eliminate malignant cells. For autologous T cell therapy, tumor antigen-specific lymphocytes are isolated from the patient, selected, expanded *ex vivo* and re-infused into the patient (Farkona et al, 2016). ACT using autologous tumor infiltrating lymphocytes (TILs) showed promising clinical results. Treatment of lymphodepleted patients suffering from metastatic melanoma with autologous TILs in combination with IL-2 administration achieved a complete tumor regression in 22 % of the treated patients (Rosenberg et al, 2011). To further improve ACT, isolated peripheral blood T cells are used which are genetically engineered to express a T cell receptor (TCR) specific for a tumor antigen. This therapy is in principle applicable to patients whose tumor expresses the matching human leukocyte antigen (HLA) as well as the respective tumor antigen. Furthermore, the specificity of T cells can be engineered by chimeric antigen receptors (CARs). CARs are artificial receptors

composed of an extracellular domain enabling antigen recognition (usually a single-chain variable fragment (scFv)) fused to an intracellular T cell activation domain (e.g. CD3ζ). CARs provide the advantage of an HLA-independent recognition of cell surface antigens leading to tumor cell destruction (Farkona et al, 2016; Rosenberg & Restifo, 2015). Among the most advanced CARs in clinical trials are CD19-targeted CAR T cells for the treatment of B-cell malignancies (Oluwole & Davila, 2016).

1.1.4 Immune checkpoint inhibitors

One of the most promising approaches in cancer immunotherapy involves the blockade of immune checkpoints by mAbs. Among the most advanced immune checkpoint inhibitors are mAbs directed against the cytotoxic T-lymphocyte-associated antigen (CTLA-4), programmed cell death protein-1 (PD-1) and its ligand PD-L1. These immune checkpoints are crucial to maintain immunological homeostasis by regulating the activity of T cells but are also involved in tumor immune escape. The mechanisms of regulating T cell activation and inhibiting antitumor immune responses are different for CTLA-4 and PD-1/PD-L1 as described in the following section (Topalian et al, 2015).

T cell activation is an antigen-dependent process that requires at least two signals to induce the differentiation and proliferation of naïve T cells into effector cells. Activation is initiated by the engagement of the TCR to antigenic peptides bound to MHC molecules on APCs (signal 1). For productive activation of T cells, additional co-stimulatory signals are needed. This T cell co-stimulation can be mediated by the binding of CD28 on the T cell surface to B7 proteins (e.g. B7-1 (CD80) and B7-2 (CD86)) on APCs (signal 2). However, this priming phase of T cell activation is modulated by the upregulation of CTLA-4 on activated T cells. CTLA-4 has a higher affinity for B7 proteins than CD28, thereby dampening T cell activity by outcompeting CD28 for binding to B7 molecules and consequently downregulates T cell responses (Chen, 2004; Sharma et al, 2011; Pardoll, 2012). Additionally, CTLA-4 is supposed to directly trigger inhibitory signals in T cells, to interfere with the 'TCR Stop Signal' required for stable conjugate formation between T cells and APCs and to induce the depletion of B7 proteins from the APCs by trans-endocytosis (Lee et al, 1998; Schneider et al, 2006; Qureshi et al, 2011). Furthermore, CTLA-4 is predominantly expressed on helper $CD4^+$ T cells and plays a major role in enhancing the immunosuppressive function of T_{reg} cells (Wing et al, 2008; Topalian et al, 2015).

The level of T cell activation by co-stimulation with CD28 and co-inhibition with CTLA-4 is regulated by the time point of surface expression and the strength of TCR signaling.

Naïve and resting T cells express high levels of CD28 but no CTLA-4 on the cell surface and thus co-stimulation dominates upon antigen recognition (Lindsten et al, 1993; Pardoll, 2012). However, surface expression of CTLA-4 is induced upon binding of the TCR to the MHC-presented antigen at levels depending on the strength of the TCR signaling and thus can result in an inhibition after antigen recognition (Egen & Allison, 2002).

T cell activity is additionally regulated in peripheral tissue by PD-1 that is expressed on antigen-experienced T cells. Expression of PD-L1 or PD-L2, the ligands of PD-1, is upregulated on tissue in response to inflammation. Binding of PD-1 to one of its ligands leads to the inhibition of T cell activity (Freeman et al, 2000; Latchman et al, 2001; Pardoll, 2012). Through this mechanism, PD-1 regulates the balance of T cell activity in the periphery at the time of an inflammatory response in order to limit autoimmunity (Pardoll, 2012).

Recently, B7-1 was identified as a further interaction partner of PD-L1. B7-1 expressed on T cells binds PD-L1 with an affinity intermediate to that of B7-1 to CD28 and B7-1 to CTLA-4. This interaction also induces inhibitory signals in T cells (Butte et al, 2007). Furthermore, it was demonstrated that the PD-L1/B7-1 pathway is also required for the maintenance of peripheral T cell tolerance (Park et al, 2010).

PD-1 and its ligand PD-L1 are expressed on a variety of different cell types. PD-1 is not only expressed on activated T cells but also on T_{reg} cells, B cells, monocytes, NK cells and DCs. Its ligand PD-L1 is expressed on immune cells including activated T cells and DCs as well as on a wide range of non-hematopoietic tissue such as lung cells (Keir et al, 2008; Pardoll, 2012). However, PD-1 is also expressed on the majority of TILs, including T_{reg} cells and $CD8^+$ T cells, and PD-L1 is commonly upregulated on the cell surface of various solid tumor types (Ahmadzadeh et al, 2009; Thompson et al, 2007; Sfanos et al, 2009; Dong et al, 2002; Thompson et al, 2004; Ohigashi et al, 2005; Hino et al, 2010). Two different mechanisms are described for the upregulation of PD-1 ligands on tumor cells: intrinsic and adaptive immune resistance. The intrinsic immune resistance describes the upregulation due to constitutive oncogenic signaling (e.g. activation of AKT pathway). Adaptive immune resistance refers to the induction of PD-1 ligand expression on tumor cells in response to inflammatory signals. In particular, IFNγ, mainly produced by T cells attempting to elicit tumor-specific immune responses, is claimed to induce the upregulation of PD-1 ligands (Topalian et al, 2015).

Accordingly, the PD-1/PD-L1 interaction is a major immune escape mechanism of cancer cells. Different tumor growth promoting mechanisms are described for the PD-1/PD-L1 pathway. One described mechanism is the promotion of tumor cell survival by

delivering anti-apoptotic signals via PD-L1 into tumor cells (Azuma et al, 2008). Additionally, the PD-1/PD-L1 axis mediates tumor immune escape through the inhibition of signaling pathways in T cells required for differentiation, expansion and survival of T cells (Bardhan et al, 2016). Furthermore, permanent antigen exposure by cancer cells is supposed to mediate persistent expression of PD-1 on $CD8^+$ TILs eventually inducing T cell exhaustion (Topalian et al, 2015; Ahmadzadeh et al, 2009).
The findings that PD-L1 is upregulated on the vast majority of malignancies and PD-1 is expressed on TILs was the rationale to design antibodies to block the PD-1/PD-L1 interaction in order to restore T cell activation and thereby prevent immune evasion of cancer cells. Blockade of the PD-1/PD-L1 axis is supposed to mainly provoke antitumoral effects within the tumor microenvironment since the ligands are overexpressed by tumor cells and TILs (Topalian et al, 2015). However, due to the expression of PD-L1 on APCs inhibition of the PD-1/PD-L1 interaction might also play a role in the secondary lymphoid tissue (Curiel et al, 2003). Antibody-mediated blockage of CTLA-4 is supposed to mediate antitumor immune responses by systemic T cell activation upon antigen encounter (Topalian et al, 2015). However, αCTLA-4 mAbs might also stimulate antitumor immune responses within the tumor microenvironment by directly depleting tumor-infiltrating T_{reg} cells or by affecting their immunosuppressive functions (Peggs et al, 2009; Topalian et al, 2015; Simpson et al, 2013). In conclusion, αCTLA-4, αPD-1 and αPD-L1 antibodies block different inhibitory interactions and thus induce the stimulation of antitumor immune responses by different ways (Figure 1).

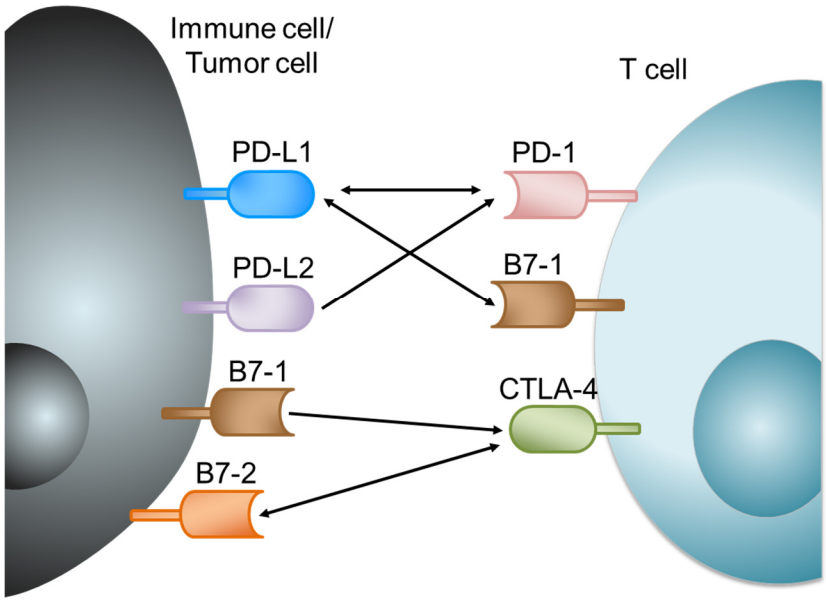

Figure 1: Possible inhibitory interactions blocked by αCTLA-4, αPD-1 and αPD-L1 mAbs. αCTLA-4 mAbs block the binding of CTLA-4 to B7-1 and B7-2. αPD-1 mAbs block the interaction between PD-1 and PD-L1 as well as PD-L2. αPD-L1 mAbs inhibit the binding of PD-L1 to PD-1 and to B7-1**.** According to the information provided in (Topalian et al, 2015).

Ipilimumab, an αCTLA-4 mAb, was one of the first immune checkpoint inhibitors that entered clinical trials and was approved in the US and EU in 2011 for the treatment of advanced melanoma (Topalian et al, 2015). A long-term follow up study for ipilimumab-treated melanoma patients demonstrated a durable survival of about 20 % with observation periods lasting up to 10 years (Schadendorf et al, 2015). The success of αCTLA-4 mAbs paved the way for the clinical development of further immune checkpoint inhibitors including mAbs targeting PD-1 and PD-L1. In 2014, two PD-1 specific mAbs, namely nivolumab and pembrolizumab, achieved marketing authorization by the FDA for therapy of advanced melanoma. Later on both PD-1 blocking mAbs were also approved for the treatment of non-small cell lung cancer (NSCLC) and nivolumab additionally achieved marketing authorization for therapy of several cancer types including renal cell carcinoma (RCC) (Bardhan et al, 2016). Nivolumab and pembrolizumab demonstrated superior clinical benefit in melanoma patients compared to ipilimumab (Larkin et al, 2015; Robert et al, 2015b). Recently, also a PD-L1-specific mAb (avelumab) received marketing authorization in the US for the treatment of metastatic Merkel cell carcinoma (MCC) (Kim, 2017).

While the clinical response in some patients with advanced cancer is impressive, there are also downsides including absence of response in a fraction of patients and toxicity induced by immune checkpoint modulation. Due to non-specific immunostimulation, these novel immunotherapeutics induce inflammation in tissues affecting multiple organs such as skin, gut, digestive tract, lung and liver. These so-called ‘immune-related

adverse events' (irAE) include vitiligo, skin rash, colitis, pneumonitis as well as hepatitis and their severity can range from mild to fatal (Naidoo et al, 2016; Abdel-Wahab et al, 2016). The irAEs are mainly managed with immunomodulatory medications such as steroids or immunosuppressive antibodies like tumor necrosis factor-alpha antagonists (infliximab) (Spain et al, 2016).

1.1.5 Oncolytic immunotherapy

Many of the aforementioned cancer immune escape mechanisms (chapter 1.1) result in a restricted ability of neoplastic cells to respond to viral infections compared to healthy cells (Lichty et al, 2014). In addition, malignant cells develop aberrant deregulated cell signaling pathways during carcinogenesis that also support productive viral infection. This includes the activation of the Ras signaling pathway and a deregulation of the type I IFN immune response (Kirn et al, 2001; Noser et al, 2007; Zhang et al, 2010). The parallels between the requirements for viral replication in mammalian cells and the mechanisms driving cancer cell growth have led to the development of oncolytic viruses (Lichty et al, 2014). Oncolytic viruses are a novel class of antitumor therapeutics that preferentially replicate and kill cancer cells while sparing normal tissue. They can be categorized into two groups: (i) viruses that have a natural preference to replicate in cancer cells (e.g. new castle disease virus, reovirus) and (ii) viruses that are engineered for cancer cell selectivity (e.g. herpes simplex virus, vaccinia virus) (Russell et al, 2012).
Oncolytic viruses are especially promising anticancer agents as they promote antitumor responses through different mechanisms of action. First, oncolytic viruses cause tumor debulking due to viral infection and cell lysis, a process called oncolysis. Released viral particles infect neighboring tumor cells resulting in viral amplification and spread throughout the tumor tissue. However, this cycle is likely to be hampered by induced antiviral immune response mechanisms (Marchini et al, 2016). Second, some oncolytic viruses are described to trigger a tumor vasculature disruption and thereby elicit apoptosis or necrosis of uninfected tumor cells (Breitbach et al, 2013; Benencia et al, 2005; Marchini et al, 2016). Furthermore, there is increasing evidence that oncolytic virotherapy induces a systemic antitumor immune response that is decisive for therapy efficacy. Thus, oncolytic virus-mediated cancer therapy is now referred more and more frequently as 'oncolytic immunotherapy' (Guo et al, 2017). In recent years, it was claimed that the induction of immunogenic cell death (ICD) by oncolytic virus-mediated cell killing is a key mechanism to promote a durable antitumor immune response. ICD describes modes of cell death like necroptosis, autophagic cell death and pyroptosis of

cancer cells that trigger the induction of immune responses. The oncolysis-induced inflammatory milieu in combination with the release and presentation of pathogen-associated molecular patterns (PAMPs), danger-associated molecular patterns (DAMPs) and TAAs from the lysed tumor cells stimulate the recruitment and maturation of APCs, such as DCs (Guo et al, 2017; Marchini et al, 2016). DAMPs are endogenous molecules in the inside of a cell that are usually not recognized by the host immune system but initiate danger signaling after the release by dying cells (e.g. cell-surface exposure of calreticulin, release of heat-shock-proteins, secretion of ATP) (Galluzzi et al, 2017). Typical PAMPs in the context of oncolytic virotherapy include viral nucleic acids or viral proteins. Antigen-loaded DCs migrate to tumor draining lymph nodes promoting antigen presentation to immune cells. Ideally, antitumor immune responses are induced mediating killing of infected and uninfected tumor cells (Guo et al, 2017; Marchini et al, 2016).

Various transgenes have been incorporated into the genome of oncolytic viruses to improve their therapeutic efficacy and to further enhance the induction of an antitumor immunity. This includes the modification of oncolytic viruses to encode inflammatory cytokines or T cell co-stimulatory proteins (Lichty et al, 2014). The most advanced oncolytic virus in clinical development is Talimogene laherparepvec (T-Vec), which has been approved by the FDA in 2015 for the treatment of advanced metastatic melanoma (Farkona et al, 2016). T-Vec is an attenuated oncolytic herpes simplex virus-1 (HSV-1) that is engineered for tumor-selective replication, minimal pathogenicity and stimulation of a tumor-specific immune response (Hughes et al, 2014; Kaufman et al, 2015; Liu et al, 2003). This is accomplished by deleting genes in the viral genome that are not essential for viral replication in cancer cells and by incorporating an immunostimulatory transgene. Removal of both copies of the 'neurovirulence factor' ICP34.5 required for viral immune evasion renders the virus tumor-selective and reduces its neurovirulence thereby attenuating viral pathogenicity (Chou et al, 1990; Sarinella et al, 2006; Liu et al, 2003; Hughes et al, 2014). Due to the deletion of the viral gene ICP47, that usually blocks antigen presentation in HSV-infected cells, the induction of T cell immunity is enhanced by improving antigen processing and presentation (York et al, 1994; Früh et al, 1995; Hughes et al, 2014; Liu et al, 2003). In addition, deletion of ICP47 leads to the early activation of the HSV promotor US11 thereby supporting viral growth (Mohr et al, 2001; Liu et al, 2003; Hughes et al, 2014). Additionally, T-Vec is engineered to express the immunomodulating cytokine GM-CSF to stimulate antitumor immune responses (Hughes et al, 2014). GM-CSF is described to play a critical role in the development and maturation of DCs, promotes the survival and activation of

macrophages, neutrophils as well as eosinophils and mobilizes myeloid populations from the bone marrow into blood (Hamilton, 2008). Thus, the rational to use GM-CSF in the context of oncolytic immunotherapy is to improve the recruitment of DCs into the tumor microenvironment resulting in an increased antigen presentation to T cells and thereby enhancing the induction of antitumor immune responses (Hughes et al, 2014).
Another cytokine stimulating the maturation and proliferation of DCs that has been investigated in cancer immunotherapy is FMS-like tyrosine kinase 3 ligand (Flt3L) (Maraskovsky et al, 1996; Shurin et al, 1997). Treatment of different cancer types with either recombinant or viral-encoded Flt3L showed promising antitumor efficacy and the induction of an immunological memory (Chen et al, 1997; Wang et al, 2000; King et al, 2008; Lynch et al, 1997).

1.2 Vesicular stomatitis virus

Vesicular stomatitis virus (VSV) is an enveloped, single-stranded RNA virus belonging to the family *Rhabdoviridae*. It is an arthropod-borne virus and natural hosts mainly include rodents, horse, cattle and swine. VSV can lead to an acute disease in livestocks that is characterized by vesicular lesions in the oral cavity, teats and feets that usually resolves within a few weeks without fatality. VSV is zoonotic but human infections are rare and are usually asymptomatic or only accompanied by mild-flu like symptoms in some individuals (Lichty et al, 2004). Only a single case of VSV-associated human encephalitis has been reported (Quiroz et al, 1988). The two predominant serotypes found in America are New Jersey and Indiana, whereas the New Jersey serotype is considered to be the agriculturally relevant pathogen. Oncolytic VSV agents are derived from the Indiana serotype (Lichty et al, 2004).

1.2.1 VSV biology

VSV is a membrane-enveloped virus having a bullet-shaped morphology with an approximate size of 185 x 75 nm (Ge et al, 2010; Hastie & Grdzelishvili, 2012). The virions contain a single-stranded RNA genome with negative polarity (ss(-)RNA) that exhibits a size of approximately 11,000 nucleotides. The genome encodes the five viral proteins nucleoprotein (N), phosphoprotein (P), matrix protein (M), glycoprotein (G) and large polymerase (L) (Figure 2).

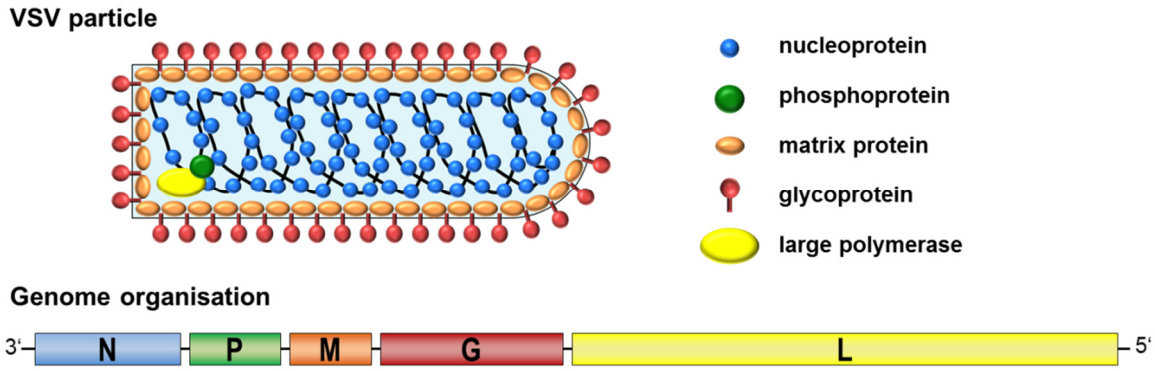

Figure 2: Schematic representation of VSV virions and of their genome. The negative, single-stranded RNA genome encodes five viral proteins: Nucleoprotein (N), phosphoprotein (P), matrix protein (M), glycoprotein (G) and large polymerase (L). The viral proteins and a lipid envelope build up bullet-shaped VSV virions. According to the information provided in (Lichty et al, 2004).

The N protein is tightly associated with the ss(-)RNA genome rendering the genome nuclease-resistant. Moreover, the ss(-)RNA-N protein complex constitutes the template for transcription as well as replication by the RNA-dependent RNA-polymerase (RdRP). The RdRP consists of the catalytically large subunit, the L protein, and the essential phosphoprotein cofactor, the P protein (Hastie & Grdzelishvili, 2012). The N-encapsidated VSV genome together with the RdRP forms the ribonucleoprotein (RNP) complex. The M protein has multiple functions including virus assembly and budding. Additionally, it is an important virulence factor as it is involved in the induction of apoptosis and disruption of host antiviral mechanisms (Lichty et al, 2004). In particular, the M protein interrupts the host transcriptional machinery and blocks the mRNA export from the nucleus and thereby interferes with the expression of antiviral genes such as IFN (Black & Lyles, 1992; Petersen et al, 2000; Ahmed et al, 2003; Lichty et al, 2004). The G protein binds to the cell surface via the ubiquitously expressed low density lipoprotein (LDL) receptor and mediates fusion of the viral and cellular membranes (Finkelshtein et al, 2013; Sun et al, 2010). The virus is internalized into the cell by actin- and clathrin-dependent endocytosis (Sun et al, 2005; Cureton et al, 2010). Acidification in the endosome (pH<6.2) triggers a conformational change in the G protein leading to the fusion of the viral envelope with the endosomal membrane finally causing the release of the infectious RNP complex into the cytoplasm (White et al, 1981; Sun et al, 2010). The subsequent transcription and replication of the viral genome entirely occurs in the cytosol. Due to a single polymerase entry site on the 3'-end of the VSV genome transcription is obligatory sequential (Ball & White, 1976; Emerson, 1982). Highly conserved *cis*-acting elements within the intergenic regions provide start/stop signals required for transcriptional regulation (Barr et al, 2002; Rose, 1980; McGeoch, 1979). However, reinitation of transcription by the RdRP complex at each gene junction does

not always occur, resulting in 29-33 % fewer transcripts of downstream genes compared to the previous genes (Iverson & Rose, 1981). The resulting transcriptional gradient causes a decrease in mRNA and thus protein abundance from the 3' to the 5' located genes (Villarreal et al, 1976; Barr et al, 2002). Later on, the VSV genome is also replicated by the viral RdRP. During replication, full-length positive-sense VSV antigenomes are synthesized which in turn are used as template for the synthesis of the negative-sense VSV genomes. These genomes are either utilized as template for second transcription or packaged into progeny VSV virions (Barr et al, 2002).

1.2.2 VSV – an oncolytic virus

VSV is a promising oncolytic virus candidate showing impressive antitumor activity in a variety of animal models. It is under intense development due to several favorable characteristics including its cytoplasmic replication without the risk of host-cell-transformation, its well-studied biology, a rapid replication cycle, a genome that is genetically stable as well as easily manipulable and its producibility to high virus yields. Furthermore, VSV primarily affects rodents and livestocks. Human infections are rare and are mainly limited to agricultural as well as laboratory workers. Thus, the occurrence of VSV-specific antibodies in the general human population is low. Due to the absence of preexisting immunity, neutralization of VSV during virotherapy treatment is reduced and further allows the systemic administration of VSV agents to treat also disseminated cancer (Hastie & Grdzelishvili, 2012). In addition, VSV exhibits inherent tumor selectivity due to its exquisitely sensitivity to type I IFN-induced antiviral responses (Stojdl et al, 2000; Stojdl et al, 2003; Liu et al, 2013). Many tumor cells acquired deregulated type I IFN signaling pathways during carcinogenesis. This includes the downregulation of genes associated with type I IFN responses such as the IFN receptor (IFNAR) or epigenetic silencing of IFN-responsive transcription factors (Zhang et al, 2010; Li & Tainsky, 2011). In addition, IFN signaling can be inhibited by Ras signaling pathways that are often activated in malignant cells (Noser et al, 2007).

Different strategies have been investigated to further improve the efficacy of VSV therapeutics. This involves the combination of VSV therapy with chemical agents, radiotherapy or viral expression of suicide genes (Goel et al, 2007; Fernandez et al, 2002; Hastie & Grdzelishvili, 2012). Additionally, numerous approaches have been developed to prevent premature clearance of VSV-based oncolytic viruses by the host immunity (Hastie & Grdzelishvili, 2012). This includes physical delivery methods to mask the virus from immune cells or engineering VSV to escape the host immune

response (Kottke et al, 2008; Muik et al, 2014). Since it is claimed that fully effective oncolytic virotherapy requires the activation of tumor-specific immune responses, VSV constructs have also been developed that encode for TAAs or cytokines (Hastie & Grdzelishvili, 2012; Pulido et al, 2012; Fernandez et al, 2002; Bergman et al, 2007).
However, VSV exhibits inherent neurotoxicity which has hindered clinical development. VSV invasion of the central nervous system has been observed in rodent's models after different application routes as well as in non-human primates finally leading to severe neurological diseases (Muik et al, 2012; Johnson et al, 2007; Bi et al, 1995; Shinozaki et al, 2005).

1.2.2.1 Improving the safety of VSV

Different strategies have been evaluated to improve the safety profile of VSV. One promising approach includes VSV-MΔ51 or VSV-M51R viruses exploiting the lack of IFN response in certain cancer types. The deletion or mutation of the methionine residue at position 51 prevents the matrix protein from blocking the nucleocytoplasmic transport of mRNA and from inhibiting host-cell gene expression. This enables the expression of antiviral genes such as IFN. Thereby, such VSV mutants retain their oncolytic activity in cancer cells defective for the IFN pathway while being attenuated in healthy tissue (Stojdl et al, 2003). A further strategy to exploit the defects in IFN signaling in cancer cells involves the development of recombinant VSV viruses engineered to encode IFN (e.g. VSV-IFNβ). The resultant virus protected non-malignant tissue from off-target toxicity while retaining oncolytic activity (Obuchi et al, 2003). Due to promising results in preclinical studies, VSV encoding IFNβ is currently evaluated in ongoing clinical trials (ClinicalTrials.gov identifier: NCT01628640, NCT02923466, NCT03120624).
One of the key determinant of VSV neurovirulence is the VSV-G glycoprotein (Cooper et al, 2008; Clarke et al, 2007; Martinez et al, 2003). Thus, a further promising approach to improve the safety profile was the exchange of the VSV-G with the non-neurotropic envelope glycoprotein of the lymphocytic choriomeningitis virus WE strain (LCMV-GP). Tropism analysis showed that LCMV-GP pseudotyped single-cycle infectious VSV (VSVΔG-GP) showed enhanced infectivity of malignant glioma cells while sparing primary human and murine neurons *in vitro* and *in vivo.* Furthermore, immune cells (such as stimulated T cells and DCs) were less susceptible to VSVΔG-GP as compared to VSV-G complemented VSVΔG vectors (Muik et al, 2011). Pseudotyping replication-competent VSV with LCMV-GP (rVSV(GP)) abrogates neurotoxicity while retaining potent antitumor activity. In addition, rVSV(GP) was proven to escape humoral immunity and resisted complement-mediated inactivation in normal human serum and

thus potentially allows repeated rVSV(GP) application without impaired therapeutic efficacy (Muik et al, 2014).

A further approach to overcome the neurotoxicity of VSV was the development of a semireplication-competent VSV vector system (srVSV) which is based on two *trans*-complementing, propagation-deficient VSV vectors (Figure 3) (Muik et al, 2012).

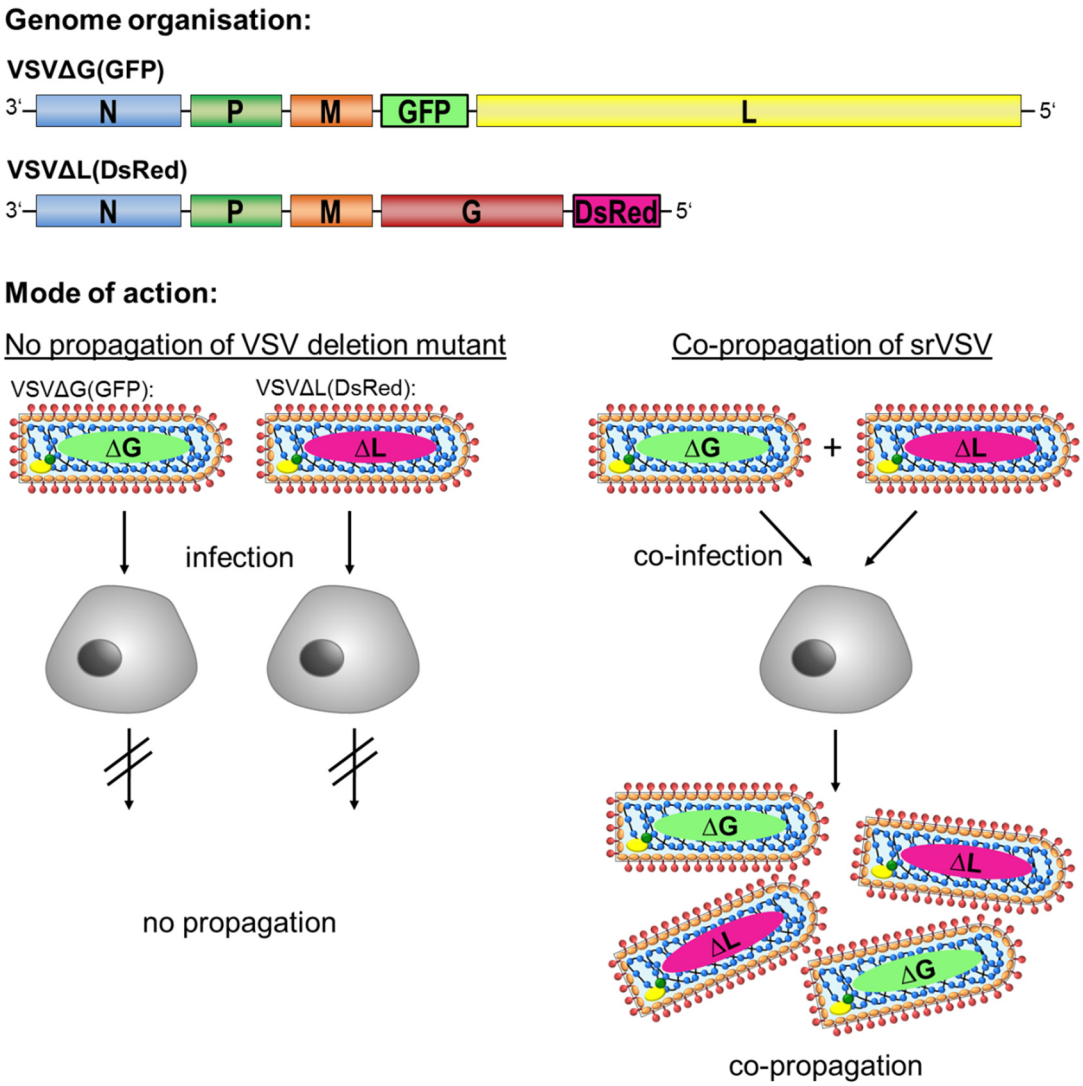

Figure 3: Genome organization and mode of action of srVSV. srVSV is composed of two complementary VSV deletion mutants, namely VSVΔG and VSVΔL. In the genome of the VSVΔG vector the gene of the G protein was substituted with GFP and in the genome of the VSVΔL vector the gene encoding the L protein was substituted with DsRed. Both individual VSV deletion mutants are propagation-deficient alone. After co-infection with VSVΔG(GFP) together with VSVΔL(DsRed), they can co-replicate and co-propagate leading to viral spread. According to the information provided in (Muik et al, 2012).

In particular, srVSV is composed of a VSVΔG vector lacking the G gene and a VSVΔL vector being deleted for the L gene. VSVΔG and VSVΔL cannot propagate alone and thus infectious progeny can only be produced in double infected cells. Consequently, co-propagation is limited to foci of high vector concentrations such as the injection site and adjacent areas of the topically treated tumor reducing the risk of toxicity. srVSV was

shown to propagate without reversion to replication-competent virus, proved to be highly oncolytic *in vitro* and induced long-term tumor regression in a xenograft tumor mouse model. Treatment of tumor-bearing mice or direct intracranial administration in healthy mice was not associated with any side effects of neurotoxicity. It was also shown that srVSV exhibited a similar IFN-inducing capacity as VSV-M51R. Thus, next to its intrinsic mode of co-propagation resulting in limited viral spread, srVSV restriction to tumor tissue could additionally be caused by its effective induction of type I IFN (Muik et al, 2012).

Further strategies to improve the safety of VSV include mutation in the VSV-G protein, adaption to cancer cells by serial passaging or insertion of targets for microRNA into the VSV genomes that are solely expressed in normal cells (Hastie & Grdzelishvili, 2012).

1.3 Adeno-associated virus

Adeno-associated viruses (AAV) are nonpathogenic, single-stranded DNA viruses belonging to the family *Parvoviridae* (Gonçalves, 2005). AAV is classified to the genus *dependovirus* as successful replication and production of AAV particles requires the co-infection with a helper virus such as adenovirus or HSV (Casto et al, 1967; Buller et al, 1981, Gonçalves, 2005). In the absence of a helper-virus the AAV genome preferentially integrates site-specifically into chromosome 19 of the host's genome and persists in a latent form (Kotin et al, 1990; Samulski et al, 1991). The virus has an icosahedral capsid architecture with a diameter of approximately 22 nm and is formed by 60 subunits of the viral proteins (VP) VP1, VP2 and VP3 (Xie et al, 2002; Gonçalves, 2005).

AAVs package a linear, single-stranded DNA genome of approximately 4.7 kb that can have negative or positive polarity (Samulski & Muzyczka, 2014; Srivastava et al, 1983). The genome consists of two open reading frames (ORF), *rep* and *cap*, that are flanked by inverted terminal repeats (ITR) serving as origin of replication and encapsidation signal (Samulski & Muzyczka, 2014; Senapathy et al, 1984; McLaughlin et al, 1988). The *rep* ORF encodes the four regulatory proteins Rep78, Rep68, Rep52 and Rep40 that are required for the regulation of gene expression, chromosomal integration, DNA replication, viral assembly and genome packaging (Im & Muzyczka, 1992; Im & Muzyczka, 1990; Smith & Kotin, 1998; Collaco et al, 2003; Pereira et al, 1997; Weitzman et al, 1994; King et al, 2001). The *cap* ORF encodes the structural proteins VP1, VP2 and VP3 (Samulski & Muzyczka, 2014). Recently, a third ORF within *cap* has been identified encoding the assembly-activating protein (AAP) that is required for capsid formation (Sonntag et al, 2010).

Various AAV serotypes have been isolated from human, non-human primates and other species such as horse. The different serotypes have a similar genome organization and size but differ in the amino acid composition of their capsid resulting in varying tissue tropisms. Further differences include their transduction efficiencies and prevalence of preexisting immunity. AAV serotype 2 (AAV2) is the best characterized as well as most abundant strain in the human population and was used by a vast majority of AAV gene transfer studies (Wu et al, 2006; Asokan et al, 2012). The primary receptor of AAV2 is heparin sulfate proteoglycan (HSPG), with residues R585 and R588 of AAV2 being primarily responsible for heparin sulfate binding (Summerford & Samulski, 1998; Kern et al, 2003; Opie et al, 2003). Recently, AAVR was identified as a further essential host receptor required for AAV infection and also other surface proteins including fibroblast growth factor, laminin receptor and integrin αVβ5 have been described as putative AAV2 co-receptors (Pillay et al, 2016; Qing et al, 1999; Akache et al, 2006; Summerford et al, 1999).

1.3.1 AAV-based gene transfer vectors

Over the past decade, AAV gained considerable interest as gene therapy vector due to some of its advantageous properties such as lack of pathogenicity, high stability, low immunogenicity, capability of transducing dividing and non-dividing cells and to establish a long-term transgene expression (Coura & Nardi, 2007). AAV vectors are investigated in numerous clinical studies addressing monogenetic diseases such as hemophilia B, retinal diseases or muscular dystrophy. In 2012, the AAV vector Glybera® was the first gene therapy medicinal product that achieved marketing authorization in the western nation. The AAV1-based vector delivers the human lipoprotein lipase (LPL) gene to muscle cells following intramuscular injection into patients suffering from a rare genetic disease in lipid metabolism. Further clinical trials utilize AAV vectors to treat also other diseases such as Parkinson's disease or heart failure (Kotterman et al, 2015).
For gene therapeutic applications, recombinant AAV vectors are generated by incorporating a gene of interest into the viral genome. For this, the *rep* and *cap* ORFs are deleted from the AAV genome and replaced by the transgene that is now flanked by the ITRs, the only *cis*-acting elements required for DNA encapsidation (hereafter designated as 'transfer vector'). The *rep* and *cap* genes as well as the adenoviral helper functions are provided in *trans* on separate plasmids during vector production. After transfection of these plasmids into producer cell lines, rAAV vectors carrying the desired transgene are purified (Gonçalves, 2005). Due to the construction of rAAV vectors that do not encode

Rep proteins and lack the integration efficiency element (IEE), both required for site-specific integration, the transferred transgene primarily persists episomally (Philpott et al, 2002; Daya & Berns, 2008).

One of the rate-limiting steps during AAV transduction is the conversion of the single-stranded into double-stranded DNA genome which is required prior to transgene expression. To avoid the delayed start of gene expression after transduction, this step can be circumvented by using self-complementary AAV vectors (scAAV). Such scAAVs contain an AAV genome with a deleted terminal resolution site sequence from one ITR preventing the Rep-mediated DNA nick and thus leading to the generation of self-complementary, double-stranded AAV genomes. Even though scAAV vectors lost about half of their coding capacity, they showed increased transduction efficiency relative to single-stranded AAV (ssAAV) in various animal models (McCarty, 2008).

1.3.2 Surface engineering of AAV vectors

Different strategies have been developed to enable effective AAV-mediated gene transfer to specific tissues or relevant cell types to increase efficiency and safety of gene therapy applications, especially after systemic vector administration. One approach includes the control of gene expression using cell type-specific promotors and microRNA target sequences (Nettelbeck et al, 2000; Gentner & Naldini, 2012). However, these vector particles can still enter non-target cells which potentially reduce the efficiency of gene transfer.

A further approach is based on capsid engineering either by directed evolution efforts or rational design. Directed evolution approaches use AAV libraries that are created by modification of the *cap* genes. This includes (i) the usage of libraries carrying a mutation in the *cap* ORF introduced by error-prone PCR, (ii) capsid shuffling which is based on fragmenting the capsid DNA sequences of different serotypes that is followed by random assembly of the sequences and (iii) random peptide sequences that are genetically introduced into the AAV capsid. The capsid libraries are put under selective pressure *in vitro* or in a suitable animal model to isolate an AAV vector with the desired properties. Finally, the capsid modifications of the selected AAV variants are identified enabling the development of the corresponding vector. Thereby, AAV vectors can be identified that enter the cell type of choice and allow intracellular processing of AAVs (Kotterman & Schaffer, 2014; Büning et al, 2015).

Rational design approaches rely on the identification of cell surface receptors that are expressed on the relevant cell type (Buchholz et al, 2015). Recently, successful

redirection of the AAV2 receptor usage has been achieved by incorporating designed ankyrin repeat proteins (DARPin) as high-affinity ligands into the AAV capsid. The concept is based on ablating natural receptor binding of AAV2 to HSPG by introducing two point mutations into the VP proteins (R585A, R588A). Next, genetic fusion of a DARPin to the N-terminus of the VP2 protein enabled the binding to the cell surface receptor of choice (Münch et al, 2013) (Figure 4).

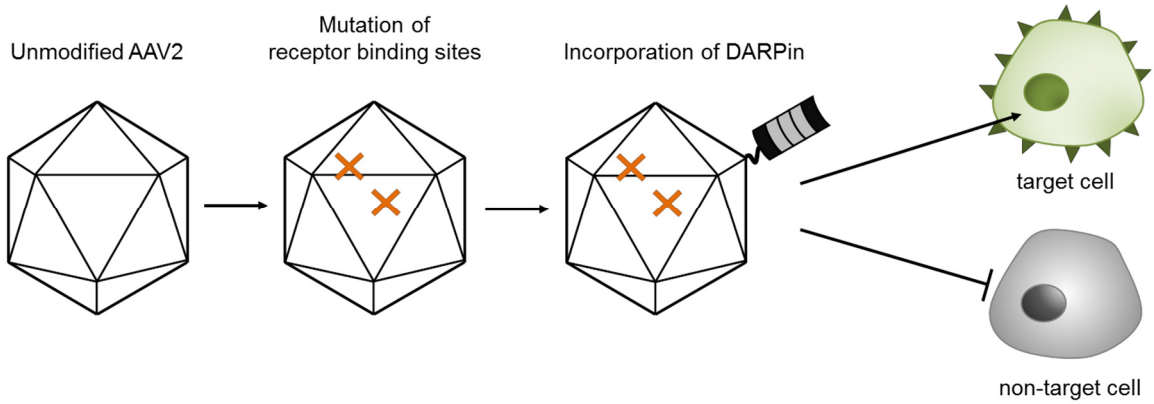

Figure 4: Rational engineering of receptor-targeted AAV. Generation of receptor-targeted AAV vectors involves two steps. First, natural receptor binding to HSPG is ablated by introducing two point mutations into the capsid proteins (indicated in orange). Second, a DARPin specific for a cell surface receptor of choice is fused to the capsid proteins on genetic level enabling the transduction of receptor-positive cells. According to the information provided in (Buchholz et al, 2015).

Among these receptor-targeted AAV vectors is a tumor-specific vector displaying a Her2/neu-specific DARPin on the capsid surface (Her2-AAV). Her2-AAV enabled specific gene transfer into subcutaneous and disseminated Her2/neu-positive tumor cells in a xenograft tumor mouse model, while non-targeted AAV2 retained in the liver (Münch et al, 2013; Münch et al, 2015). In addition, application of Her2-AAV equipped with the suicide gene thymidine kinase from HSV was sufficient to control tumor growth and to substantially prolong survival in a therapeutic xenograft mouse model. In contrast, non-targeted AAV2 showed decreased survival compared to untreated animals due to liver toxicity (Münch et al, 2013). The system was proven to be highly flexible, since the incorporation of further DARPins, specific for CD4 or epithelial cell adhesion molecule (EpCAM), also enabled selective transduction of target cells even if they were highly underrepresented (Münch et al, 2015).

1.4 Objectives

Aim of this study was the generation and characterization of two different types of viral gene transfer systems for applications in cancer immunotherapy. The first project aimed at the development of srVSV as a novel vector system for oncolytic immunotherapy. Combining the oncolytic activity of srVSV with the expression of immunotherapeutic transgenes was assumed to interfere with tumor immune escape mechanisms leading to a long-lasting antitumor immunity. Tumor cells acquired a variety of mechanisms to evade the immune response in order to favor cancer progression including reduced numbers as well as functionally impaired DCs, low TAA presentation due to downregulation of MHC molecules and secretion of factors suppressing the activity of cytotoxic T cells (Melzer et al, 2017; Zou, 2005). Thus, srVSV should be armed with the cytokines GM-CSF or Flt3L to stimulate the generation and recruitment of DCs into the tumor microenvironment. Furthermore, srVSV should be equipped with the coding sequence of the TAA Her2/neu or of a fusion protein comprised of CTLA-4 and Her2/neu in order to directly deliver the respective TAA to B7-expressing APCs. Additionally, srVSV should be armed with the T cell co-immunostimulatory molecule B7. To this end, the different immunostimulatory transgenes (GM-CSF, Flt3L, B7) and TAAs (Her2/neu, CTLA-4-Her2/neu) had to be cloned into the genome of VSVΔG and VSVΔL vectors. The different binary srVSV systems had to be generated *de novo* and analyzed for their capacity to mediate transgene expression. In order to investigate the antitumoral efficacy of the generated srVSV systems *in vivo*, a suitable tumor mouse model should be identified. For this purpose, different murine tumor cell lines had to be analyzed in regard to their sensitivity to type I IFN-induced antiviral responses. Finally, antitumoral efficacy of srVSV armed with immunotherapeutic transgenes had to be evaluated in a subcutaneous tumor mouse model.

The second part of the thesis aimed at developing receptor-targeted AAV vectors for tumor-specific delivery of immune checkpoint inhibitors. While immune checkpoint blockade is promising, this therapy is associated with a number of irAEs. These toxicities are fostered by the systemic administration of these antibodies which do not only lead to the activation of the immune response at sites of tumor lesions but also in healthy tissue. Thus, the aim of this study was the specific delivery of αPD-1 and αPD-L1 precisely to sites of tumor growth. As potential vehicle for the delivery of the immune checkpoint inhibitors tumor-targeted AAV vectors should be investigated. In particular, Her2/neu-specific AAV vectors should be used as gene transfer system, as they had been well characterized for their specificity *in vitro* as well as for their targeting capacity in

immunodeficient tumor-bearing mice (Münch et al, 2013; Münch et al, 2015). To this end, the ORF of PD-1- and PD-L1-specific molecules had to be incorporated into AAV transfer vectors. Generated AAV vector particles had to be characterized regarding their genomic titers, packaging efficiency and transgene expression. For quantification and detection of AAV-encoded αPD-1 and αPD-L1 in cell culture supernatants as well as in mice organs an ELISA had to be developed. Since the immune system is mandatory for immune checkpoint modulation, a suitable syngeneic tumor mouse model for the investigation of tumor-targeted delivery of immune checkpoint inhibitors by AAV vectors had to be identified and Her2-AAV tumor targeting had to be investigated in immunocompetent mice. Finally, the capability of Her2-AAV to mediate tumor-targeted delivery of immune checkpoint inhibitors *in vivo* should be assessed.

2 Material and Methods

2.1 Material

Consumables used for cell culture, molecular biology, protein biochemistry and animal work were obtained from Braun, TPP, BD Bioscience, Greiner Bio-One, GE Healthcare, Biozym, Nerbe, Biotix, Thermo Fisher Scientific, Merck Millipore, Micronic, Beckman Coulter, Bio-Rad, BD Microfine, Fujifilm, Sarstedt, VWR and MP Biomedical. Chemicals were generally obtained from Biozym, Carl Roth, Sigma-Aldrich, Applichem, VWR or *Medienküche* of the Paul-Ehrlich-Institut and more details of commonly used reagents are given in Table 1.

2.1.1 Reagents, chemicals, recombinant proteins and cytokines

Table 1: Reagents, chemicals, recombinant proteins and cytokines

Name	Supplier
1-Step™ Ultra TMB substrate	Thermo Fisher Scientific
2-log DNA ladder	New England Biolabs
Ampicillin	Roche
Concanavalin A (ConA) from *canavalia ensiformis* (Jack bean)	Sigma-Aldrich
D-Luciferin	Perkin Elmer
Dulbecco's Modified Eagle Medium (DMEM)	Biowest
Fetal calf serum (FCS)	Biochrom
FuGENE® HD Transfection Reagent	Promega
Geneticin®	life technologies
Ionomycin	Sigma-Aldrich
Kanamycin	Sigma-Aldrich
Lipofectamine™ LTX Reagent with PLUS™ Reagent	Invitrogen
Midori Green DNA, Direct loading dye	Nippon Genetics
Mouse IFNα	Miltenyi Biotec
Mouse IFNγ	Miltenyi Biotec
OptiMEM® (1x) + GlutaMAX™	life technologies
PageBlue™ Protein Staining Solution	Thermo Fisher Scientific
PageRuler™ Plus Prestained Protein Ladder	Thermo Fisher Scientific
Panexin NTA	PanBiotech
Passive Lysis Buffer	Promega
PBS (w/o Mg^{2+}/Ca^{2+})	Lonza, Paul-Ehrlich-Institut
PBS(w/o Mg^{2+}/Ca^{2+})/EDTA (1 mM), pH 7.1	Paul-Ehrlich-Institut

Penicillin/Streptomycin (PenStrep)	Paul-Ehrlich-Institut
Phorbol 12-myristate 13-acetate (PMA)	Sigma-Aldrich
Pierce BCA Protein Assay Kit	Thermo Fisher Scientific
Pierce™ ECL Western Blotting substrate	Thermo Fisher Scientific
Protease inhibitor cocktail, complete ULTRA Tablets	Roche
Puromycin	life technologies
Quick Start™ Bradford 1x dye	Bio-Rad
Quick Start™ BSA Standard Set	Bio-Rad
Recombinant PD-1	Life technologies
Recombinant PD-L1	Life technologies
Rec-Protein A-Sepharose® 4B Conjugate	Invitrogen
RPMI 1640 medium	Biowest
VP-SFM	life technologies

2.1.2 Commercially available kits

Table 2: Kits

Name	**Supplier**
AAV2 Titration ELISA	Progen
DNeasy® Blood & Tissue Kit	Qiagen
eBioscience™ Fixable Viability Dye eFluor™ 450	Thermo Fisher Scientific
Flt3 Ligand Human ELISA Kit	Abcam
GeneJET Gel Extraction Kit	Thermo Fisher Scientific
GeneJET Plasmid Miniprep Kit	Thermo Fisher Scientific
JETSTAR 2.0 Plasmid Maxiprep Kit	Genomed
JETSTAR 2.0 Plasmid Midiprep Kit	Genomed
Mouse GM-CSF ELISA Kit	Thermo Fisher Scientific
Mouse IFN gamma ELISPOT Ready-Set-Go!®-Kit	eBioscience
NucleoBond® Xtra Midi	Macherey-Nagel
Rapid DNA Ligation Kit	Thermo Fisher Scientific
SensiFAST™ Probe No-ROX Kit	Bioline
WST-1 Cell Proliferation Assay Kit	Takara Clontech

2.1.3 Enzymes

Table 3: Enzymes

Name	Supplier
Antarctic Phosphatase	New England Biolabs
Benzonase® Nuclease	Sigma-Aldrich
KOD Hot Start DNA Polymerase	Merck Millipore
Restriction endonucleases	New England Biolabs
Trypsin 2.5 %	Paul-Ehrlich-Institut

2.1.4 Buffers

Table 4: Buffer composition

Name	Composition
AAV lysis buffer	50 mM Tris-HCl 150 mM NaCl H_2O pH 8.5
ELISA blocking buffer	5 % (v/v) FCS (filtered through 0.45 µm) 0.05 % (v/v) Tween PBS
ELISA washing buffer	0.05 % (v/v) Tween PBS
FACS fix	1 % formaldehyde PBS
FACS washing buffer	2 % (v/v) FCS 0.1 % (v/v) NaN_3 PBS
Freezing medium	90 % (v/v) FCS 10 % (v/v) DMSO
PBS M/K	2.5 mM KCl 1 mM $MgCl_2$ PBS
PEI	18 mM polyethylenimine in H_2O
Protein A collection buffer	1 M Tris PBS pH 8.8
Protein A elution buffer	100 mM glycine PBS pH 2.7
Protein A storage buffer	0.1 % (v/v) NaN_3 PBS

Red Blood Cell Lysis Buffer (provided by *Medienküche* Paul-Ehrlich-Institut)	155 mM NH_4Cl 10 mM Tris H_2O pH 7.5
SDS loading dye (4x)	250 mM Tris/HCl (pH 6.8) 4 % (w/v) SDS 20 % (v/v) glycerol 20 mg/l bromphenolblue 10 % β-Mercaptoethanol H_2O
SDS running buffer (10x buffer provided by *Medienküche* Paul-Ehrlich-Institut)	25 mM Tris 192 mM glycine 1 % (w/v) SDS H_2O
TAE buffer (20x TAE buffer provided by *Medienküche* Paul-Ehrlich-Institut)	40 mM Tris 20 mM acetic acid 1 mM EDTA H_2O
TBS-T (10x TBS buffer provided by *Medienküche* Paul-Ehrlich-Institut)	50 mM Tris 150 mM NaCl 0.1 % (v/v) Tween H_2O pH 7.4
Western blot transfer buffer	48 mM Tris 39 mM glycine 20 % (v/v) methanol H_2O

2.1.5 Antibodies

Table 5: Antibodies

Antibody		**Application & Dilution**	**Supplier**
α-Myc-tag (Myc.A7)	mouse	WB[a] (1:1,000)	abcam
α-His-PE (GG11-8F3.5.1.)	mouse	FC[b] (1:50-1:100)	Miltenyi Biotec
α-human-CD86-FITC (FM95)	mouse	FC (1:50-1:100)	Miltenyi Biotec
α-human-CD80-PE (2D10)	mouse	FC (1:50-1:100)	Miltenyi Biotec
α-human IgG (Fc specific), HRP-coupled	goat	WB (1:10,000) ELISA (1:10,000)	Sigma-Aldrich
α-mouse-CD28-PE (37.51)	hamster	FC (1:50-1:100)	Miltenyi Biotec
$F(ab')_2$ α-human IgG-FITC	goat	FC (1:100)	Biozol (Southern Biotech)
α-murine GM-CSF	rabbit	WB (1:500)	Peprotech

α-human Flt3L	rabbit	WB (1:500)	Peprotech
α-HA-tag (16B12)	mouse	WB (1:1,000) ELISA (1:200)	abcam
α-HA-Biotin (3F10)	rat	ELISA (1:500)	Roche
α-mouse-PD-L1-PE (MIH5)	rat	FC (1:300)	eBioscience
α-mouse-PD-1-PE (HA2-7B1)	rat	FC (1:10-1:100)	Miltenyi Biotec
α-rabbit, HRP-conjugated	goat	WB (1:2,000)	Dako
α-mouse, HRP-conjugated	rabbit	WB (1:2,000)	Dako
Rat IgG2b, isotype control		FC (1:10)	Miltenyi Biotec
FcR blocking reagent, mouse	-	FC (1:10)	Miltenyi Biotec

[a] WB: Western blot, [b] FC: flow cytometry

2.1.6 Oligonucleotides

All oligonucleotides were synthesized by the company Sigma-Aldrich or Eurofins MWG Operon.

Table 6: Primer

Name	Oligonucleotides (5'→ 3')
ΔL_GMCSF_for	CGATGGATCCATGTGGCTGCAGAATTTACTTTTCCTG
ΔL_GMCSF_rev	CAGTGCGGCCGCTCATTTTTGGACTGGTTTTTTGCATTCAAAG
ΔG_Flt3L_for	ATTCGATCCCGGGATGACAGTGCTGGCTCCTGCATG
ΔG_Flt3L_rev	TATTGCGGCCGCTCAGGATGTC
ΔL_TAA_for	CGATGGATCCATGGAGACAGACACACTCCTGCTATGG
ΔG_TAA_for	ATTCGATCCCGGGATGGAGACAGACACACTCCTGCTATGG
ΔL/ΔG_TAA_rev	CAGTGCGGCCGCTCAATGATGATGATGATGATGGTC
ΔL_B7_for	GAGCGATAGATCTATGGCTTGCAATTGTCAGTTG
ΔG_B7_for	GAGCGATACCGGTATGGCTTGCAATTGTCAGTTG
ΔL/ΔG_B7_rev	ATTAGCGGCCGCTTATTTACCCGGGGACAGGG
pB7_for	CGGCTTAATTAAATGGCTTGCAATTGTCAG
pB7_rev	CGATGCTAGCCTTACCTGTCTTGCTATCAGGAG
pIRES-G_for	GGCGCGACATGTATGAAGTGCCTTTTGTACTTAG
pIRES-G_rev	CCGCGGAATTCTTACTTTCCAAGTCGGTTCATC
scAAV-αPD-1/αPD-L1_for	TGCCACCATGGAGACAGACAC
scAAV-αPD-1/αPD-L1_rev	ATATGGGCGGCCGCTTCAATTCAGATCTTCTTCTGAGATG
Fc-only_for	ATATAGGCCCAGCCGGCCGTCGACGAGGCCAAATCTTG
Fc-only_rev	GCATGCGGCCGCTTCAATTCAGATC
ITR2_for	GGAACCCCTAGTGATGGAGTT
ITR2_rev	CGGCCTCAGTGAGCGA
ITR2_probe	6FAM-CACTCCCTCTCTGCGCGCTCG-TAMRA

2.1.7 Plasmids

Table 7: Plasmids

Name	Description	Source
pGM-CSF	cDNA encoding GM-CSF	O. Ebert, TU München, München
pEX-A-sFlt3L	cDNA encoding human Flt3L; on the 5' and 3' prime ends restrictions sites *BamHI* and *NotI* were included	Eurofins MWG operon
pCR-B7IG	Plasmid containing the B7-1-IgG cassette	S.D. Rabkin, Massachusetts General Hospital, MA, USA
phuFc-endoglin	cDNA of endoglin fused to human IgG1-Fc	G. Braun, Paul-Ehrlich-Institut, Langen
phuFc-B7-1	Plasmid with B7-1-IgG cassette used as template for cloning of VSV vectors	This thesis (3.1.1)
pSecTag2B-Her2/neu pSecTag2B-CTLA-4-Her2/neu	Plasmid encoding Her2/neu or CTLA-4-Her2/neu	W. Wels, Georg-Speyer-Haus, Frankfurt
pVSVΔG(GM-CSF)[a] pVSVΔG(Flt3L)[a] pVSVΔG(B7)[a] pVSVΔG(Her2)[a] pVSVΔG(C-Her2)[a]	G deletion mutant of the VSV genome encoding GM-CSF, Flt3L, B7, Her2, C-Her2	This thesis (3.1.1)
pVSVΔL(GM-CSF)[a] pVSVΔL(Flt3L)[a] pVSVΔL(B7)[a] pVSVΔL(Her2)[a] pVSVΔL(C-Her2)[a]	L deletion mutant of the VSV genome encoding GM-CSF, Flt3L, B7, Her2, C-Her2	This thesis (3.1.1)
pVSVΔL(DsRed)[a]	L deletion mutant of the VSV genome encoding the fluorescent protein DsRed	A. Muik, Georg-Speyer-Haus, Frankfurt (Muik et al, 2012)
pVSV(GP)[a]	VSV-WT genome encoding LCMV-GP instead of VSV-G	A. Muik, Georg-Speyer-Haus, Frankfurt
pBSII-G-ΔL-HDVR	Cloning vector: DsRed is flanked by the G-L intergenic regions and a part of the G-gene of VSV as well as the L-HDV (Hepatitis Delta Virus) ribozyme region	A. Muik, Georg-Speyer-Haus, Frankfurt (Muik et al, 2012)

pBSII-M-ΔG-L	Cloning vector: LCMV-GP is flanked by the M-G intergenic regions and a part of the M gene as well as G-L intergenic region of VSV	A. Muik, Georg-Speyer-Haus, Frankfurt
pBSIIΔL-GM-CSF pBSIIΔL-Flt3L pBSIIΔL-B7 pBSIIΔL-Her2 pBSIIΔL-C-Her2	Cloning vector: transgene (GM-CSF, Flt3L, B7, Her2 or C-Her2) is flanked by the G-L intergenic regions and a part of the G-gene of VSV as well as the L-HDV (Hepatitis Delta Virus) ribozyme region	This thesis (3.1.1)
pBSIIΔG-GM-CSF	Cloning vector: GM-CSF is flanked by the M-G intergenic regions and a part of the M gene as well as G-L intergenic region of VSV	This thesis (3.1.1)
pIRES-N pIRES-P pIRES-L	Helper plasmids required for VSV rescue: based on pBS II (+) plasmids containing ECMV IRES and the VSV viral proteins N, P, L under the control of a T7 promotor	M. J. Schnell, Thomas Jefferson University, PA, USA
pIRES-G	Helper plasmid required for VSVΔG rescue: based on pBS II (+) plasmid containing ECMV IRES and the VSV viral protein G under the control of a T7 promotor	This thesis (3.1.2)
pS-GluRD-IP-W	Bicistronic HIV-1 transfer vector encoding the murine glutamate receptor subunit D and an IRES-driven puromycin resistance gene under control of the SFFV promotor; used as backbone for cloning of pS-mPD1-IP-W and pS-CD28-IP-W	R. Bender, Paul-Ehrlich-Institut, Langen
pmCD28_BamHI_SpeI	cDNA encoding mouse CD28; on the 5' and 3' prime ends restrictions sites *BamHI* and *SpeI* were included	Invitrogen™ GeneArt™
pS-CD28-IP-W	Bicistronic HIV-1 transfer vector encoding mouse CD28 and an IRES-driven puromycin resistance gene under control of the SFFV promotor	This thesis (3.1.3) Cloned by D. Beckmann as part of a supervised student internship

pCG-sa-PD-1 pCG-sa-PD-L1	Expression plasmid encoding αPD-1 (scFv derived from the clone J43) or αPD-L1 (scFv derived from the clone YW243.55.S70) under the control of a CMV promotor	G. Ungerechts, NCT[b], Heidelberg
pXX6-80	Adenoviral helper plasmid encoding the adenoviral genes VA RNA, E2A and E4	H.Büning, ZMMK[c], Cologne
pRC	Encodes the AAV2 rep and cap proteins	H.Büning, ZMMK, Cologne
pRC-VP2$_{KO}$-HSPG$_{mut}$	Encodes the AAV2 rep proteins and capsid proteins VP1and VP3, VP2 start codon is mutated, capsid proteins contain the point mutations R585A and R588A	H.Büning, ZMMK, Cologne
pHer2/neu$^{D9.29}$-HisXa-VP2$_{KO}$	Encodes the His-tagged DARPin-9.29 fused to the N-terminus of the AAV2 VP2 protein (start codon mutated) containing the point mutations R585A and R588A under the control of a CMV promotor	R. Münch, Paul-Ehrlich-Institut, Langen (Münch et al, 2015)
pscαPD-1-SFFV	scAAV transfer vector encoding αPD-1 under the control of the SFFV promotor; BGH polyA	This thesis (3.2.1)
pscαPD-L1-SFFV	scAAV transfer vector encoding αPD-L1 under the control of the SFFV promotor, BGH-polyA	This thesis (3.2.1)
pscIgG-Fc-SFFV	scAAV transfer vector encoding IgG-Fc under the control of the SFFV promotor, BGH-polyA	This thesis (3.2.1)
pscGFP-SFFV_2.0	scAAV transfer vector encoding GFP under the control of the SFFV promotor; BGH-polyA	T. Abel, Paul-Ehrlich-Institut, Langen
pscGFP-SFFV	scAAV transfer vector encoding GFP under the control of the SFFV promotor, SV40-polyA	R. Münch, Paul-Ehrlich-Institut, Langen (Münch et al, 2013)
pscluc-SFFV	scAAV transfer vector encoding luciferase under the control of the SFFV promotor, SV40-polyA	R. Münch, Paul-Ehrlich-Institut, Langen (Münch et al, 2013)
pmPD1_BamHI_SpeI	cDNA encoding mouse PD-1; on the 5' and 3' prime ends restrictions sites *BamHI* and *SpeI* were included	Invitrogen™ GeneArt™

pS-mPD1-IP-W	Bicistronic HIV-1 transfer vector encoding mouse PD-1 and an IRES-driven puromycin resistance gene under control of the SFFV promotor	This thesis (3.2.6)
pMDG-2	Encodes the glycoprotein of VSV	D. Trono, École Polytechnique Fédérale De Lausanne, Switzerland
pCMVΔR8.91	HIV-1 packaging plasmid	U. Blömer, University Hospital Kiel (Zufferey et al, 1998)
pCG1	Empty expression plasmid for mock control	R. Cattaneo, Mayo Clinic, USA

[a]All used pVSV as well as pVSVΔG/pVSVΔL genomes are originally derived from pVSV-XN2 that consists of a pBS SK(+) backbone containing the full-length cDNA genome of VSV, Indiana serotype, under the control of a T7 promotor; [b]NCT: Nationales Centrum für Tumorerkrankungen; [c]ZMMK: Zentrum für Molekulare Medizin

2.1.8 Bacterial & eukaryotic cells

Medium used for the cultivation of bacterial or eukaryotic cells are described in detail in chapter 2.2.2 or 2.4.1, respectively.

Table 8: Bacterial & eukaryotic cells

Name	Description
4T1	Mouse mammary carcinoma cell line; ATCC®, CRL-2539™
B16-F10	Mouse melanoma cell line; ATCC®, CRL-6475™
BHK-21	Baby hamster kidney cells, derived from a Syrian gold hamster; ATCC®, CCL-10™
BHK21-GP	BHK-21 cells genetically engineered to express the glycoprotein of LCMV; provided by G. Zimmer, Institute of Virology and Immunoprophylaxis, Switzerland
E. coli (Top10)	Highly transformable laboratory strain of *Escherichia coli* (Invitrogen)
E0771	Mouse metastatic breast cancer model, provided by M. Mühlebach, Paul-Ehrlich-Institut, Langen
HEK293-NPeGFPL	HEK-293 cells stably expressing VSV-N, -P and -L protein (clone 206); provided by A. Pattnaik, University of Nebraska, Lincoln, USA (Panda et al, 2010)
HEK-293T	Human fetal kidney epithelial cells, transformed to express the adenoviral SV40 T antigen; ATCC®, CRL-11268™
HT1080	Human fibrosarcoma cell line; ATCC®, CCL-121™
HT1080-CD28	Human fibrosarcoma cell line genetically engineered to express mouse CD28; generated in this thesis by D. Beckmann as part of a supervised student internship (3.1.3)

HT1080-PD-1	Human fibrosarcoma cell line genetically engineered to express mouse PD-1; generated in this thesis (3.2.6)
MC38	Mouse colon adenocarcinoma cell line; provided by H. Abken, ZMMK, Cologne
MC38-ek-Her2/neu	MC38 cells stably expressing the ectodomain of human Her2/neu displayed on the transmembrane domain of the platelet-derived growth factor receptor (PDGFR); provided by M. Mühlebach/V. Scheuplein, Paul-Ehrlich-Institut, Langen
Molt 4.8	Human T cell leukemia cell line
Raji	Human B lymphoblast cell line; ATCC®, CCL-86™
RENCA-Her2/neu	Mouse renal carcinoma cells (RENCA cells), stably expressing β-galactosidase and human Her2/neu; provided by W. Wels, Georg-Speyer-Haus, Frankfurt (Maurer-Gebhard et al, 1998)

2.1.9 Viruses

All viruses not listed in Table 9 were generated during this thesis and are described in more detail in the results part.

Table 9: Viruses

Virus	Description	Source
MVA-T7pol	Modified vaccinia virus Ankara (MVA) expressing T7 RNA polymerase; highly attenuated and host range restricted strain (Sutter et al, 1995)	A. Muik, Georg-Speyer-Haus, Frankfurt
rVSV(GFP)	Replication-competent VSV *Indiana* coding for GFP as reporter	A. Muik, Georg-Speyer-Haus, Frankfurt
VSVΔG(GFP)	Propagation-defective VSVΔG vector coding for GFP as reporter instead of VSV-G	G. Zimmer, Institute of Virology and Immunoprophylaxis, Switzerland
VSVΔL(DsRed)	Propagation-defective VSVΔL vector coding for DsRed as reporter instead of VSV-L	A. Muik, Georg-Speyer-Haus, Frankfurt (Muik et al, 2012)

2.2 Molecular biology

2.2.1 Transformation of chemically competent bacteria

For the amplification of plasmid DNA, chemically competent *E. coli* (Top10) was used. Bacteria (100 µl) were thawed on ice and after adding of approximately 50 ng plasmid DNA or 5 µl ligation reaction mix, bacteria were incubated on ice for 30 min.

Subsequently, a heat shock at 42°C for 45 s was performed and bacteria were immediately cooled on ice. After the addition of 100 µl SOC medium (2 % (w/v) tryptone, 0.5 % (w/v) yeast extract, 8.6 mM NaCl, 2.5 mM KCl, 10 mM $MgCl_2$, 20 mM glucose in H_2O, pH 7.0; provided by *Medienküche* Paul-Ehrlich-Institut), bacteria were incubated at 37°C, 600 rpm for 30 – 60 min in a thermomixer (Eppendorf). Bacteria suspension was plated on Luria-Bertani (LB) agar plates containing the corresponding antibiotic (4 % (w/v) LB-Agar, 100 mg/l ampicillin or kanamycin; provided by *Medienküche* Paul-Ehrlich-Institut) and either cultivated overnight at 37°C, overnight at 30°C or for three days at 25°C in a bacteria incubator (Innova 4200, New Brunswick Scientific).

For retransformation of purified plasmid DNA, around 50 ng plasmid DNA were added to thawed *E. coli* (Top10) cells and incubated for 5 min at 37°C in a thermomixer (Eppendorf). Subsequently, bacteria suspension was applied on LB agar plates containing the corresponding antibiotic and either incubated overnight at 37°C, overnight at 30°C or for three days at 25°C in a bacteria incubator (Innova 4200, New Brunswick Scientific).

2.2.2 Plasmid preparation

Preparation of plasmid DNA from transformed and cultured bacteria was performed using GeneJET Plasmid Miniprep Kit (Thermo Fisher Scientific), JETSTAR 2.0 Plasmid Midiprep Kit (Genomed) or JETSTAR 2.0 Plasmid Maxiprep Kit (Genomed) according to the manufacturer's instructions. Accordingly, 5 ml, 50 ml or 250 ml LB medium (1 % (w/v) tryptone, 0.5 % (w/v) yeast extract, 1 % (w/v) NaCl in H_2O, pH 7.0; provided by *Medienküche* Paul-Ehrlich-Institut) supplemented with the corresponding antibiotic (100 mg/l ampicillin or 35 mg/l kanamycin) were inoculated with a single bacteria clone and incubated with constant shaking (180 rpm) either over night at 37°C, overnight at 30°C or for three days at 25°C in a bacteria incubator (Innova 4200, New Brunswick Scientific). Alternatively, NucleBond® Xtra Midi Kit (Macherey-Nagel) was used and bacterial cells were grown in 200 ml LB-Medium supplemented with the appropriate antibiotics. Bacteria were harvested by centrifugation at 4,566 xg for 10 min (Multifuge 3S-R, Heraeus) (Miniprep, Midiprep) or at 6,000 rpm for 15 min (Sorvall® RC 26 plus, Rotor: Sorvall® SLA-1500) (Maxiprep) and the resulting pellet was used for plasmid DNA purification. The extracted DNA was eluted or resuspended in Tris-EDTA buffer (TE-buffer) and concentration of extracted DNA was determined photometrically (NanoDrop™ 2000c, Thermo Fisher Scientifc). Purified plasmid DNA was analyzed by

restriction endonuclease digestion (2.2.3) and subsequent agarose gel electrophoresis (2.2.4).

2.2.3 Restriction of DNA

Analytical and preparative DNA digestions were performed using restriction endonucleases from New England Biolabs according to the manufacturer's instructions. Generally, for analytical DNA digestions 1 µg DNA was mixed with 3-5 U of the corresponding enzyme and incubated under the recommended buffer conditions and temperature (standard 37°C) for around 2-4 h in a thermomixer (Eppendorf). Preparative DNA digestions were performed using 3-5 µg DNA mixed with 10-20 U enzyme as well as with the recommended buffer and incubated for 4-16 h at the recommended temperature in a thermomixer (Eppendorf). Restriction samples were analyzed by agarose gel electrophoresis (2.2.4) and if required, respective DNA fragments were further purified by GeneJET Gel Extraction Kit (Thermo Fisher Scientific).

2.2.4 Agarose gel electrophoresis

Analytical and preparative plasmid DNA digestions were analyzed by agarose gel electrophoresis that separates DNA fragments according to their size. Generally, 1 % (w/v) DNA agarose gels were used for analyses. For the preparation of the agarose gels, the required amount of agarose powder was dissolved in TAE buffer by heating in a microwave prior to casting the solution into a tray for polymerization. For visualization of DNA, either ethidium bromide or Midori Green was used. When using ethidium bromide, 50 µg/ml were added to the liquid agarose gel solution and DNA samples were mixed with 6x DNA loading buffer (New England Biolabs) prior to loading into the gel pockets of the polymerized agarose gel. When using the Midori Green technology, DNA samples were mixed with Midori Green Direct Loading dye (Nippon Genetics) according to the manufacturer's instructions prior to loading into the gel pockets. Electrophoresis was performed at 70-120 V in a Wide Mini-Sub® Cell GT chamber (Bio-Rad) and as reference the 2-log DNA ladder (New England Biolabs) was used. Separated DNA fragments were analyzed under ultraviolet light for ethidium bromide or blue/green LED light for Midori Green in a gel documentation imager (Intas).

If required, gel pieces containing DNA fragments with the desired size were excised from agarose gels and purified using the GeneJET Gel Extraction Kit (Thermo Fisher Scientific) according to manufacturer's instructions.

2.2.5 Dephosphorylation and ligation of DNA

In case linearized backbone DNA with two compatible ends was used for ligation, re-ligation was prevented by dephosphorylation of the 5'-ends using the antarctic phosphatase (New England Biolabs). For this, approximately 300 ng linearized backbone DNA was mixed with 5 U antarctic phosphatase, 3 µl of the corresponding antarctic phosphatase buffer and the reaction mix was filled up to 30 µl with H_2O. The reaction was incubated for 30 min at 37°C followed by 5 min enzyme inactivation at 65°C.

DNA ligation was performed using the Rapid DNA Ligation Kit (Thermo Fisher Scientific) according to the manufacturer's protocol. Briefly, 50 ng of linearized backbone DNA and a three-fold molar excess of insert DNA were mixed with 4 µl rapid ligation buffer, 5 U T4 ligase and with H_2O to a final volume of 20 µl. The ligation sample was mixed, incubated for at least 5 min at 22°C and 5 µl were used for transformation (2.2.1).

2.2.6 Polymerase chain reaction

Polymerase chain reaction (PCR) was used for the specific amplification of DNA sequences using specific oligonucleotide primers (Table 6). When required for cloning, DNA primers additionally contained the desired endonuclease restriction sites. A typical PCR reaction consists of a series of temperature changes allowing the initial denaturation of DNA, the annealing of the primers to the complementary DNA strand and finally the DNA elongation by the DNA polymerase. Annealing temperatures and elongation times were adjusted to the primer pair (Table 6) and the DNA length. Amplification of DNA sequences for cloning was performed using the KOD Hot Start DNA Polymerase (Merck Millipore) according to the manufacturer's instructions. The reaction mix was prepared as followings:

Table 10: Standard reaction set up for PCR

Template DNA	10 ng
10x Buffer for KOD Hot Start DNA polymerase	5 µl
$MgSO_4$	1.5 mM
dNTPs	0.2 mM
Sense (5') Primer	0.3 µM
Antisense (3') Primer	0.3 µM
KOD Hot Start DNA Polymerase	0.02 U/µl
H_2O	Add to 50 µl

The PCR reaction was performed according to the manufacturer's instructions using a PCR thermal cycler (Bio-Rad). The steps 2-4 were repeated 20-40 times:

Table 11: Cycling conditions

Step	Temperature	Time
Polymerase activation	95°C	2 min
Denature	95°C	20 s
Annealing	Lowest Primer T_m[a]	10 s
Extension	70°C	10-25 s/kb[b]

[a] melting temperature of primer

[b] depending on PCR product length (<500 bp: 10 s/kb; 500-1,000 bp: 15 s/kb; 1,000-3,000 bp: 20 s/kb; >3,000 bp: 25 s/kb)

PCR products were analyzed by agarose gel electrophoresis (2.2.4) and purified using the GeneJET Gel Extraction Kit (Thermo Fisher Scientific) according to manufacturer's instructions.

2.2.7 DNA sequencing

Plasmid DNA was either sequenced by Eurofins MWG Operon or GATC Biotech. Samples were prepared according to the guidelines of the company and standard or customized primer sets were used for sequencing. For sequencing by Eurofins MWG Operon about 50-100 ng/µl plasmid DNA diluted in a total volume of 15 µl H_2O were used. For sequencing by GATC Biotech 80-100 ng/µl plasmid DNA were combined with 5 µM primer in a total volume of 10 µl H_2O. Sequencing results were analyzed by the software ContigExpress in the Vector NTI Suite (Invitrogen).

2.2.8 Quantitative polymerase chain reaction

Genomic titers of AAV vector preparations were determined by TaqMan®-based quantitative PCR (qPCR) using ITR-specific primers. The DNA isolation from AAV vector particles as well as the determination of the genomic titers by qPCR were routinely performed by the technical assistant Manuela Gallet.

DNA isolated from AAV vectors were used as template. For this, 10 µl iodixanol density gradient purified vector was mixed with 190 µl PBS. Subsequently, DNA was purified using the DNeasy® Blood and Tissue Kit (Qiagen) according to the manual for the isolation of genomic DNA from cultured cells.

To determine AAV genomic titers, the SensiFAST™ Probe No-ROX Kit (Bioline) was used according to manufacturer's instructions. Briefly, 10 µl template DNA (isolated from AAV)/standard/control, 0.2 µM ITR2_for, 0.68 µM ITR2_rev and 0.2 µM ITR2_probe were mixed with the SensiFAST™ Probe No-ROX mix and the solution was filled up with H_2O to a final volume of 25 µl. A ten-fold serial dilution of the linearized AAV transfer vector plasmid pscGFP-SFFV was used as standard and pure H_20 served as negative control. Eventually, the qPCR was performed on a LightCycler® 480 Real-Time PCR System (Roche) applying the below described cycling conditions:

Table 12: Cycling conditions of qPCR

	Polymerase activation	95°C	15 min	4.4 °C/s
x40 cycles	Denaturation	95°C	15 s	4.4 °C/s
	Annealing and extension	60°C	72 s	2.2 °C/s
	Cooling	40°C	30 s	1.5°C/s

2.3 Protein biochemical methods

2.3.1 Determination of protein concentrations

Concentrations of purified proteins were determined by the Quick Start™ Bradford 1x dye reagent (BioRad) according to the manufacturer's instructions. Briefly, 5 µl of sample or protein standard (Quick Start™ BSA Standard Set, Bio-Rad) were mixed with 250 µl Bradford reagent in a flat bottom microplate well. After incubation for about 5 min at room temperature, the absorbance was measured between 580 – 610 nm on a microplate reader (EMax® Plus, Molecular Devices). The corresponding buffer solution

was used as blank and the protein concentrations of the unknown samples were calculated with the help of a standard curve.

Protein concentrations of organ lysates were determined using the Pierce BCA Protein Assay Kit (Thermo Fisher Scientific) according to the manufacturer's instructions. Accordingly, 25 µl of sample or protein standard (Quick Start™ BSA Standard Set, Bio-Rad) were pipetted into a flat bottom microplate well and mixed with 200 µl BCA working reagent (50:1 of A:B). The plate was covered with foil and incubated at 37°C for 30 min. After the samples were cooled down to room temperature, the absorbance was measured between 540 – 590 nm on a microplate reader (EMax® Plus, Molecular Devices). The corresponding buffer solution was used as blank and the protein concentrations of the unknown samples were calculated with the help of a standard curve.

2.3.2 SDS-polyacrylamide gel electrophoresis

The sodium dodecyl sulfate-polyacrylamide gel electrophoresis (SDS-PAGE) allows the separation of proteins according to their molecular weight. Purified proteins or cell culture supernatants of infected or transduced cells were mixed with the appropriate amount of SDS-loading dye (4x) and boiled at 95°C for 10 min in a thermoblock (FALC). Depending on the molecular weight of the analyzed proteins, samples were either loaded on 10 % (separation of large proteins) or on 12 % (separation of smaller proteins) SDS polyacrylamide gels (Table 13).

Table 13: Composition of resolving and stacking gel.

	Resolving Gel		**Stacking Gel**
	10 %	**12 %**	**5 %**
30% acrylamide solution (Rotiphorese® Gel 30)	2.5 ml	3 ml	0.83 ml
1 M Tris, pH 8.8	2.93 ml	2.93 ml	-
1 M Tris, pH 6.8	-	-	0.63 ml
50 % glycerine	0.65 ml	0.65 ml	
10 % SDS	85 µl	85 µl	50 µl
H_2O	1.34 ml	0.83 ml	3.5 ml
TEMED	6.25 µl	6.25 µl	6.25 µl
20 % APS	20 µl	20 µl	20 µl

The PageRuler™ Plus Prestained Protein Ladder (Thermo Fisher Scientific) served as protein standard. Samples were separated using Mini-Protean® 3 cell chamber (Bio-

Rad) filled with SDS running buffer. Separation was carried out at 70 V until samples entered the resolving gel and thereafter at 120 V until the desired protein separation was achieved. Afterwards SDS polyacrylamide gels were either subjected to Coomassie staining (2.3.3) or Western blot analysis (2.3.4).

2.3.3 Coomassie staining of SDS-PAGE

After SDS-PAGE, proteins in the gels were visualized by the PageBlue™ Protein Staining Solution (Thermo Fisher Scientific). For this purpose, the SDS polyacrylamide gel was first washed for 10 min with 10 % acetic acid for fixation. Then, the gels were washed twice with H_2O for 10 min and stained with the PageBlue™ Protein Staining Solution (Thermo Fisher Scientific) for at least 2 h at room temperature while shaking. Finally, the gels were destained by several wash steps with H_2O until the protein bands became visible.

2.3.4 Western blot analysis

After separation by SDS-PAGE, proteins were transferred to a nitrocellulose membrane and analyzed by immunostaining. Whatman filter papers (GE Healthcare), the nitrocellulose membrane (Amersham Protran 0.2 µm nitrocelluose blotting membrane, GE Healthcare) and the SDS polyacrylamide gel were soaked in transfer buffer and layered into the Trans-Blot® SD semi-dry transfer cell (Bio-Rad). Generally, proteins were blotted to the membrane using 180 mA at max. 20 V for 60 – 90 min for one gel. After blotting, the membrane was blocked with an appropriate blocking buffer (Table 14) on an orbital shaker for at least 1 h at room temperature. Thereafter, membranes were incubated with primary antibody diluted in blocking buffer (Table 14) over night at 4°C at constant shaking. Then, the membranes were washed five times with TBS-T. If the primary antibody was not labeled with the horseradish peroxidase (HRP), membranes were incubated with the respective secondary antibody conjugated to HRP on an orbital shaker for at least 1 h at room temperature and thereafter, were again washed five times with TBS-T. Proteins were detected with Pierce™ ECL Plus Western blotting substrate (Thermo Fisher Scientific) according to manufacturer's instructions and luminescence was detected using Super RX x-ray films (Fujifilm) and a x-ray film developer (Curix 60, AGFA).

Table 14: Antibodies and corresponding blocking buffer used for Western blot analysis.

	Antibody		Dilution	Blocking puffer
primary antibodies	α-Myc-tag (Myc.A7)	mouse	1:1,000	5 % (v/v) horse serum in TBS-T
	α-human IgG, HRP-conjugated	goat	1:10,000	2 % (w/v) milk powder in TBS-T
	α-human Flt3L	rabbit	1:500	5 % (w/v) milk powder in TBS-T
	α-murine GM-CSF	rabbit	1:500	5 % (w/v) milk powder in TBS-T
	α-HA-tag (16B12)	mouse	1:1,000	5 % (v/v) horse serum in TBS-T
secondary antibodies	α-rabbit, HRP-conjugated	goat	1:2,000	Same blocking buffer as used for the primary antibody
	α-mouse, HRP-conjugated	rabbit	1:2,000	Same blocking buffer as used for the primary antibody

2.3.5 Enzyme-linked immunosorbent assay

Enzyme-linked immunosorbent assays (ELISA) were used for the quantification of GM-CSF and Flt3L in cell culture supernatants of srVSV-infected cells, for the quantification of intact AAV capsids in vector preparations and for the quantification of immune checkpoint inhibitors in the cell culture supernatants of AAV-transduced cells as well as in organ lysates.

For quantification of GM-CSF in cell culture supernatants, the Mouse GM-CSF Elisa Kit (Thermo Fisher Scientific) and for the quantification of Flt3L in cell culture supernatant the Flt3 Ligand Human ELISA Kit (abcam) were used according to the manufacturer's instructions. Cell culture supernatants of cells infected with srVSV(GFP/DsRed) were used as blank.

For quantification of intact AAV capsids, the AAV2 Titration ELISA (Progen) was used according to the manufacturer's instructions. The dilution buffer was used as blank.

2.3.5.1 Immune checkpoint inhibitor ELISA: Approach 1

Adapted according to Engeland *et al*. (Engeland et al, 2014). 96-well immunoplates (Nunc MaxiSorp™, Thermo Fisher Scientific) were coated with 200 ng recombinant PD-1 or PD-L1 (Life Technologies) in a total volume of 100 µl PBS for 2 h at room temperature. Thereafter, the plates were washed twice with 200 µl PBS and then, blocked with 200 µl ELISA blocking buffer for 2-3 h at room temperature. After incubation, plates were washed three times with 200 µl PBS. Sample dilutions were prepared using PBS as diluent and 100 µl of each sample were added per well. The

plates were covered with foil and incubated overnight at 4°C. On the next day, the plates were washed five times with 300 µl ELISA washing buffer and subsequently, were incubated with 100 µl of biotin-conjugated anti-HA-tag antibody (clone 3F10; Roche) diluted 1:500 in ELISA blocking buffer. The plates were incubated for 1 h at room temperature. After the plates were washed five times with 300 µl ELISA washing buffer, 100 µl HRP-streptavidin (Jackson Immuno Research, Dianova) diluted 1:500 in blocking buffer were added per well and incubated for 1 h at room temperature. During all incubation steps by now, the plates were slowly shaken on an orbital shaker. Finally, plates were washed again five times with 300 µl ELISA washing buffer and 100 µl 1-Step™ Ultra TMB substrate (Thermo Fisher Scientific) were added. After 20 min of incubation, the reaction was stopped by adding 100 µl 1 N H_2SO_4 and absorbance was measured at 450 nm within 30 min using a microplate reader (EMax® Plus, Molecular Devices).

2.3.5.2 Immune checkpoint inhibitor ELISA: Approach 2

96-well immunoplates (Nunc MaxiSorp™, Thermo Fisher Scientific) were coated with 250 ng α-HA-tag antibody (clone 16B12; abcam) in a total volume of 50 µl PBS for 2-3 h at room temperature. Thereafter, the plates were washed twice with 200 µl PBS and then, blocked with 200 µl ELISA blocking buffer for 2-3 h at room temperature. After incubation, plates were washed three times with 200 µl PBS. Unless otherwise stated, serial sample dilutions were prepared using PBS as diluent and 100 µl sample was applied per well. The plates were covered with foil and incubated overnight at 4°C. On the next day, plates were washed five times with 300 µl ELISA washing buffer and 100 µl of α-human-IgG conjugated with HRP (Sigma-Aldrich) diluted 1:10,000 in ELISA blocking buffer were added per well. After 3 h of incubation, the plates were again washed five times with 300 µl ELISA washing buffer. During all aforementioned incubation steps, plates were slowly shaken on an orbital shaker. Finally, 100 µl 1-Step™ Ultra TMB substrate (Thermo Fisher Scientific) were added per well and reactions were stopped with 100 µl 1 N H_2SO_4 after the desired color had been developed. Within 30 min absorbance was measured at 450 nm using a microplate reader (EMax® Plus, Molecular Devices).

The respective blank was subtracted prior quantification. For the mice samples the organ lysates of PBS-treated mice were used as blank. Protein concentrations were calculated using αPD-1 and αPD-L1 protein standards (2.4.4, 2.3.6).

2.3.6 Protein affinity tag purification from cell culture supernatant

Recombinant αPD-1 and αPD-L1 were purified out of cell culture supernatants of transfected HEK-293T cells by Protein A affinity purification. For this purpose, 20 ml sterile-filtered cell culture supernatant (2.4.4) were mixed with 10 µl Protein A beads (rec-Protein A-Sepharose® 4B Conjugate, Invitrogen) and the solution was incubated overnight at 4°C on a roller bottle shaker. After equilibration of an empty gravity-flow Econo-Pac® chromatography column (Bio-Rad) with 10 column volumes (CV) of PBS, protein-bound Protein A beads were loaded and washed with 20 CV of PBS. Proteins were eluted by incubation of the beads with 5 ml acidic elution buffer (pH 2.7) and the protein was collected in 1 ml fractions. The acidic pH was neutralized by elution into 500 µl (1/10 of elution volume) collection puffer. Protein A beads were regenerated by adding 10 CV of PBS and stored in storage buffer at 4°C. All purification steps were performed at 4°C and with ice cold buffer.
Purified proteins were concentrated via Amicon® Ultra centrifugal filter devices (Merck Millipore). Amicons were equilibrated with 0.1 % Pluronic® in PBS, the elution fractions of the Protein A purification were supplemented with Pluronic® to a final concentration of 0.001 % (v/v) and were concentrated with 4,000 xg at 4°C (Multifuge 3S-R, Heraeus). Then, the concentrated protein solution was washed several times with PBS to exchange the buffer. For long-term storage at -80°C, protein solution was supplemented with protease inhibitor cocktail (Roche) and 5 % (v/v) glycerol. The protein concentration was determined via Bradford Assay (2.3.1).

2.4 Cell culture and virological methods

2.4.1 Cultivation of eukaryotic cell lines

Cells were cultured in the appropriate culture medium in a cell culture incubator at 37°C, 5 % CO_2 and 90 % humidity (Hereaus BBD 6220, Thermo Fisher Scientific). HEK-293T, BHK-21, MC38, B16-F10, E0771 and HT1080 cells were cultivated in Dulbecco's Modified Eagles Medium (DMEM) supplemented with 10 % fetal calf serum (FCS) and 2 mM L-glutamine (thereafter abbreviated with $DMEM^{complete}$). HEK-293NPeGFPL cells were grown in $DMEM^{complete}$ supplemented with 2 mg/ml Geneticin® and MC38-ek-Her2/neu cells were grown in $DMEM^{complete}$ supplemented with 0.75 mg/ml Geneticin®. BHK21-GP, HT1080-CD28 and HT1080-PD-1 cells were cultivated in $DMEM^{complete}$ supplemented with 10 µg/ml puromycin. Raji, Molt 4.8 and 4T1 cells were cultivated in

Roswell Park Memorial Institute (RPMI) 1640 medium supplemented with 10 % FCS and 2 mM L-glutamine (abbreviated with RPMI^{complete}). RENCA-Her2/neu cells were grown in RPMI^{complete} either supplemented with 0.48 mg/ml Geneticin® or with 0.48 mg/ml Geneticin® and 0.25 mg/ml Zeocin.
Cells were passaged twice a week under sterile conditions using a laminar flow cabinet (SterilGARD® III Advance, The Baker Company). For this, the medium was aspirated from adherent cells, cells were washed with PBS and then detached with 0.25 % trypsin solution (PBS/1 mM EDTA). Fresh medium was added, cells were resuspended and an appropriate fraction of detached cells were seeded into a new cell culture flask with fresh medium. Suspension cells were passaged by resuspending the cells and then an appropriate fraction of cells were directly transferred into a new cell culture flask with fresh medium. Morphology and growth characteristics of the cells were monitored by microscopy (Axiovert™ 25, Carl Zeiss). Furthermore, cell lines were checked for mycoplasma contamination by PCR on a regular basis.

2.4.2 Freezing and thawing of cells

After the cells were detached and resuspended in an appropriate amount of medium (2.4.1), they were pelleted at 140 xg for 4 min at 4°C (Heraeus™ Multifuge™ X3R, Thermo Fisher Scientific). The pellet was resuspended in ice cold freezing medium, aliquoted into cryotubes and frozen at -80°C using a Mr.Frosty™ Freezing Container (Nalgene). On the next day, cells were transferred to the gas phase of a liquid nitrogen tank and stored at -155°C.
Frozen cells were thawed in a water bath at 37°C. Immediately, thawed cells were transferred into pre-warmed medium in a new cell culture flask. On the next day, cell culture medium was exchanged.

2.4.3 Transfection of BHK-21 cells

For transfection, 1x10^6 BHK-21 cells were seeded in DMEM^{complete} culture medium per well of a 6-well plate. On the next day, cells were transfected using Lipofectamine™ LTX Reagent with PLUS™ Reagent (Invitrogen). For this, 5 µg DNA (pSecTag2B-Her2/neu, pSecTag2B-CTLA-4-Her2/neu, phuFc-B7-1 or pCG1) were combined with 250 µl OptiMEM® and 5 µl PLUS™ reagent. Furthermore, 10 µl Lipofectamine™ LTX Reagent were combined with 250 µl OptiMEM®. Both solutions were mixed by inverting the tubes and incubated for 5 min at room temperature. Subsequently, solutions were

combined and mixed again by inverting the tube. The transfection mix was incubated for 20 min at room temperature. During the incubation step, cells were washed three times with PBS. After incubation, the transfection mix was added to the cells and incubated for 5 min at 37°C. Then, 1.5 ml DMEM^{complete} was added. On the next day, cells were washed three times with PBS and 2 ml serum-free VP-SFM medium was added. VP-SFM was used instead of DMEM^{complete} medium to avoid the detection of 'FCS clouds' in the Western blot analysis. Two days after transfection, cell culture supernatants were harvested, filtrated through a 0.45 µm pore size filter (Minisart® Syringe Filters, Sartorius) and stored at -80°C until needed for analysis.

2.4.4 Production of recombinant αPD-1 and αPD-L1

For the production of recombinant αPD-1 and αPD-L1, both proteins were transiently expressed in HEK-293T cells. For transfection, 1.8x10^7 HEK-293T cells were seeded in a T175 cell culture flask. On the next day, the cell culture medium was exchanged with 12 ml DMEM supplemented with 15 % FCS and 2 mM L-glutamine. Then, 35 µg DNA (pCG-sa-PD-1 or pCG-sa-PD-L1) and 140 µl PEI were each diluted with 2.3 ml DMEM without additives (DMEM$^{w/o}$) and vortexed. Both solutions were combined, vortexed thoroughly and incubated for 20 min at room temperature. After incubation, the PEI/DNA mix was added to the cells and about 5 to 7 h later, the medium was replaced with DMEM supplemented with 5 % Panexin and 2 mM L-glutamine medium. In the following three days after transfection, cell culture supernatants were collected. For this, cell culture supernatants were harvested, filtrated through a 0.45 µm pore size filter (Minisart® Syringe Filters, Sartorius) and supplemented with sodium acid to a final concentration of 0.01 % (v/v). Supernatants were stored at 4°C until used for protein affinity tag purification (2.3.6).

2.4.5 VSV rescue

A reverse genetic system was used for the *de novo* generation of VSV vectors from cDNA (Whelan et al, 1995; Lawson et al, 1995). On the day prior to transfection, 1x10^6 BHK-21 cells were seeded per well of a 6-well plate. Then, the cells were washed with PBS, infected with MVA-T7pol at a multiplicity of infection (MOI) of about 0.5 in 200 µl DMEM^{complete} for 1 h at room temperature and every 10 min plate was mildly rocked. Meanwhile, the transfection mix was prepared as follows:

Table 15: Transfection mix for VSV rescue

	Rescue of VSVΔG	**Rescue of VSVΔL**
OptiMEM®	100 µl	100 µl
pVSVΔG or pVSVΔL to be rescued	2 µg	2 µg
pIRES-N	1 µg	1 µg
pIRES-P	0.8 µg	0.8 µg
pIRES-L	0.4 µg	0.4 µg
pIRES-G	0.25 µg	-
FuGENE® HD	18 µl	18 µl

Plasmid amounts and transfection reagents were calculated for the transfection of one well of a 6-well plate (culture area 9.6 cm^2)

The transfection mix was mixed gently by inverting the tube several times and incubated for 20 min at room temperature. The MVA-T7pol inoculum was removed from the cells, the cells were washed with PBS and 2 ml DMEM supplemented with 5 % FCS and 2 mM L-glutamine were added per well. Subsequently, the transfection mix was added drop-wise and the cells were incubated at 37°C in a cell culture incubator. Three days after transfection, the supernatant was collected and filtered through 0.2 µm pore size filter (Minisart® Syringe Filters, Sartorius) to remove MVA-T7pol virions as well as cell debris. Subsequently, the supernatant was added to BHK21-GP cells ($1x10^6$ cells/well of a 6-well plate) for the rescue of VSVΔG vectors or to HEK-293NPeGFPL cells ($2x10^6$ cells/well of a 6-well plate) for the rescue of VSVΔL vectors. After three days, cells were inspected for cytopathic effects, the supernatants of wells exhibiting cytopathic-effect-positive cells were filtered through 0.2 µm pore size filters (Minisart® Syringe Filters, Sartorius) and subsequently stored at -80°C until plaque purification.

2.4.6 Plaque purification of VSV and preparation of virus stocks

After successful VSV rescue, a clonal vector population was generated by plaque purification. Additionally, any possible remaining MVA-T7pol contaminations were removed by this purification step. For the plaque purification of VSVΔG vectors, BHK21-GP cells and for the plaque purification of VSVΔL vectors, HEK-293NPeGFPL cells were used. Cells were seeded either in 6-well or 12-well plates with a cell number leading to confluent cell monolayers on the day of infection (generally one day prior to infection: $3x10^5$ BHK21-GP cells/well of a 6-well plate; $8x10^5$–$1.5x10^6$ HEK-293NPeGFPL cells/well of a 12-well plate). Cells were infected with different dilutions of rescued VSV vectors and incubated for 1 h at 37°C. Meanwhile, 1.8 % plaque agarose was melt and combined 1:1 with pre-warmed $DMEM^{complete}$ medium. After incubation, the inoculum

was removed and the cells were washed with pure DMEM^{complete} medium or PBS. The melted DMEM/plaque agarose mixture was added carefully to the cells (1 ml/well for 12-well plate; 2 ml/well for 6-well plate) and allowed to gel. After an incubation time of one to two days at 37°C, single plaques were microscopically visible. Eventually, a single plaque was isolated with a pipette tip and used to inoculate fresh BHK21-GP or HEK-293NPeGFPL cells seeded in a 6-well plate. Infected cells were incubated for one up to two days at 37°C until cytopathic effects were fully visible. Then, cell culture supernatants were harvested, filtrated through a 0.45 µm pore size filter (Minisart® Syringe Filters, Sartorius), aliquoted and stored at -80°C.

Plaque-purified VSV vectors were titrated (2.4.7) and used for the large-scale production of 'P2' VSV vector stocks. Generally, for amplification of VSVΔG vectors 6x10^6 BHK21-GP cells and for amplification of VSVΔL vectors 1.5x10^7 HEK-293NPeGFPL cells were seeded in a T75 cell culture flask one day prior to infection. Cells were infected with a low MOI ranging between 0.01 and 0.03 in 8 ml DMEM^{complete} medium and were incubated for one up to two days at 37°C until cytopathic effects were visible. Eventually, cell culture supernatants were filtrated through 0.45 µm pore size filter (Minisart® Syringe Filters, Sartorius), aliquoted and stored at -80°C. After the $TCID_{50}$ of the VSV stocks were determined, they were subjected to co-plaque purification.

In order to generate srVSV vector preparations that are composed of VSVΔL and VSVΔG vectors a co-plaque purification was performed. For this, 1.5x10^5 BHK-21 or 4x10^5 BHK-21 cells were seeded in a well of a 12-well plate or a 6-well plate, respectively. The next day, cells were co-infected with serial dilutions of VSVΔG and VSVΔL vectors (generally MOI ranged between 0.0001 and 0.1). Cells were overlaid with plaque agarose and a single clone was picked as described before for the plaque purification of VSV vectors. Eventually, a single clone was isolated and amplified on fresh BHK-21 cells seeded in a 6-well plate. Cells were incubated for at least one day at 37°C until cytopathic effects were microscopically visible. Subsequently, cell culture supernatants were collected, filtrated through 0.45 µm pore size filters (Minisart® Syringe Filters, Sartorius), aliquoted and stored at -80°C.

Plaque-purified srVSV preparations were titrated (2.4.7) and used for the large-scale production of 'P2' vector stocks. Generally, 6x10^6 cells were seeded in a T75 cell culture flask one day prior to infection and were infected with plaque-purified srVSV at a low MOI ranging between 0.01 and 0.03 in 8 ml DMEM^{complete}. When cytopathic effects were visible, generally on the next day, cell culture supernatants were collected, filtrated through 0.45 µm pore size filter (Minisart® Syringe Filters, Sartorius), aliquoted and

stored at -80°C. Generated srVSV stocks were subjected to virus titer determination (2.4.7).

2.4.7 Determination of the 50 % tissue culture infective dose

Viral titers of VSV vectors and of srVSV preparations were determined using the 50 % tissue culture infective dose ($TCID_{50}$) method according to Kärber (Kärber, 1931). For titration of VSVΔG vectors, $5x10^3$ BHK21-GP cells, of VSVΔL vectors $1x10^4$ HEK-293NPeGFPL cells and of srVSV $5x10^3$ BHK-21 cells were seeded per well of a 96-well plate. On the next day, a 10-fold serial dilution of the respective vector stock was prepared using $DMEM^{complete}$ medium as diluent. Dilutions used for titration ranged between 10^{-2}–10^{-9}. Finally, 20 µl of each dilution was added to the cells in eight replicates. After three days of incubation at 37°C, the titration was analyzed by microscopy. Infection was detected by cytopathic effects or expression of marker proteins such as GFP or DsRed. Finally, the titer was calculated according to following equation:

$$TCID_{50}/ml = x * 10^{-(log_{10}A-(B-0.5))}$$

x: extrapolation factor arising from the volume of virus dilution used per well
A: value of the last dilution step where all eight wells showed cytopathic effects
B: summation of the proportion of positive wells including both the last 100 % up to the first 0 % infectious dilution

2.4.8 Infection

For infection, 10^6 cells were seeded per well of a 6-well plate and generally cells were infected with virus at a MOI of 0.1. On the next day, cell culture supernatant was harvested, filtrated through 0.45 µm pore size filters (Minisart® Syringe Filters, Sartorius) and stored at 4°C or -80°C until used for ELISA (2.3.5), Western blot (2.3.4) or flow cytometry analysis (2.4.13). If required, medium was replaced with serum free VP-SFM medium in order to prevent the detection of 'FCS clouds' in the Western blot analysis.
Expression of the marker proteins DsRed and GFP was analyzed by microcopy using the fluorescence microscope Axiovert200 (Carl Zeiss). Pictures were taken with the fluorescence microscope Axiovert200, the AxioCam HRc (Carl Zeiss) and the software AxioVision 4.8 (Carl Zeiss).

2.4.9 Cell viability assay

Cell viability was analyzed using the WST-1 cell proliferation assay kit (Takara Clontech). Mouse cancer cell lines ($4x10^3$ cells/well) were seeded into 96-well plates and stimulated with different concentrations of mouse IFNα for 24 h. Two days after infection, cell viability was analyzed by WST-1 assay. For this, 10 µl WST-1 substrate was added per well and incubated for 4 h at 37°C. Eventually, absorption was measured between 420-480 nm using a multiplate reader. Pure medium served as blank and cell viability was normalized to uninfected control cells that were stimulated with the same IFNα concentrations. The type I IFN sensitivity assay was adapted according to Liu *et al.* (Liu et al, 2013).

2.4.10 AAV vector production and concentration

AAV vectors were generated by an adenovirus-helper free, four plasmid transfection system using PEI as transfection reagent (Xiao et al, 1998; Münch et al, 2013). The AAV transfer vector plasmid (pscGFP-SFFV, pscluc-SFFV, pscαPD-1-SFFV, pscαPD-L1-SFFV or pscIgG-Fc-SFFV), pRC and pXX6-80 were co-transfected into HEK-293T cells in a ratio of 1:1:3 for the production of AAV2 vectors. For the production of Her2-AAV vectors, the AAV transfer vector plasmid, pRC-$VP2_{KO}$-$HSPG_{mut,}$ pHer2/$neu^{D9.29}$-HisXa-$VP2_{KO}$ and pXX6-80 were co-transfected in a ratio of 1:1:1:3 into HEK-293T cells.
One day prior to transfection, $1.8\text{-}2x10^7$ HEK-293T cells were seeded in a 15 cm cell culture dish. On the next day, medium was replaced with 14 ml DMEM supplemented with 15 % FCS and 2 mM L-glutamine. Subsequently, the transfection mix was prepared as follows:

Table 16: Transfection mix for AAV production

	AAV2	Her2-AAV
$DMEM^{w/o}$	1,958.4 µl	1,958.4 µl
AAV transfer vector	5.91 µg	4.93 µg
pXX6-80	17.74 µg	14.78 µg
pRC	5.91 µg	-
pRC-$VP2_{KO}$-$HSPG_{mut}$	-	4.93 µg
pHer2/$neu^{D9.29}$-HisXa-$VP2_{KO}$	-	4.93 µg

Plasmid amounts are calculated for the transfection of one 15 cm cell culture dish (culture area 148 cm^2)

Additionally, 118 µl PEI solution was mixed with 1,958.4 µl $DMEM^{w/o}$. Each solution was mixed shortly by vortexing. Subsequently, both solutions were combined and again vortexed thoroughly. After an incubation of 20 min at room temperature, the

transfection mix was added to the cells. On the next morning, the medium was exchanged with fresh DMEM^{complete} medium.

Two days after transfection, cells were scraped off the cell culture dish and pelleted for 7 min at 218 xg, 4°C (Multifuge™ 3-S-R, Hereaus). The supernatant was discarded and the pellet was resuspended in 500 µl AAV lysis buffer per 15 cm cell culture dish. Subsequently, the lysate was subjected to three freeze/thaw cycles in liquid nitrogen and a 37°C water bath. After benzonase digestion (50 U/ml) for 30 min at 37°C (rocking every 10 min), cell debris were pelleted for 20 min at 3,700 xg and 4°C (Multifuge™ 3-S-R, Hereaus). Vector particle containing supernatant was diluted in PBS M/K and transferred to Quick-Seal® Ultra-Clear™ ultracentrifugation tubes (1x3½ in.) (Beckman Coulter). For purification by density gradient centrifugation, the supernatant was under layered with 9 ml 15 %, 6 ml 25 %, 5 ml 40 % and up to 7.5 ml 60 % iodixanol solution (Table 17).

Table 17: Composition of iodixanol solutions

	15% iodixanol	**25% iodixanol**	**40% iodixanol**	**60% iodixanol**
PBS (10x)	1 ml	0.8 ml	0.8 ml	-
$MgCl_2$ (1 M)	10 µl	8 µl	8 µl	8 µl
KCl (1 M)	25 µl	20 µl	20 µl	20 µl
NaCl (5 M)	2 ml	-	-	-
Phenolred (0.5%)	15 µl	12 µl	-	12 µl
H_2O	4.45 ml	3.8 ml	1.8 ml	-
OptiPrep™ (60%)	2.5 ml	3.3 ml	5.33 ml	8 ml

The gradient was centrifuged for 2 h in a 70 Ti rotor (Beckman-Coulter) at 63,000 rpm and 4°C (Optima™L-70k, Beckman Coulter) and AAV vector particles were recovered from the 40 % iodixanol fraction, aliquoted and stored at -80°C.

2.4.11 Transduction

In order to analyze AAV-mediated transgene expression, $8x10^3$ or $8\text{-}9x10^4$ RENCA-Her2/neu cells were seeded per well of a 96-well plate or of a 12-well plate, respectively. On the next day, cells were transduced with AAV2 or Her2-AAV at genome containing particles per cell (GOI) ranging between 450,000 and 500,000. The next day, the medium was exchanged with fresh RPMI^{complete} medium. For Western blot analysis, cells were washed three times with PBS and serum-free VP-SFM medium instead of RPMI^{complete} medium was added to the cells in order to avoid the detection of 'FCS clouds'. Four days after transduction, cell culture supernatants were harvested and

centrifuged to remove cell debris. Cleared supernatants were stored either at 4°C or -80°C until used for Western blot (2.3.4), ELISA (2.3.5.1; 2.3.5.2) or flow cytometry analysis (2.4.13).

2.4.12 Generation of stably transgenic cell lines

Cell lines stably expressing a transgene were generated by transduction with lentiviral vectors (LV) encoding the transgene and an IRES-driven puromycin resistance gene.
LVs pseudotyped with the VSV glycoprotein were generated in a 6-well scale format. For this, $1.8x10^6$ HEK-293T cells were seeded per well of a 6-well plate and on the following day were transfected with PEI as transfection reagent. For this, 3.4 µg pMDG-2, 6.3 µg pCMVΔR8.91 and 0.96 µg LV transfer vector plasmid (pS-CD28-IP-W; pS-mPD1-IP-W) were combined with 130 µl $DMEM^{w/o}$. Additionally, 8 µl PEI solution was combined with 120 µl $DMEM^{w/o}$. Each solution was mixed by vortexing. Then, both solutions were combined, mixed again by vortexing and incubated for 20 min at room temperature. Meanwhile, medium of the cells were replaced with 1 ml DMEM supplemented with 15 % FCS and 2 mM L-glutamine. After incubation, the transfection mix was added to the cells. On the next morning, medium was replaced with 2 ml fresh $DMEM^{complete}$. Two days after transfection, vector particle containing supernatant was collected, filtrated through 0.45 µm pore size filter (Minisart® Syringe Filters, Sartorius) and used for the transduction of HT1080 cells. For this, $5\text{-}6x10^4$ HT1080 cells were seeded per well of a 12-well plate and transduced with different volumes of LV containing supernatant (25 µl up to 500 µl). Three days after transduction, transduced cells were selected by the addition of puromycin (10 µg/ml) and cultures were expanded to establish a stably transgenic cell line.

2.4.13 Flow cytometry

Flow cytometry analyses were used to examine cell surface expression of proteins and to investigate specific binding of srVSV- or AAV-encoded transgenes.
To investigate cell surface expression of stably transgenic cell lines, adherent cells were detached (2.4.1), resuspended and subjected to antibody staining. For this, $5x10^4$–$1x10^5$ cells per sample were washed twice with 500 µl FACS washing buffer (314 xg, 4 min, 4°C) (Hereaus™ Multifuge™ X3R, Thermo Fisher Scientific) and stained with fluorophore-labelled primary antibody (Table 5). Subsequently, cells were washed again twice and fixed with 200 µl FACS fix.

To investigate binding of srVSV- or AAV-encoded proteins to their target, $5x10^4$–$1x10^5$ cells were washed twice as described above and were then incubated with 400–600 µl cell culture supernatant or with 4-5 µg recombinant protein for 30-60 min at 4°C. Subsequently, cells were pelleted, the supernatant was discarded and cells were washed twice as described above. Then, binding was detected with an appropriate fluorophore-labelled secondary antibody. Eventually, cells were washed again twice and were finally fixed with 200 µl FACS fix.

For flow cytometry analyses of mouse splenocytes, $3x10^5$ stimulated cells (2.5.5) were subjected to the analysis. After washing the cells twice with 500 µl PBS (314 xg, 5 min, 4°C) (Hereaus™ Multifuge™ X3R, Thermo Fisher Scientific), a live/dead staining using eBioscience™ Fixable Viability Dye eFluor™ 450 (Thermo Fisher Scientific) according to the manufacturer's instructions was performed in order to exclude dead cells from the analysis. Prior to antibody staining, FcR blocking reagent was added to the cell suspensions and incubated for 10 min at 4°C. Eventually, cell surface staining or binding assay was performed as described above.

Flow cytometry measurements were performed using MACSQuant® analyzer 10 (Miltenyi Biotec) and data were analyzed with FCS Express™ software (DeNovo Software™).

2.4.14 ELISpot

Tumor-specific immune cells isolated from spleens of cured mice 14 days after tumor re-challenge were analyzed by enzyme-linked immune spot assay (ELISpot) using the Mouse IFN gamma ELISPOT Ready-Set-Go!®-Kit (eBioscience). First, 96-well MultiScreen® filter plates with hydrophobic high protein binding immobilon®-P PVDF membrane (MultiScreen®-IP, Merck Millipore) were activated with 50 µl 70 % ethanol per well. After adding 200 µl H_2O per well, the fluid was discarded and the plate was washed again twice with 200 µl H_2O followed by a single washing step with 200 µl PBS. Further assay procedures were performed according to the manufacturer's instructions. Following splenocyte isolation (2.5.5), $5x10^5$ splenocytes were resuspended in 100 µl RPMI supplemented with 10 % FCS, 2 mM L-glutamine and 1 % PenStrep ($RPMI^{+PenStrep}$) and added per well of a 96-well round bottom plate. Then, splenocytes were mixed with 100 µl stimulants or controls that were also diluted in $RPMI^{+PenStrep}$ medium. Cells were either stimulated with γ-irradiated (60 Gy) MC38 tumor cells (two cell counts tested: $5x10^4$ and $1x10^5$) or with MC38 tumor cell lysates (two cell counts tested: $8x10^4$ or $2.5x10^5$). For the preparation of the MC38 tumor cell lysates, MC38 cells were detached

with PBS supplemented with 1 mM EDTA, resuspended in RPMI$^{+PenStrep}$ medium and lysed via five freeze/thaw cycles using liquid nitrogen and a 55°C water bath. Cell debris were pelleted and supernatant was used for ELISpot assay. Stimulation of splenocytes with 10 µg/ml ConA served as positive control and plain medium as negative control. The mixtures of stimulants and splenocytes were transferred to the blocked MultiScreen®-IP filter plates and incubated for 36 h in a cell culture incubator at 37°C, 5 % CO_2 and 90 % humidity. IFNγ-secreting cells were detected according to manufacturer's instructions and the counts were documented with an ELISpot Reader (Eli.Scan; software ELI. Analyse; A.EL.VIS).

2.5 Experimental mouse work

2.5.1 Injection of tumor cells

Tumor cell lines were cultured and detached as described in 2.4.1. Then, cells were pooled, pelleted at 314 xg, 4°C for 5 min (Hereaus™ Multifuge™ X3R, Thermo Fisher Scientific) and washed with PBS. Cells were counted and resuspended in the desired amount of PBS. Mice were anesthetized with 2-3 % isoflurane using an anesthetic machine with an isoflurane vaporizer and an oxygen concentrator (indulab-vet). Prior to tumor implantation, aliquoted cell suspensions were briefly vortexed and 100 µl tumor cell suspension was subcutaneously injected using a 23 or 29 gauge needle into one flank of the mouse. $2x10^6$ MC38 cells in 100 µl PBS were injected per C57BL/6 mouse (provided by the animal facility of the Paul-Ehrlich-Institut or purchased from Harlan Nederland). $5x10^6$ RENCA-Her2/neu cells in 100 µl PBS were injected per BALB/c mouse (Charles River) or NOD.Cg-Prkdc^{scid} Il2rg^{tm1Wjl}/SzJ (NSG) mouse (provided by the animal facility of the Paul-Ehrlich-Institut). The tumor growth was monitored by digital caliper measurements and tumor size was calculated according to the volume of an ellipsoid by the following equation:

$$tumor\ volume\ [cm^3] = 0.4 * length\ [cm] * (width\ [cm])^2$$

2.5.2 Injection of vector particles

When MC38 tumors reached a specified volume, they were intratumorally injected with 50 µl srVSV using a 30 gauge needle. For injection, mice were anesthetized with 2-3 % isoflurane using an anesthetic machine with an isoflurane vaporizer and an oxygen concentrator (indulab-vet).

For intravenous injection, mice were prewarmed under a heat-lamp in order to dilate the veins and transferred to a mouse–restrainer. 200 µl AAV vector particles were injected into one of the lateral tail veins using a 29 gauge needle.

2.5.3 Blood sampling

Mice were anesthetized with 2-3 % isoflurane using an anesthetic machine with an isoflurane vaporizer and an oxygen concentrator (indulab-vet) and blood was collected by retro-orbital bleeding using thin glass capillaries. Blood was transferred into EDTA-coated tubes (Microvette® CB 300 K2E, Sarstedt) and serum was recovered by centrifugation at 2,000 xg for 5 min. Eventually, serum was aliquoted and stored at -80°C until analysis.

2.5.4 *In vivo* Imaging

AAV-mediated luciferase expression in living mice was analyzed by *in vivo* imaging using the IVIS® Imaging System 200 (Caliper Life Science) as described previously (Münch et al, 2013). For this purpose, mice were injected intraperitoneally with 150 mg D-Luciferin (Perkin Elmer) per kg body weight using a 29 gauge needle. About five minutes later, mice were anesthetized with 2-3 % isoflurane using a XGI-8 Gas Anesthesia system (Caliper Life Sciences). Finally, imaging data were recorded 10 to 20 min post substrate injection and data analyses were performed using the Living Image 4.3 software (Caliper Life Science).

2.5.5 Isolation and cultivation of splenocytes from mice

Prior to removal of the spleen, mice were sacrificed by cervical dislocation under isoflurane anesthesia. The spleen was explanted, placed onto a 70 µm cell strainer (BD Bioscience) and pushed through the strainer using the plunger end of a syringe. The strainer was washed with RPMI$^{+PenStrep}$ medium and cells were pelleted for 5 min at 314 xg and 4°C (Hereaus™ Multifuge™ X3R, Thermo Fisher Scientific). Erythrocytes were lysed by incubation of the cells in 5 ml red blood cell lysis buffer for 2 min at room temperature. After adding 5 ml RPMI$^{+PenStrep}$ medium, cells were pelleted as described above, the supernatant was discarded and cells were resuspended in 5 ml RPMI$^{+PenStrep}$. Cells were filtered again through a 70 µm cell strainer (BD Bioscience), counted and either cultivated or used for ELISpot analysis (2.4.14).

For cultivation, $5x10^5$ splenoctyes were seeded per well of a round-bottom 96-well plate and cells were cultivated in $RPMI^{+PenStrep}$ supplemented with 10 ng/ml PMA and 500 ng/ml ionomycin (del Rio et al, 2005). Two days after stimulation, cells were used for flow cytometry analysis (2.4.13).

2.5.6 Preparation of mouse organ lysates

In order to detect *in vivo* delivered immune checkpoint inhibitors by AAV vectors, organ lysates were prepared. For this, mice were sacrificed by cervical dislocation under isoflurane anesthesia, organs were explanted, snap frozen in liquid nitrogen and stored at -80°C. For preparation of organ lysates, organs were thawed on ice, cut in small pieces and transferred into lysing matrix D tubes (MP Biomedicals). Passive lysis buffer (Promega) supplemented with protease-inhibitor cocktail (Roche) was applied to the tubes (generally: 2 µl buffer per 1 mg tumor; 1.25 µl buffer per 1 mg liver) and organs were homogenized using a Fast-Prep-24® instrument (MP Biomedicals) equipped with a cooling rotor. Thereafter, cell homogenates were incubated for further 15 min at room temperature. Cell homogenates were transferred to fresh tubes and cell debris were removed by two centrifugation steps (1. centrifugation: 16,200 xg, 4°C, 20 min; 2. centrifugation: 16,200 xg, 4°C, 10 min) (Biofuge Fresco, Heraeus). Supernatant was aliquoted and stored at -80°C until used for analysis.
Samples were thawed on ice prior to ELISA and centrifuged again (16,200 xg, 4°C, 10 min) (Biofuge Fresco, Heraeus) to remove remaining precipitates. Protein concentrations of the organ lysates were determined by BCA assay (2.3.1).

3 Results

This thesis describes the generation and characterization of oncolytic srVSV and receptor-targeted AAV vectors as gene transfer systems for applications in cancer immunotherapy. In the first part of the thesis srVSV encoding different immunotherapeutic transgenes was developed as a novel vector system for oncolytic immunotherapy. This approach aimed at combining immunostimulatory transgene expression with srVSV-mediated oncolysis to induce a long-lasting antitumor immunity. After demonstrating functionality of the *de novo* generated srVSV encoding APC-recruiting cytokines, TAA or B7 T cell co-immunostimulators, their therapeutic efficacy was investigated in a subcutaneous tumor mouse model.
The second part of this thesis describes the development of receptor-targeted AAV vectors for tumor-specific delivery of immune checkpoint inhibitors. Her2/neu-targeted AAV vectors were generated encoding the immune checkpoint inhibitors αPD-1 or αPD-L1. *In vitro* analyses revealed that the vectors were able to mediate expression of functional inhibitors upon transduction of cancer cell lines. Furthermore, Her2-AAV vectors successfully redirected immune checkpoint inhibitors from liver to Her2/neu-positive tumor tissue upon systemic injection into tumor-bearing mice.

3.1 Development of semireplication-competent VSV as a novel vector system for oncolytic immunotherapy

This project aimed at the development of srVSV as a novel vector system for oncolytic immunotherapy by combining the oncolytic activity of srVSV with its ability to accommodate multiple transgenes. To this end, srVSV was engineered to express different immunostimulatory transgenes and its therapeutic efficacy was investigated in a subcutaneous tumor mouse model.

3.1.1 Incorporation of immunotherapeutic transgenes into VSV vector genomes

With the aim of inducing a durable antitumor immune response by srVSV, different immunostimulatory transgenes were incorporated into the VSV vector genomes. First, the APC-recruiting cytokines GM-CSF as well as Flt3L were investigated in this study as potential transgenes to improve antitumor immune responses (Figure 5A). The coding sequence of mouse GM-CSF was cloned into the genomes of the VSV deletion mutants VSVΔG and VSVΔL (Figure 5B). Due to the described cross-reactivity of mouse and

human Flt3L, the cDNA encoding the soluble form of human FlT3L (Isoform 2 P49771-2 found at UniProt database) was cloned into the VSV vector genomes (Maraskovsky et al, 1996; Brasel et al, 1996) (Figure 5B).

A further promising approach to break cancer immune tolerance is the induction or maintenance of T cell activation in the tumor microenvironment. In this context, B7 family members, being crucial for T cell activation and tolerance, have been described to be effective in tumor immunotherapy (Zang & Allison, 2007; Capece et al, 2012). Thus, in a further approach srVSV was armed with B7, a protein required for T cell co-stimulation. The utilized construct was composed of the extracellular domain of mouse B7-1 (B7-$1_{1\text{-}245}$ according to isoform 1 Q00609-1 found at UniProt database) fused to the Fc portion of human IgG1 (IgG-Fc) (hereafter abbreviated with B7) (Figure 5A). In order to generate the respective fusion construct, the extracellular domain of mouse B7-1 was amplified from pCR-B7IG using the primer pair pB7_for and pB7_rev and was cloned via the restriction sites *PacI/NheI* into phuFc-endoglin, thereby replacing the endoglin coding sequence with that for the extracellular domain of mouse B7-1. The resulting plasmid phuFc-B7-1 was used as template for cloning the coding sequence of B7 into the two different VSV vector genomes VSVΔG and VSVΔL (Figure 5B).

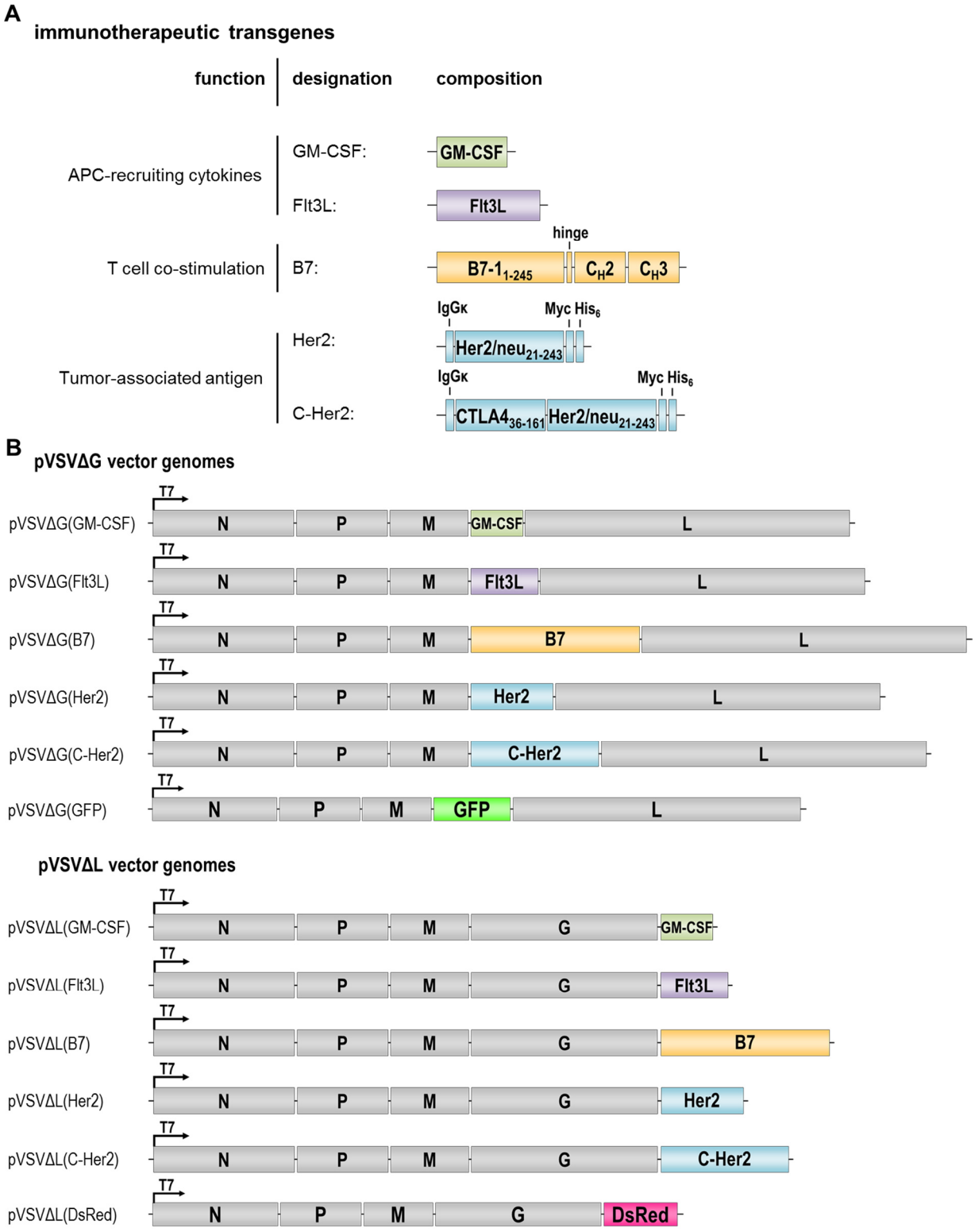

Figure 5: Schematic representation of the incorporated immunotherapeutic transgenes and the resulting VSV vector genomes. (A) The immunostimulatory transgenes GM-CSF, Flt3L, B7, Her2 and C-Her2 were cloned into the in (B) indicated positions of the VSVΔG and VSVΔL vector genomes. Conserved intergenic regions between the viral genes were left unchanged during cloning. IgGκ leader sequence and small epitope tags (Myc, His_6) are indicated. The amino acid position of B7-1 refers to the accession number Q00609-1, of Her2/neu to P04626-1 and of CTLA-4 to P16410 found at UniProt database. Furthermore, VSVΔG vector genome encoding the reporter protein GFP and the VSVΔL vector genome encoding the reporter protein DsRed are shown. C_H: constant region of the heavy chain

Besides direct recruitment of immune cells and stimulation of antitumoral T cell responses, the equipment of oncolytic viruses with TAAs is another feasible strategy to enhance immune stimulation (Pulido et al, 2012; Vigil et al, 2008; Diaz et al, 2007). As a consequence, srVSV was armed with TAAs as a third strategy to enhance antitumor immunity. First, VSV vector genomes were cloned encoding the N-terminal part of human Her2/neu (Her2/neu$_{21-243}$ according to isoform 1 P04626-1 found at UniProt database) (hereafter abbreviated with Her2) (Figure 5B). This part of Her2/neu contains the immunodominant peptide epitope TYLPTNASL which is described to be efficiently presented by mouse MHC class I molecules (Nagata et al, 1997). In addition, the construct encodes an N-terminal IgGκ leader sequence for secretion and C-terminal His$_6$- and Myc-tags (Figure 5A). In order to facilitate targeted delivery of tumor antigens to APCs, constructs had been generated that are composed of the extracellular domain of human CTLA-4 (CTLA-4$_{36-161}$ according to isoform 1 P16410 found at UniProt database) fused to Her2 (hereafter abbreviated with C-Her2) (Sloots et al, 2008; Rohrbach et al, 2005) (Figure 5A). In this approach, CTLA-4 acts as binding domain for B7 proteins on APCs and thereby facilities antigen uptake (Sloots et al, 2008; Rohrbach et al, 2005). Furthermore, using human CTLA-4 is feasible for studies in murine tumor models since it has been described to interact functionally with mouse B7 proteins (Rohrbach et al, 2005; Freeman et al, 1993). Hence, the ORF of C-Her2 was also cloned into the VSVΔG and VSVΔL vector genomes (Figure 5B).

The cloning strategies are summarized in Table 18. For cloning it was necessary to ensure that the intergenic regions between the viral genes are kept unchanged as they provide essential *cis*-acting elements required for viral transcription (Schnell et al, 1996). If no suitable single cutting sites were present in the intergenic regions, the transgene was initially cloned into a pBluescriptII (pBSII) cloning vector, either pBSII-G-ΔL-HDVR for cloning of pVSVΔL or pBSII-M-ΔG-L for cloning of pVSVΔG. These cloning vectors had been designed in a way that the inserted gene is framed by the respective VSV gene junctions. Furthermore, unique cutting sites had been inserted into the cloning vector to enable easy cloning of the gene into the VSV vector genome. After cloning, the inserts of the generated plasmids were sequenced in order to confirm the absence of mutations and subsequently used for the *de novo* generation of replication-deficient VSVΔG and VSVΔL vectors.

Table 18: Cloning strategies to generate VSV vector genomes encoding different immunotherapeutic transgenes

Cloned construct	Template	Cloning of the transgene into cloning vector pBluescriptII (pBSII)			Cloning of the transgene into VSV vector genome		
		Primer[a]	Restriction sites[b]	Backbone[c]	Primer[a]	Restriction sites[b]	Backbone[c]
pVSVΔL(GM-CSF)	pGM-CSF	ΔL_GMCSF_for/ΔL_GMCSF_rev	*BamHI/NotI*	pBSII-G-ΔL-HDVR[d]	-	*KpnI/SpeI* of pBSIIΔL-GM-CSF[g]	pVSVΔL(DsRed)
pVSVΔG(GM-CSF)		ΔL_GMCSF_for/ΔL_GMCSF_rev	*BamHI/NotI*	pBSII-M-ΔG-L[e]	-	*MluI/HpaI* of pBSIIΔG-GM-CSF[h]	pVSV(GP)
pVSVΔL(Flt3L)	pEX-A-sFlt3L	-	*BamHI/NotI*	pBSII-G-ΔL-HDVR[d]	-	*KpnI/SpeI* of pBSIIΔL-Flt3L[g]	pVSVΔL(DsRed)
pVSVΔG(Flt3L)		-	-	-	ΔG_Flt3L_for/ΔG_Flt3L_rev	*XmaI/NotI* of PCR product	pVSV(GP)
pVSVΔL(B7)	phuFc-B7-1	ΔL_B7_for/ΔL/ΔG_B7_rev	*BglII/NotI*[f]	pBSII-G-ΔL-HDVR[d]	-	*KpnI/SpeI* of pBSIIΔL-B7[g]	pVSVΔL(DsRed)
pVSVΔG(B7)		-	-	-	ΔG_B7_for/ΔL/ΔG_B7_rev	*AgeI/NotI* of PCR product[i]	pVSV(GP)
pVSVΔL(Her2)	pSecTag2B-Her2/neu	ΔL_TAA_for/ΔL/ΔG_TAA_rev	*BamHI/NotI*	pBSII-G-ΔL-HDVR[d]	-	*NheI/SpeI* of pBSIIΔL-Her2[g]	pVSVΔL(DsRed)
pVSVΔG(Her2)		-	-	-	ΔG_TAA_for/ΔL/ΔG_TAA_rev	*XmaI/NotI* of PCR product	pVSV(GP)
pVSVΔL(C-Her2)	pSecTag2B-CTLA-4-Her2/neu	ΔL_TAA_for/ΔL/ΔG_TAA_rev	*BamHI/NotI*	pBSII-G-ΔL-HDVR[d]	-	*NheI/SpeI* of pBSIIΔL-C-Her2[g]	pVSVΔL(DsRed)
pVSVΔG(C-Her2)		-	-	-	ΔG_TAA_for/ΔL/ΔG_TAA_rev	*XmaINotI* of PCR product	pVSV(GP)

[a] primer pair used for the amplification of the insert (= immunotherapeutic transgene), [b] restriction sites used for the digestion of the the PCR product/plasmid, [c] unless otherwise noted backbone is digested with the same restriction enzymes as stated in column "restriction sites", [d] pBSII-G-ΔL-HDVR cloning vector: inserted transgene is flanked by the G-L intergenic regions and a part of the G-gene as well as the L-HDV (Hepatitis Delta Virus) ribozyme region, [e] pBSII-M-ΔG-L cloning vector: inserted transgene is flanked by the M-G intergenic regions and a part of the M-gene as well as the G-L intergenic region , [f] PCR product was digested with *BglII/NotI* and cloned into pBSII-G-ΔL-HDVR digested with *BamHI/NotI*, [g] pBSII-G-ΔL-HDVR cloning vector with incorporated transgene, [h] pBSII-M-ΔG-L cloning vector with incorporated transgene, [i] PCR product was digested with *AgeI/NotI* and cloned into pVSV(GP) digested with *XmaI/NotI*

3.1.2 *De novo* generation of srVSV

A reverse genetic system was used for the *de novo* generation of VSVΔG and VSVΔL vectors from cDNA (Whelan et al, 1995; Lawson et al, 1995) (Figure 6). For this, BHK-21 cells were transfected with the full length antigenomic cDNA of the respective VSV vector variant (Figure 5B: pVSVΔG or pVSVΔL) encoding for one of the described immunotherapeutic transgenes. Using the antigenomic cDNA for viral rescue is important to avoid hybridization of the viral genomic RNA and transcribed N, P and L mRNAs supplied from the helper plasmids (Lawson et al, 1995; Schnell et al, 1994). The nucleocapsid protein, the phosphoprotein as well as the RNA-dependent RNA-polymerase required for the initiation of viral replication were provided by co-transfection with the helper plasmids pIRES-N, pIRES-P and pIRES-L (Lawson et al, 1995). The rescue of VSVΔG vectors required an additional helper plasmid encoding the glycoprotein of VSV-G (Boritz et al, 1999). The helper plasmid pIRES-G was cloned by amplifying the coding sequence of VSV-G from the cDNA of the VSV genome using the primer pair pIRES-G_for and pIRES-G_rev. Next, the PCR product was digested with *PcI/EcoRI* and inserted into the *NcoI/EcoRI* digested pIRES-P plasmid, thereby replacing the sequence of the P-gene with the G-gene. Since all plasmids are under the control of a bacteriophage T7 RNA promotor, BHK-21 cells were infected with recombinant modified vaccinia virus expressing T7 RNA polymerase prior to transfection. Propagation-defective VSV vectors were recovered from the cell culture supernatants three days post transfection. The recovered VSV vectors were amplified by passaging supernatants on cells complementing the deleted VSV protein. For propagation of VSVΔG vectors, BHK-21 cells were used that had been engineered to express the glycoprotein of LCMV (BHK21-GP). For amplification of VSVΔL vectors, modified HEK293 cells expressing the VSV-N, VSV-P and VSV-L proteins were utilized (HEK293-NPeGFPL).

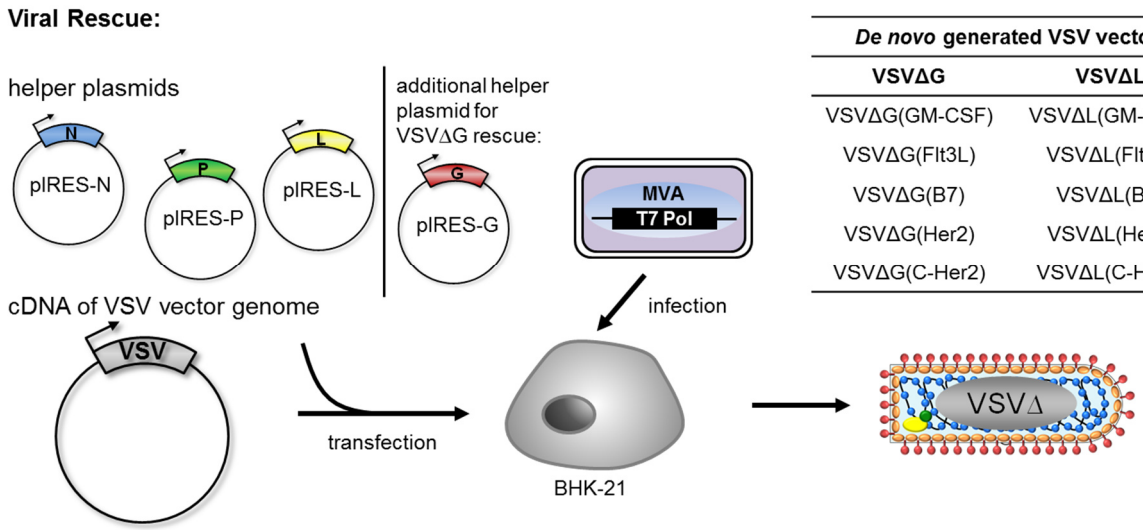

De novo generated VSV vectors	
VSVΔG	**VSVΔL**
VSVΔG(GM-CSF)	VSVΔL(GM-CSF)
VSVΔG(Flt3L)	VSVΔL(Flt3L)
VSVΔG(B7)	VSVΔL(B7)
VSVΔG(Her2)	VSVΔL(Her2)
VSVΔG(C-Her2)	VSVΔL(C-Her2)

Figure 6: Viral rescue of recombinant VSV deletion mutants. Helper plasmids encoding VSV-N, -P and -L protein (pIRES-N, pIRES-P, pIRES-L) as well as the full-length antigenomic cDNA of the respective VSV genome (pVSVΔG or pVSVΔL) were co-transfected into BHK-21 cells. The rescue of VSVΔG vectors required an additional helper plasmid encoding the glycoprotein of VSV (pIRES-G). All plasmids are driven by a bacteriophage T7 promotor. The T7 RNA polymerase was provided by infection of BHK-21 cells with modified vaccinia virus Ankara coding for the T7 polymerase (MVA-T7pol). The shown table summarizes the in this thesis *de novo* generated VSVΔG as well as VSVΔL vectors.

Following rescue, the recovered VSVΔG and VSVΔL vectors were analyzed for their ability to *trans*-complement and co-propagate after co-infection with their respective complementing VSV vector. For this, BHK-21 cells were co-infected with VSVΔG(transgene) and VSVΔL(DsRed) or with VSVΔL(transgene) and VSVΔG(GFP). 'Transgene' refers to the different immunostimulatory transgenes GM-CSF, Flt3L, B7, Her2 or C-Her2. As control, cells were co-infected with VSV vectors deleted for the same VSV protein: VSVΔG(transgene) and VSVΔG(GFP) or with VSVΔL(transgene) and VSVΔL(DsRed). On the following day, cell culture supernatants were transferred to freshly seeded BHK-21 cells and another day later cells were analyzed for cytopathic effects as well as for the expression of the fluorescent proteins by microscopy. An example for the fluorescence microscopy is shown in Figure 7. The analyses showed that the VSVΔG as well as VSVΔL vectors did only generate progeny virions in cell cultures when the respective deleted viral gene was provided by the complementing VSV vector (Figure 7).

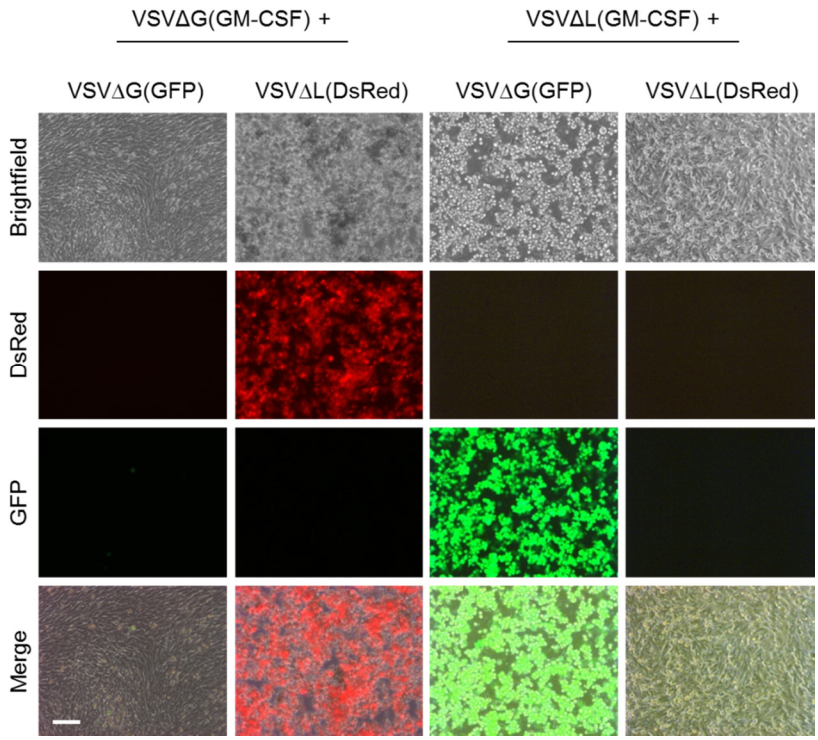

Figure 7: *Trans*-complementation of VSVΔG(GM-CSF) and VSVΔL(GM-CSF). BHK-21 cells were co-infected with VSVΔG(GM-CSF) and VSVΔL(GM-CSF) together with VSVΔG(GFP) or VSVΔL(DsRed). On the following day, supernatants were transferred to freshly seeded BHK-21 cells. One hour later, the cells were washed and fresh medium was added. On the next day, cells were analyzed by fluorescence microscopy. VSV vector variants encoding GM-CSF are shown as representative example. (Scale bar: 200 µm)

When *trans*-complementation of the recovered VSV vector variants was observed, as exemplarily shown for VSVΔG(GM-CSF) and VSVΔL(GM-CSF), the recovered vector preparations were subjected to plaque purification in order to purify a clonal vector population arising from a 'single' VSV vector. For plaque purifications as well as for the subsequent amplifications and titrations BHK21-GP and HEK293-NPeGFPL cells were used for VSVΔG and for VSVΔL vectors, respectively (Figure 8). After amplification of the plaque-purified vector stocks, the titers were determined as $TCID_{50}$/ml.

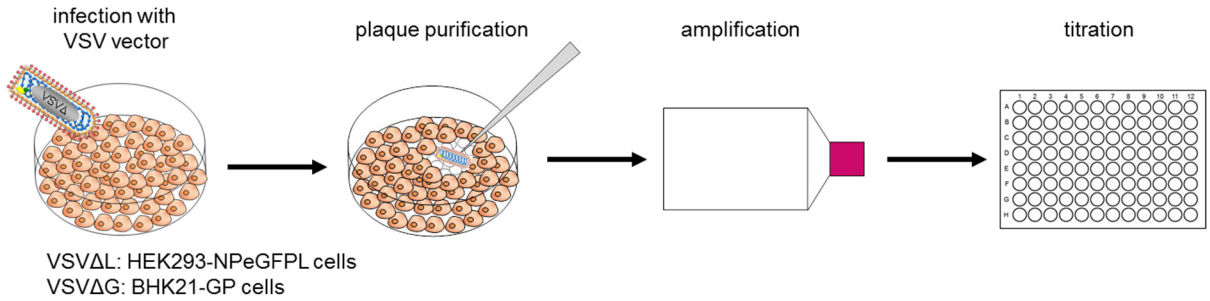

Figure 8: Generation of clonal VSVΔG and VSVΔL vectors. Plaque purifications were performed by infection of cells with serial dilutions of VSVΔG or VSVΔL vectors. The cells were overlaid with 0.9 % agarose solution to limit viral spread. A clonal vector population was purified by isolating an individual plaque. Subsequently, VSV vectors were amplified and titers determined. For this, BHK21-GP or HEK293-NPeGFPL cells were infected with ten-fold serial dilutions of the respective VSV vector variant. Three days later cells were analyzed for cytopathic effects by microscopy and titers were determined as $TCID_{50}$/ml. Titers of the newly generated VSV vector variants are summarized in Table 19.

Table 19: $TCID_{50}$/ml of VSV vectors after single plaque purification

	VSVΔG	VSVΔL
GFP	$5x10^5$	-
DsRed	-	$1.6x10^7$
GM-CSF	$1.6x10^5$	$3.8x10^6$
Flt3L	$3.8x10^5$	$6.7x10^6$
B7	$5x10^6$	$6.7x10^6$
Her2	$1.2x10^5$	$3.7x10^7$
C-Her2	$1.6x10^5$	$2.8x10^7$

Titrations revealed that the titers for VSVΔG vectors were approximately one up to two log levels lower compared to VSVΔL vector preparations (Table 19). The average titer for VSVΔG vector preparations was around $1.1x10^6 \pm 1.9x10^6$ $TCID_{50}$/ml (n=6, mean ± SD) and for VSVΔL around $1.6x10^7 \pm 1.3x10^7$ $TCID_{50}$/ml (n=6, mean ± SD). However, the observed differences can presumably be explained by the different cell lines used for vector amplification and titration. Overall, all VSV vector variants encoding the different immunostimulatory transgenes were successfully rescued.

In order to generate srVSV stocks, a plaque purification was performed after co-infection of BHK-21 cells with VSVΔG and VSVΔL vectors (Figure 9A). Single clones were amplified and subsequently titrated on BHK-21 cells. The resulting srVSV preparations were either composed of a VSVΔG(transgene) vector together with a VSVΔL(DsRed) vector (mixture of those two vector types is further referred to as srVSV(transgene/DsRed)) or of a VSVΔG(GFP) vector together with a VSVΔL(transgene)

vector (mixture of those two vector types is further referred to as srVSV(GFP/transgene)) (Figure 9B). Generated srVSV preparations are summarized in Figure 9C.

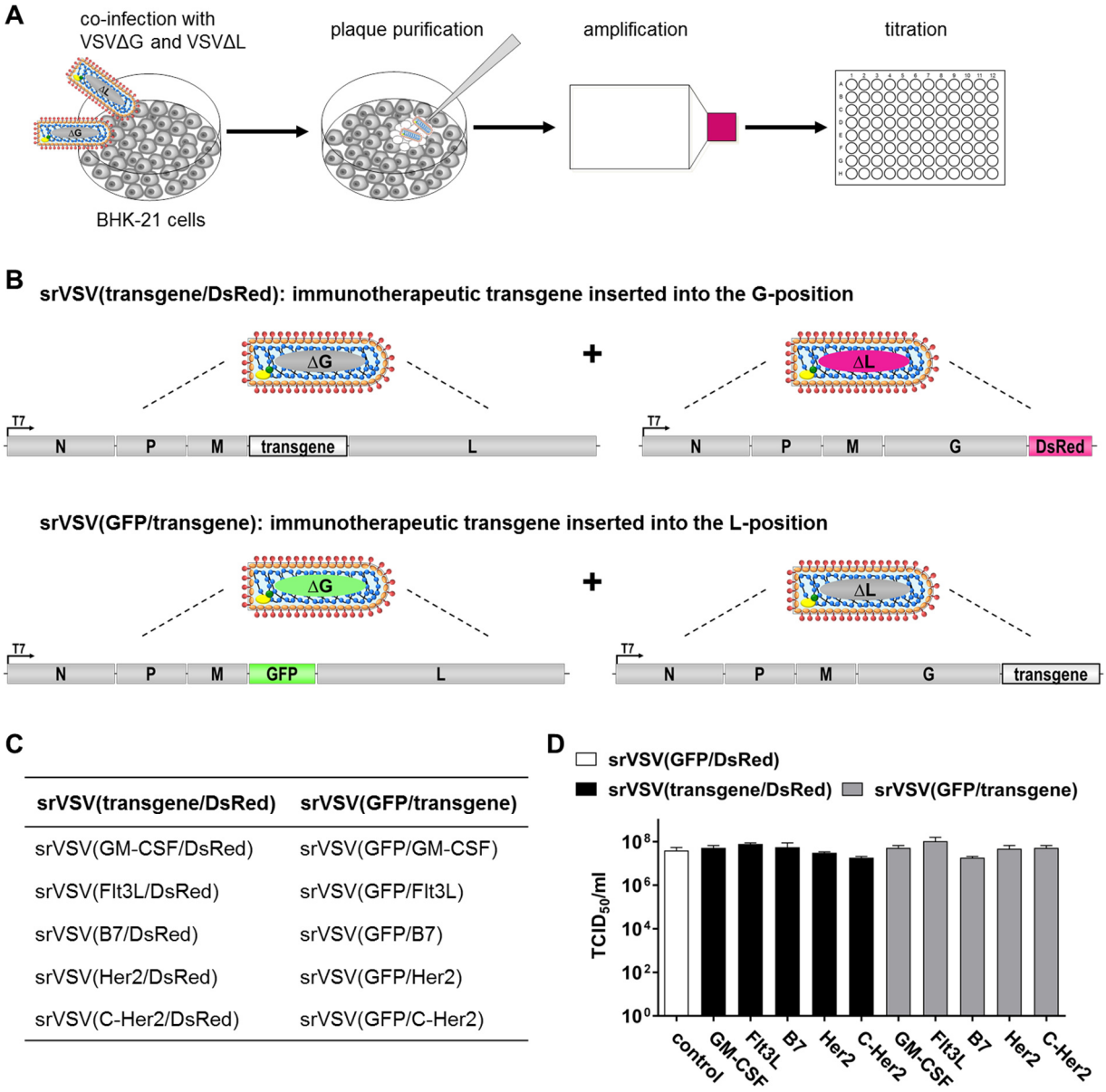

srVSV(transgene/DsRed)	srVSV(GFP/transgene)
srVSV(GM-CSF/DsRed)	srVSV(GFP/GM-CSF)
srVSV(Flt3L/DsRed)	srVSV(GFP/Flt3L)
srVSV(B7/DsRed)	srVSV(GFP/B7)
srVSV(Her2/DsRed)	srVSV(GFP/Her2)
srVSV(C-Her2/DsRed)	srVSV(GFP/C-Her2)

Figure 9: Generation and titration of srVSV. (A) srVSV stocks were generated by co-infection of BHK-21 cells with serial dilutions of VSVΔG together with VSVΔL vectors. On the following day, a single plaque was isolated and amplified on BHK-21 cells. Subsequently, titers were determined as $TCID_{50}$/ml. (B) Schematic drawing of the generated srVSV variants. For srVSV(transgene/DsRed), the immunotherapeutic transgene replaces the G-gene in the VSV vector genome and for srVSV(GFP/transgene), the immunotherapeutic transgene replaces the L-gene. 'Transgene' refers to the immunotherapeutic transgenes GM-CSF, Flt3L, B7, Her2 or C-Her2. (C) Summary of the generated srVSV variants. (D) $TCID_{50}$/ml of the generated srVSV preparations. For titration, BHK-21 cells were infected with ten-fold serial dilutions of srVSV. Three days later cells were analyzed for cytopathic effects by microscopy and titers were determined as $TCID_{50}$/ml. (n=2, means ± SD)

The titers of the different srVSV vector preparations were quite similar among the different transgenes having an average value of $4.2x10^7 \pm 2.3x10^7$ $TCID_{50}$/ml (n=11, mean ± SD) (Figure 9D). Thus, different srVSV vectors encoding either GM-CSF, Flt3L, B7, Her2 or C-Her2 were available for further studies.

3.1.3 Analyzing srVSV-mediated expression of immunostimulatory proteins

The previous chapter described the successful *de novo* generation of srVSV encoding various immunotherapeutic transgenes. Next, it was analyzed whether the newly generated srVSVs mediate transgene expression. For this, cells were infected with srVSV and on the next day cell culture supernatants were collected and subjected to ELISA, Western blot or flow cytometry analyses in order to confirm the presence of the srVSV-encoded immunotherapeutic proteins.

In order to assess the transgene expression of the APC-recruiting cytokine Flt3L, the murine melanoma cell line B16-F10, the murine renal cancer cell line RENCA-Her2/neu and BHK-21 cells were infected with srVSV(Flt3L/DsRed) or srVSV(GFP/Flt3L). To analyze the transgene expression of GM-CSF, B16-F10 and RENCA-Her2/neu cells were infected with srVSV(GM-CSF/DsRed) or srVSV(GFP/GM-CSF). On the next day, cell culture supernatants were analyzed by ELISA.

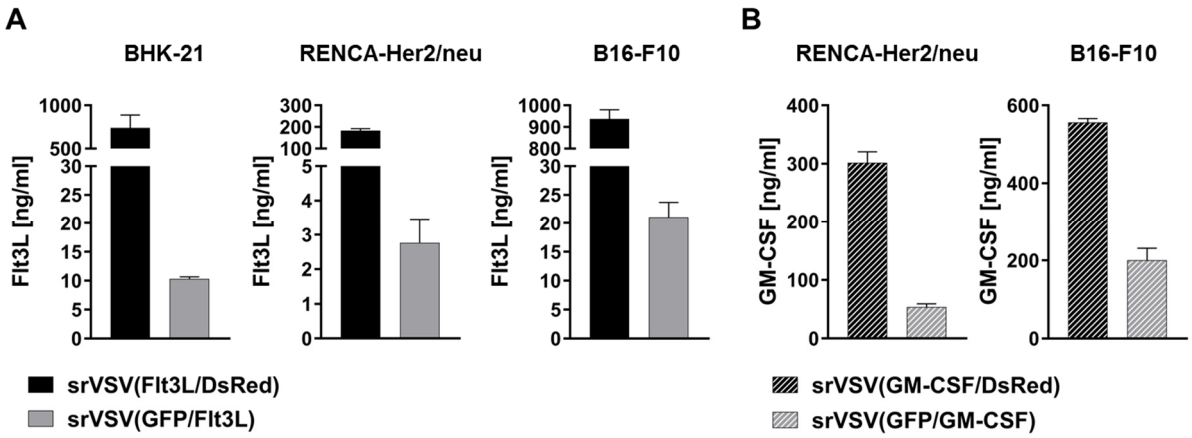

Figure 10: srVSV-mediated expression of Flt3L and GM-CSF. (A) BHK-21, RENCA-Her2/neu and B16-F10 cells were infected with srVSV(Flt3L/DsRed) or srVSV(GFP/Flt3L) (MOI 0.1). On the following day, cell culture supernatants were collected for the quantification of srVSV-encoded Flt3L by ELISA. (n=3, means ± SD) (B) RENCA-Her2/neu and B16-F10 cells were infected with srVSV(GM-CSF/DsRed) or srVSV(GFP/GM-CSF) (MOI 0.1). On the next day, the amount of srVSV-encoded GM-CSF was quantified in cell culture supernatants by ELISA. (n=3, means ± SD)

The analyses revealed srVSV-mediated expression of GM-CSF and Flt3L on various cell lines for all srVSV constructs tested (Figure 10). The amount of detected Flt3L and GM-

CSF was higher in cell culture supernatants of infected B16-F10 compared to RENCA-Her2/neu tumor cells. In cell culture supernatants of srVSV(Flt3L/DsRed)-infected cells an average amount of 182 ± 10 ng/ml (n=3, mean ± SD) were detected for RENCA-Her2/neu cells, 937 ± 42 ng/ml (n=3, mean ± SD) for B16-F10 cells and 740 ± 149 ng/ml (n=3, mean ± SD) for BHK-21 cells (Figure 10A). The amount of Flt3L in cell culture supernatants of srVSV(GFP/Flt3L)-infected cells was in average 2.8 ± 0.7 ng/ml (n=3, mean ± SD) for RENCA-Her2/neu cells, 21 ± 2.6 ng/ml (n=3, mean ± SD) for B16-F10 cells and 10 ± 0.4 ng/ml (n=3, mean ± SD) for BHK-21 cells. In cell culture supernatants of srVSV(GM-CSF/DsRed)-infected cells concentrations of 300 ± 18 ng/ml (n=3, mean ± SD) were measured for RENCA-Her2/neu cells and 556 ± 10 ng/ml (n=3, mean ± SD) for B16-F10 cells (Figure 10B). The amount of GM-CSF in cell culture supernatants of srVSV(GFP/GM-CSF)-infected cells was in average 53 ± 5.6 ng/ml (n=3, mean ± SD) for RENCA-Her2/neu cells and 200 ± 30 ng/ml (n=3, mean ± SD) for B16-F10 cells. Taken together, the results revealed higher levels of transgene expressions for the constructs having the cytokine-gene inserted into the G-position than for those having the cytokine reading frame inserted into the L-position of the VSV vector genome.

Transgene expression of Her2 and C-Her2 was analyzed in cell culture supernatants of srVSV-infected BHK-21 cells by Western blot analysis using a Myc-tag-specific antibody. Cell culture supernatants of BHK-21 cells that had been transfected with expression plasmids encoding the same Her2 or C-Her2 protein as the srVSV variant served as positive control. Western blot analysis revealed specific bands for Her2 at the expected size between 36 and 55 kDa for srVSV(Her2/DsRed) as well as srVSV(GFP/Her2) (Figure 11A). Moreover, the analysis showed the expression of the fusion protein C-Her2 for both srVSV variants.

Functionality of srVSV-encoded C-Her2 was assessed by flow cytometry using the Raji B cell lymphoma cell line constitutively expressing the B7 molecules B7-1 (CD80) and B7-2 (CD86) (Figure 11B). For the analysis, Raji cells were incubated with cell culture supernatants of BHK-21 cells that had been infected with srVSV(C-Her2/DsRed) or srVSV(GFP/C-Her2). B7-negative Molt4.8 cells as well as cell culture supernatants of BHK-21 cells that had been infected with srVSV encoding Her2 served as negative controls. Binding to cell surface was detected using a fluorophore-labeled His-tag-specific antibody. The analysis revealed specific binding of C-Her2 to Raji cells whereas no binding was detectable for the negative controls (Figure 11C).

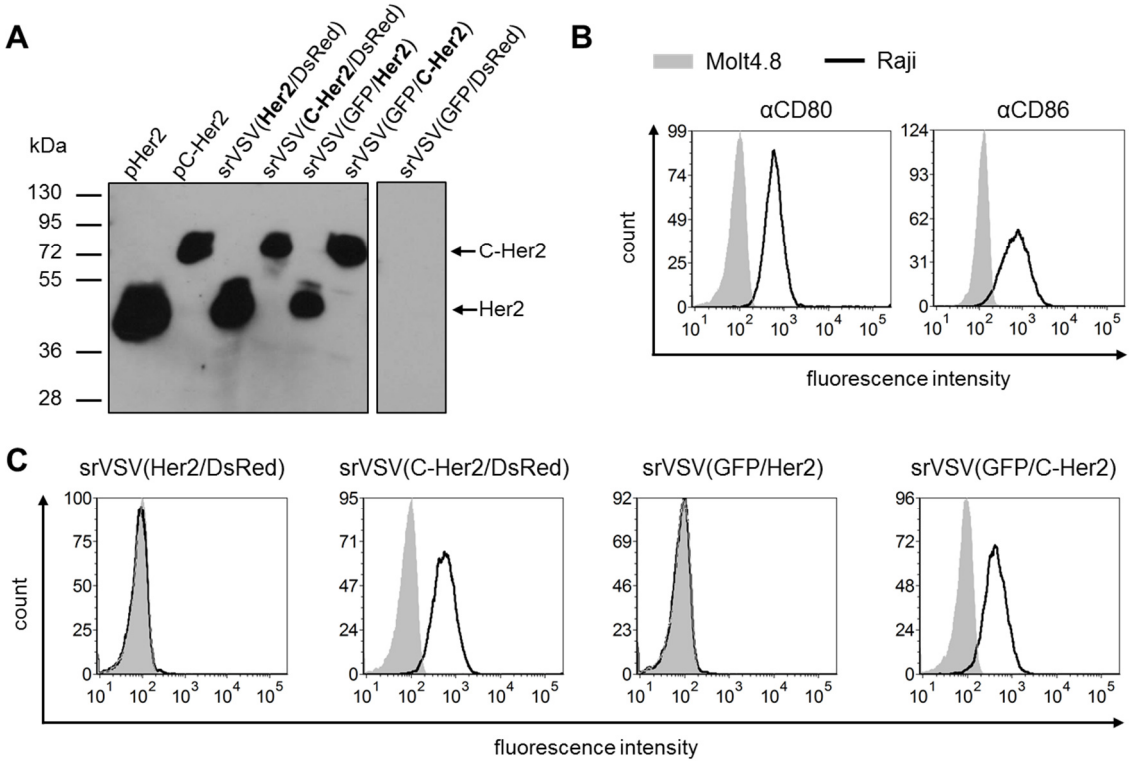

Figure 11: srVSV-mediated expression of Her2 and C-Her2. (A) BHK-21 cells were infected with srVSV(Her2/DsRed), srVSV(C-Her2/DsRed), srVSV(GFP/Her2), srVSV(GFP/C-Her2) and srVSV(GFP/DsRed) (MOI 0.1). On the following day, cell culture supernatants were collected and examined for C-Her2 or Her2 by Western blot analysis using a Myc-tag-specific antibody. As positive control, cell culture supernatants of BHK-21 cells that had been transfected with the expression plasmids pSecTag2B-Her2/neu (pHer2) or pSecTag2B-CTLA-4-Her2/neu (pC-Her2) were included to the analysis. (B) Surface expression of CD80 (B7-1) and CD86 (B7-2) on Raji cells was analyzed using PE-labelled CD80- and FITC-labelled CD86-specific antibodies and flow cytometry (αCD86 clone: FM95; αCD80 clone: 2D10). (C) Specific binding of C-Her2 to B7 molecules was analyzed by incubating Raji cells (black empty curve) with 400 µl cell culture supernatants of BHK-21 cells that had been infected with srVSV(C-Her2/DsRed) or srVSV(GFP/C-Her2) (MOI 0.1). As control, Raji cells were incubated with cell culture supernatants of srVSV(Her2/DsRed)- or srVSV(GFP/Her2)-infected BHK-21 cells. In addition, cell culture supernatants were incubated with B7-negative Molt4.8 cells (grey filled curve). Binding to cell surface was assessed by flow cytometry measurements using a PE-labelled His-tag-specific antibody.

Next, srVSV-mediated expression of B7 was assessed. Transgene expression in cell culture supernatants of BHK-21 cells that had been infected with srVSV(B7/DsRed) or srVSV(GFP/B7) was confirmed by Western blot analysis using a Fc-specific antibody (Figure 12A). The detected band at ~95 kDa corresponded to B7 and the additional band at the size between 28 and 36 kDa presumably represents a cleaved Fc-part. As already observed for the previously described transgenes GM-CSF as well as Flt3L, Western blot analysis also indicated a higher level of transgene expression for B7 when the gene was inserted into the G-position in the VSV vector genome.

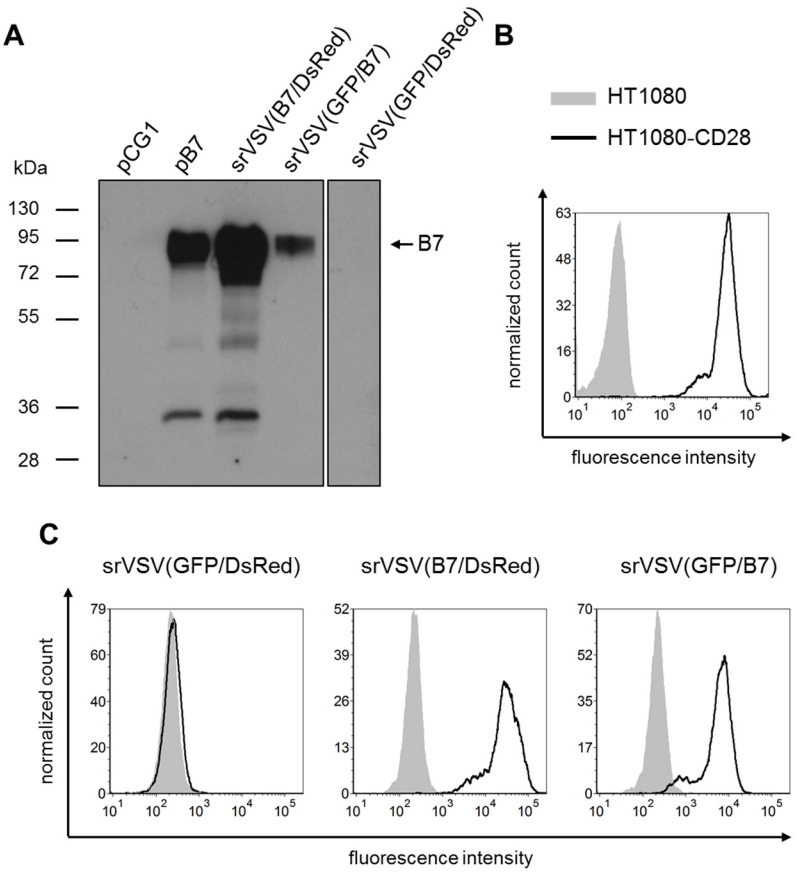

Figure 12: srVSV-mediated expression of B7. (A) BHK-21 cells were infected with srVSV(B7/DsRed) or srVSV(GFP/B7) (MOI 0.1). As negative control, cells were infected with srVSV(GFP/DsRed). On the next day, supernatants were collected and analyzed by Western blot using a Fc-specific antibody. Cell culture supernatant of BHK-21 cells that had been transfected with the expression plasmid phuFc-B7-1 encoding B7 (pB7) was used as positive control. Cell culture supernatant of BHK-21 cells that had been transfected with an empty plasmid (pCG1) served as further negative control. (B) CD28 expressing HT1080 cells were generated by transduction with VSV-G pseudotyped lentiviral vectors encoding mouse CD28 and puromycin resistance. Subsequently, transduced cells were selected by addition of puromycin to the cell culture medium. Surface expression of CD28 was analyzed by flow cytometry using a PE-labelled CD28-specific antibody (clone: 37.51). (C) Parental HT1080 (grey filled curve) and HT1080-CD28 (black empty curve) were incubated with 600 µl cell culture supernatant of BHK-21 cells that had been infected with srVSV(B7/DsRed) or srVSV(GFP/B7) (MOI 0.1). As control, cells were incubated with supernatant of srVSV(GFP/DsRed)-infected BHK-21 cells. Binding to cell surface was detected by a FITC-labelled Fc-specific antibody followed by flow cytometry analysis. Peaks were normalized to number of events.

To investigate functionality of srVSV-encoded B7, HT1080 cells stably expressing CD28 were generated. For this, the cDNA sequence of mouse CD28 (NCBI NM_007642.4) was cloned into a lentiviral transfer vector plasmid via the restriction sites *BamHI*/*SpeI* resulting in pS-CD28-IP-W. In this construct, the ORF for CD28 and for the puromycin antibiotic resistance are linked by an internal ribosomal entry site (IRES) allowing the expression of both genes from a single mRNA. The transfer vector plasmid was packaged into VSV-G pseudotyped lentiviral vectors and the resulting vectors were used for the transduction of HT1080 cells. Successfully transduced cells were selected using the antibiotic puromycin. Surface expression of CD28 on the newly generated HT1080-CD28

cells was confirmed by staining the cells with a fluorophore-labelled CD28-specific antibody and flow cytometry analysis (Figure 12B).
Specific binding of srVSV-encoded B7 to CD28 was investigated by incubating HT1080-CD28 or parental HT1080 cells with cell culture supernatants of srVSV-infected BHK-21 cells. Cell culture supernatant of cells that had been infected with srVSV(GFP/DsRed) was used as control. Subsequently, cells were stained with a fluorophore-labeled Fc-specific antibody and analyzed by flow cytometry. Analysis confirmed specific binding of srVSV-encoded B7 to CD28-positive HT1080 cells and no binding was detected for the negative controls (Figure 12C). Furthermore, a higher mean fluorescence intensity was observed for srVSV(B7/DsRed) as compared to srVSV(GFP/B7) indicating again a higher level of transgene expression for constructs that had incorporated the transgene into the G-position of the VSV vector genome compared to the L-position.

In summary, the data demonstrate that the generated srVSV variants mediated transgene expression of the different immunostimulatory proteins. Furthermore, the analysis revealed a higher level of transgene expression of the constructs having the transgene inserted into the G-position than for those having the transgene inserted into the L-position of the VSV vector genome.

3.1.4 Sensitivity of murine tumor cell lines to the antiviral effects of type I IFN

In order to investigate antitumor efficacy of the srVSV systems *in vivo,* a suitable VSV-permissive syngeneic tumor mouse model had to be identified. VSV is exquisitely sensitive to type I IFN-induced antiviral responses. Hence, defective IFN pathways in cancer cells are described to be the key determinant of VSV oncoselectivity (Stojdl et al, 2000; Stojdl et al, 2003; Liu et al, 2013; Hastie & Grdzelishvili, 2012). However, not all cancer cells have a deregulated IFN response and thus resist to VSV infection (Liu et al, 2013; Dold et al, 2016). Therefore, five different murine cancer cell lines were analyzed concerning their IFN sensitivity.
The breast cancer cell line 4T1, the renal cancer cell line RENCA-Her2/neu, the melanoma cell line B16-F10, the colon cancer cell line MC38 or the breast cancer cell line E0771 were pretreated for 24 h with different concentrations of IFNα and subsequently infected either with replication-competent rVSV(GFP) or srVSV(GFP/DsRed). Two days later, the different cancer cell lines were analyzed by fluorescence microscopy revealing different sensitivity to the antiviral effects of IFNα (Figure 13). The analysis showed that

4T1 and B16-F10 cells were productively infected with VSV up to a concentration of 1 U/ml IFNα. At a concentration of 10 U/ml IFNα only single infected cells were observable but no viral spread. RENCA-Her2/neu cells showed the highest IFN sensitivity as these cells were only infectable with VSV up to a concentration of 0.1 U/ml IFNα. In contrast, MC38 and E0771 cells were infectable even when pretreated with the highest tested IFNα dose of 1000 U/ml. However, at high concentrations of IFNα fluorescence microscopy indicated less infected cells for MC38 and E0771 as compared to cells that were not pretreated with IFNα. The same was observed for cells that were infected with srVSV (not shown).

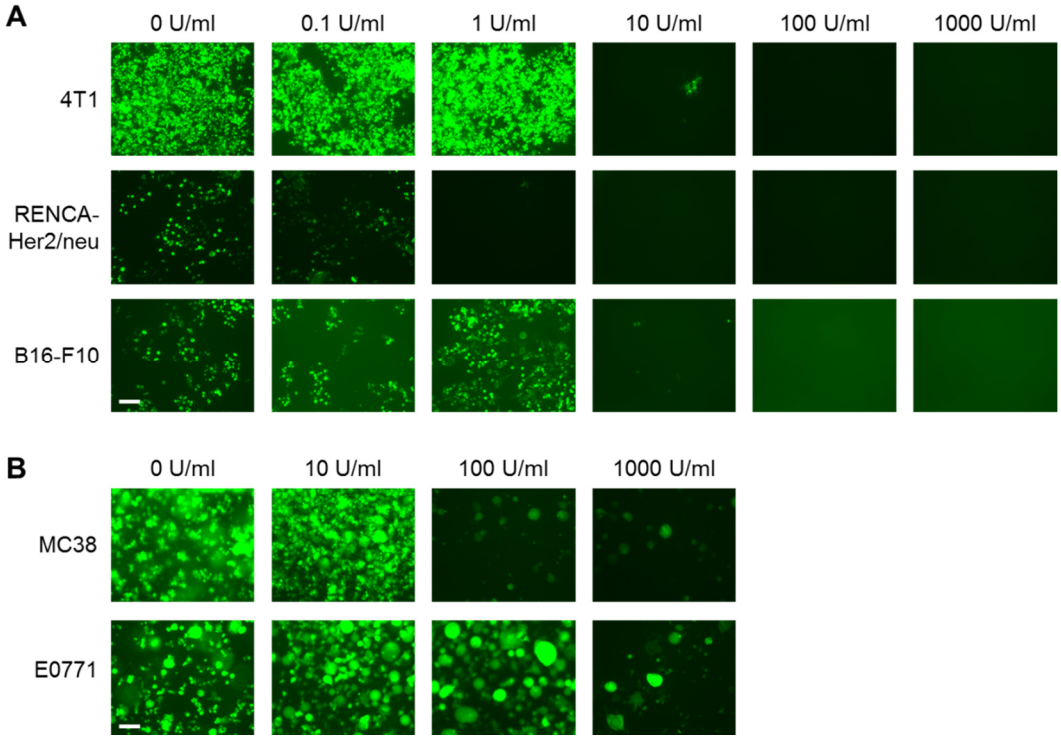

Figure 13: Susceptibility of IFNα-stimulated murine cancer cell lines to VSV infection. (A) 4T1, RENCA-Her2/neu, B16-F10 and (B) MC38, E0771 cells were pretreated with the indicated concentrations of mouse IFNα for 24 h prior to rVSV(GFP) infection. Two days post infection cells were analyzed by fluorescence microscopy. (Scale bar: 200 μm)

To further examine the relative sensitivity of the cancer cell lines to protection by IFNα, the cell viability was examined by WST-1 assay. Results obtained from the fluorescence microscopy analyses were mainly confirmed by the WST-1 assay. RENCA-Her2/neu cells were exquisitely sensitive to the antiviral effects of IFNα (Figure 14). Only 1 U/ml IFNα was sufficient to protect all RENCA-Her2/neu cells from rVSV- as well as srVSV-mediated oncolysis. 10 U/ml IFNα was sufficient to protect 4T1 and B16-F10 cells from

VSV-mediated cell killing. In contrast to the other examined cancer cell lines, 30-40 % of E0771 cells were still viable even if the cells were not pretreated with IFNα. Moreover, pretreatment with IFNα influenced the susceptibility of E0771 cells to VSV infection. Thus, albeit E0771 cells were infectable by VSV, even at high IFNα concentrations, the susceptibility to VSV-mediated cell killing seemed to be restricted or decelerated compared to the other tested cancer cell lines. MC38 cells showed the best susceptibility to VSV-mediated oncolysis and cells pretreated with IFNα up to a dose of 10 U/ml were not protected from VSV-mediated oncolysis. However, incubation with higher doses of IFNα still revealed cell viability of about 30 % for srVSV- and about 60 % for VSV-treated MC38 cells. Thus, even though MC38 cells retained highly susceptible to VSV infection at high concentrations of IFNα, none of the tested cancer lines were proven to be completely unresponsive to type I IFN-induced antiviral responses. Overall, the fluorescence microscopy analyses and the WST-1 assay showed the same antiviral effects of IFNα against both tested VSV systems, the replication-competent rVSV and the semireplication competent srVSV.

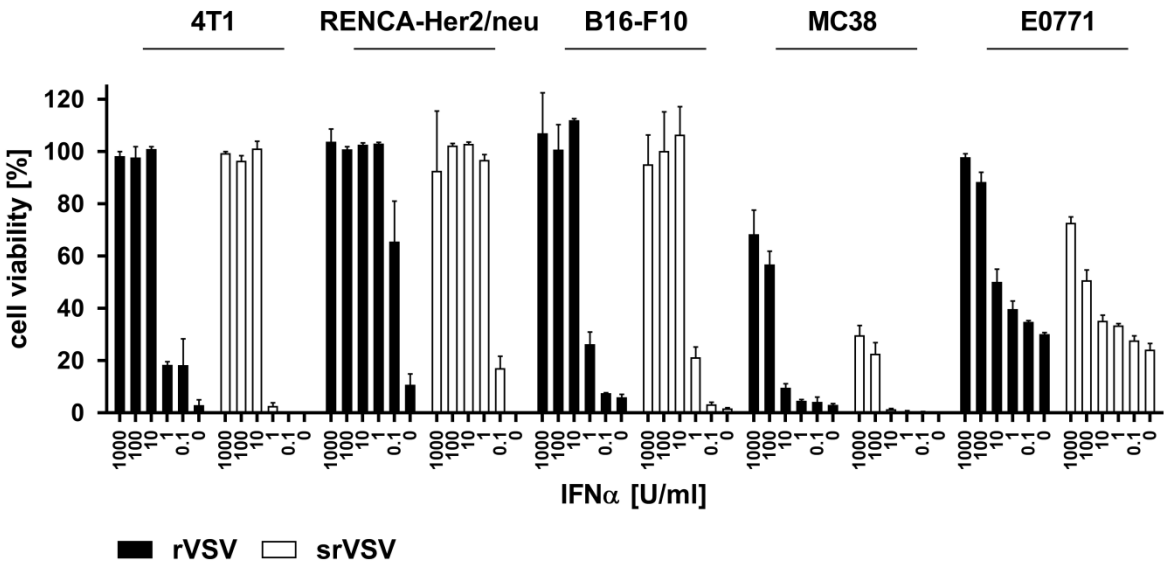

Figure 14: VSV-mediated oncolysis of murine cancer cell lines after pretreatment with IFNα. Murine cancer cell lines were pretreated with the indicated concentrations of mouse IFNα for 24 h prior to rVSV(GFP) or srVSV(GFP/DsRed) infection. Cell viability was measured two days post infection by WST-1 assay and is presented as percentage to the uninfected control. (n=3, means ± SD)

In order to investigate the antitumor effects of srVSV encoding the TAA Her2, the usage of a Her2/neu-positive tumor model is mandatory. However, the previous experiment showed that RENCA-Her2/neu cells are quite sensitive to the antiviral effects of IFNα. Thus, this cancer cell line is not a suitable tumor model to investigate the therapeutic

efficacy of srVSV *in vivo*. As MC38 cells showed the best susceptible to VSV oncolysis after pretreatment with IFNα, this cancer cell line was considered to be a potential tumor model. Therefore, MC38 cells genetically engineered to express the ectodomain of Her2/neu (MC38-ek-Her2/neu) were also analyzed in regard to their sensitivity to IFNα. For this, MC38 and MC38-ek-Her2/neu cells were pretreated with different concentrations of IFNα for 24 h and subsequently infected with srVSV(GFP/DsRed) or rVSV(GFP).

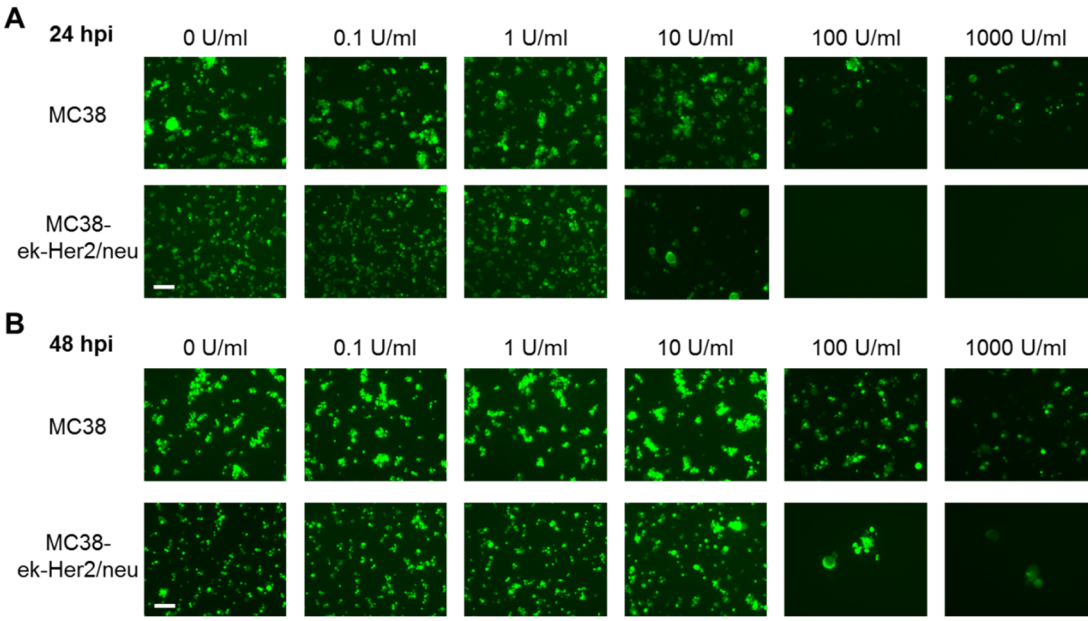

Figure 15: Different susceptibility of MC38 and MC38-ek-Her2/neu cells to VSV infection after pretreatment with IFNα. MC38 and MC38-ek-Her2/neu cells were pretreated with the indicated concentrations of IFNα for 24 h. (A) 24 h and (B) 48 h post infection with rVSV(GFP) cells were analyzed by fluorescence microscopy. hpi: hours post infection. (Scale bar: 200 µm)

Surprisingly, fluorescence microscopy analysis 24 h post infection indicated a different sensitivity of MC38 and MC38-ek-Her2/neu cells to the antiviral effects of IFNα (Figure 15). As expected, MC38 cells were infectable up to a concentration of 1000 U/ml IFNα. In contrast, MC38-ek-Her2/neu cells showed an infection only up to an IFNα dose of 10 U/ml and no infected cells were observable at higher IFNα concentrations. Two days after infection, MC38-ek-Her2/neu cells showed single infected cells at 100 U/ml and 1000 U/ml but no viral spread. These observations were confirmed by measuring the cell viability by WST-1 assay. In contrast to MC38 cells, MC38-ek-Her2/neu cells showed no VSV-induced cell killing at high IFNα doses of 100 U/ml and 1000 U/ml (Figure 16).

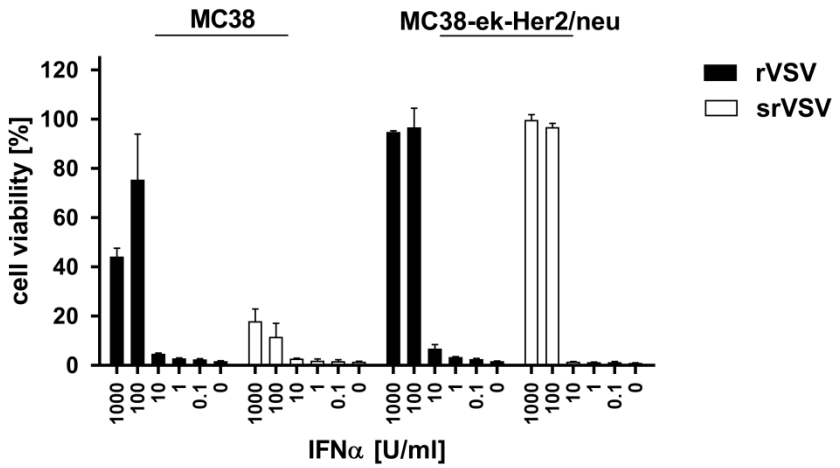

Figure 16: VSV-mediated cell killing of MC38 and MC38-ek-Her2/neu cells after IFNα treatment. MC38 and MC38-ek-Her2/neu cells were pretreated for 24 h with the indicated concentrations of mouse IFNα prior to rVSV(GFP) or to srVSV(GFP/DsRed) infection. Cell viability was measured two days after infection by WST-1 assay and is presented as percentage to the uninfected control. (n=3, means ± SD)

These results revealed a slightly increased sensitivity of MC38-ek-Her2/neu cells to the antiviral effects of IFNα as compared to parental MC38 cells. During the generation of the transgenic MC38-ek-Her2/neu cell line, probably a single clone had been selected exhibiting a higher IFN sensitivity compared to parental MC38 cells. It cannot be excluded that the integration of the gene encoding ek-Her2/neu into the genome upon transduction with the lentiviral vector altered the characteristics of the generated cell line.

Overall, most of the tested mouse cancer cell lines were quite sensitive to the antiviral effects of IFNα indicating that the IFN-signaling seems to be at least partially intact in these cells. The parental murine colon cancer cell line MC38 showed the best susceptibility to VSV infection post IFNα incubation and thus was considered to be a suitable tumor model to investigate the therapeutic efficacy of srVSV *in vivo*.

3.1.5 Generation and characterization of srVSV for the *in vivo* studies

So far, srVSVs encoding a single immunotherapeutic transgene together with a fluorescent protein were generated and it could be shown that srVSV can be engineered to express cytokines or TAAs. However, srVSV is an especially promising platform for the use in cancer immunotherapy as it is a suitable system to easily deliver two therapeutic transgenes, one transgene incorporated into the VSVΔG and one into the

VSVΔL vector genome. To take advantage of this property, srVSV encoding two different immunotherapeutic transgenes were generated for the *in vivo* studies. However, the previously tested mouse cancer cell lines expressing the TAA Her2/neu were quite sensitive to the antiviral effects of IFNα. Thus, no tumor mouse model could be identified so far that is suitable to investigate the antitumoral efficacy of srVSV encoding Her2 or C-Her2 *in vivo*. As a consequence, it was initially focused on srVSV delivering the APC-recruiting cytokines GM-CSF and Flt3L as well as the T cell co-immunostimulator B7.

To this end, srVSV encoding GM-CSF and B7 (srVSV(GM-CSF/B7)) and srVSV encoding Flt3L and B7(srVSV(Flt3L/B7)) were generated as described in chapter 3.1.2 (Figure 17). Titers of the generated srVSV preparations were in the expected range of $2.2x10^7 \pm 8.5x10^6$ $TCID_{50}$/ml (mean ± SD, n=2) for srVSV(GM-CSF/B7) and $3.9x10^7 \pm 1.56x10^7$ $TCID_{50}$/ml (mean ± SD, n=2) for srVSV(Flt3L/B7).

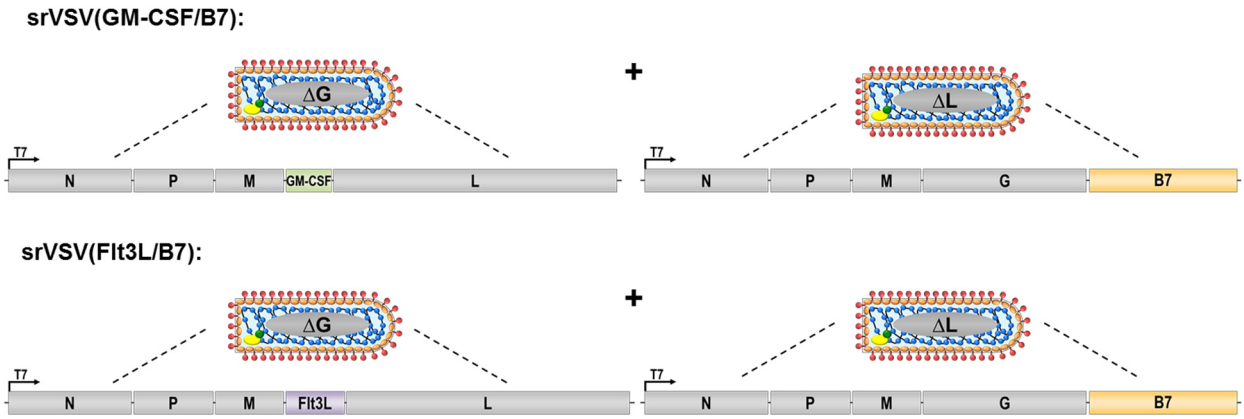

Figure 17: Schematic representation of srVSV(GM-CSF/B7) and srVSV(Flt3L/B7). srVSV(GM-CSF/B7) is composed of VSVΔG(GM-CSF) and VSVΔL(B7) and srVSV(Flt3L/B7) is composed of VSVΔG(Flt3L) and VSVΔL(B7).

To confirm functionality of the newly generated srVSV stocks, transgene expression was analyzed in cell culture supernatants of srVSV-infected MC38 cells. The expression of the APC-recruiting cytokines GM-CSF and Flt3L was investigated by Western blot using GM-CSF or Flt3L-specific antibodies. As control, cell culture supernatants of cells infected with srVSV(GM-CSF/DsRed) or srVSV(Flt3L/DsRed), whose expression was already confirmed by ELISA (Figure 10), were also subjected to the Western blot analysis. As additional control, not only supernatants of infected MC38 cells but also of infected BHK-21 cells were analyzed.

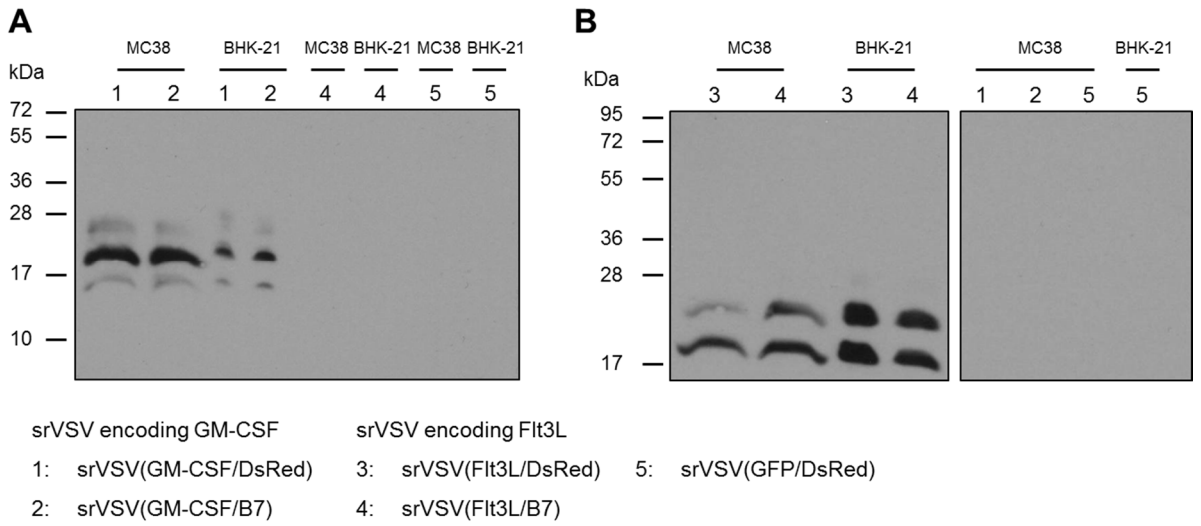

Figure 18: Expression of GM-CSF and Flt3L by srVSV-infected MC38 cells. MC38 cells were infected with the indicated srVSV variants. On the following day, cell culture supernatants were collected and analyzed by Western blot using a (A) GM-CSF- or (B) Flt3L-specific antibody. As control, cell culture supernatants of srVSV-infected BHK-21 cells were used.

Western blot analyses proved the expression of the APC-recruiting cytokines GM-CSF and Flt3L by srVSV-infected MC38 cells (Figure 18). The same specific bands were identified in cell culture supernatants of infected MC38 and BHK-21 cells. However, analysis revealed next to a strong band at ~19 kDa two further distinct bands for GM-CSF in the Western blot analysis (Figure 18A). The different molecular weights observed for GM-CSF are also described in the literature and originates from varying degrees of glycosylation (Miyajima et al, 1986). GM-CSF is a monomeric protein composed of 141 amino acids having two potential N-linked and two potential O-linked glycosylation sites (according UniProt database P01587 and 'NetNGlyc' predictor). Thus, the apparent molecular mass of the protein varies from around ~16 kDa for unglycosylated GM-CSF to ~19 kDa and ~24 kDa for glycosylated GM-CSF.

Analysis of supernatants collected from cells infected with srVSV encoding Flt3L identified two specific bands at a size of ~20 kDa and ~25 kDa confirming the expression of the cytokine (Figure 18B). As already described for GM-CSF, also two predicted N-linked glycosylation sites exist for Flt3L (according UniProt database P49771 and 'NetNGlyc' predictor) presumably explaining the detection of two bands instead of one single band. Also in literature it is described that purified, recombinant Flt3L exhibited two specific bands in Western blot analysis (Zhang et al, 2005).

Next, srVSV(GM-CSF/B7) and srVSV(Flt3L/B7) were characterized with respect to their capacity to express functional B7 after infection of MC38 cells. First, supernatants of

infected cells were examined for transgene expression by Western blot analysis using a Fc-specific antibody. A specific band at the expected size of ~95 kDa was detectable confirming the presence of B7 in cell culture supernatants of srVSV-infected MC38 cells (Figure 19A).

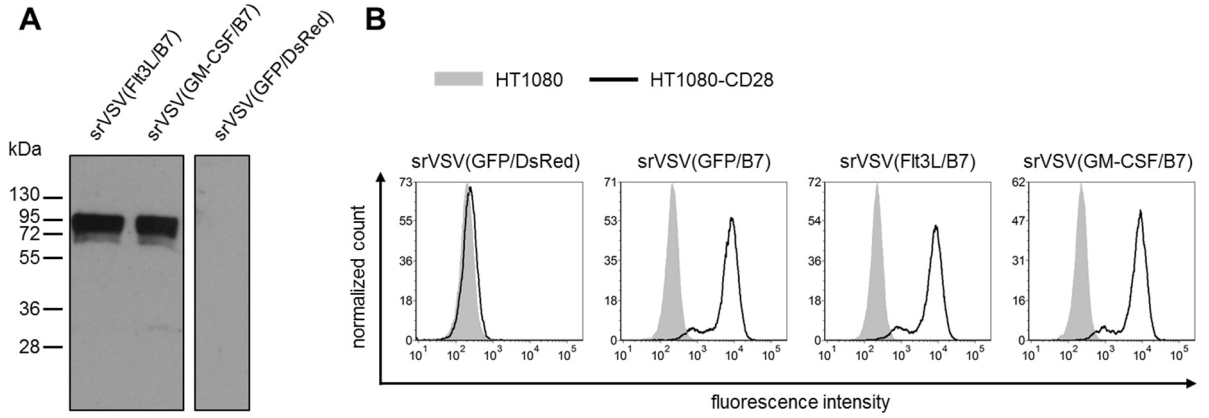

Figure 19: Expression of B7 by srVSV-infected MC38 cells. (A) MC38 cells were infected with srVSV(Flt3L/B7), srVSV(GM-CSF/B7) or srVSV(GFP/DsRed) (MOI 0.1). On the next day, cell culture supernatants were collected and analyzed by Western blot using a Fc-specific antibody. (B) Parental HT1080 (grey filled curve) and HT1080-CD28 cells (empty black curve) were incubated with 600 µl cell culture supernatant of MC38 cells that had been infected with srVSV(GFP/B7), srVSV(Flt3L/B7) or srVSV(GM-CSF/B7) (MOI 0.1). As control, cells were incubated with supernatants of srVSV(GFP/DsRed)-infected MC38 cells. Binding to cell surface was detected by FITC-labelled Fc-specific antibody followed by flow cytometry analysis. Peaks were normalized to number of events.

Functionality of srVSV(GM-CSF/B7)- and srVSV(Flt3L/B7)-encoded B7 after infection of MC38 cells were investigated by specific binding to CD28-positive HT1080 cells as described previously (chapter 3.1.3). As positive control, cell culture supernatant of MC38 cells infected with the previously characterized srVSV(GFP/B7) was used. The flow cytometry analysis showed specific binding of B7 to CD28-positive HT1080 cells demonstrating the expression of functional B7 by srVSV-infected MC38 cells (Figure 19B).

Taken together, the obtained results demonstrate the successful generation of srVSV(GM-CSF/B7) and srVSV(Flt3L/B7). Generated srVSV productions yielded high titers and transgene expression was proven in cell culture supernatants of infected MC38 cells.

3.1.6 Analyzing therapeutic efficacy of srVSV equipped with immunotherapeutic transgenes *in vivo*

The previous chapters showed the identification of a VSV-permissive mouse cancer cell line and the successful generation as well as characterization of srVSV encoding different immunotherapeutic transgenes. Next, it was analyzed whether the generated srVSVs encoding immunotherapeutic transgenes exhibit a superior antitumoral effect as compared to srVSV(GFP/DsRed). For this, MC38 cells were subcutaneously transplanted into C57BL/6 mice and tumor growth was monitored until the tumors reached an average volume of about 0.1 cm^3. Subsequently, animals were injected intratumorally with srVSV(GFP/DsRed), srVSV(GM-CSF/B7) or srVSV(Flt3L/B7).

The analysis revealed complete tumor regression for two out of four mice treated with srVSV(Flt3L/B7) and for one out of three mice treated with srVSV(GM-CSF/B7) (Figure 20A). However, also one mouse injected with srVSV(GFP/DsRed) revealed complete tumor regression. All mock-treated mice showed progressing tumor growth. Altogether, tumor response to therapy treatment was dichotomous, with some mice responding and some mice not responding within a cohort. Remarkably, all mice showing complete tumor regression were female. In contrast, only one male mouse showed a delayed tumor growth in the srVSV(GFP/DsRed) cohort, whereas the tumors of the other male mice showed progressing growth. This difference in treatment response might be explained by the growth inhibition of MC38 cells by female sex steroids, such as estrone and progesterone (Motylewska & Melen-Mucha, 2009). Thus, possibly hormones supported the antitumor effects in female mice.

Comparing the tumor volumes on day 15, the last day when all mice were alive, revealed no differences between the different srVSV treatment groups (Figure 20B). However, an easier comparison of the tumor growth can be achieved by calculating the area under the curve (AUC). The obtained AUC value reflects the entire tumor growth curve through a single number and considers the total observation period from srVSV injection until the mouse had to be sacrificed (Duan et al, 2012). The analysis indicated an improved therapeutic efficacy of srVSV(GM-CSF/B7) or srVSV(Flt3L/B7) as compared to srVSV(GFP/DsRed) (Figure 20C). Survival analysis revealed a clear benefit of srVSV-treated mice in comparison to the mock cohort (Figure 20D). Furthermore, srVSV equipped with immunostimulatory transgenes indicated a modest increase in overall survival as compared to srVSV(GFP/DsRed) (Figure 20D).

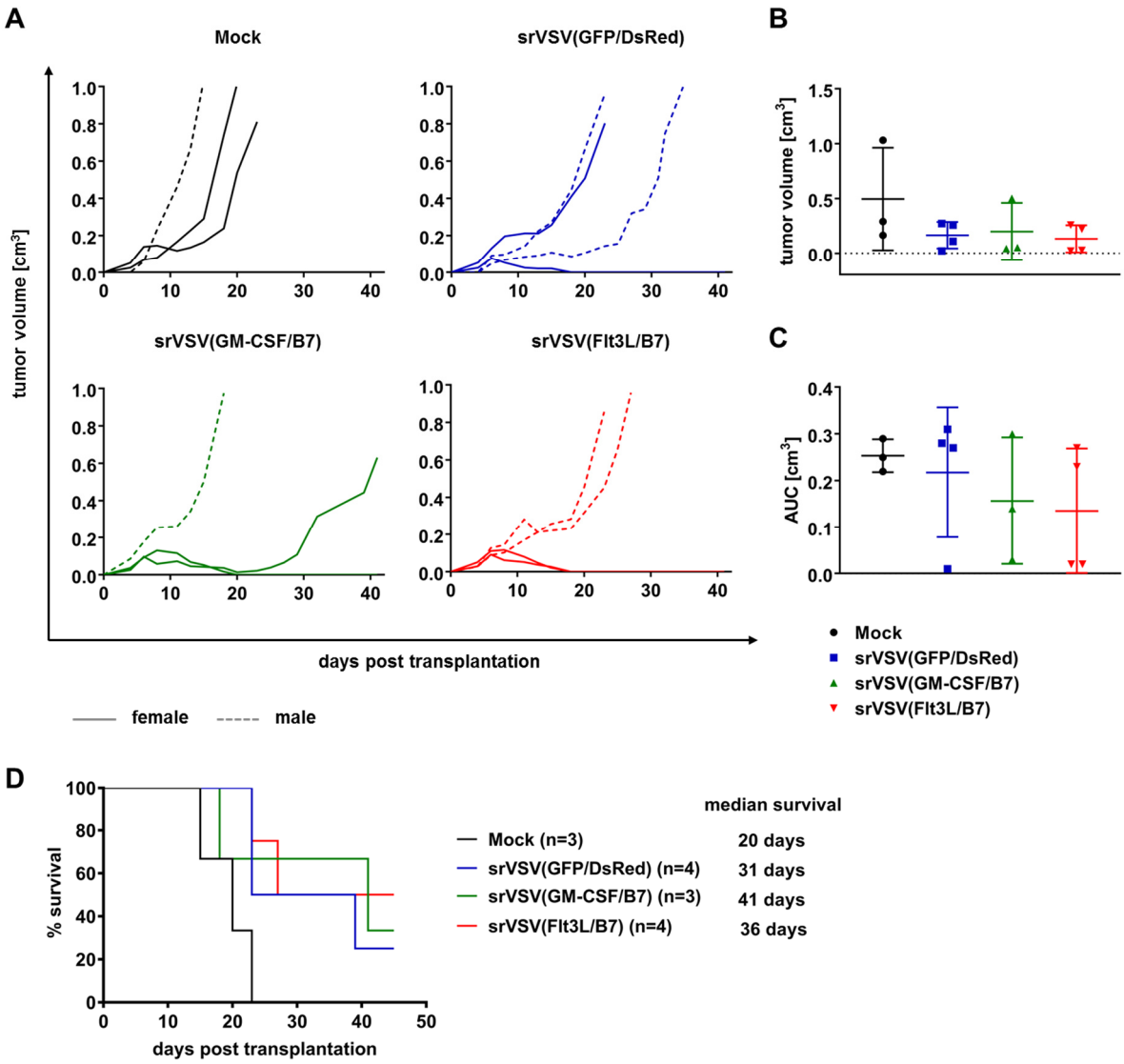

Figure 20: Therapeutic efficacy of srVSV in a subcutaneous syngeneic tumor mouse model. C57BL/6 mice were subcutaneously transplanted with $2x10^6$ MC38 tumor cells. Once the tumors had reached an average size of 0.1 cm^3, animals were assigned to four different treatment groups with each having the same mean tumor volume. Mice were subjected to intratumoral injections of $1x10^6$ $TCID_{50}$ with srVSV(GFP/DsRed) (n=4), srVSV(GM-CSF/B7) (n=3) or srVSV(Flt3L/B7) (n=4) (5 injections: 6, 8, 11, 13 and 15 days post tumor implantation). Control animals were injected with the same volume PBS (Mock). (A) Tumor growth curves of individual mice are shown. Curves of female mice are displayed as continuous lines and curves of male mice are displayed as dashed lines. (B) Distribution of tumor volumes of each group on day 15 post tumor implantation. Dots represent tumor volume of each mouse. (means ± SD) (C) Group comparison was performed by calculating the AUC for each animal normalized to the day when the respective mouse was sacrificed. (means ± SD) (D) Kaplan-Meyer survival analysis. AUC: area under the curve

3.1.6.1 Induction of an antitumor immune response

Next, it was tested whether cured mice conferred protective antitumor immunity against tumor cells. For this, cured mice were rechallenged with a subcutaneous injection of MC38 cells on their flanks contralateral to their initial tumor challenge. As control, naïve mice were transplanted with MC38 tumor cells. Control mice showed progressing tumor growth (Figure 21). In contrast, mice that were cured by srVSV

treatment rejected the tumors indicating the induction of a long-term antitumor immune response by the srVSV tumor therapy.

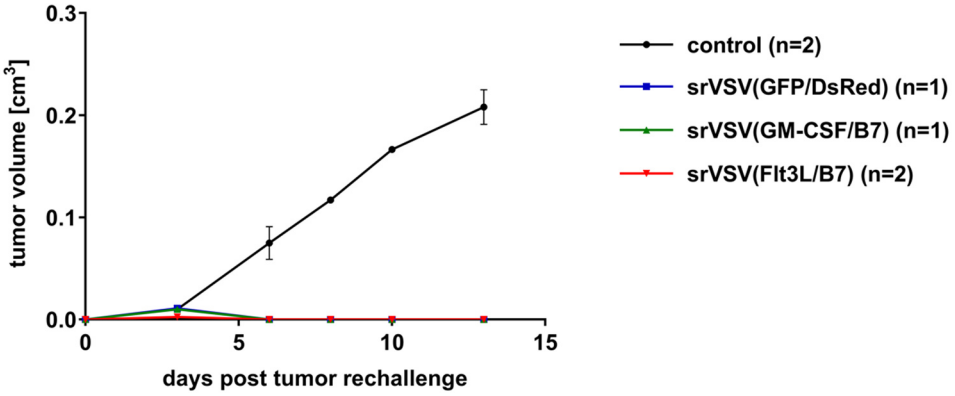

Figure 21: Mice cured by srVSV treatment were protected from tumor rechallenge. Naïve mice or mice cured from MC38 tumors by srVSV treatment were rechallenged with a subcutaneous injection of MC38 cells ($2x10^6$ cells) at the opposite flank to their original tumor application. Growth curves represent the average tumor volumes. (means ± SD)

To assess whether the srVSV treatment induced a tumor-specific cellular immune response, splenocytes of animals were analyzed for antigen-specific IFNγ-secretion by ELISpot assay. Mice were sacrificed 14 days after tumor rechallenge and splenocytes were isolated. Two different approaches were tested to stimulate isolated splenocytes. In a first approach, cells were stimulated with irradiated MC38 tumor cells. In a second stimulation variant, cells were stimulated with MC38 tumor lysates. In addition, two different stimulants to splenocyte ratios were tested for each approach: 1:10 and 1:5 for irradiated tumor cells and 1:6 and 1:2 for MC38 tumor lysates. Thus, IFNγ release by the splenocytes was measured in the presence of irradiated MC38 tumor cells or MC38 tumor lysates as source of *in vitro* stimulating antigens. As positive control, cells were stimulated with ConA and cells incubated with medium only served as negative control.
The analysis showed that incubation of splenocytes with irradiated MC38 tumor cells indeed stimulated immune cells. This was true for both stimulant to splenocyte ratios tested (Figure 22). However, almost no IFNγ-secreting immune cells were detectable when splenoyctes were stimulated with MC38 tumor lysates. Furthermore, IFNγ-secreting splenocytes were only clearly detectable in spleens of mice that were cured by the srVSV treatment and not in spleens of the control mice. Stimulation of splenocytes with ConA revealed IFNγ-secreting cells in the spleens of control mouse and of cured mice confirming the reactivity of the splenocytes. Furthermore, the observed amount of IFNγ-secreting immune cells after stimulation with MC38 antigen of cured mice was

definitely higher as compared to the medium negative control. Altogether, the ELISpot assay indicated the induction of a tumor-specific cellular immune response in mice that were cured by srVSV treatment and thus further supports the previous data that the treatment induced a durable antitumor immune response.

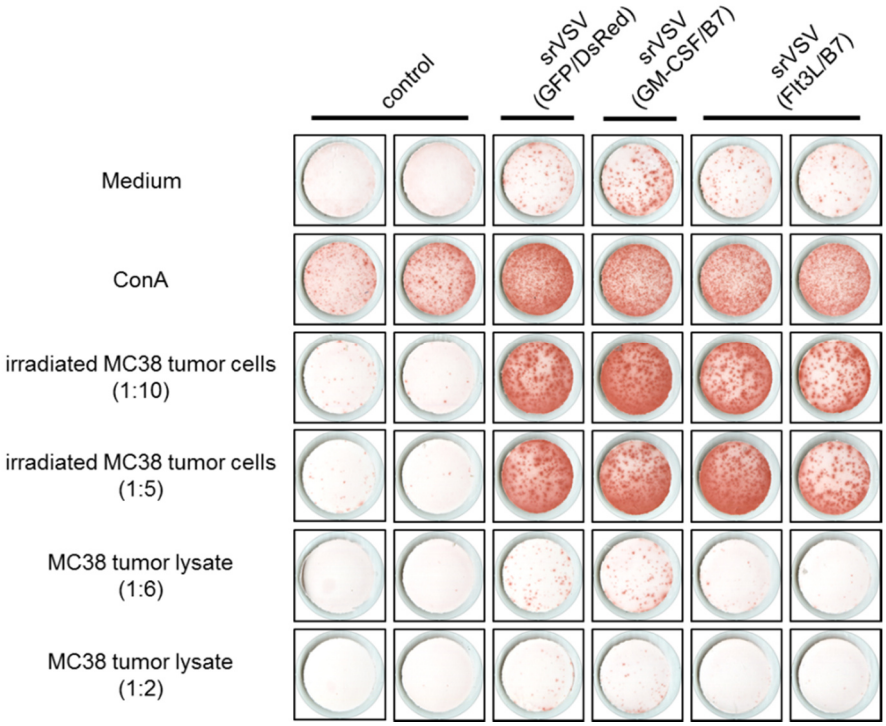

Figure 22: Analyzing IFNγ secretion by splenocytes from srVSV-cured mice after tumor rechallenge. 14 days after tumor rechallenge splenocytes were isolated and subjected to ELISpot analysis to assess the amount of tumor-specific, IFNγ-secreting immune cells. For antigen-specific recall, isolated splenocytes were stimulated either with irradiated MC38 tumor cells (ratio of tumor cells to spleen cells: 1:10 or 1:5) or with MC38 tumor lysates (ratio of tumor cells to spleen cells: 1:6 or 1:2) before they were tested in IFNγ ELISpot assay for the presence of reactive cells. Plain medium served as negative control and Concanavalin A (ConA) served as positive control. Representative wells for each mice and stimulant are shown.

3.1.7 Evaluating viral dose on therapy efficacy

The previous data described that srVSV armed with immunotherapeutic payload was curative for a fraction of treated mice. However, also one mouse treated with srVSV(GFP/DsRed) showed complete tumor remission. In the next *in vivo* experiment it was investigated whether a lower viral dose might enhance the antitumoral effect of transgene-armed srVSV as compared to srVSV(GFP/DsRed) since lower viral doses might diminish the effect of direct viral oncolysis and thereby enhance the influence of transgene expression on therapy efficacy. Furthermore, in that context it was investigated whether the viral dose has a strong influence on therapeutic efficacy. The previous experiment showed a slightly improved treatment response of

srVSV(Flt3L/B7) as compared to srVSV(GM-CSF/B7)-injected mice. Therefore, in the next *in vivo* experiment the therapeutic efficacy of srVSV(GFP/DsRed) was compared to srVSV(Flt3L/B7). As female mice showed an improved treatment response as compared to male mice, only female mice were used in the next *in vivo* study.

To this end, increasing doses of srVSV(Flt3L/B7) or srVSV(GFP/DsRed) (10^4, 10^5, 10^6 $TCID_{50}$) were injected intratumorally into MC38-bearing C57BL/6 mice and tumor growth was followed by caliper measurements.

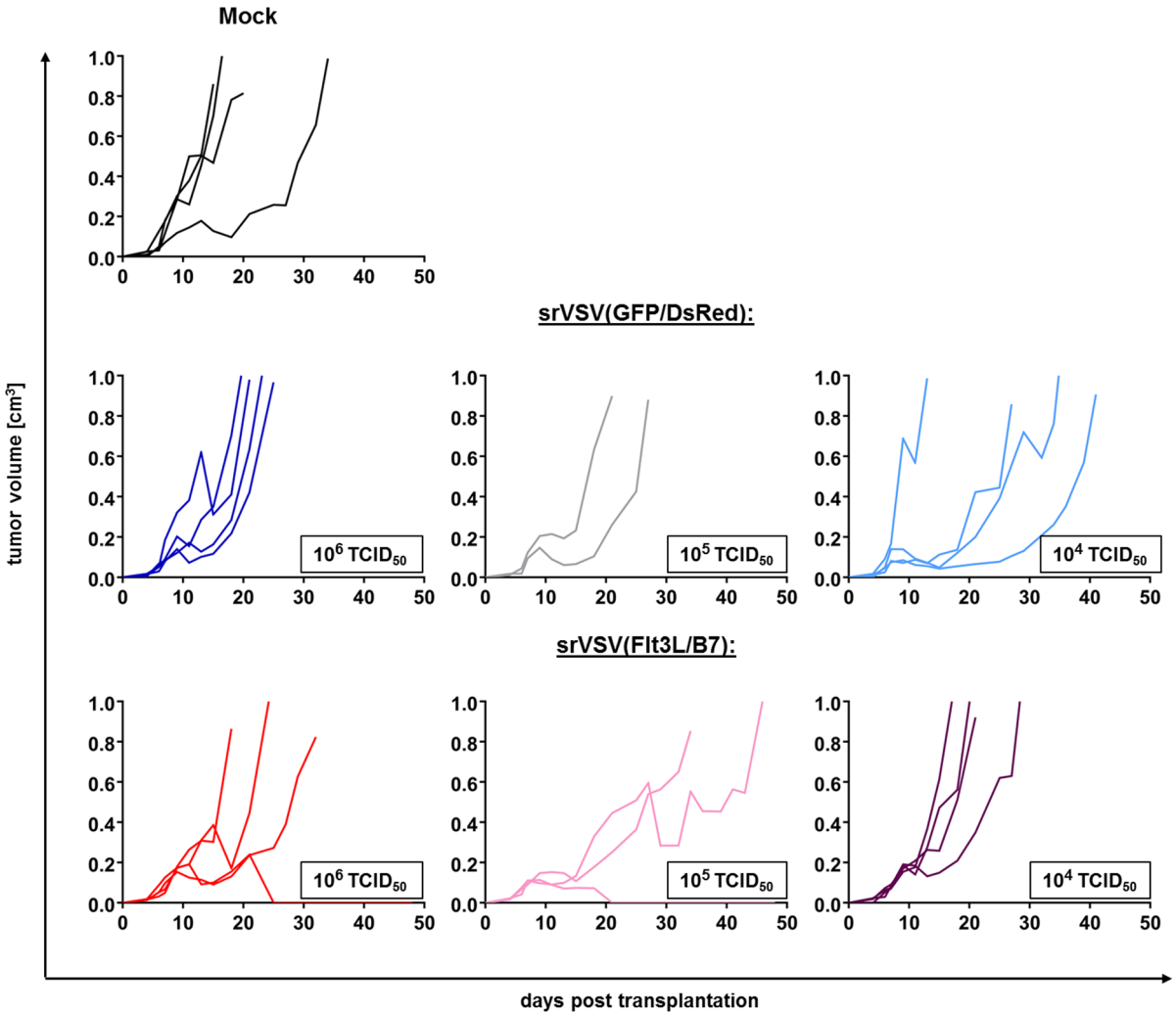

Figure 23: Tumor growth curves of subcutaneously growing MC38 tumors after intratumoral injections with different viral doses of srVSV(GFP/DsRed) or srVSV(Flt3L/B7). 2x10^6 MC38 tumor cells were subcutaneously implanted into the right flank of C57BL/6 mice. At an approximate size of 0.1 cm^3, tumors were injected intratumorally with escalating doses of 10^4, 10^5 and 10^6 $TCID_{50}$ srVSV(GFP/DsRed) or srVSV(Flt3L/B7) (5 injections: 7, 9, 11, 13 and 15 days post tumor implantation). Control mice received the same volume DMEM (Mock). Tumor growth curves of individual mice are shown.

Surprisingly, there was no pronounced difference observable between the different viral doses in both srVSV treatment groups (Figure 23). An increasing viral dose was not clearly correlated with an improved treatment response. A slight improvement for

srVSV(Flt3L/B7) as compared to srVSV(GFP/DsRed) was observable in the 10^5 $TCID_{50}$ cohort. However, this was not applicable to the 10^4 $TCID_{50}$ cohort. In conclusion, the data showed that there was no pronounced improvement in the therapeutic efficacy for srVSV(Flt3L/B7) as compared to srVSV(GFP/DsRed) detectable when a low viral dose was injected. Accordingly, injection of lower viral doses did not confirm an increased influence of srVSV-encoded Flt3L or B7 on the tumor growth of treated mice.

Also the overall tumor response to srVSV treatment was not as pronounced as observed in the previous *in vivo* experiment. Only two out of eleven srVSV(Flt3L/B7)-treated mice showed complete tumor regression. Treatment with srVSV(GFP/DsRed) was not curative at all. In contrast, four out of six female mice were cured by srVSV treatment in the previous experiment (srVSV(GFP/DsRed): 1/2; srVSV(GM-CSF/B7): 1/2; srVSV(Flt3L/B7): 2/2).

Thus, it remained to evaluate whether srVSV(Flt3L/B7) treatment induced a superior antitumoral effect compared to srVSV(GFP/DsRed) at all. To allow a more straightforward comparison, tumor volume and survival of srVSV(Flt3L/B7)- and srVSV(GFP/DsRed)-treated mice were compared independently of the viral dose.

The tumor sizes on day 13, the last day when all mice were alive, were quite comparable for both srVSV treatment groups (Figure 24A). The results of the AUC calculation showed a slightly increased treatment response for srVSV(Flt3L/B7) as compared to srVSV(GFP/DsRed), presumably arising due to the two tumor-free mice in the srVSV(Flt3L/B7) group (Figure 24B). However, the difference was not proven to be statistically significant. Mice of the srVSV(Flt3L/B7) group showed with an overall survival of 29 days a slightly prolonged survival as compared to srVSV(GFP/DsRed)-treated mice which showed an overall survival of 25 days (Figure 24C). However, the difference was again not statistically significant.

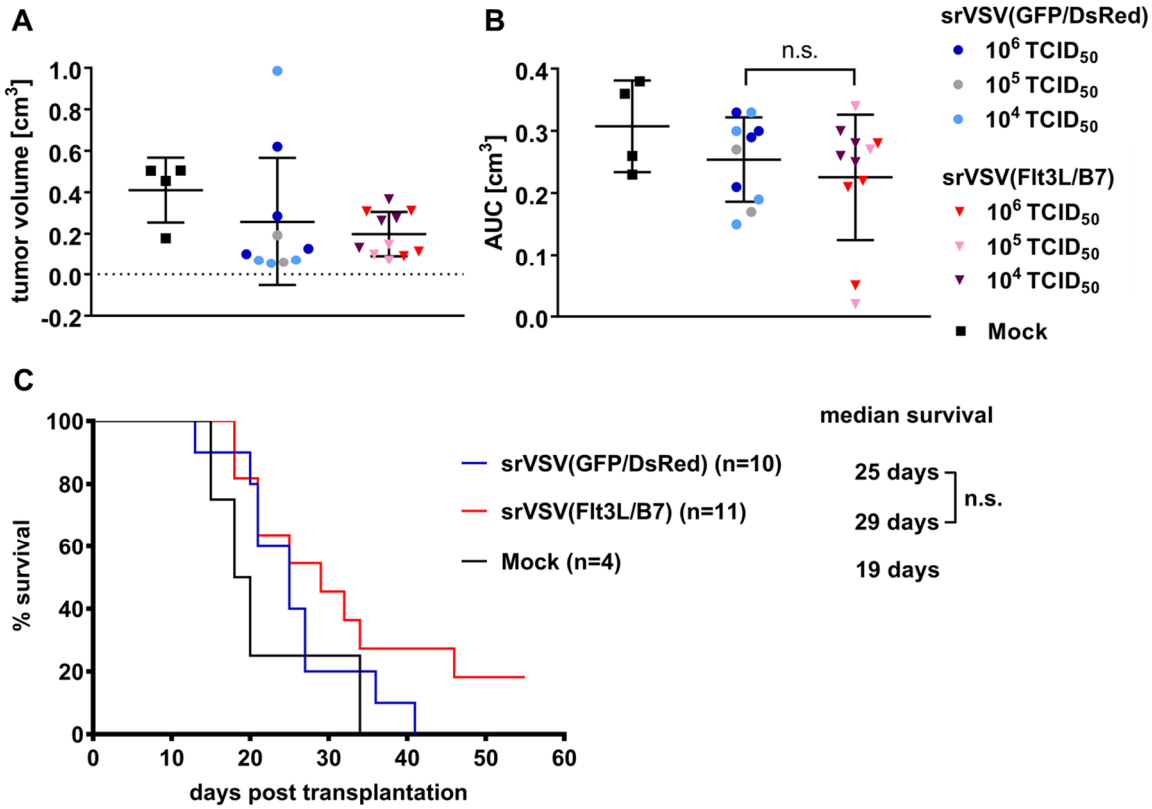

Figure 24: Comparison of the antitumor efficacy of srVSV(GFP/DsRed) and srVSV(Flt3L/B7). Mice treated with srVSV(GFP/DsRed) or srVSV(Flt3L/B7) as described in Figure 23 were compared in regard to tumor size and survival. (A) Distribution of tumor volumes of each group on day 13 post tumor implantation. Dots represent tumor volumes of each mouse. (means ± SD) (B) Group comparison was performed by calculating the AUC for each animal normalized to the day when the respective mouse was sacrificed. (means ± SD) n.s., not significant by unpaired t-test. (C) Kaplan-Meyer survival analysis. n.s. not significant by log-rank test. AUC: area under the curve

Overall, the first as well as the latest *in vivo* experiment indicated only a slightly improved treatment response for srVSV encoding immunotherapeutic transgenes as compared to srVSV(GFP/DsRed). However, the differences obtained in the present preclinical studies were not proven to be statistically significant.

3.2 Towards tumor-targeted delivery of immune checkpoint inhibitors by receptor-targeted AAV

One of the most promising approaches in cancer immunotherapy involves the inhibition of immune checkpoint receptors by PD-1- or PD-L1-specific mAbs. While the clinical response of these antibodies is at least in some cancer patients impressive, therapy is associated with a number of irAEs such as colitis and pneumonitis (Hamanishi et al, 2016; Michot et al, 2016). The toxicities are presumably fostered by the systemic administration of these antibodies that does not only promote the activation of immune responses at sites of tumor lesions but also in healthy organs. Therefore, this project aimed at the specific delivery of immune checkpoint inhibitors precisely to sites of tumor growth.

To this end, a strategy based on receptor-targeted AAV vectors was investigated for the tumor-specific delivery of immune checkpoint inhibitors. Her2/neu-targeted AAV vectors encoding αPD-1 and αPD-L1 were generated and characterized. After identifying a suitable syngeneic tumor mouse model for the *in vivo* studies, the generated vectors were analyzed for their capacity to mediate tumor-targeted delivery of immune checkpoint inhibitors.

3.2.1 Generation and characterization of AAV encoding αPD-1 and αPD-L1

In order to achieve the aim of tumor-targeted delivery of immune checkpoint inhibitors, Her2-AAV vectors packaging the coding sequence of αPD-1 and αPD-L1 were generated. For this purpose, the required AAV transfer vector plasmids encoding these inhibitors were cloned. The immune checkpoint inhibitors that were investigated in this study are composed of a scFv specific for mouse PD-1 or mouse PD-L1 and the Fc-portion of an human immunoglobulin IgG1 (Figure 25A). Furthermore, small epitope tags (HA, Myc) enabling protein detection are fused to the N- or C-terminal ends. The respective ORFs were amplified from the template plasmids pCG-sa-PD-1 or pCG-sa-PD-L1 using the primer pair scAAV-αPD-1/αPD-L1_for and scAAV-αPD-1/αPD-L1_rev. Subsequently, the amplified sequences were cloned into the AAV2 derived self-complementary transfer vector plasmid pscGFP-SFFV_2.0 using the restriction sites *NcoI/NotI* thereby replacing the GFP coding sequence and resulting in pscαPD-1-SFFV or pscαPD-L1-SFFV (Figure 25B). As control, a similar transfer vector plasmid was cloned that encodes only the constant region of immunoglobulin IgG1 (IgG-Fc) as well as the HA- and Myc-tag on the

N- and C-terminal ends, respectively. The coding sequence of IgG-Fc was amplified from pscαPD-L1-SFFV by the primer pair Fc-only_for and Fc-only_rev and ligated into the transfer vector plasmid via the restriction sites *Sfi/NotI* resulting in pscIgG-Fc-SFFV. The inserts of the resulting plasmids were sequenced confirming the absence of mutations. Subsequently, the cloned transfer vector plasmids were used for the production of either AAV vectors carrying a Her2/neu-specific DARPin or of AAV2 having an unmodified capsid.

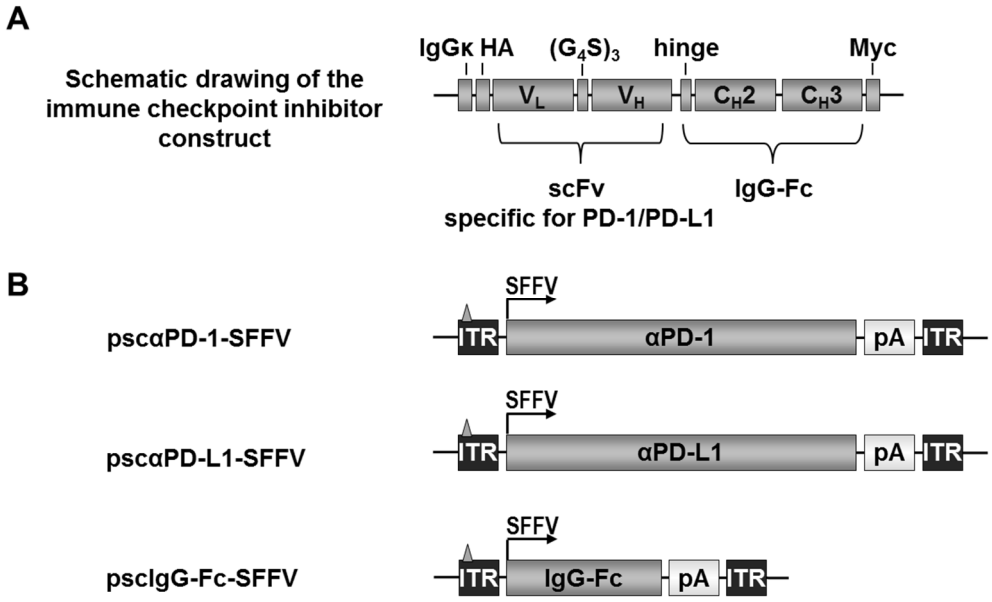

Figure 25: Cloning of AAV transfer vectors. (A) Schematic representation of the used immune checkpoint inhibitors: single-chain variable fragment (scFv) specific for mouse PD-1 or mouse PD-L1 is fused to the constant region of an IgG1 (IgG-Fc). IgGκ leader sequence for secretion and an HA- and Myc-tag for detection are fused to the N- and C-terminal ends, respectively. HA: hemagglutinin, v_H: variable region of the heavy chain, v_L: variable region of the light chain, c_H: constant region of the heavy chain, $(G_4S)_3$: Glycine-Serine-linker (B) Schematic representation of the cloned AAV transfer vectors. Triangle in the inverted terminal repeat (ITR) indicates the deleted terminal resolution site sequence from one ITR (McCarty, 2008). SFFV: spleen focus forming virus, pA: bovine growth hormone polyadenylation signal.

Receptor-targeted AAV vectors were generated by an adenovirus-helper free, four plasmid transfection system (Figure 26) (Xiao et al, 1998; Münch et al, 2013). The adenoviral helper functions for successful AAV production were provided by the plasmid pxx6-80 encoding the required helper genes E2A, E4 and VA RNA, but lacking the adenoviral structural and replication genes (Xiao et al, 1998). The AAV transfer vector encodes the transgene under the control of the spleen focus forming virus (SFFV) promotor and is packaged into the AAV capsid via the ITRs during vector production. The rep and cap genes, which are required for the replication of the ITR flanked transgene, for the synthesis of the capsid proteins and for the genome packaging, are

provided by the plasmid pRC-VP2$_{KO}$-HSPG$_{mut}$ (Münch et al, 2013). Compared to pRC, used for the production of AAV2, the plasmid pRC-VP2$_{KO}$-HSPG$_{mut}$ carries the two point mutations R585A and R588A in order to ablate natural receptor binding to HSPG (Kern et al, 2003; Opie et al, 2003; Münch et al, 2013). In addition, incorporation of unmodified VP2 was prevented by mutating the start codon required for the expression of VP2 (Münch et al, 2013). For the incorporation of the Her2/neu-specific DARPin D9.29, the plasmid pHer2/neu$^{D9.29}$-HisXa-VP2$_{KO}$ encoding the DARPin-VP2-fusion protein was used. The latter plasmid has the same mutations as described for pRC-VP2$_{KO}$-HSPG$_{mut}$ (Münch et al, 2013). Upon co-transfection of these plasmids into HEK-293T cells, recombinant AAV vector particles were produced and purified via iodixanol density gradient purification.

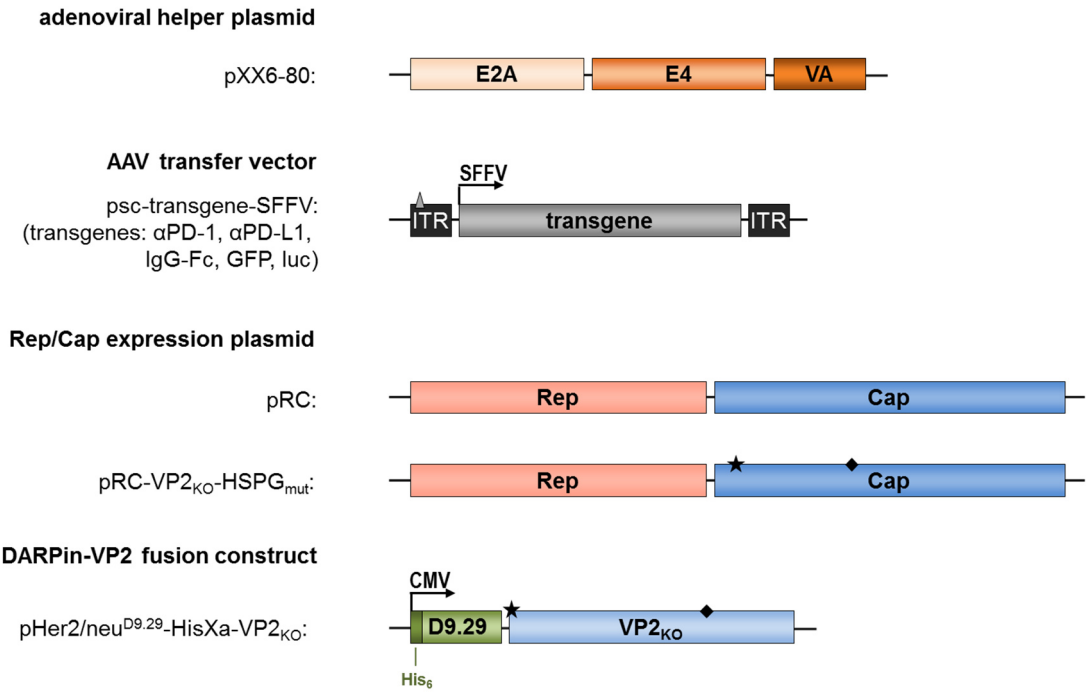

Figure 26: Schematic representation of constructs required for the production of recombinant AAV vectors. The adenoviral helper plasmid pXX6-80 delivers the adenoviral helper genes E2A, A4 and VA RNA required for AAV production. The transfer vector encodes the transgene (αPD-1, αPD-L1, IgG-Fc, GFP, luciferase (luc)) that is flanked by two inverted terminal repeats (ITR). The grey triangle in the ITR indicates the deleted terminal resolution site sequence from one ITR (McCarty, 2008). The non-structural proteins AAP, Rep78, Rep68, Rep52, Rep40 and the capsid proteins VP1, VP2 and VP3 are provided by pRC. For the generation of receptor-targeted AAV vectors pRC-VP2$_{KO}$-HSPG$_{mut}$ was used instead. Here the natural receptor binding to HSPG was deleted by introducing the two point mutations R585A and R588A (indicated with a black diamond). Furthermore, incorporation of unmodified VP2 is prevented by deleting the VP2 start codon (indicated with a black star). The Her2/neu-specific DARPin D9.29 fused to the N-terminus of the VP2 capsid protein is delivered by pHer2/neu$^{D9.29}$-HisXa-VP2$_{KO}$. SFFV: spleen-focus forming virus, CMV: cytomegalovirus.

In order to characterize AAV preparations, DNA containing vector particles were quantified by qPCR using a primer pair specific for the ITRs (D'Costa et al, 2016).

Defined copy numbers of the linearized transfer vector plasmid pscGFP-SFFV were used as a standard for quantification.

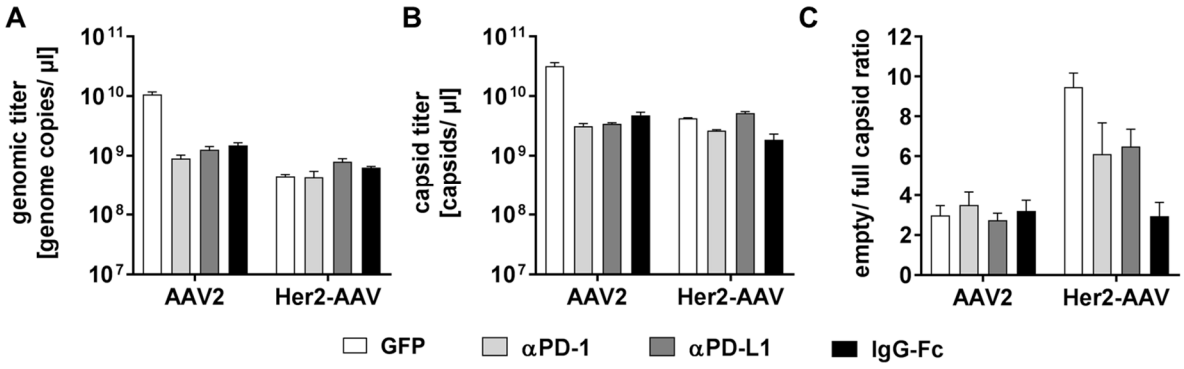

Figure 27: Genomic titers, capsid titers and packaging efficiency of iodixanol-purified vector stocks. (A) DNA-containing AAV particles per µl were quantified by qPCR using ITR-specific primers (genomic titer). (n=3, means ± SD) (B) The amount of empty and DNA-containing capsids per µl was determined by ELISA using the αAAV2 antibody clone A20 that is specific for intact AAV capsids. (n=3, means ± SD) (C) The quotient of capsid to genomic titer provides the empty/full capsid ratio and represents the packaging efficiency of the vector. The errors for the empty/full capsid ratios were calculated by Gaussian error propagation. (n=3, means ± SD)

Overall, the genomic titers of the different AAV vector preparations were similar, even though the data showed a trend for slightly higher genomic titers for AAV2 (about 2-fold) as compared to Her2-AAV (Figure 27A). The AAV preparations among the different transgenes were proven to be similar in regard to genomic titers, with an exception for $AAV2^{GFP}$.

The amount of DNA-containing and empty vector particles was analyzed by an ELISA using a capsid-specific antibody. The results revealed again similar capsid titers for the different AAV vector preparations (Figure 27B). The packaging efficiencies calculated as quotient of the capsid and the genomic titer were similar for the different transgenes in AAV2 vector preparations (Figure 27C). The best packaging efficiency in Her2-AAV preparations was observed for the smallest transfer vector construct IgG-Fc, suggesting that the size of the transgene may have influenced the number of empty particles. However, the empty/full capsid ratios for the other Her2-AAV vector preparations were increased as compared to AAV2. Taken together, these data demonstrate that Her2-AAV vectors encoding αPD-1 and αPD-L1 were producible with comparable titers and packaging efficiencies to that of the GFP-encoding counterpart.

3.2.2 AAV-mediated expression of αPD-1 and αPD-L1

Renal cell carcinoma (RCC) is considered to be an immunogenic tumor and has been subjected to various immunotherapeutic approaches (Itsumi & Tatsugami, 2010). Immune checkpoint blockade of the PD-1/PD-L1 axis has shown promising clinical results for patients with advanced RCC eventually leading to the marketing authorization of nivolumab for the treatment of this malignancy (McDermott et al, 2015; Bardhan et al, 2016). Therefore, the newly generated AAV vector particles encoding αPD-1 and αPD-L1 were characterized on the mouse RCC cell line RENCA. Furthermore, this cell line has been proven to be responsive to PD-1/PD-L1 inhibition (Hirayama et al, 2016). However, in order to enable the cell entry of Her2/neu-retargeted AAV vectors, RENCA cells were used for analysis that had been genetically engineered to express the target receptor Her2/neu (RENCA-Her2/neu) (Maurer-Gebhard et al, 1998).

AAV-mediated transgene expression of αPD-1, αPD-L1 and IgG-Fc was analyzed in cell culture supernatants of AAV-transduced RENCA-Her2/neu cells by Western blot analysis using an HA-tag-specific antibody. Cell culture supernatants of cells transduced with $AAV2^{GFP}$ and $Her2\text{-}AAV^{GFP}$ served as negative control.

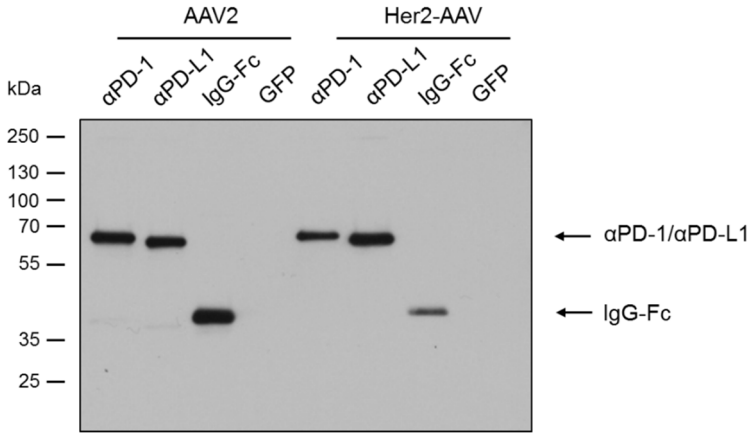

Figure 28: Transgene expression following AAV transduction of RENCA-Her2/neu cells. RENCA-Her2/neu cells were incubated with AAV2 or Her2-AAV encoding αPD-1, αPD-L1, IgG-Fc or GFP (GOI: 450,000). Cell culture supernatants were harvested four days post transduction and analyzed by Western blot analysis using a HA-tag-specific antibody.

Specific bands were detected for αPD-1 and αPD-L1 between 55-70 kDa as well as for IgG-Fc between 35-55 kDa revealing the successful expression of the respective protein following gene transfer by AAV2 and Her2-AAV (Figure 28). The proteins were detected at the expected size (Engeland et al, 2014).

3.2.3 Establishing an ELISA for the detection of αPD-1 and αPD-L1

After showing the successful AAV-mediated expression of αPD-1 and αPD-L1, the next step was the quantification of αPD-1 and αPD-L1 protein amounts in cell culture supernatants of AAV-transduced cells. For this purpose, an ELISA was established. Initially, two different ELISA approaches were compared for their ability to detect αPD-1 and αPD-L1. In the first approach, commercially available recombinant PD-L1 or PD-1 were coated on the ELISA plate and protein binding was detected via an HA-tag-specific antibody (Approach 1, Figure 29A) (Engeland et al, 2014). In the second approach, an HA-tag-specific antibody was used as capture antibody and αPD-1/αPD-L1 binding was detected via an Fc-specific antibody (Approach 2, Figure 29B). To compare both approaches, RENCA-Her2/neu cells were transduced with AAV vectors encoding αPD-1 or αPD-L1 and cell culture supernatants were analyzed by the aforementioned ELISA approaches. Cell culture supernatants of cells transduced with AAV2 and Her2-AAV encoding GFP served as negative control.

Only for approach 2 a specific detection of both inhibitors was feasible (Figure 29D). Approach 1 revealed a lower signal for αPD-L1 or a signal close to the background for αPD-1 (Figure 29C). A reason for the variable outcome could be the better accessibility of the detection antibody to its antigen in approach 2 as compared to approach 1. Another possible reason could be a higher affinity of the αHA antibody to the HA-tag (Approach 2) as compared to the affinity of αPD-L1/αPD-1 to their target proteins PD-L1/PD-1 (Approach 1). Furthermore, it cannot be excluded that the PD-1 and PD-L1 proteins used for coating of the ELISA plates are not correctly folded. Consequently, in the following analysis protein amounts were quantified by sandwich ELISA using Fc- and HA-tag-specific antibodies according to approach 2.

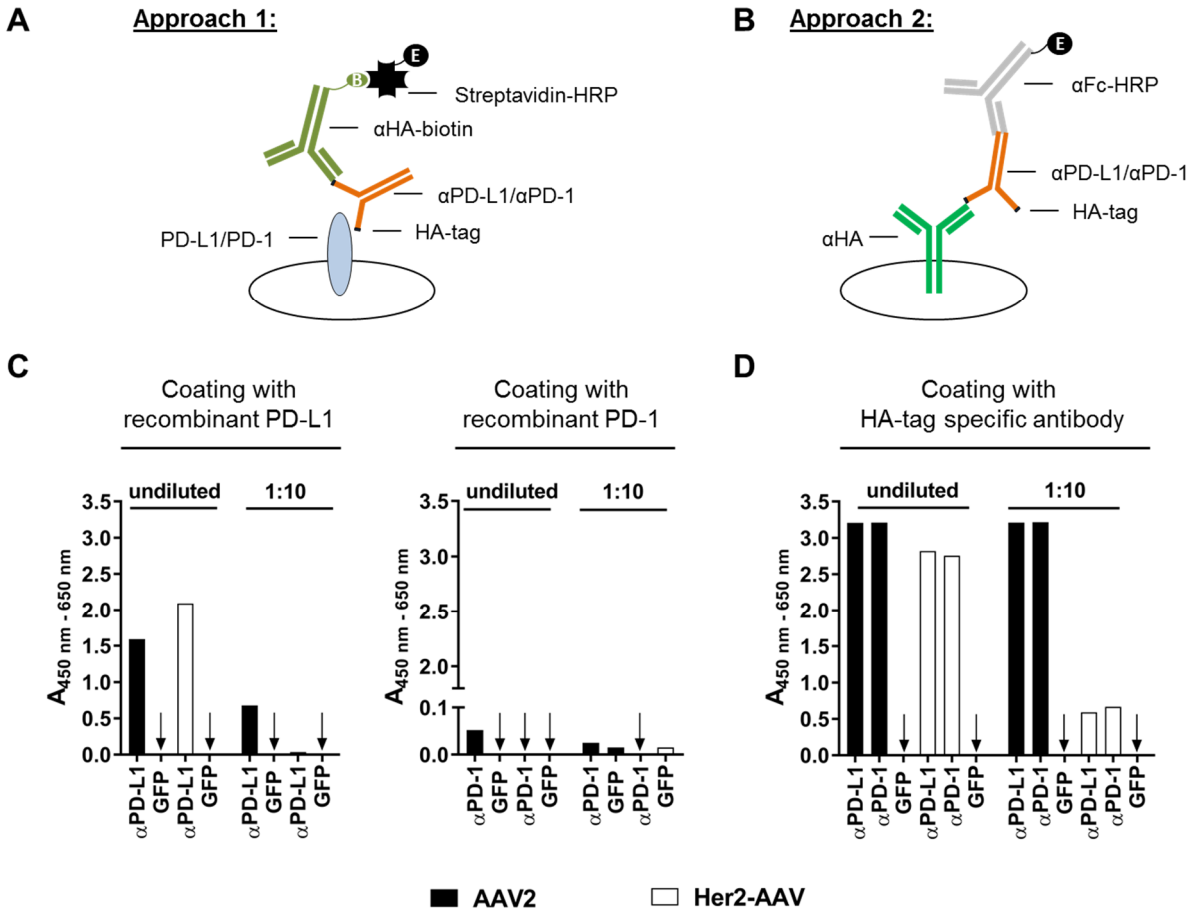

Figure 29: Establishing an ELISA for the detection of αPD-1 and αPD-L1. Schematic representations of two different ELISA approaches either using (A) recombinant PD-L1 or PD-1 (Approach 1) or (B) an HA-tag-specific antibody (Approach 2) to capture αPD-L1 or αPD-1. To assess both approaches, $8*10^3$ RENCA-Her2/neu cells were seeded per well of a 96-well plate and transduced with AAV2$^{\alpha PD\text{-}L1}$, AAV2$^{\alpha PD\text{-}1}$, Her2-AAV$^{\alpha PD\text{-}L1}$ or Her2-AAV2$^{\alpha PD\text{-}1}$ (5 µl) on the next day. As mock control, cells were transduced with AAV2^{GFP} or Her2-AAV^{GFP}. Cell culture supernatants were collected four days after transduction and subjected to the ELISA either undiluted or diluted 1:10 in PBS. Samples were analyzed by (C) approach 1 or (D) approach 2. Arrow indicates that no signal above background was detected.

The established ELISA was also considered to be a suitable approach to detect *in vivo* delivered immune checkpoint inhibitors in organ lysates after systemic administration of AAV vectors into tumor-bearing mice. Since mouse organ lysates will be not only prepared with mechanical but also with chemical methods using an appropriate lysis buffer, the influence of the used lysis buffer on protein detection in the ELISA was investigated. In addition, it was assessed whether a freeze/thaw cycle of the sample impaired the detectability of the analyzed proteins. To investigate the influence of the lysis buffer, three-fold serial dilutions of cell culture supernatants of AAV2$^{\alpha PD\text{-}1}$-, Her2-AAV$^{\alpha PD\text{-}1}$-, AAV2$^{\alpha PD\text{-}L1}$- and of Her2-AAV$^{\alpha PD\text{-}L1}$-transduced RENCA-Her2/neu cells were prepared using the lysis buffer as diluent and analyzed by ELISA. In addition, cell culture

supernatants were stored for one day either at 4°C or frozen at -80°C and diluted in PBS for the ELISA.

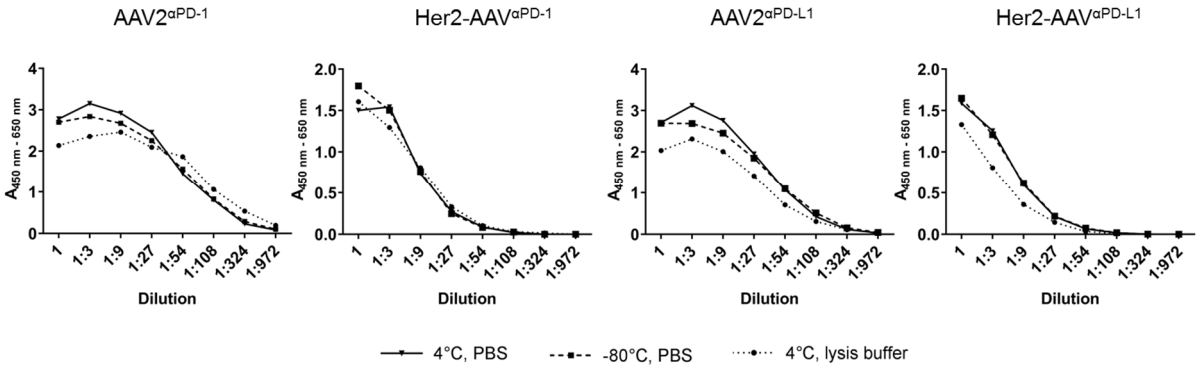

Figure 30: Influence of sample storage conditions and diluting buffer on protein detectability in the ELISA. $8*10^3$ RENCA-Her2/neu cells were seeded per well of a 96-well plate and on the following day transduced with 5 µl AAV2$^{\alpha PD\text{-}1}$, Her2-AAV$^{\alpha PD\text{-}1}$, AAV2$^{\alpha PD\text{-}L1}$ or Her2-AAV$^{\alpha PD\text{-}L1}$. Cell culture supernatants were collected four days after transduction and stored for one day either at 4°C or frozen at -80°C. Serial three-fold dilutions of the supernatants were prepared using PBS or lysis buffer as diluent and subsequently subjected to the ELISA.

The curves obtained under the different conditions were quite similar for all four samples tested (Figure 30). This observation indicated that the lysis buffer did not impair the detectability of αPD-1 and αPD-L1. Furthermore, a freeze/thaw cycle of the sample did not affect protein detection. Accordingly, the used lysis buffer is suitable for the preparation of the organ lysates and the subsequent detection of *in vivo* expressed αPD-1 and αPD-L1 by ELISA.

3.2.4 Quantification of AAV-encoded αPD-1 and αPD-L1

For quantification of the αPD-1 and αPD-L1 amounts by the established ELISA, protein standards were generated. For this purpose, αPD-1 and αPD-L1 were transiently expressed in HEK-293T cells and purified out of the cell culture supernatants with high purity by Protein A affinity purification. Purified proteins were analyzed by Coomassie-stained SDS-PAGE (Figure 31A) and Western blot analysis (Figure 31B) revealing signals at the expected size.

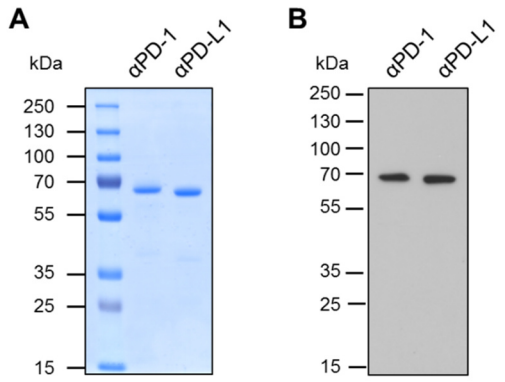

Figure 31: Affinity purification of αPD-1 and αPD-L1. 1.8x10^7 HEK-293T cells were seeded per 175 cm^2 flask and transfected with 35 µg of the respective pCG-derived expression plasmids on the next day. Supernatants were harvested 24 h, 48 h and 72 h post transfection. Proteins were affinity-purified by Protein A beads. (A) Coomassie-stained SDS-PAGE and (B) Western blot analysis from affinity-purified αPD-1 and αPD-L1 are shown. 1 µg protein was applied for the Coomassie-stained SDS-PAGE and 100 ng for Western blot analysis. In the Western blot analysis a Myc-tag-specific antibody was used for the specific detection of αPD-1 and αPD-L1.

To assess the sensitivity of the established ELISA, the assay was performed with serial two-fold dilutions of the generated αPD-1 or αPD-L1 standard. Surprisingly, the ELISA data showed a higher sensitivity for αPD-1 as compared to αPD-L1 (Figure 32). Since the HA-tag is directly fused to the scFv, binding of the HA-tag-specific capture antibody to the immune checkpoint inhibitor could be influenced by different biochemical properties of the scFv's, such as folding or stability, probably explaining the difference in sensitivity. The lower limits of protein amounts that could be detected in different experiments varied from 1.6 ng/ml down to 0.4 ng/ml for αPD-1. For αPD-L1 protein amounts ranging from 3.2 ng/ml down to 1.6 ng/ml were detectable by the ELISA.

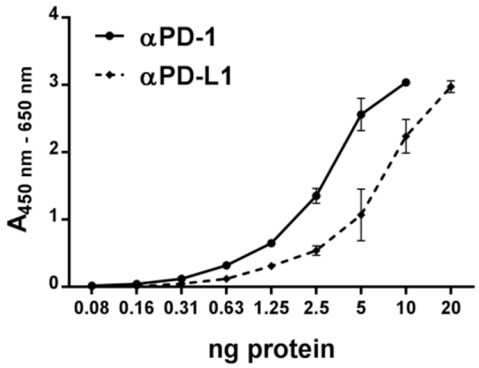

Figure 32: Sensitivity of the established ELISA. Serial two-fold dilutions of purified αPD-1 and αPD-L1 were prepared and applied to the ELISA. Proteins were detected by HA-tag- and Fc-specific antibodies as described previously. (n=2; means ± SD)

Next, the amount of AAV-encoded αPD-1 and αPD-L1 was quantified in cell culture supernatants of RENCA-Her2/neu cells that had been transduced with AAV2$^{\alpha PD\text{-}1}$,

AAV2$^{\alpha PD\text{-}L1}$, Her2-AAV$^{\alpha PD\text{-}1}$ and Her2-AAV$^{\alpha PD\text{-}L1}$. As negative control, cell culture supernatants of AAV2^{GFP}- and Her2-AAV^{GFP} -transduced cells were used.

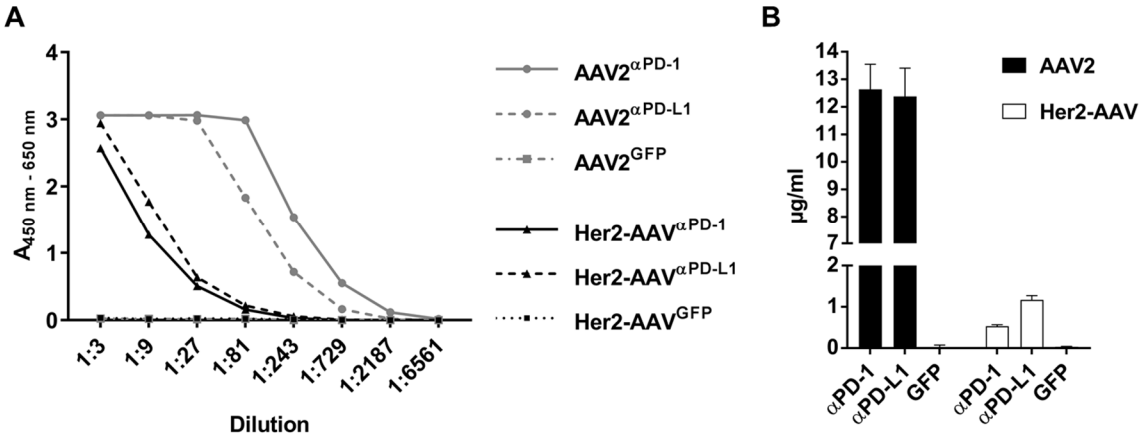

Figure 33: Quantification of AAV-encoded αPD-1 and αPD-L1 in cell culture supernatants. (A) RENCA-Her2/neu cells were incubated with AAV2$^{\alpha PD\text{-}1}$, AAV2$^{\alpha PD\text{-}L1}$, AAV2^{GFP}, Her2-AAV$^{\alpha PD\text{-}1}$, Her2-AAV$^{\alpha PD\text{-}L1}$ or Her2-AAV^{GFP} (GOI 450,000) and four days later cell culture supernatants were harvested. Serial three-fold dilutions of cell culture supernatants were prepared and subjected to the ELISA. (B) For the quantification of αPD-1 and αPD-L1 in cell culture supernatants, purified αPD-1 and αPD-L1 were used as standard. (n=3, means ± SD)

The analysis revealed a higher amount of αPD-1 and αPD-L1 in cell culture supernatants of AAV2-transduced cells as compared to Her2-AAV (Figure 33A). Quantification of the data using the generated protein standards revealed concentrations of 12.6 ± 0.9 µg/ml for AAV2$^{\alpha PD\text{-}1}$ (n=3, mean ± SD), 12.4 ± 1.0 µg/ml for AAV2$^{\alpha PD\text{-}L1}$ (n=3, mean ± SD), 0.53 ± 0.04 µg/ml for Her2-AAV$^{\alpha PD\text{-}1}$ (n=3, mean ± SD) and 1.2 ± 0.1 µg/ml for Her2-AAV$^{\alpha PD\text{-}L1}$ (n=3, mean ± SD) (Figure 33B). In summary, the Western blot and ELISA analyses proved the AAV-mediated expression of αPD-1 as well as αPD-L1 after transduction of RENCA-Her2/neu cells.

3.2.5 Functionality of AAV-encoded αPD-L1

In the previous chapters it was shown that AAV-encoded αPD-1 and αPD-L1 were expressed after transduction of RENCA-Her2/neu cells. But whether these AAV-expressed inhibitors recognize their target antigen PD-L1 or PD-1 still needs to be answered.

The melanoma cell line B16-F10 expresses PD-L1 and upregulates the expression of PD-L1 upon stimulation with IFNγ (Fu et al, 2014; Nagato et al, 2014). Thus, specific binding of AAV-encoded αPD-L1 to its antigen was analyzed by incubating IFNγ-stimulated or unstimulated B16-F10 tumor cells with cell culture supernatants of AAV-transduced

RENCA-Her2/neu cells. In addition, specific binding of AAV-encoded αPD-L1 to PD-L1 expressed on RENCA-Her2/neu cells was investigated. Binding was analyzed by flow cytometry using a fluorophore-labelled Fc-specific antibody. To exclude that the Fc-part mediated cell surface binding, cell culture supernatants of cells transduced with AAVs encoding IgG-Fc were used as negative controls. Furthermore, tumor cells were incubated with purified recombinant αPD-L1. Upregulation of PD-L1 expression on IFNγ-stimulated tumor cells was assessed by the commercially available αPD-L1 antibody MIH5.

The flow cytometry results showed a higher PD-L1 expression level on unstimulated RENCA-Her2/neu cells as compared to unstimulated B16-F10 cells (Figure 34). Stimulation with IFNγ induced an upregulation of PD-L1 expression on both tumor cell lines. The binding analysis revealed a specific binding of recombinant and AAV-encoded αPD-L1 on IFNγ-stimulated tumor cells. For AAV2$^{\alpha PD\text{-}L1}$ and recombinant αPD-L1 a comparatively low binding was observed on unstimulated RENCA-Her2/neu cells and no binding on unstimulated B16-F10 cells. No binding was detected for Her2-AAV$^{\alpha PD\text{-}L1}$ on both unstimulated tumor cells. This correlation between the level of PD-L1 on the tumor cell surface and the binding efficiency of recombinant and AAV-encoded αPD-L1 indicates the specificity of the inhibitor for PD-L1. Furthermore, no signals were detected for the negative controls AAV2^{GFP} and Her2-AAV^{GFP} as well as for AAV2$^{IgG\text{-}Fc}$ and Her2-AAV$^{IgG\text{-}Fc}$. Consequently, the flow cytometry analysis demonstrated that AAV-encoded αPD-L1 specifically recognized its target antigen PD-L1.

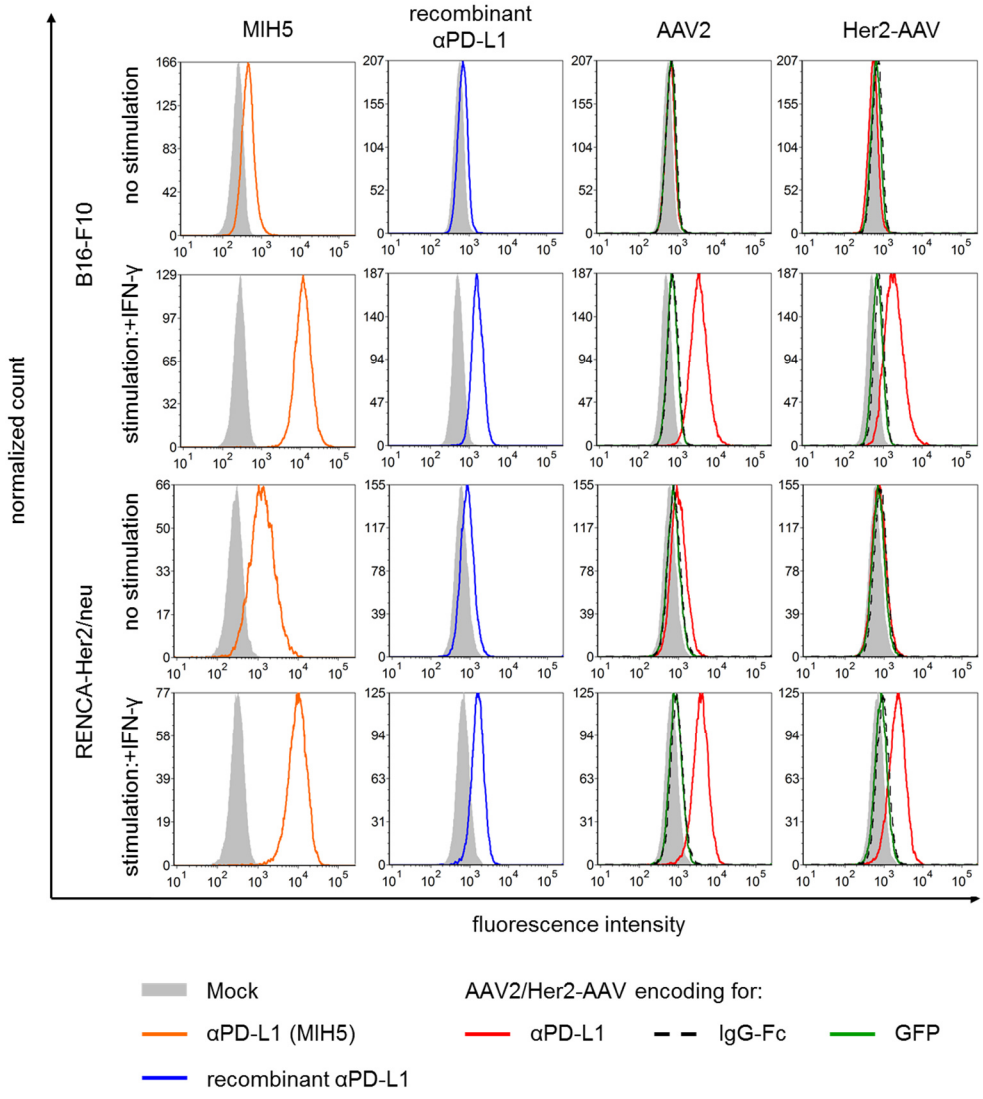

Figure 34: Specific binding of AAV-encoded αPD-L1 to IFNγ-stimulated tumor cells. B16-F10 and RENCA-Her2/neu cells were stimulated with 500 U/ml IFNγ for three days and used for the analysis of αPD-L1 binding by flow cytometry. 1. Colum: B16-F10 and RENCA-Her2/neu tumor cells were stained with commercially available PE-labelled αPD-L1 antibody (clone: MIH5) to analyze PD-L1 surface expression on unstimulated and IFNγ-stimulated tumor cells. As control, cells were incubated with the respective isotype control (Mock). 2. Colum: Unstimulated or IFNγ-stimulated tumor cells were incubated with 5 µg purified recombinant αPD-L1 and binding was detected using a FITC-labelled Fc-specific antibody. As control, cells were incubated with the Fc-specific antibody only (Mock). 3. & 4. Colum: RENCA-Her2/neu cells were transduced with $AAV2^{\alpha PD\text{-}L1}$, $AAV2^{IgG\text{-}Fc}$, $AAV2^{GFP}$, $Her2\text{-}AAV^{\alpha PD\text{-}L1}$, $Her2\text{-}AAV^{IgG\text{-}Fc}$ or $Her2\text{-}AAV^{GFP}$ (GOI 450,000) and cell culture supernatants were harvested four days later. Stimulated or unstimulated tumor cells were incubated with 400 µl of the respective cell culture supernatants. Binding to the cell surface was detected using a FITC-labelled Fc-specific antibody followed by flow cytometry. Mock-treated cells were incubated with the Fc-specific antibody only. Cell counts were normalized to peak value.

3.2.6 Functionality of AAV-encoded αPD-1

In order to assess PD-1 recognition of AAV-encoded αPD-1, HT1080 cells were genetically engineered to express PD-1. The cDNA sequence of mouse PD-1 (NCBI X67914.1) was cloned into a lentiviral transfer vector plasmid via the restriction sites

SpeI/BamHI resulting in pS-mPD1-IP-W. The inserts of the resulting plasmid was sequenced confirming the absence of mutations. VSV-G pseudotyped lentiviral vectors were generated using the cloned transfer vector plasmid. Subsequently, these vectors were used for the transduction of HT1080 cells. Successfully transduced cells were selected via the antibiotic puromycin for PD-1 positive cells. Surface expression of PD-1 on the newly generated HT1080-PD-1 cells was proven by flow cytometry using a PD-1-specific antibody (clone HA2-7B1) (Figure 35A).

Parental HT1080 and HT1080-PD-1 cells were used to analyze the functionality of AAV-encoded αPD-1. For this, HT1080 or HT1080-PD-1 cells were incubated with cell culture supernatants of AAV-transduced RENCA-Her2/neu cells. Subsequently, binding was analyzed by flow cytometry using a fluorophore-labeled Fc-specific antibody. Recombinant αPD-1 was also applied to the assay. As negative control, supernatants of cells that had been transduced with AAV vectors encoding IgG-Fc were used. Specific binding to PD-1 expressing HT1080 cells was detected for recombinant αPD-1, AAV2$^{\alpha PD\text{-}1}$ and Her-AAV$^{\alpha PD\text{-}1}$ (Figure 35B). In contrast, no binding was observed for the negative controls AAV2$^{IgG\text{-}Fc}$ and Her2-AAV$^{IgG\text{-}Fc}$.

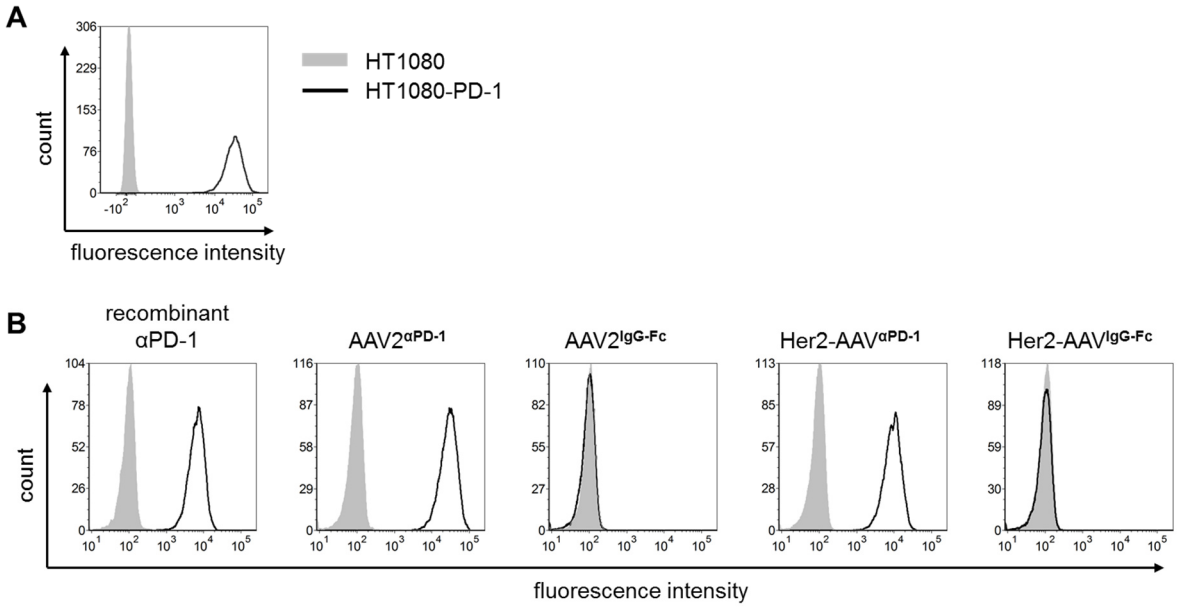

Figure 35: Specific binding of AAV-encoded αPD-1 to HT1080 cells stably expressing PD-1. (A) Generation and characterization of transgenic HT1080 cells expressing mouse PD-1. Parental HT1080 cells were transduced with VSV-G pseudotyped lentiviral vectors encoding mouse PD-1 as well as a puromycin resistance. After selecting puromycin resistant cells, surface expression of mouse PD-1 was proven by flow cytometry using a PE-labelled PD-1-specific antibody (clone: HA2-7B1). As negative control, parental HT1080 cells were used. (B) Parental HT1080 (grey filled curve) or HT1080-PD-1 cells (black empty curve) were either incubated with recombinant, purified αPD-1 (4 µg) or with 400 µl cell culture supernatants of AAV-transduced RENCA-Her2/neu cells (GOI 450,000). Binding to cell surface was detected using a FITC-labelled Fc-specific antibody followed by flow cytometry analysis.

PD-1 is physiologically not expressed on HT1080 cells but on immune cells such as activated T cells. Accordingly, binding of AAV-encoded αPD-1 was also investigated on activated mouse splenocytes. For this, mouse splenocytes were isolated from C57BL/6 mice, depleted of red blood cells and subsequently activated with PMA and ionomycin for two days to induce PD-1 expression. For the binding assay, the stimulated splenocytes were incubated with cell culture supernatants of AAV2$^{αPD-1}$-transduced RENCA-Her2/neu cells or purified recombinant αPD-1. As negative controls, supernatants of cells transduced with AAV2^{GFP} or AAV2^{IgG-Fc} were used. Binding was analyzed by flow cytometry using a fluorophore-labelled Fc-specific antibody.

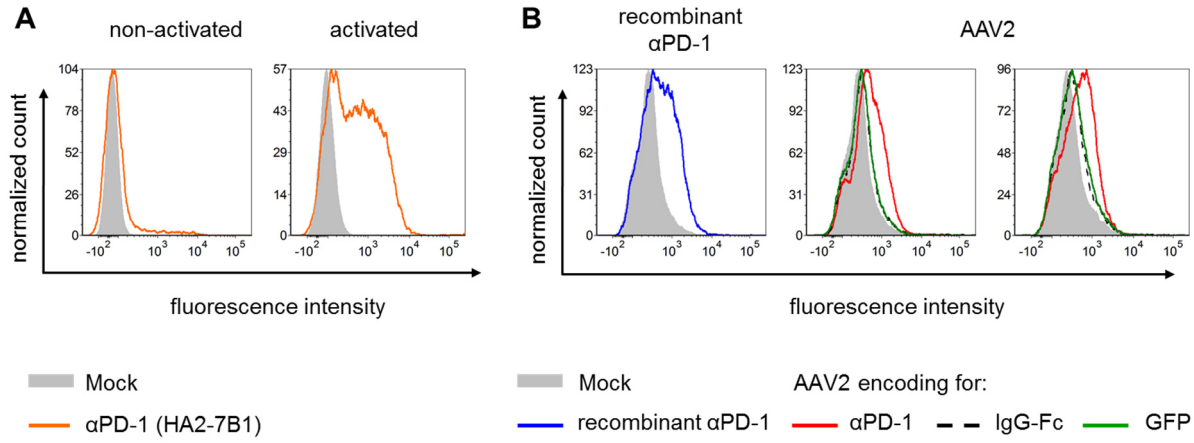

Figure 36: Binding of AAV2-encoded αPD-1 to stimulated mouse splenocytes. (A) Splenocytes from C57BL/6 mice were activated for two days with PMA and ionomycin. Subsequently, cells were stained using a PE-labelled PD-1-specific antibody (clone: HA2-7B1) and analyzed by flow cytometry. As negative control, cells were incubated with an appropriate isotype control (Mock). Live/dead staining was performed to exclude dead cells from the analysis. (B) RENCA-Her2/neu cells were incubated with AAV2 encoding αPD-1, IgG-Fc or GFP (GOI: 500,000) and cell culture supernatants were collected four days later. For analysis, activated mouse splenocytes were incubated either with purified recombinant αPD-1 (4 µg) or with 400 µl cell culture supernatants of AAV-transduced RENCA-Her2/neu cells. Binding to the cell surface was detected using a FITC-labelled Fc-specific antibody and flow cytometry. As control, cells were incubated with the Fc-specific antibody only (Mock). Live/dead staining was performed to exclude dead cells from the analysis. For AAV2 two different donors and representative histograms are shown. Cell counts were normalized to peak value.

PD-1 expression of the activated splenocytes was confirmed by flow cytometry using the commercially available PD-1-specific-antibody HA2-7B1 (Figure 36A). The binding assay revealed binding for recombinant and AAV2-encoded αPD-1 whereas IgG-Fc showed no binding on activated splenocytes (Figure 36B). Taken together, these data demonstrate that AAV-encoded αPD-1 specifically recognized its target antigen.

3.2.7 Detection of *in vivo* delivered immune checkpoint inhibitors

The previous chapters proved the generation of Her2-AAV vectors expressing functional αPD-1 and αPD-L1. Consequently, the next step was to investigate whether the generated vectors enable the delivery of these inhibitors *in vivo*.

In previous studies tumor-specific gene transfer by Her2-AAV was shown in xenograft tumor mouse models but has not been analyzed in immunocompetent mice so far (Münch et al, 2013; Münch et al, 2015). Hence, in a pilot-experiment the AAV-mediated *in vivo* delivery of immune checkpoint inhibitors was assessed in immunodeficient mice first. Thereby, it was possible to investigate whether αPD-1 and αPD-L1 are expressed *in vivo* without the aggravating factor of the immune system which possibly reduces the efficiency of the *in vivo* gene transfer.

RENCA-Her2/neu cells were subcutaneously transplanted into NSG mice and tumor growth was monitored until tumors reached a volume of about 70 mm^3. Subsequently, $AAV2^{\alpha PD\text{-}1}$, $AAV2^{\alpha PD\text{-}L1}$, $Her2\text{-}AAV^{\alpha PD\text{-}1}$ or $Her2\text{-}AAV^{\alpha PD\text{-}L1}$ were injected intratumorally. The local administration route was chosen to evaluate whether AAV2 and Her2-AAV mediate the transgene expression in RENCA-Her/neu tumors *in vivo* at all. To additionally investigate whether the transgenes can be delivered into the tumor after systemic vector administration, $Her2\text{-}AAV^{\alpha PD\text{-}1}$ and $Her2\text{-}AAV^{\alpha PD\text{-}L1}$ were injected intravenously through the lateral tail vein of tumor-bearing NSG mice. As control, $AAV2^{\alpha PD\text{-}L1}$ was also applied intravenously. An untreated RENCA-Her2/neu-bearing NSG mouse served as negative control. Seven days post vector application, tumors were explanted and tumor lysates were prepared. For the detection of αPD-1 and αPD-L1 the prepared tumor lysates were applied to the established ELISA (chapter 3.2.3).

The ELISA proved the presence of αPD-1 and αPD-L1 in all tumor lysates of mice injected intratumorally with AAV showing that both vector types mediated transgene expression after local AAV application (Figure 37). Higher signals were detectable for AAV2- than for Her2-AAV-mediated gene transfer. This observation is consistent with the previous *in vitro* data that also revealed higher transgene expression for AAV2 than for Her2-AAV. Interestingly, when vectors were injected intravenously, αPD-1 and αPD-L1 were only detectable in tumor lysates explanted from mice that had received Her2-AAV. In contrast, no signal above the background was detectable in the tumor of the mouse treated with $AAV2^{\alpha PD\text{-}L1}$. In summary, these data confirm the AAV-mediated expression of the immune checkpoint inhibitors *in vivo*. Furthermore, these results

demonstrate that the method chosen for organ disruption and the subsequent ELISA are eligible for the detection of αPD-1 and αPD-L1 in tumor lysates.

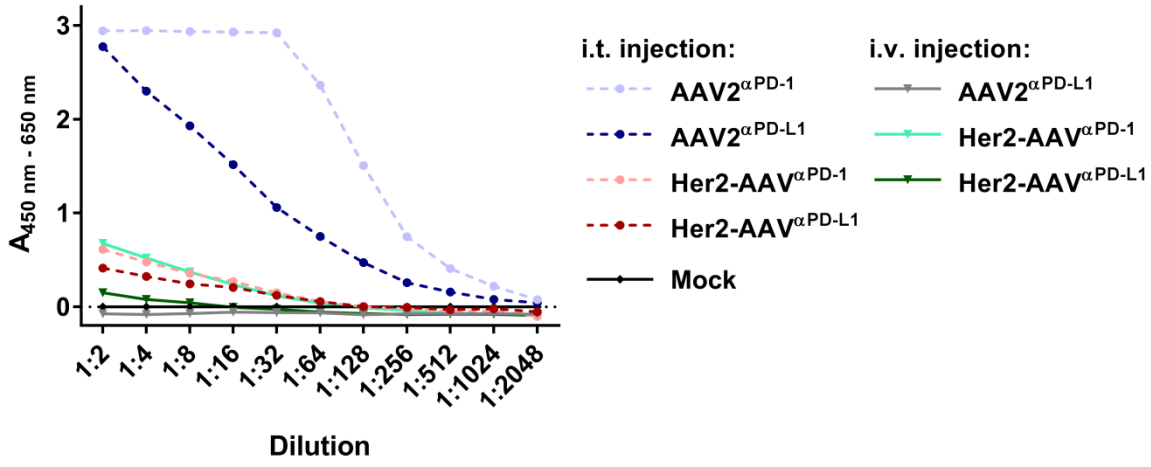

Figure 37: Detection of immune checkpoint inhibitors in tumors explanted from immunodeficient mice treated with AAV vectors. The indicated vectors were either injected intratumorally or intravenously into RENCA-Her2/neu-bearing NSG mice. Seven days after vector administration, mice were sacrificed and tumors isolated. Serial two-fold dilutions of the generated tumor lysates were prepared and subjected to the ELISA to analyze αPD-1 and αPD-L1 levels. Tumors explanted from RENCA-Her2/neu-bearing NSG mice that had not received AAV vectors served as negative control (Mock).

Since it is well established that AAV2 transduces liver after systemic administration (Münch et al, 2013), liver lysates from mice treated intravenously with the AAV vectors were prepared and analyzed by ELISA. Signals were detected in the liver lysates of the mouse which had received AAV2$^{\alpha PD\text{-}L1}$ but no signals clearly above the background were detectable in livers of mice that had received Her2-AAV$^{\alpha PD\text{-}1}$ or Her2-AAV$^{\alpha PD\text{-}L1}$ (Figure 38A). This observation indicated that AAV2 mediated the transgene expression in liver upon systemic vector applications whereas this was not applicable for Her2-AAV. To analyze whether the organ lysates can be stored frozen prior they are analyzed in the ELISA, liver lysates were also applied to the assay after they had been subjected to a single freeze/thaw cycle. The data showed in accordance with the analysis of the cell culture supernatants (Figure 30), that a freeze/thaw cycle did not influence the detectability of the proteins. The same was observed for tumor lysates (data not shown).

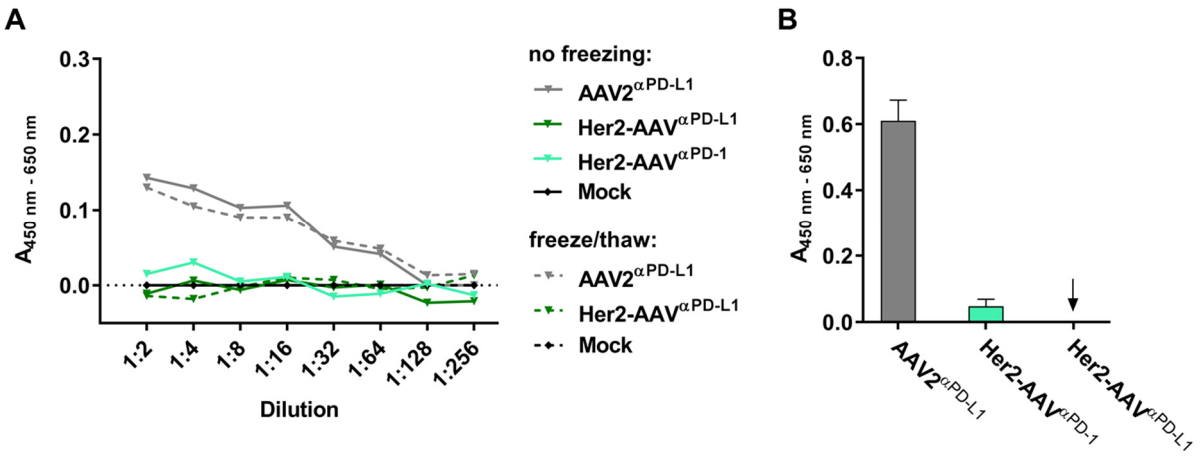

Figure 38: Detection of αPD-1 and αPD-L1 in liver and serum from immunodeficient mice systemically injected with AAV vectors. Liver and serum from RENCA-Her2/neu-bearing NSG mice that are derived from the experiment described in Figure 37 were analyzed by ELISA. Untreated RENCA-Her2/neu-bearing mice served as negative control (Mock). (A) αPD-1 and αPD-L1 levels in livers were analyzed by applying serial two-fold dilutions of the prepared liver lysates to the ELISA. (B) Analysis of αPD-1 and αPD-L1 levels in sera of mice. Arrow indicates that no signal above background was detectable. (n=2, means ± SD)

These results confirmed that the established ELISA is suitable for the detection of αPD-1 and αPD-L1 in tumor and liver lysates. In addition, analysis of the sera of mice treated intravenously with AAV vectors revealed that the ELISA is also suitable for the detection of the inhibitors in blood. The results also showed that only in sera from the mouse that had been treated intravenously with AAV2$^{\alpha PD\text{-}L1}$ a signal clearly above the background was detectable (Figure 38B). In contrast, for Her2-AAV$^{\alpha PD\text{-}1}$ and Her2-AAV$^{\alpha PD\text{-}L1}$ the signals were close to background or even not detectable.

Overall, the data provide first evidence that the generated AAV vectors can mediate expression of αPD-1 and αPD-L1 *in vivo* and that Her2-AAV is a suitable tool to deliver the immune checkpoint inhibitors to the tumor even after systemic vector administration. Furthermore, the results show that the applied method for organ disruption and the subsequent ELISA can be used to detect the inhibitors in tumor organ lysates, in liver organ lysates and in serum.

3.2.8 Her2-AAV tumor-targeting in immunocompetent mice

The tumor-targeting capacity of Her2-AAV has been investigated only in immunodeficient mouse models so far (Münch et al, 2013; Münch et al, 2015). Since the therapeutic effects of the immune checkpoint blockade therapy require the immune system, the Her2-AAV tumor-targeting in immunocompetent mice was analyzed in a next step. The previous data demonstrate that RENCA-Her2/neu cells were susceptible

to AAV transduction *in vitro* and *in vivo* and that they expressed functional αPD-1 and αPD-L1 upon vector transduction. Accordingly, Her2-AAV tumor-targeting was analyzed using a syngeneic tumor mouse model based on immunocompetent BALB/c mice carrying subcutaneously growing RENCA-Her2/neu tumors.

In order to follow tumor-targeting *in vivo,* Her2-AAV and AAV2 vectors were equipped with a luciferase reporter gene. This reporter system enables the non-invasive monitoring of the vector biodistribution by measuring the luciferase activity. For the experiment, BALB/c mice were subcutaneously injected with RENCA-Her2/neu cells and Her2-AAV^{luc} or AAV2^{luc} were administered systemically through the lateral tail vein once the tumors had reached an average size of about 80 mm^3. Seven days after vector application mice were analyzed by *in vivo* imaging.

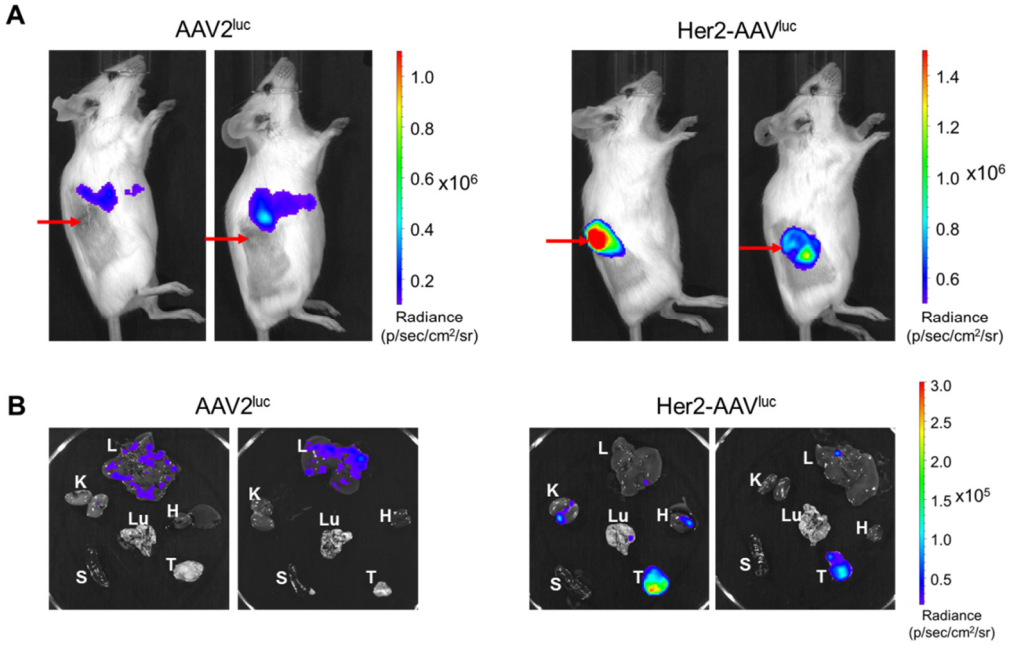

Figure 39: Her2-AAV tumor-targeting in immunocompetent mice. BALB/c mice were subcutaneously transplanted with 5x10^6 RENCA-Her2/neu tumor cells (red arrow). Once the tumors had reached a size of about 80 mm^3, mice were intravenously injected with 1x10^{11} genome copies of AAV2 or Her2-AAV transferring the luciferase gene. One week after vector administration, AAV targeting was analyzed by *in vivo* imaging in (A) living mice and (B) isolated organs (L: liver, K: kidney, H: heart, Lu: lung, S: spleen, T: tumor). Luciferase signal intensity is expressed as photons/seconds/square centimeter/steradian (p/sec/cm^2/sr).

AAV2-injected mice showed a signal in the upper abdominal region (Figure 39A). In contrast, Her2-AAV-injected mice revealed strong luciferase activity in the tumor. Immediately after *in vivo* imaging, mice were sacrificed and luciferase signals of the isolated organs were analyzed. Analysis of the organs revealed that the signal in AAV2-injected mice originates from the liver (Figure 39B). The strongest signal for Her2-AAV-treated mice was observed in the tumor. No luciferase activity was detectable

in the liver of these mice showing that Her2-AAV was successfully redirected from liver to tumor tissue. However, when mice were imaged in the dorsal position luciferase signals were observed for Her2-AAV that presumably did not originate from the tumor (Figure 40A). Analysis of the explanted organs indicated that presumably the mammary fat pads as well as other fat tissue in the abdomen gave rise to the additional signals (Figure 40B). For AAV2-injected mice the expected signal in the upper abdominal region was detectable and the mammary fat pad did not show luciferase activity.

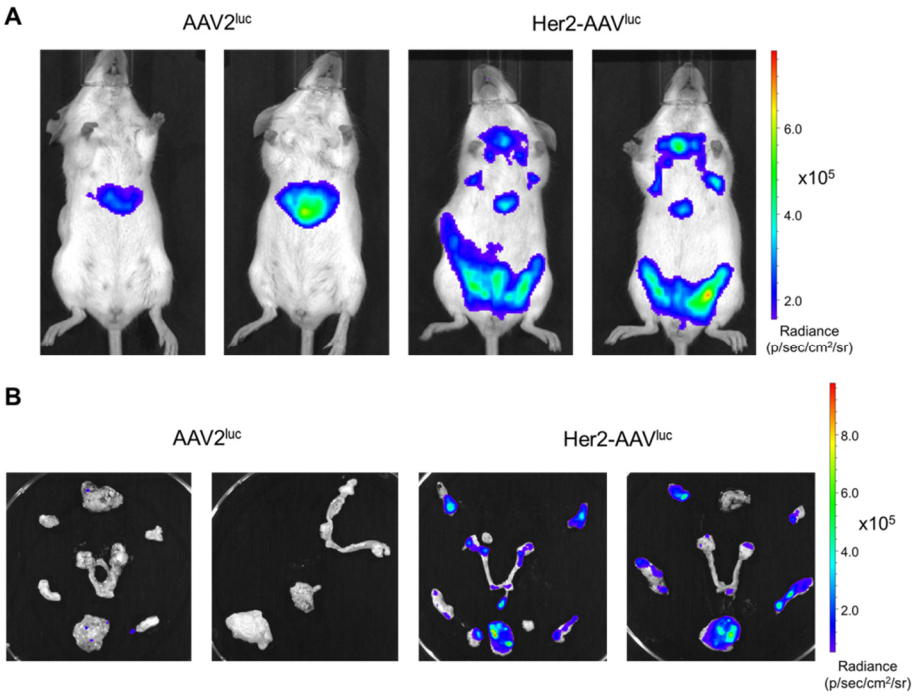

Figure 40: Off-targeting after systemic administration of Her2-AAV. Mice that were treated as described in Figure 39 were imaged in (A) a dorsal position and subsequently, (B) mammary fat pad and fat tissue in the abdomen were isolated and analyzed. Luciferase signal intensity is expressed as photons/seconds/square centimeter/steradian (p/sec/cm^2/sr).

Taken together, these data demonstrate that also in immunocompetent mice Her2-AAV is successfully redirected from liver to tumor tissue when injected intravenously, while non-targeted AAV2 retained in liver. Thus, as observed for the immunodeficient mouse models the ablation of natural receptor binding to HSPG and the incorporation of a Her2/neu-specific DARPin successfully redirected the Her2-AAV-mediated gene transfer from liver to tumor lesions.

3.2.9 Tumor-targeted delivery of αPD-1 by Her2-AAV

The successful production of AAV vectors encoding αPD-1 as well as αPD-L1 and the identification of a suitable syngeneic tumor mouse model for the investigation of AAV-mediated tumor-targeted delivery of immune checkpoint inhibitors were described above. Finally, the tumor-targeted delivery of immune checkpoint inhibitors by Her2-AAV in immunocompetent mice was investigated. For the final analysis, αPD-1 was chosen as transgene since the ELISA of the pilot-experiment (chapter 3.2.7) revealed higher signals for αPD-1 than for αPD-L1. For the experiment, Her2-AAV$^{αPD-1}$ or AAV2$^{αPD-1}$ were systemically injected through the lateral tail vein into RENCA-Her2/neu-bearing mice. Mice that were injected with PBS served as negative control and were used as blank for the ELISA analysis. One week after vector administration, mice were sacrificed and organs isolated as well as blood collected. Tumor lysates, liver lysates and serum were analyzed in regard to the αPD-1 level by ELISA. The quantity of αPD-1 in the organ extracts was calculated using the αPD-1 protein standard and normalized to the total protein yield of the organ lysates.

The analysis showed tumor-targeted delivery of αPD-1 by systemically administered Her2-AAV (Figure 41A). The αPD-1 levels in the tumors were similar for all three mice injected. However, AAV2-treated mice showed comparable αPD-1 levels in the tumor. Presumably, these signals did not arise from AAV2-mediated expression of αPD-1 in the tumor, rather from the transport of liver expressed αPD-1 via the blood stream to other organs such as the tumor. On average, the levels of αPD-1 in the tumor of the three different mice per group was for Her2-AAV in the range of 1.9 ± 0.11 ng αPD-1/mg protein (n=3, mean ± SD) and for AAV2 in the range of 3.28 ± 1.22 ng αPD-1/mg protein (n=3, mean ± SD) (Figure 41B). In contrast, αPD-1 levels in the livers were significantly higher for AAV2 than for Her2-AAV. The αPD-1 levels in the liver for Her2-AAV were quite low. The average αPD-1 amount in the livers for Her2-AAV was 0.17 ± 0.01 ng αPD-1/mg protein (n=3, mean ± SD) and for AAV2 5.12 ± 1.24 ng αPD-1/mg protein (n=3, mean ± SD). Comparing the αPD-1 levels in blood serum, AAV2-injected mice showed a fourfold higher level as compared to Her2-AAV-treated mice. The average amount of αPD-1 in sera from the different mice treated with Her2-AAV was 447.3 ± 36.7 ng/ml (n=3, mean ± SD) and for AAV2 1,896.25 ± 378.5 ng/ml (n=3, mean ± SD).

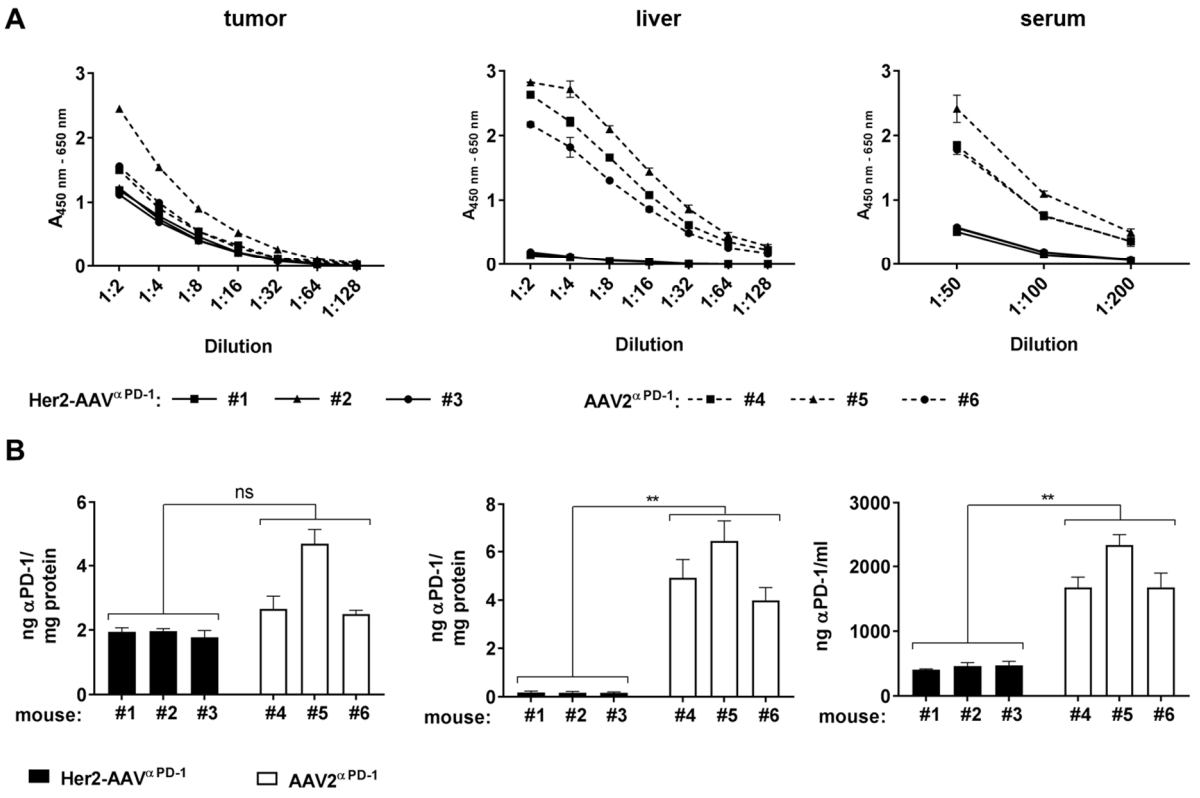

Figure 41: Analyzing αPD-1 levels in tumor, liver and serum of mice after systemic administration of Her2-AAV or AAV2. RENCA-Her2/neu-bearing BALB/c mice received a single intravenous injection of Her2-AAV or AAV2 encoding αPD-1 ($1.1x10^{10}$ genome copies) or PBS as mock control. One week after vector administration, organs were isolated and blood taken. αPD-1 levels were analyzed by the previously described sandwich ELISA using Fc- and HA-tag-specific antibodies. (A) Raw data obtained by ELISA. (tumor: n=1, liver: n=3; serum: n=3-4; means ± SD) (B) αPD-1 levels in tumor and liver were quantified using the generated αPD-1 protein standard and normalized to the total protein yields. The amount of αPD-1 in serum was calculated as ng/ml. (tumor: n=3; liver: n=9; serum: n=5-7; means ± SD); **, $p<0.01$; ns, not significant by unpaired t-test (n=3)

Overall, these results confirmed the tumor-targeted delivery of the immune checkpoint inhibitor αPD-1 in a syngeneic tumor mouse model by Her2-AAV. This model will pave the way for further investigations addressing toxicity and efficacy of vector-mediated immune checkpoint modulation.

4 Discussion

Treatment strategies in cancer therapy are currently shifting from targeting exclusively tumor cells towards stimulating the host immune system to attack the malignancy. Indeed, one of America's leading scientific journals - *Science* - deemed cancer immunotherapy as 'Breakthrough of the Year 2013' due to substantial benefit observed in clinical trials (Couzin-Frankel, 2013). Improving this type of therapy will likely require the combination with other treatment modalities and possibly the application of viral based systems may contribute to further increase efficacy and safety of cancer immunotherapeutic approaches. In fact, recent advances in oncolytic virotherapy as well as viral gene therapy have proven that viral systems can be a powerful tool for medical applications, including the treatment of cancer (Rehman et al, 2016; Büning, 2013). In this thesis, oncolytic srVSV as well as receptor-targeted AAV were developed as novel systems for applications in cancer immunotherapy. To this end, oncolytic srVSV was armed with immunotherapeutic cargo to enhance its capacity to induce an antitumor immune response. Moreover, receptor-targeted AAV vectors were equipped with the coding sequence of αPD-1 as well as αPD-L1 in order to enable tumor-directed delivery of immune checkpoint inhibitors upon systemic vector administration.

4.1 Arming VSV with immunotherapeutic transgenes

Oncolytic VSV is currently developed as biological anticancer therapeutic and different strategies have been investigated to further improve its antitumoral efficacy. This involves a variety of approaches to increase the potential of VSV to induce a long-lasting antitumor immune response (Hastie & Grdzelishvili, 2012). In this context, VSV has been designed to encode TAAs or cytokines such as IL-4, IL-12, Ftl3L or GM-CSF (Pulido et al, 2012; Fernandez et al, 2002; Shin et al, 2007; Leveille et al, 2011; Bergman et al, 2007).
One aim of this thesis included arming of srVSV with immunotherapeutic transgenes. The srVSV system was developed by Muik *et al.* and was proven to be genetically stable, exhibited no neurotoxicity and showed potent antitumor activity (Muik et al, 2012). Furthermore, a key benefit of srVSV is the increased coding capacity for therapeutic transgenes making the system attractive for oncolytic immunotherapy. Accordingly, both viral vectors, the VSVΔG and VSVΔL vector, can be armed to enhance srVSV-mediated antitumor immune responses. Also other oncolytic viruses were already

equipped with more than one immunotherapeutic transgene in order to enhance their antitumor efficacy. For instance, oncolytic adenovirus or HSV armed with the T cell costimulatory molecule B7-1 together with GM-CSF, IL-12 or IL-18 were shown to improve the efficacy of virotherapy (Choi et al, 2006; Lee et al, 2006; Fukuhara et al, 2005).

In this thesis, srVSV was armed with the immunostimulatory transgenes GM-CSF, Flt3L, B7 as well as with the TAA Her2/neu and CTLA4-Her2/neu. The different immunostimulatory transgenes were cloned into the VSVΔG and VSVΔL vector genomes, all VSV vectors were successfully generated *de novo* and functional analyses revealed srVSV-mediated transgene expression *in vitro.* Transgenes inserted into the G-position were expressed at higher levels as those inserted into the L-position of the VSV vector genome. This observation is in perfect agreement with the transcriptional gradient described for VSV leading to a decrease in mRNA and thus protein abundance from the 3' to the 5' located genes (Villarreal et al, 1976; Barr et al, 2002).

4.1.1 Mechanisms of action of the incorporated immunotherapeutic transgenes

The mechanisms of inducing antitumor immunity by the used immunostimulatory transgenes have been studied before in the context of virotherapy and cancer immunotherapy. Especially, GM-CSF is highly promising as a variety of advanced oncolytic viruses code for GM-CSF including T-Vec, an approved oncolytic virus for the treatment of metastatic melanoma (Rehman et al, 2016; Lichty et al, 2014). GM-CSF is considered to improve antitumor effects due to the stimulation of the development and maturation of APCs such as DCs (Kaufman et al, 2014; Pan et al, 2004). These DCs in turn are recruited to the tumor microenvironment, process tumor antigens and promote antigen presentation that finally stimulates T cell responses augmenting antitumor immune responses (Figure 42) (Pan et al, 2004).

Flt3L is also a cytokine stimulating maturation and proliferation of DCs that has shown promising antitumor efficacy and the induction of an immunological memory in various tumor models (Maraskovsky et al, 1996; Shurin et al, 1997; Chen et al, 1997; Wang et al, 2000; King et al, 2008; Lynch et al, 1997). However, even if both cytokines have the capability to increase the amount of tumor-infiltrating DCs, studies directly comparing the efficiency of GM-CSF and Flt3L to mount an antitumor immunity revealed either an superior efficacy for Flt3L over GM-CSF or vice versa (Braun et al, 1999; Mach et al,

2000). Several differences exist between the DCs elicited by GM-CSF and Flt3L. GM-CSF stimulates exclusively the generation of myeloid-type DCs, whereas Flt3L drives the generation of both, lymphoid- and myeloid-type DCs. Moreover, GM-CSF induces the upregulation of the costimulatory molecule B7 on DCs and has the capability to induce a broad T cell cytokine response, whereas Flt3L only shows a Th1 response (Mach et al, 2000). Furthermore, Flt3L is not only known to stimulate DCs but also to stimulate NK cell generation *in vivo* (Shaw et al, 1998). Accordingly, Flt3L-induced antitumoral effects were described to also depend on NK cells (Péron et al, 1998; Braun et al, 1999). In the present study, both cytokines were incorporated into srVSV. A pilot-experiment indicated a superior performance for srVSV(Flt3L/B7) treatment resulting in two tumor-free mice out of four over srVSV(GM-CSF/B7) treatment resulting in one tumor-free mouse out of three. However, this was only a pilot-experiment and further studies with more animals will be required to confirm this tendency.

Furthermore, srVSV was equipped with the coding sequence of soluble B7, which was composed of the extracellular domain of mouse B7-1 and the constant region of an IgG1, in order to promote antitumor T cell activity (Figure 42). B7-1-IgG fusion proteins demonstrated antitumor effects in multiple murine tumor models in the context of tumor cell vaccines as well as oncolytic virotherapy (Todo et al, 2001; Zhou et al, 2003; Sturmhoefel et al, 1999; Ino et al, 2006). Several hypotheses are discussed for the underlying mechanism by which B7-1-IgG fusion proteins assist the induction of antitumor immune responses since B7-1 is described to bind to CD28, CTLA-4 and PD-L1 (Sturmhoefel et al, 1999; Zhou et al, 2003; Chen, 2004; Butte et al, 2007). Thus, B7-1-IgG molecules probably enhance T cell co-stimulation by engaging CD28. This might be relevant for naïve T cells that express CD28 but no CTLA-4 on their surface. Furthermore, it is feasible that soluble B7-1-IgG functions like an immune checkpoint inhibitor. Accordingly, B7-1-IgG probably binds to CTLA-4 on activated T cells or to PD-L1 and thereby, might antagonize T cell inhibition (Zhou et al, 2003; Sturmhoefel et al, 1999).

The third followed strategy to enhance tumor-specific immune responses was the equipment of srVSV with the TAA Her2/neu. Since the presentation of TAAs by DCs is critical for the induction of tumor-specific T cell responses, srVSV was also armed with the fusion protein CTLA4-Her2/neu. This construct is supposed to facilitate tumor-antigen uptake by mediating the binding to B7 molecules on DCs via CTLA-4. In the context of other cancer vaccination studies, the CTLA4-Her2/neu fusion construct was

already shown to be internalized upon specific binding to B7-expressing cells eventually leading to intracellular protein degradation (Rohrbach et al, 2005). Comparing Her2/neu and CTLA4-Her2/neu in tumor mouse models revealed a superior capability of the fusion protein to protect mice from tumor challenge and to induce a potent antitumor response in terms of tumor growth and survival (Rohrbach et al, 2005; Sloots et al, 2008).

4.1.2 Therapeutic efficacy of srVSV armed with immunotherapeutic cargo

Taken together, srVSV is considered to be a promising oncolytic virotherapeutic due to its potent antitumor efficacy in xenograft tumor mouse models and its increased safety profile (Muik et al, 2012). Furthermore, the immunotherapeutic transgenes that were incorporated into srVSV in the present study are capable to enhance antitumor immunity as well as to increase the efficacy of virotherapy as demonstrated in the context of other cancer immunotherapy studies. Thus, combining srVSV with immunotherapeutic transgene expression was expected to improve srVSV cancer therapy. However, the present study could not confirm a clearly improved therapeutic efficacy of srVSV armed with immunostimulatory transgenes as compared to srVSV(GFP/DsRed) in an immunocompetent tumor mouse model. The *in vivo* pilot-experiment compared srVSV(GM-CSF/B7), srVSV(Flt3L/B7) and srVSV(GFP/DsRed). Indeed, some srVSV-treated mice showed complete tumor regression. However, this was true for all three srVSV variants tested. Remarkably, all mice showing complete tumor regression were female with one tumor-free out of two treated female mice for srVSV(GM-CSF/B7), two tumor-free out of two treated female mice for srVSV(Flt3L/B7) and one tumor-free out of two treated female mice for srVSV(GFP/DsRed). This observation might be explained by the growth inhibition of MC38 cells by female sex steroids that possibly supported the antitumor effects in female mice (Motylewska & Melen-Mucha, 2009). Cured mice were protected against tumor rechallenge and showed tumor-specific immune cells in isolated splenocytes as determined by IFNγ ELISpot showing that the mice exhibited protective immunity against tumor cells. However, even though cured mice were observed in all srVSV cohorts, the tumor growth and the median survival indicated an improved treatment response for srVSV(GM-CSF/B7) and srVSV(Flt3L/B7) as compared to srVSV(GFP/DsRed), whereby srVSV(Flt3L/B7) indicated the best therapeutic effect. Thus, the *in vivo* experiment was repeated with

female mice only to confirm the improved efficacy of srVSV(Flt3L/B7) versus srVSV(GFP/DsRed). In addition, it was evaluated whether a lower viral dosage might improve the antitumoral effect of srVSV(Flt3L/B7) compared to srVSV(GFP/DsRed) as this set-up might enhance the influence of transgene expression and diminish the effect of direct viral oncolysis. However, when the same viral dosage was applied as in the first *in vivo* experiment the therapeutic effect of srVSV-treated mice in both cohorts was not as pronounced as observed in the previous *in vivo* experiment. Only one out of four female mice showed complete tumor regression in the srVSV(Flt3L/B7) cohort and no mouse was cured by srVSV(GFP/DsRed) treatment. Furthermore, an increased therapeutic efficacy of srVSV(Flt3L/B7) compared to srVSV(GFP/DsRed) with lower viral doses was not observed. After all, srVSV(Flt3L/B7) treatment showed again a slightly improved treatment response as compared to srVSV(GFP/DsRed). However, the results did not reveal a statistically significant superior therapeutic efficacy of srVSV(Flt3L/B7) as compared to srVSV(GFP/DsRed). Consequently, the therapeutic efficacy of srVSV armed with immunotherapeutic cargo was not clearly improved as compared to srVSV(GFP/DsRed) treatment as initially assumed. Thus, much larger cohort sizes will be required to clarify whether arming of srVSV with immunostimulatory transgenes improves srVSV therapy efficacy.

4.2 Oncolytic immunotherapy requires a balance between antitumor and antiviral immune responses

The host immune response is critical for the efficacy of oncolytic virotherapy. On the one hand, viral oncolysis potentially elicits beneficial antitumor immunity and on the other hand, provokes detrimental antiviral immune responses. For example, induced antiviral immune responses might eliminate virus-infected tumor cells and thereby enhance therapy efficacy due to tumor regression and otherwise also dampen efficacy due to early viral clearance. Thus, a fine balance between viral and tumor elimination is required for successful oncolytic immunotherapy (Prestwich et al, 2008).

Even VSV that was not armed with additional immunotherapeutic transgenes was capable to elicit antitumor immune responses. Diaz and colleagues showed that the efficacy of VSV in an immunocompetent melanoma mouse model did not only depend on its oncolytic activity but also on host-derived immune cells, in particular on $CD8^+$ T cells. In this study, not only tumor-specific but also VSV-specific T cells were induced during

therapy. Arming VSV with a tumor-antigen induced a similar number of antiviral T cells, while the number of tumor-antigen-specific T cells were increased eventually leading to an improved therapy efficacy (Diaz et al, 2007). Thus, equipping srVSV with the TAA Her2/neu or CTLA4-Her2/neu might also be able to increase the amount of tumor-specific T cells and to improve efficacy as compared to parental srVSV. However, since no suitable Her2/neu-positive tumor model was available, these srVSV constructs have not been investigated *in vivo* so far.

4.2.1 Type I IFN-induced antiviral immune responses

A major barrier for successful VSV oncolytic immunotherapy is the innate immune response as VSV is particularly sensitive to type I IFN-induced antiviral responses. Thus, defective IFN pathways in cancer cells are described to be the key determinant of VSV oncoselectivity and are decisive for effective VSV therapy (Stojdl et al, 2000; Stojdl et al, 2003; Liu et al, 2013; Hastie & Grdzelishvili, 2012). Even though many tumor cells have acquired deregulated IFN-responsiveness, the extent of the defects are highly variable between different cancers (Liu et al, 2013; Stojdl et al, 2003; Dold et al, 2016). Therefore, in the present study different murine cancer cell lines were analyzed concerning their IFN sensitivity to identify a suitable mouse model to investigate the therapeutic efficacy of srVSV *in vivo*. Analyses revealed that the murine colon cancer cell line MC38 could be an appropriate tumor model since MC38 cells were infectable even when pretreated with high doses of IFNα. However, albeit MC38 cells remained susceptible to VSV infection after pretreatment with the highest tested IFNα doses of 100 U/ml and 1000 U/ml, cell viability was increased compared to untreated control cells showing that even MC38 cells were not totally unresponsive to the antiviral effects of IFNα. Accordingly, partially intact antiviral mechanisms in MC38 tumor cells probably limited the efficacy of the srVSV treatment in the MC38 tumor model (Figure 42). To investigate in future experiments whether MC38 cells are resistant to srVSV infection *in vivo*, immunohistochemical staining of VSV proteins in isolated tumors would be feasible for example.

It was shown that even if cancer cells have functional IFN response pathways, they are permissive to VSV infection *in vitro* due to the absence of accessory cells which produce IFN. In contrast, those cancer cells are protected from VSV infection *in vivo* due to stromal cells of the tumor microenvironment such as tumor-associated macrophages

that produce IFN (Liu et al, 2013). Accordingly, one strategy of Lemay and colleagues to harness VSV-mediated antitumor immunity was the usage of an infected cell vaccine. Here, B16-F10 cells, which are not VSV-permissive *in vivo*, were infected *in vitro* with VSV to bypass the requirement for *in vivo* replication to elicit an antitumor immune response. Those VSV-infected cell vaccines were used to immunize mice and were shown to protect some animals against a subsequent tumor challenge in a prophylactic setting. Using B16-F10 cells infected with VSV encoding GM-CSF (VSV-GMCSF) protected even more mice against future tumor challenge and also showed antitumor efficacy in therapeutic models of subcutaneously or metastatically growing B16-F10 tumors. In contrast, B16-F10-tumor-bearing mice that were solely treated with VSV or VSV-GMCSF, the same approach as used in the present study, did not respond to VSV treatment most likely due to the lack of intratumoral viral replication (Lemay et al, 2012).

Other studies aimed at suppressing IFN signaling in the tumor microenvironment in order to support VSV spread and oncolysis. In that context, localized expression of B18R, a type I IFN antagonist that is originally derived from vaccinia virus, was shown to enhance viral spread and tumor destruction of tumor cells exhibiting low VSV-susceptibility (Alcami et al, 2000; Le Boeuf et al, 2010; Cronin et al, 2014). In another study the IFN sensitivity of ovarian cancer cells was overcome by inhibiting the Janus kinase/signal transducer and activator of transcription (JAK/STAT) pathway, which is involved in the induction of IFN responsive antiviral genes, using the drug ruxolitinib. The combination of VSV treatment and ruxolitinib administration showed an improved therapeutic efficacy in a subcutaneous as well as in an orthotopic tumor mouse model (Dold et al, 2016). Thus, if the srVSV treatment failed to elicit a pronounced antitumor effect due to the partial sensitivity of MC38 cells to the antiviral effects of IFN, combination of srVSV with B18R or ruxolitinib probably might improve srVSV treatment outcome.

However, tumor selectivity of VSV is mainly mediated via intact IFN pathways of healthy cells. Accordingly, combination therapy of B18R or ruxolitinib might lead to VSV replication in healthy tissue resulting in damage of nontumor cells. Anyway, so far no signs of toxicity have been reported for the combination therapy of VSV with one of these IFN modulators (Dold et al, 2016; Cronin et al, 2014; Le Boeuf et al, 2010). Moreover, the risk of toxicity for srVSV might be even lower as compared to fully replication-competent VSV, due to its mode of co-propagation. Furthermore, it must be considered that inhibition of type I IFN responses in the tumor microenvironment might

not only support viral oncolysis but might also dampen antitumoral immune responses (Sikora et al, 2009; Hiroishi et al, 2000; Smyth et al, 2004).

4.2.2 Humoral immune responses

A further factor of the immune system potentially limiting efficacy of oncolytic virotherapy is the humoral adaptive immunity. VSV was shown to trigger a rapid and robust neutralizing antibody (nAb) response beginning at day 3 post intravenous VSV administration (Muik et al, 2014; Pinschewer et al, 2004). Single intratumoral application of srVSV also resulted in a nAb response beginning at day 5 post application and was increased until the end of the observation period on day 14 (data not shown). Thus, it has to be expected that the induction of nAbs probably will also limit the therapy efficiency of srVSV (Figure 42). One promising strategy to prevent the induction of a nAb response against srVSV could be the exchange of the VSV glycoprotein (VSV-G) with the glycoprotein of LCMV (LCMV-GP) (WE strain). Replication-competent VSV pseudotyped with LCMV-GP (rVSV(GP)) was already shown to escape nAb response after a single intravenous injection and was efficiently delivered to subcutaneous growing tumors in preimmunized mice (Muik et al, 2014). Thus, in the present study srVSV was also pseudotyped with the glycoprotein of LCMV (srVSV(GP)) to investigate whether this construct also evades humoral immune responses and indeed, srVSV(GP) did not elicit a nAb response after a single intratumoral injection (data not shown). Furthermore, previous work by Muik *et al*. demonstrated that immune cells were less susceptible to VSVΔG pseudotyped with LCMV-GP (VSVΔG-GP) as compared to VSV-G complemented VSVΔG vectors (VSVΔG-G). In particular, VSVΔG-GP was shown to spare stimulated T cells and DCs that were in contrast infected by the VSVΔG-G vector (Muik et al, 2011). Thus, pseudotyping srVSV with LCMV-GP may not only avoid the induction of nAbs but also prevent the infection of immune cells that are recruited into the tumor microenvironment. Leveille *et al.* showed that tumor-associated DCs were infected by VSV *in vivo* reducing their viability as well as preventing their migration to the draining lymph nodes to prime a tumor-specific T cell response (Leveille et al, 2011). Accordingly, infection of DCs by VSV potentially interferes with tumor-antigen presentation being crucial to induce an antitumor immune response and on the contrary, might enhance VSV-specific immune responses. Possibly, infection of recruited

DCs, T cells or other immune cells by srVSV also hampered therapy efficacy in the present study (Figure 42).

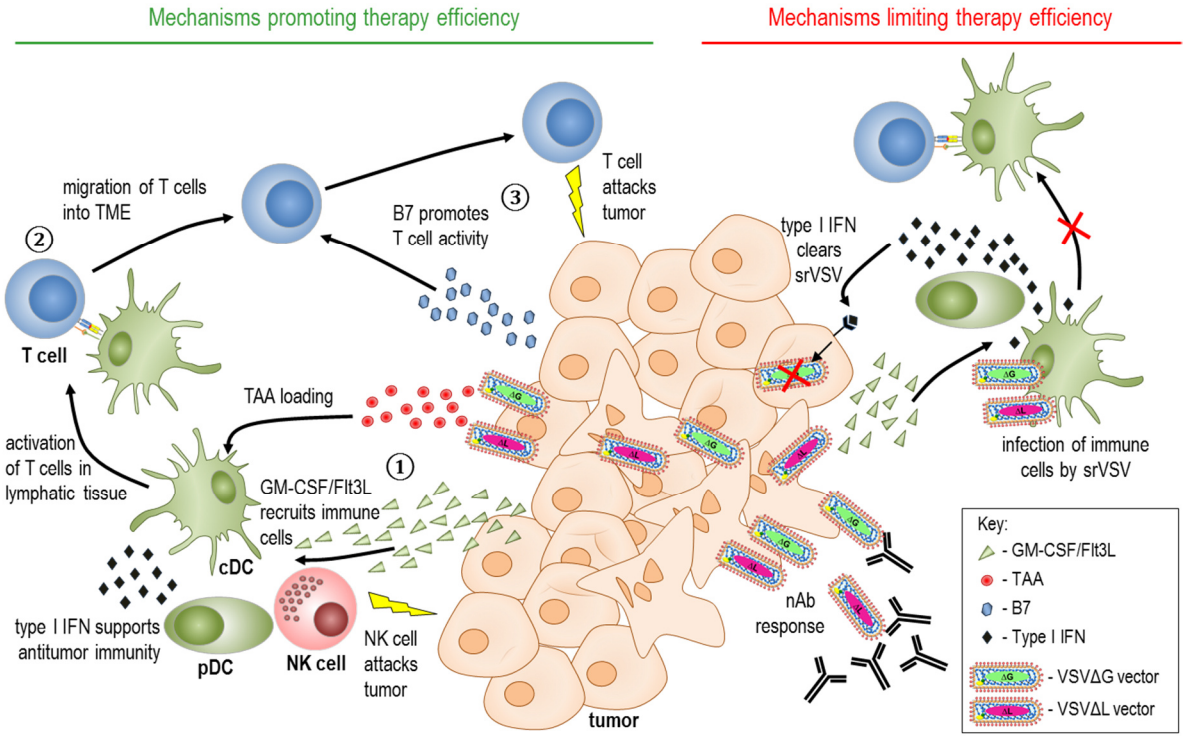

Figure 42: Schematic drawing of possible mechanisms promoting or limiting srVSV therapy efficiency. Possible mechanisms promoting therapy efficiency: Infection of tumor cells by srVSV causes direct virus-mediated cell lysis and the recruitment of conventional dendritic cells (cDCs) as a result of srVSV-mediated GM-CSF or FLt3L expression (①) as well as by release of PAMPs and DAMPs. Released tumor-associated antigens (TAAs) are captured and processed by the recruited cDCs that migrate to lymphatic organs in order to stimulate tumor-specific T cells (②). Tumor-specific T cells migrate into the tumor microenvironment (TME) where B7, expressed by srVSV-infected tumor cells, support their activity (③). Finally, T cells potentially directly attack tumor cells leading to tumor debulking. In addition to increasing the amount of cDCs, Flt3L potentially also triggers the generation of plasmacytoid DCs (pDCs) and natural killer (NK) cells (Shortman et al, 2013; Shaw et al, 1998). pDCs are the major interferon (IFN)-producing cell type and thus, intratumoral production of type I IFN by pDCs might also contribute to antitumor immunity through the upregulation of MHC molecules on tumor cells or via stimulating TAA-specific T cells for instance (Smyth et al, 2004). Recruited NK cells potentially also trigger tumor cell killing (Marcus et al, 2014). Possible mechanisms limiting therapy efficiency: srVSV possibly infects recruited DCs and thereby prevents the migration of DCs into lymphatic organs. This event interferes with tumor-antigen presentation and activation of tumor-specific T cells. Secreted type I IFN might affect srVSV spread within tumor cells that exhibit at least partial sensitivity to type I IFN induced antiviral responses. The induction of neutralizing antibody (nAb) response might further hamper viral spread. Altogether, antiviral immune responses also shorten the duration of srVSV-mediated transgene expression.

4.2.3 Antiviral immune responses may interfere with srVSV-mediated expression of immunomodulatory proteins

Innate and adaptive antiviral immune responses also shorten the duration of viral-mediated transgene expression. However, some immunotherapeutic proteins might need a certain time to fulfill their immunostimulatory function. For example, Flt3L has been shown to trigger the increase of DCs in mice after 8 to 10 days following daily

administration (Maraskovsky et al, 1996). Accordingly, srVSV-mediated Flt3L expression might not be sustained for a sufficient time to augment the DC numbers in the tumor-microenvironment. Similarly, it was demonstrated that the combination therapy of VSV and of recombinant Flt3L (daily administration over 10 days) exhibited a pronounced survival advantage as compared to parental VSV, whereas VSV engineered to encode Flt3L could only provide modest or even no survival improvement in the different tumor mouse models tested (Leveille et al, 2011). Consequently, srVSV engineered to encode immunotherapeutic transgenes probably did not elicit a pronounced superior therapeutic effect as compared to srVSV(GFP/DsRed) in the present study, since the duration of srVSV-mediated transgene expression was not sufficient to benefit from the immunostimulatory properties of the viral-encoded cargo.
In order to examine the aforementioned assumptions the analysis of srVSV replication in MC38 tumor cells *in vivo*, the investigation of antiviral immune responses as well as of the duration of srVSV-mediated transgene expression in MC38 tumors would be necessary.

4.2.4 Possible strategies to improve srVSV therapy

Taken together, srVSV treatment probably failed to induce a potent antitumor effect due to induced innate and adaptive antiviral immune responses. To avoid antiviral innate immune responses, the usage of tumor mouse models that are totally unresponsive to type I IFN antiviral responses, such as 5TGM1 or MPC-11, would be reasonable in future experiments (Liu et al, 2013). Alternatively, combining IFN modulators with srVSV therapy would be a further feasible strategy to overcome IFN sensitivity of tumor cells. Furthermore, using srVSV pseudotyped with the glycoprotein of LCMV could also enhance the outcome of srVSV oncolytic immunotherapy by evading humoral immunity and preventing the infection of recruited immune cells. In conclusion, combining these strategies might prolong the duration of srVSV-mediated transgene expression and thus, potentially also enhance the therapeutic efficacy of srVSV armed with immunostimulatory transgenes as compared to srVSV(GFP/DsRed).

4.3 Local delivery of immune checkpoint inhibitors

Monoclonal antibodies directed against immune checkpoints, such as PD-1 and PD-L1, have revolutionized cancer therapy with now several products on the market that

substantially prolong survival of end stage cancer patients (Bardhan et al, 2016). Despite the exciting clinical results obtained for the treatment of several malignancies using αPD-1 and αPD-L1 mAbs, there is an urgent need of further improving immune checkpoint blockade therapy. First, not all cancer patients respond to PD-1/PD-L1 blockade therapy whereas the objective response rates range between 15 % up to 40 % for the approved antibodies (Weber et al, 2015; Robert et al, 2015a; Topalian et al, 2014; Robert et al, 2015b; Robert et al, 2014; Rosenberg et al, 2016). Second, PD-1/PD-L1 immune checkpoint blockade therapy is associated with a number of immune-related toxicities. Grade 3 – 4 adverse events are observed in about 5 % up to 16 % of treated patients (Weber et al, 2015; Robert et al, 2015a; Robert et al, 2015b; Rosenberg et al, 2016). Third, the treatment entails high costs due to the amount of inhibitors needed. Generally, patients are treated with the respective mAbs in regular intervals until disease progression or unacceptable toxic effects are observed (Weber et al, 2015; Robert et al, 2014).

Local delivery of immune checkpoint inhibitors is a promising approach potentially addressing the aforementioned drawbacks. Toxicities elicited through autoimmune or inflammatory side effects might be limited by local mAbs delivery due to lower systemic exposure (Aznar et al, 2017). Furthermore, off-target binding of immune checkpoint inhibitors to healthy tissue might not only promote toxicity but also reduce the efficacy of the treatment. Local administration may circumvent low tumor tissue penetration by systemically injected mAbs (Aznar et al, 2017). It was shown by immuno-positron emission tomography (PET) imaging that only around 5 % to 10 % of systemically injected αPD-1 was accumulated in tumor tissue of treated mice (Natarajan et al, 2015).

Various approaches were investigated to achieve local delivery of immune checkpoint inhibitors. This included generation of tumor cell lines stably expressing the respective mAbs or novel delivery systems such as polymeric microparticles or Montanide emulsions that are loaded with mAbs (e.g. αCTLA-4) (Simmons et al, 2008; Rahimian et al, 2015; Fransen et al, 2013). A further strategy to increase the safety of checkpoint blockade therapy was based on dual-targeting bispecific antibodies that targeted a TAA as well as a checkpoint receptor (Dheilly et al, 2017). In the present thesis, Her2-AAV vectors were investigated as potential vehicles for the tumor-targeted delivery of the immune checkpoint inhibitors αPD-1 and αPD-L1.

4.3.1 Delivery of antibodies and antibody-like molecules by AAV vectors

AAV vectors are currently under investigations as platform for the delivery of antibodies. In contrast to passive immunization where neutralizing antibodies are directly administered into the patient, viral vector-mediated antibody gene transfer delivers the respective gene to the target cell being subsequently expressed *in vivo* (Schnepp & Johnson, 2014).

AAV vectors exhibit a limited packaging capacity that ranges about 4.7 kb for ssAAV and is even reduced for scAAV packaging a double-stranded DNA (McCarty, 2008). Wu *et al*. suggested a maximum packaging capacity of scAAV vectors of around 3.3 kb (Wu et al, 2007). Thus, scAAVs are not able to accommodate the heavy and the light chain required for a full-length immunoglobulin G (IgG) antibody. Nevertheless, scAAV vectors achieve considerably higher levels of transgene expression *in vitro* as well as *in vivo* and therefore, different approaches were investigated to enable scAAV-mediated expression of antibodies or antibody-like molecules (McCarty et al, 2001; McCarty et al, 2003; Fuchs et al, 2016). AAV vectors are under intense development especially for the delivery of anti-human immunodeficiency virus (HIV) antibodies in order to prevent or treat the disease and various strategies for antibody delivery by AAV vectors were investigated in that context (Schnepp & Johnson, 2014; Fuchs & Desrosiers, 2016; Deal & Balazs, 2015). One approach relied on the usage of antibody-like molecules composed of a simian immunodeficiency virus (SIV)-specific scFv attached to a rhesus IgG2-derived Fc-part. Upon expression the scFv-Fc dimerizes and forms the so-called 'immunoadhesins'. The respective coding sequence was packaged into an AAV serotype 1 (AAV1)-derived vector and resulting AAVs were administered intramuscularly into rhesus macaques. Using this approach, SIV-specific immunoadhesins were expressed *in vivo* and were detectable in sera of some treated animals up to 12 months that were furthermore protected against SIV infection. Additionally, transgene expression levels of immunoadhesins that were packaged into scAAV vectors were higher as compared to ssAAV vectors (Johnson et al, 2009).

One aim of this thesis was the generation of AAV vectors encoding immune checkpoint inhibitors targeting PD-1 or PD-L1. The molecular architecture of the inhibitors used in the present study was comparable to that of the above described SIV-specific immunoadhesins that were successfully delivered by AAV vectors *in vivo* and exhibited biological function (Johnson et al, 2009). The αPD-1 and αPD-L1 constructs used in this thesis were composed of a scFv specific for mouse PD-1 or PD-L1 and a constant region

of a human IgG1. Immune checkpoint inhibitors exhibiting the same molecular architecture were already proven to show antitumoral efficacy in preclinical mouse models when encoded by an oncolytic virus (Engeland et al, 2014).

The ORFs of αPD-1 or αPD-L1 were cloned into AAV2-derived self-complementary transfer vectors and together with both ITRs as well as the SFFV promotor, the transfer vector constructs finally exhibited a size of about 2.6 kb. Thus, the generated AAV transfer vectors encoding αPD-1 and αPD-L1 matched to the packaging capacity required for scAAV vectors (Wu et al, 2007). Successful encapsidation of the AAV transfer vectors by scAAV particles was proven by determining the genomic titers by qPCR. The genomic titers were mainly comparable among the different transgenes GFP (size transfer vector: 2,217 bp), αPD-1 (size transfer vector: 2,594 bp), αPD-L1 (size of transfer vector 2,588 bp) and IgG-Fc (size transfer vector 1,862 bp) ranging between $5x10^8$ and $1x10^9$ gc/µl and thus, demonstrated that the vectors were producible to similar yields. Only $AAV2^{GFP}$ exhibited a slightly higher titer of about $1x10^{10}$ gc/µl. Calculating the ratio of capsid to genomic titer revealed a slightly decreased packaging efficiency of Her2-AAV vectors having the larger constructs encapsidated (GFP, αPD-1, αPD-L1) as compared to non-targeted AAV2. However, it has been described previously that the fusion of a DARPin to the N-terminus of VP2 and even small alterations in the AAV capsid can influence the packaging efficiency of AAV vectors (Münch et al, 2013; Wu et al, 2000). Furthermore, the empty-full capsid ratio of Her2-AAV encoding IgG-Fc was improved as compared to the other Her2-AAV vectors indicating that the size of the transfer vector construct can influence the packaging efficiency.

The AAV2 and Her2-AAV vectors were proven to successfully mediate the expression of αPD-1 and αPD-L1 after transduction of the mouse RCC cell line RENCA-Her2/neu and the expressed immune checkpoint inhibitors specifically recognized their target protein PD-1 or PD-L1. However, the analyses revealed higher levels of transgene expression for AAV2 as compared to Her2-AAV vectors even though the same GOI was applied for transduction. This result can probably be explained by previous observations showing that Her2-AAV vector preparations are not only composed of DARPin-displaying AAVs but also of vector particles that had not incorporated the DARPin-VP2 fusion protein and are build up by VP1 and VP3 proteins only (Münch et al, 2015). Those VP1/VP3 particles have also packaged the vector genome but they can neither bind to Her2/neu nor to HSPG and thus do not contribute to gene transfer. Therefore, the transduction of AAV2 is probably more efficient than for Her2-AAV even though the same GOI was applied

resulting in different protein yields in cell culture supernatants of transduced cells. However, this could be obviated including a further purification step during AAV production. Münch and colleagues showed that affinity purification can be used to separate DARPin-displaying from DARPin-deficient AAV particles enabling the generation of vector preparations solely composed of DARPin-displaying AAV vectors (Münch et al, 2015).

To study antitumoral effects by immune checkpoint blockade therapy, immunocompetent models are mandatory. Therefore, RENCA cells that are syngeneic to fully immunocompetent BALB/c mice were investigated as a potential mouse model. In order to enable the cell entry of Her2-AAV, RENCA cells were used that had been genetically engineered to express the target receptor Her2/neu (Maurer-Gebhard et al, 1998). The results of the present study showed that RENCA-Her2/neu cells were transducable by Her2-AAV vectors and expressed functional αPD-1 and αPD-L1 upon AAV transduction. In addition, Hirayama *et al.* demonstrated that RENCA derived tumors are responsive to the inhibition of the PD-1/PD-L1 axis (Hirayama et al, 2016). Furthermore, immune checkpoint blockade therapy was successfully used for the treatment of RCC in clinics (McDermott et al, 2015). Taken together, these observations demonstrate that RENCA-Her2/neu is a reasonable syngeneic tumor mouse model to investigate immune checkpoint blockade therapy after systemic AAV vector administration. Therefore, the tumor-targeting capacity of Her2-AAV was analyzed in an immunocompetent BALB/c mouse model bearing subcutaneous growing RENCA-Her2/neu tumor cells after intravenous vector administration. Her2-AAV^{luc} vectors showed a high luciferase signal in the tumor tissue, whereas the highest signal of non-targeted AAV2^{luc} was detectable in the liver. This is in accordance with the previously performed AAV-targeting experiments in immunodeficient mice in which also successful redirection of Her2-AAV^{luc} from liver to tumor tissue was shown (Münch et al, 2013; Münch et al, 2015). The residual off-target signals observed for Her2-AAV^{luc} vectors are likely elicited by VP1/VP3 vector particles that had not incorporated the DARPin-VP2 fusion protein (Münch et al, 2015). Finally, tumor-targeted delivery of αPD-1 by Her2-AAV$^{\alpha PD\text{-}1}$ vectors was shown. Upon systemic administration of Her2-AAV$^{\alpha PD\text{-}1}$ into the aforementioned tumor mouse model, higher αPD-1 levels were detectable in the tumor as compared to the liver. In contrast, mice injected with non-targeted AAV2$^{\alpha PD\text{-}1}$ revealed the highest level of αPD-1 in the liver.

Approved immune checkpoint inhibitors that are used for the treatment of end-stage cancer patients are full-length IgG mAbs. Thus, to translate the AAV vector technology from pre-clinical models to clinical studies, it would be preferably to equip the vectors with the sequence encoding for one of the approved mAbs. This would require the incorporation of the heavy and the light chain of an IgG into AAV vectors. Different studies already attempted to use AAV vectors for the delivery of full-length IgG molecules in order to treat or prevent infectious diseases as well as to treat Alzheimer's disease or methamphetamine addiction (Fuchs et al, 2015; Skaricic et al, 2008; Shimada et al, 2013; Chen et al, 2017). One approach enabling the expression of a full-length antibody specific for HIV by ssAAV vectors is the dual promotor approach. Here, the vector encodes a CMV promotor for the heavy chain and an EF1α promotor for the light chain (Lewis et al, 2002).

Another study by Fuchs *et al.* used scAAV as well as ssAAV vectors for the *in vivo* delivery of full-length versions of IgG antibodies specific for SIV. Due to the limited packaging capacity of scAAV vectors, those vectors were generated by placing the heavy and the light chain on two separate scAAV vectors (two vector approach). For the generation of ssAAV vectors, the heavy and the light chain sequences were placed onto one single ssAAV vector separated by the 2A self-cleaving sequence from foot-and-mouth disease virus (F2A) (one vector approach). The respective AAV transfer vectors were packaged into rAAV1 capsids and injected intramuscularly into rhesus macaques. SIV-specific antibodies were measured in the serum through 44 weeks with concentrations ranging from 1 to 270 µg/ml that seemed to be dependent on the presence of anti-antibody responses. In one animal high antibody levels persisted for more than two years. The presence of AAV-delivered SIV-specific antibodies showed significant antiviral effects (Fuchs et al, 2015). Remarkably, the efficiencies of scAAV and ssAAV vectors were similar in the study of Fuchs *et al.*, in contrast to numerous other studies exhibiting a superior efficiency of scAAV vectors (McCarty, 2008; McCarty et al, 2001; Gao et al, 2006; Wang et al, 2003; Natkunarajah et al, 2008). This can probably be explained by the principle of the two vector approach that is based on the idea that high concentrations of scAAV particles are injected into localized areas of tissue leading to a high likelihood that a majority of the cells will take up many particles. This is crucial since the heavy and the light chains encoded of the respective scAAV vector must come together to form the full length IgG (Fuchs et al, 2015; Fuchs et al, 2016). Therefore, the

two vector approach using scAAV is probably even less suitable for receptor-targeted AAV that are administered systemically.

Finally, different studies have shown that AAV vectors can be used for the delivery of full-length antibodies making their application for the tumor-targeted delivery of immune checkpoint inhibitors that are used in clinics also feasible. However, due to the potential limitations of the two vector approach using scAAV vectors, ssAAV vectors should probably be preferred for the delivery of full-length antibodies especially when receptor-targeted vectors are used.

4.3.1.1 Duration of AAV-mediated antibody expression

An often mentioned advantage of AAV vectors for the delivery of antibodies is their capability to mediate a long-term transgene expression making re-administration of antibodies not necessary that, in contrast, is generally required for passive immunization due to the short half-life of antibodies (Deal & Balazs, 2015). Even though AAV genomes persist predominantly episomally in the cells, the protein will be expressed for the lifetime of the cell and as long as the transgene product is not recognized as foreign by the immune system (Schnepp et al, 2003; Schnepp et al, 2016; Johnson et al, 2009; Fuchs et al, 2015; Rivera et al, 2005; Mueller et al, 2017; Fuchs & Desrosiers, 2016). When long-term delivery of the transgene product is desired, AAV vectors are generally delivered to post-mitotic organs such as muscle, brain or liver resulting in a sustained transgene expression that can continue up to years (Mueller et al, 2017; Fuchs et al, 2015; Korbelin et al, 2016; Nakai et al, 1998). Intramuscular injection of AAV vectors delivering antibodies for cancer therapy resulted in a stable antibody expression for at least 70 to 85 days in mice. The serum concentrations strongly varied between the studies and were found to be in the range of 1 µg/ml up to 1,000 µg/ml (Lv et al, 2011; Ho et al, 2009; Principe et al, 2015). Intraperitoneal injections of AAV vectors into mice also enabled long-term transgene expression including one study by Xie *et al*. that used an AAV vector encoding an antibody for the treatment of ovarian cancer (Chen et al, 2017; Xie et al, 2014). Xie *et al.* observed persistent and high levels of AAV-delivered antibodies in intraperitoneal organs (lavage, omentum, mesentery and diaphragm) with concentrations between 200 ng/mg total protein up to 1,000 ng/mg total protein in the different organs 9 weeks after vector administration. Thus, their concentrations were around 100- up to 500-times higher as compared to the αPD-1 amounts in tumor tissue of Her2-AAV$^{\alpha PD\text{-}1}$-treated mice measured in the present study (2 ng/mg total protein). However, this can probably be

explained due to differences in the study design such as different time points of analysis (Xie *et al.*: 9 weeks; this thesis: 7 days after vector administration), different tissues encoding the antibody (Xie *et al.*: intraperitoneal organs; this thesis: tumor) or design of the AAV vector (Xie et al.: rhesus serotype 10 AAV (AAVrh10); this thesis: receptor-targeted Her2-AAV).

Also for immune checkpoint blockade in cancer therapy a sustained transgene expression might be advantageous since multiple administrations of immune checkpoint inhibitors are performed in pre-clinical models as well as for the treatment of patients in clinics (Kim et al, 2014; Duraiswamy et al, 2013; Larkin et al, 2015; Robert et al, 2015b). The present study aimed at the AAV-mediated delivery of immune checkpoint inhibitors to cancer cells that belong to mitotically active tissue. Accordingly, as long as the tumor cell is alive the transgene can probably be expressed by the cell enabling a sustained AAV-mediated expression of immune checkpoint inhibitors. But as soon as the tumor cell dies due to necrosis for instance this particular cell cannot further contribute to transgene expression. Thus, expression of the immune checkpoint inhibitors might decline over time. So far, the current study provided evidence for AAV-mediated expression of αPD-1 and αPD-L1 in the tumor 7 days after vector administration. It remains to be evaluated in more detail which amounts of immune checkpoint inhibitors are present in the tumor over time.

4.3.2 Further strategies to achieve local delivery of immune checkpoint inhibitors

As discussed in the previous chapter AAV vectors are a promising tool for the delivery of antibodies in order to treat different diseases. Furthermore, the current study provided first evidence that receptor-targeted Her2-AAV vectors are suitable for the tumor-specific delivery of immune checkpoint inhibitors. However, at present it is not exactly known to what extent the immune checkpoint inhibitors αPD-1 and αPD-L1 solely provoke their antitumor activity locally in the tumor microenvironment or whether immune checkpoint modulation in lymphoid organs might also play a decisive role for their efficacy. Nevertheless, as discussed in the following section other studies already investigated the therapeutic efficacy of locally administered αPD-1 as well as αPD-L1 immune checkpoint inhibitors showing a superior antitumor response for locally compared to systemically delivered inhibitors.

Li *et al.* used an alginate hydrogel system to locally deliver PD-1 specific mAbs (Table 20). A single local injection of hydrogels encapsulated with αPD-1 (100 µg/mouse) into the region adjacent to subcutaneous growing tumors showed an improved therapeutic efficacy as compared to a single systemic injection (intraperitoneal) of free αPD-1 (100 µg/mouse) in a syngeneic melanoma mouse model. The hydrogel-mediated local delivery resulted in sustained high levels of αPD-1 in serum and in tumor as compared to systemically applied αPD-1. In the serum, αPD-1 delivered from the hydrogel system achieved a stable αPD-1 serum concentration of about 10 µg/ml over a period of two weeks after treatment, whereas the αPD-1 levels of animals that were systemically injected with free αPD-1 started to decline on day 7 post medication achieving a level of about 2 µg/ml on day 14. In the tumor, the hydrogel delivery system achieved up to 50 µg αPD-1 per gram tumor tissue on day 1 post treatment and declined to a value of about 10 µg αPD-1 per gram tumor tissue two weeks later. In contrast, systemically injected αPD-1 resulted in comparatively lower antibody concentrations in the tumor with about 10 µg per gram tumor tissue on day 1 and no detectable levels on day 14 (Li et al, 2015). As in the present AAV study, Li *et al.* determined the αPD-1 levels in serum and in the tumor by ELISA and achieved higher levels as compared to the AAV-targeting approach. Using Her2-AAV vectors, an αPD-1 level of about 0.5 µg/ml was detected in the serum of mice and of about 0.13 µg αPD-1 per gram tumor tissue was measured in the tumor 7 days after vector administration. Thus, the measured αPD-1 concentrations in the present AAV study was around 20-times lower in the serum and about 80- to 400-times lower in the tumor. However, when comparing these two approaches it must be considered that Li *et al.* directly injected 100 µg αPD-1 encapsulated into hydrogels. In contrast, in the present AAV-targeting approach the αPD-1 protein is not directly injected into the mice rather an AAV vector encoding the immune checkpoint inhibitor. Moreover, it is possible that 7 days after vector administration is not sufficient to reach the peak of AAV-mediated transgene expression. Accordingly, higher expression levels might be achieved at later time points after vector application.

It remains to be investigated whether the amount of Her2-AAV-delivered αPD-1 is sufficient to mediate a therapeutic effect. If not, it would be possible to increase the AAV vector dose used for treatment and thereby potentially increase the intratumoral level of αPD-1. The high serum levels of αPD-1 in the study of Li *et al.* could be problematic in regard to treatment-induced toxicity mediated by αPD-1 but otherwise could be also required for the induction of the observed antitumoral effect. Further investigations are

necessary to evaluate in detail which αPD-1 levels are required in tumor, serum or other organs in order to induce an antitumoral response.

Table 20: Different strategies for the local delivery of PD-1- and PD-L1-specific immune checkpoint inhibitors

	delivery of ICI[1] as protein			delivery of ICI[1] as gene	
strategy	alginate hydrogels encapsulated with αPD-1 mAbs (Li et al. 2015)	self-degradable microneedle patches composed of hyaluronic acid integrated with nanoparticles that encapsulate αPD-1 mAbs (Wang et al. 2016)	αPD-L1 mAb-conjugated platelets (Wang et al. 2017)	oncolytic virus (Engeland et al. 2014; Bartee et al. 2017)	receptor-targeted AAV (this thesis)
graphical illustration	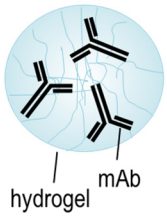	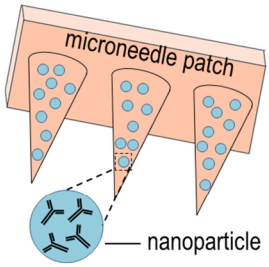	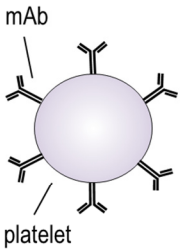	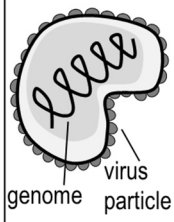	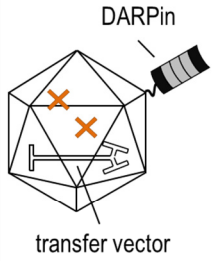
application route	injection into the region adjacent to growing tumors	local administration onto the tumor site	intravenous injection	intratumoral injection	intravenous injection

[1]Immune checkpoint inhibitor

A further approach for the sustained local delivery of αPD-1 mAbs involved self-degradable microneedle (MN) patches investigated by Wang *et al.* (Table 20). The used MN patches were loaded with dextran nanoparticles that encapsulate αPD-1 mAbs and were implanted into the skin of the mice at the site of the subcutaneous growing melanoma tumor. MN patches enabled a sustained release of αPD-1 for at least 3 days after implantation as determined by immunostaining of tumor sections. In contrast, intratumoral injection of free αPD-1 resulted in a strong antibody signal on the administration day, but signals diminished in the following 3 days. In accordance to that observation, αPD-1 delivered by MN patches exhibited a superior antitumor effect as compared to intratumorally injected αPD-1 in tumor-bearing mice and furthermore, showed an increased number of $CD8^+$ TILs. Wang and colleagues attributed this improved antitumor efficacy to the sustained release of αPD-1 into the tumor by MN

patches (Wang et al, 2016). Probably, AAV vectors might also facilitate a sustained delivery of immune checkpoint inhibitors as the vectors enable expression of their transgene for the life-time of the transduced cell (more details discussed in 4.3.1.1). Moreover, it is probable that the duration of antibody delivery might be even prolonged for AAV vectors as compared to the hydrogel system of Li *et al.* or the MN patch system of Wang *et al.*, since the respective gene that continuously expresses the immune checkpoint inhibitor is transferred. In addition, continuous delivery of immune checkpoint inhibitors by AAV vectors may counterbalance the lower antibody levels that are delivered into the tumor tissue by the vectors as compared to direct administration of mAbs. Furthermore, Wang *et al.* revealed an improved therapeutic efficacy of αPD-1 delivered locally by MN patches as compared to systemically administered (intravenous) free αPD-1 (Wang et al, 2016). This again indicates that local application of immune checkpoint inhibitors is not only beneficial as it might minimize the risk of toxicity but also as it can enhance the therapeutic effect of cancer immunotherapy. However, in contrast to the receptor-targeted AAV vectors specifically delivering immune checkpoint inhibitors directly into the tumor tissue, the hydrogel delivery and the MN patch system deliver αPD-1 mAbs in the region of the tumor and thus possibly also to local lymph nodes. Accordingly, delivery of αPD-1 mAbs in lymphatic tissue might have supported the observed antitumoral efficacy. Nevertheless, the clinical applicability of the hydrogel and the MN patch system is limited for the treatment of patients exhibiting accessible tumor sites. In contrast, Her2-AAV vectors would also enable the local delivery of immune checkpoint inhibitors to inaccessible or metastatic tumors (Münch et al, 2015).

Another strategy also investigated by Wang and colleagues that enabled the treatment of metastases used αPD-L1 conjugated to the surface of platelets (Table 20). They showed that upon intravenous injection of αPD-L1-conjugated platelets into tumor-bearing mice, platelets facilitated αPD-L1 accumulation in the tumor. Due to the enhanced local antibody concentration around the tumor cells, αPD-L1-conjugated platelets showed an improved therapeutic effect as compared to the systemic injection of free αPD-L1 (Wang et al, 2017).

In order to achieve the local delivery of PD-1- and PD-L1-specific inhibitors, other groups also examined the applicability of viral systems, especially in the context of oncolytic immunotherapy (Table 20). In contrast to the previous described strategies,

the gene rather than the protein is locally delivered to the tumor, as in the present AAV study.

Engeland *et al.* compared the therapeutic efficacy of intratumorally injected oncolytic measles virus encoding a PD-L1-specific inhibitor (MV-αPD-L1) with the combination therapy composed of systemically administered αPD-L1 mAb and intratumoral measles virus infection in a melanoma mouse model. The same PD-L1-specific inhibitor that was encoded by the measles virus in their study was also used in the present AAV study. However, Engeland and colleagues could not observe an improved treatment response for local measles virus-mediated checkpoint blockade compared to the combination treatment of measles virus with systemic αPD-L1 therapy. Therapy efficacy was similar for both approaches (Engeland et al, 2014).

Another study by Bartee and colleagues equipped oncolytic myxoma virus with the coding sequence of the soluble form of PD-1 (vPD-1) that was also proven to block the PD-1/PD-L1 checkpoints. They showed that intratumorally injected vPD-1 exhibited less toxicity and was more effective than the combination therapy using intratumoral injection of unmodified myxoma virus and systemic application of αPD-1 mAbs. However, since they used different immune checkpoint inhibitor constructs (soluble PD-1 vs αPD-1 mAb) for their comparison, the results should be considered carefully. Nevertheless, vPD-1 treatment exhibited significantly less symptoms of an autoimmune-like toxicity that was characterized by progressive alopecia as compared to the combination therapy of systemically administered αPD-1 and local myxoma virus treatment. Thus, their study is an example that locally delivered immune checkpoint inhibitors might decrease treatment-related toxicity. Furthermore, the study demonstrated an increased therapeutic efficacy of local virus-delivered immune checkpoint inhibitors as compared to systemic mAb administration. Accordingly, their investigations provide evidence that tumor-expressed immune checkpoint inhibitors may improve therapy outcome as compared to systemically applied mAbs (Bartee et al, 2017).

Taken together, immune checkpoint blockade therapy is most likely improved by strategies enabling a sustained and local delivery of the inhibitors. Thus, receptor-targeted AAV vectors are a promising vehicle for the *in vivo* delivery of immune checkpoint inhibitors as they potentially have the capability to mediate a local as well as a continuous expression of antibodies *in vivo* and are also applicable for the treatment of

inaccessible tumors. Further investigations are required to evaluate whether tumor-targeted delivery of PD-1- or PD-L1-specific inhibitors by Her2-AAV indeed reduces toxicity compared to systemic antibody administration and whether this strategy elicits a potent antitumor response.

5 References

Abdel-Wahab N, Shah M & Suarez-Almazor ME (2016) Adverse Events Associated with Immune Checkpoint Blockade in Patients with Cancer: A Systematic Review of Case Reports. PLoS ONE 11: e0160221

Ahmadzadeh M, Johnson LA, Heemskerk B, Wunderlich JR, Dudley ME, White DE & Rosenberg SA (2009) Tumor antigen-specific CD8 T cells infiltrating the tumor express high levels of PD-1 and are functionally impaired. Blood 114: 1537–1544

Ahmed M, McKenzie MO, Puckett S, Hojnacki M, Poliquin L & Lyles DS (2003) Ability of the matrix protein of vesicular stomatitis virus to suppress beta interferon gene expression is genetically correlated with the inhibition of host RNA and protein synthesis. J Virol 77: 4646–4657

Akache B, Grimm D, Pandey K, Yant SR, Xu H & Kay MA (2006) The 37/67-kilodalton laminin receptor is a receptor for adeno-associated virus serotypes 8, 2, 3, and 9. J Virol 80: 9831–9836

Alcami A, Symons JA & Smith GL (2000) The Vaccinia Virus Soluble Alpha/Beta Interferon (IFN) Receptor Binds to the Cell Surface and Protects Cells from the Antiviral Effects of IFN. Journal of Virology 74: 11230–11239

Alexandrov LB, Nik-Zainal S, Wedge DC, Aparicio SAJR, Behjati S, Biankin AV, Bignell GR, Bolli N, Borg A, Børresen-Dale A-L, Boyault S, Burkhardt B, Butler AP, Caldas C, Davies HR, Desmedt C, Eils R, Eyfjörd JE, Foekens JA & Greaves M et al (2013) Signatures of mutational processes in human cancer. Nature 500: 415–421

Asokan A, Schaffer DV & Samulski RJ (2012) The AAV vector toolkit: poised at the clinical crossroads. Mol. Ther 20: 699–708

Aznar MA, Tinari N, Rullán AJ, Sánchez-Paulete AR, Rodriguez-Ruiz ME & Melero I (2017) Intratumoral Delivery of Immunotherapy-Act Locally, Think Globally. J Immunol 198: 31–39

Azuma T, Yao S, Zhu G, Flies AS, Flies SJ & Chen L (2008) B7-H1 is a ubiquitous antiapoptotic receptor on cancer cells. Blood 111: 3635–3643

Ball LA & White CN (1976) Order of transcription of genes of vesicular stomatitis virus. Proc Natl Acad Sci U S A 73: 442–446

Bardhan K, Anagnostou T & Boussiotis VA (2016) The PD1:PD-L1/2 Pathway from Discovery to Clinical Implementation. Frontiers in immunology 7: 550

Barr JN, Whelan SPJ & Wertz GW (2002) Transcriptional control of the RNA-dependent RNA polymerase of vesicular stomatitis virus. Biochimica et biophysica acta 1577: 337–353

Bartee MY, Dunlap KM & Bartee E (2017) Tumor-Localized Secretion of Soluble PD1 Enhances Oncolytic Virotherapy. Cancer Res 77: 2952–2963

Baxevanis CN, Perez SA & Papamichail M (2009) Cancer immunotherapy. Crit Rev Clin Lab Sci 46: 167–189

Beatty GL & Gladney WL (2015) Immune escape mechanisms as a guide for cancer immunotherapy. Clin. Cancer Res 21: 687–692

Benencia F, Courreges MC, Conejo-García JR, Buckanovich RJ, Zhang L, Carroll RH, Morgan MA & Coukos G (2005) Oncolytic HSV exerts direct antiangiogenic activity in ovarian carcinoma. Hum Gene Ther 16: 765–778

Bergman I, Griffin JA, Gao Y & Whitaker-Dowling P (2007) Treatment of implanted mammary tumors with recombinant vesicular stomatitis virus targeted to Her2/neu. Int. J. Cancer 121: 425–430

Bi Z, Barna M, Komatsu T & Reiss CS (1995) Vesicular stomatitis virus infection of the central nervous system activates both innate and acquired immunity. J Virol 69: 6466–6472

Black BL & Lyles DS (1992) Vesicular stomatitis virus matrix protein inhibits host cell-directed transcription of target genes in vivo. J Virol 66: 4058–4064

Boritz E, Gerlach J, Johnson JE & Rose JK (1999) Replication-competent rhabdoviruses with human immunodeficiency virus type 1 coats and green fluorescent protein: entry by a pH-independent pathway. J Virol 73: 6937–6945

Brasel K, McKenna HJ, Morrissey PJ, Charrier K, Morris AE, Lee CC, Williams DE & Lyman SD (1996) Hematologic effects of flt3 ligand in vivo in mice. Blood 88: 2004–2012

Braun SE, Chen K, Blazar BR, Orchard PJ, Sledge G, Robertson MJ, Broxmeyer HE & Cornetta K (1999) Flt3 ligand antitumor activity in a murine breast cancer model: A comparison with granulocyte-macrophage colony-stimulating factor and a potential mechanism of action. Hum Gene Ther 10: 2141–2151

Breitbach CJ, Arulanandam R, Silva N de, Thorne SH, Patt R, Daneshmand M, Moon A, Ilkow C, Burke J, Hwang T-H, Heo J, Cho M, Chen H, Angarita FA, Addison C, McCart JA, Bell JC & Kirn DH (2013) Oncolytic vaccinia virus disrupts tumor-associated vasculature in humans. Cancer Res 73: 1265–1275

Buchholz CJ, Friedel T & Büning H (2015) Surface-Engineered Viral Vectors for Selective and Cell Type-Specific Gene Delivery. Trends in biotechnology 33: 777–790

Buller RM, Janik JE, Sebring ED & Rose JA (1981) Herpes simplex virus types 1 and 2 completely help adenovirus-associated virus replication. J Virol 40: 241–247

Büning H (2013) Gene therapy enters the pharma market: The short story of a long journey. EMBO Mol Med 5: 1–3

Büning H, Huber A, Zhang L, Meumann N & Hacker U (2015) Engineering the AAV capsid to optimize vector-host-interactions. Current opinion in pharmacology 24: 94–104

Butte MJ, Keir ME, Phamduy TB, Sharpe AH & Freeman GJ (2007) Programmed death-1 ligand 1 interacts specifically with the B7-1 costimulatory molecule to inhibit T cell responses. Immunity 27: 111–122

Capece D, Verzella D, Fischietti M, Zazzeroni F & Alesse E (2012) Targeting costimulatory molecules to improve antitumor immunity. J. Biomed. Biotechnol 2012: 926321

Casto BC, Atchison RW & Hammon WM (1967) Studies on the relationship between adeno-associated virus type I (AAV-1) and adenoviruses. I. Replication of AAV-1 in certain cell cultures and its effect on helper adenovirus. Virology 32: 52–59

Chen K, Braun S, Lyman S, Fan Y, Traycoff CM, Wiebke EA, Gaddy J, Sledge G, Broxmeyer HE & Cornetta K (1997) Antitumor activity and immunotherapeutic properties of Flt3-ligand in a murine breast cancer model. Cancer Res 57: 3511–3516

Chen L (2004) Co-inhibitory molecules of the B7-CD28 family in the control of T-cell immunity. Nat Rev Immunol 4: 336–347

Chen W, Jin W, Hardegen N, Lei K-J, Li L, Marinos N, McGrady G & Wahl SM (2003) Conversion of peripheral CD4+CD25- naive T cells to CD4+CD25+ regulatory T cells by TGF-beta induction of transcription factor Foxp3. J Exp Med 198: 1875–1886

Chen Y-H, Wu K-J, Wu K-L, Wu K-L, Tsai H-M, Chen M-L, Chen Y-W, Hsieh W, Lin C-M & Wang Y (2017) Recombinant Adeno-Associated Virus-Mediated Expression of Methamphetamine Antibody Attenuates Methamphetamine-Induced Hyperactivity in Mice. Sci Rep 7: 46301

Choi K-J, Kim J-H, Lee Y-S, Kim J, Suh B-S, Kim H, Cho S, Sohn J-H, Kim GE & Yun C-O (2006) Concurrent delivery of GM-CSF and B7-1 using an oncolytic adenovirus elicits potent antitumor effect. Gene Ther 13: 1010–1020

Chou J, Kern ER, Whitley RJ & Roizman B (1990) Mapping of herpes simplex virus-1 neurovirulence to gamma 134.5, a gene nonessential for growth in culture. Science 250: 1262–1266

Clarke DK, Nasar F, Lee M, Johnson JE, Wright K, Calderon P, Guo M, Natuk R, Cooper D, Hendry RM & Udem SA (2007) Synergistic attenuation of vesicular stomatitis virus by combination of specific G gene truncations and N gene translocations. J Virol 81: 2056–2064

Collaco RF, Kalman-Maltese V, Smith AD, Dignam JD & Trempe JP (2003) A biochemical characterization of the adeno-associated virus Rep40 helicase. J Biol Chem 278: 34011–34017

Cooper D, Wright KJ, Calderon PC, Guo M, Nasar F, Johnson JE, Coleman JW, Lee M, Kotash C, Yurgelonis I, Natuk RJ, Hendry RM, Udem SA & Clarke DK (2008) Attenuation of recombinant vesicular stomatitis virus-human immunodeficiency virus type 1 vaccine vectors by gene translocations and g gene truncation reduces neurovirulence and enhances immunogenicity in mice. J. Virol. 82: 207–219

Coura Rdos S & Nardi NB (2007) The state of the art of adeno-associated virus-based vectors in gene therapy. Virol J 4: 99

Couzin-Frankel J (2013) Breakthrough of the year 2013. Cancer immunotherapy. Science (New York, N.Y.) 342: 1432–1433

Cronin M, Le Boeuf F, Murphy C, Roy DG, Falls T, Bell JC & Tangney M (2014) Bacterial-mediated knockdown of tumor resistance to an oncolytic virus enhances therapy. Mol Ther 22: 1188–1197

Cureton DK, Massol RH, Whelan SPJ & Kirchhausen T (2010) The length of vesicular stomatitis virus particles dictates a need for actin assembly during clathrin-dependent endocytosis. PLoS Pathog 6: e1001127

Curiel TJ, Coukos G, Zou L, Alvarez X, Cheng P, Mottram P, Evdemon-Hogan M, Conejo-Garcia JR, Zhang L, Burow M, Zhu Y, Wei S, Kryczek I, Daniel B, Gordon A, Myers L, Lackner A, Disis ML, Knutson KL, Chen L & Zou W (2004) Specific recruitment of regulatory T cells in ovarian carcinoma fosters immune privilege and predicts reduced survival. Nat Med 10: 942–949

Curiel TJ, Wei S, Dong H, Alvarez X, Cheng P, Mottram P, Krzysiek R, Knutson KL, Daniel B, Zimmermann MC, David O, Burow M, Gordon A, Dhurandhar N, Myers L, Berggren R, Hemminki A, Alvarez RD, Emilie D, Curiel DT, Chen L & Zou W (2003) Blockade of B7-H1 improves myeloid dendritic cell-mediated antitumor immunity. Nat Med 9: 562–567

Daya S & Berns KI (2008) Gene Therapy Using Adeno-Associated Virus Vectors. Clinical Microbiology Reviews 21: 583–593

D'Costa S, Blouin V, Broucque F, Penaud-Budloo M, François A, Perez IC, Le Bec C, Moullier P, Snyder RO & Ayuso E (2016) Practical utilization of recombinant AAV vector reference standards: focus on vector genomes titration by free ITR qPCR. Molecular therapy. Methods & clinical development 5: 16019

Deal CE & Balazs AB (2015) Vectored antibody gene delivery for the prevention or treatment of HIV infection. Current opinion in HIV and AIDS 10: 190–197

del Rio M-L, Penuelas-Rivas G, Dominguez-Perles R, Ramirez P, Parrilla P & Rodriguez-Barbosa J-I (2005) Antibody-mediated signaling through PD-1 costimulates T cells and enhances CD28-dependent proliferation. Eur J Immunol 35: 3545–3560

Dheilly E, Moine V, Broyer L, Salgado-Pires S, Johnson Z, Papaioannou A, Cons L, Calloud S, Majocchi S, Nelson R, Rousseau F, Ferlin W, Kosco-Vilbois M, Fischer N & Masternak K (2017) Selective Blockade of the Ubiquitous Checkpoint Receptor CD47 Is Enabled by Dual-Targeting Bispecific Antibodies. Mol Ther 25: 523–533

Diaz RM, Galivo F, Kottke T, Wongthida P, Qiao J, Thompson J, Valdes M, Barber G & Vile RG (2007) Oncolytic immunovirotherapy for melanoma using vesicular stomatitis virus. Cancer Res. 67: 2840–2848

Dold C, Rodriguez Urbiola C, Wollmann G, Egerer L, Muik A, Bellmann L, Fiegl H, Marth C, Kimpel J & Laer D von (2016) Application of interferon modulators to overcome partial resistance of human ovarian cancers to VSV-GP oncolytic viral therapy. Molecular therapy oncolytics 3: 16021

Dong H, Strome SE, Salomao DR, Tamura H, Hirano F, Flies DB, Roche PC, Lu J, Zhu G, Tamada K, Lennon VA, Celis E & Chen L (2002) Tumor-associated B7-H1 promotes T-cell apoptosis: a potential mechanism of immune evasion. Nature medicine 8: 793–800

Duan F, Simeone S, Wu R, Grady J, Mandoiu I & Srivastava PK (2012) Area under the curve as a tool to measure kinetics of tumor growth in experimental animals. J Immunol Methods 382: 224–228

Duraiswamy J, Kaluza KM, Freeman GJ & Coukos G (2013) Dual blockade of PD-1 and CTLA-4 combined with tumor vaccine effectively restores T-cell rejection function in tumors. Cancer Res 73: 3591–3603

Egen JG & Allison JP (2002) Cytotoxic T lymphocyte antigen-4 accumulation in the immunological synapse is regulated by TCR signal strength. Immunity 16: 23–35

Ehrlich P (1909) Über den jetzigen Stand der Karzinomforschung. Beiträge zur experimentellen Pathologie und Chemotherapie: 117-164

Emerson SU (1982) Reconstitution studies detect a single polymerase entry site on the vesicular stomatitis virus genome. Cell 31: 635–642

Engeland CE, Grossardt C, Veinalde R, Bossow S, Lutz D, Kaufmann JK, Shevchenko I, Umansky V, Nettelbeck DM, Weichert W, Jäger D, Kalle C von & Ungerechts G (2014) CTLA-4 and PD-L1 checkpoint blockade enhances oncolytic measles virus therapy. Mol Ther 22: 1949–1959

Farkona S, Diamandis EP & Blasutig IM (2016) Cancer immunotherapy: the beginning of the end of cancer? BMC medicine 14: 73

Fernandez M, Porosnicu M, Markovic D & Barber GN (2002) Genetically Engineered Vesicular Stomatitis Virus in Gene Therapy: Application for Treatment of Malignant Disease. J Virol 76: 895–904

Ferrantini M, Capone I & Belardelli F (2007) Interferon-alpha and cancer: mechanisms of action and new perspectives of clinical use. Biochimie 89: 884–893

Finkelshtein D, Werman A, Novick D, Barak S & Rubinstein M (2013) LDL receptor and its family members serve as the cellular receptors for vesicular stomatitis virus. Proceedings of the National Academy of Sciences of the United States of America 110: 7306–7311

Fransen MF, Sluis T van der, Ossendorp F, Arens R & Melief CJ (2013) Controlled local delivery of CTLA-4 blocking antibody induces CD8+ T-cell-dependent tumor eradication and decreases risk of toxic side effects. Clin Cancer Res 19: 5381–5389

Freeman GJ, Borriello F, Hodes RJ, Reiser H, Gribben JG, Ng JW, Kim J, Goldberg JM, Hathcock K & Laszlo G (1993) Murine B7-2, an alternative CTLA4 counter-receptor that costimulates T cell proliferation and interleukin 2 production. J Exp Med 178: 2185–2192

Freeman GJ, Long AJ, Iwai Y, Bourque K, Chernova T, Nishimura H, Fitz LJ, Malenkovich N, Okazaki T, Byrne MC, Horton HF, Fouser L, Carter L, Ling V, Bowman MR, Carreno BM, Collins M, Wood CR & Honjo T (2000) Engagement of the PD-1 immunoinhibitory receptor by a novel B7 family member leads to negative regulation of lymphocyte activation. The Journal of experimental medicine 192: 1027–1034

Früh K, Ahn K, Djaballah H, Sempé P, van Endert PM, Tampé R, Peterson PA & Yang Y (1995) A viral inhibitor of peptide transporters for antigen presentation. Nature 375: 415–418

Fu J, Malm I-J, Kadayakkara DK, Levitsky H, Pardoll D & Kim YJ (2014) Preclinical evidence that PD1 blockade cooperates with cancer vaccine TEGVAX to elicit regression of established tumors. Cancer Res. 74: 4042–4052

Fuchs SP & Desrosiers RC (2016) Promise and problems associated with the use of recombinant AAV for the delivery of anti-HIV antibodies. Mol Ther Methods Clin Dev 3: 16068

Fuchs SP, Martinez-Navio JM, Gao G & Desrosiers RC (2016) Recombinant AAV Vectors for Enhanced Expression of Authentic IgG. PLoS ONE 11: e0158009

Fuchs SP, Martinez-Navio JM, Piatak M, Lifson JD, Gao G & Desrosiers RC (2015) AAV-Delivered Antibody Mediates Significant Protective Effects against SIVmac239 Challenge in the Absence of Neutralizing Activity. PLoS Pathog 11: e1005090

Fukuhara H, Ino Y, Kuroda T, Martuza RL & Todo T (2005) Triple gene-deleted oncolytic herpes simplex virus vector double-armed with interleukin 18 and soluble B7-1 constructed by bacterial artificial chromosome-mediated system. Cancer Res. 65: 10663–10668

Galluzzi L, Buqué A, Kepp O, Zitvogel L & Kroemer G (2017) Immunogenic cell death in cancer and infectious disease. Nat Rev Immunol. 17: 97–111

Gao G-P, Lu Y, Sun X, Johnston J, Calcedo R, Grant R & Wilson JM (2006) High-level transgene expression in nonhuman primate liver with novel adeno-associated virus serotypes containing self-complementary genomes. J Virol 80: 6192–6194

Ge P, Tsao J, Schein S, Green TJ, Luo M & Zhou ZH (2010) Cryo-EM model of the bullet-shaped vesicular stomatitis virus. Science (New York, N.Y.) 327: 689–693

Gentner B & Naldini L (2012) Exploiting microRNA regulation for genetic engineering. Tissue antigens 80: 393–403

Goel A, Carlson SK, Classic KL, Greiner S, Naik S, Power AT, Bell JC & Russell SJ (2007) Radioiodide imaging and radiovirotherapy of multiple myeloma using VSV(Delta51)-NIS, an attenuated vesicular stomatitis virus encoding the sodium iodide symporter gene. Blood 110: 2342–2350

Gonçalves MA (2005) Adeno-associated virus: from defective virus to effective vector. Virol J 2: 43

Gray JD, Hirokawa M & Horwitz DA (1994) The role of transforming growth factor beta in the generation of suppression: An interaction between CD8+ T and NK cells. J Exp Med 180: 1937–1942

Gubin MM, Artyomov MN, Mardis ER & Schreiber RD (2015) Tumor neoantigens: Building a framework for personalized cancer immunotherapy. The Journal of clinical investigation 125: 3413–3421

Guo ZS, Liu Z, Kowalsky S, Feist M, Kalinski P, Lu B, Storkus WJ & Bartlett DL (2017) Oncolytic Immunotherapy: Conceptual Evolution, Current Strategies, and Future Perspectives. Front Immunol 8: 555

Hamanishi J, Mandai M, Matsumura N, Abiko K, Baba T & Konishi I (2016) PD-1/PD-L1 blockade in cancer treatment: perspectives and issues. International journal of clinical oncology 21: 462–473

Hamilton JA (2008) Colony-stimulating factors in inflammation and autoimmunity. Nat Rev Immunol. 8: 533–544

Hastie E & Grdzelishvili VZ (2012) Vesicular stomatitis virus as a flexible platform for oncolytic virotherapy against cancer. Journal of General Virology 93: 2529–2545

Herrada AA, Rojas-Colonelli N, González-Figueroa P, Roco J, Oyarce C, Ligtenberg MA & Lladser A (2012) Harnessing DNA-induced immune responses for improving cancer vaccines. Human vaccines & immunotherapeutics 8: 1682–1693

Hino R, Kabashima K, Kato Y, Yagi H, Nakamura M, Honjo T, Okazaki T & Tokura Y (2010) Tumor cell expression of programmed cell death-1 ligand 1 is a prognostic factor for malignant melanoma. Cancer 116: 1757–1766

Hirayama Y, Gi M, Yamano S, Tachibana H, Okuno T, Tamada S, Nakatani T & Wanibuchi H (2016) Anti-PD-L1 treatment enhances antitumor effect of everolimus in a mouse model of renal cell carcinoma. Cancer Science 107: 1736–1744

Hiroishi K, Tuting T & Lotze MT (2000) IFN-alpha-Expressing Tumor Cells Enhance Generation and Promote Survival of Tumor-Specific CTLs. J Immunol 164: 567–572

Ho DT, Wykoff-Clary S, Gross CS, Schneider D, Jin F, Kretschmer PJ & Hermiston TW (2009) Growth inhibition of an established A431 xenograft tumor by a full-length anti-EGFR antibody following gene delivery by AAV. Cancer gene therapy 16: 184–194

Hughes T, Coffin RS, Lilley CE, Ponce R & Kaufman HL (2014) Critical analysis of an oncolytic herpesvirus encoding granulocyte-macrophage colony stimulating factor for the treatment of malignant melanoma. Oncolytic virotherapy 3: 11–20

Ichim CV (2005) Revisiting immunosurveillance and immunostimulation: Implications for cancer immunotherapy. J Transl Med 3: 8

Im DS & Muzyczka N (1990) The AAV origin binding protein Rep68 is an ATP-dependent site-specific endonuclease with DNA helicase activity. Cell 61: 447–457

Im DS & Muzyczka N (1992) Partial purification of adeno-associated virus Rep78, Rep52, and Rep40 and their biochemical characterization. J Virol 66: 1119–1128

Ino Y, Saeki Y, Fukuhara H & Todo T (2006) Triple combination of oncolytic herpes simplex virus-1 vectors armed with interleukin-12, interleukin-18, or soluble B7-1 results in enhanced antitumor efficacy. Clin Cancer Res 12: 643–652

Itsumi M & Tatsugami K (2010) Immunotherapy for renal cell carcinoma. Clinical & developmental immunology 2010: 284581

Iverson LE & Rose JK (1981) Localized attenuation and discontinuous synthesis during vesicular stomatitis virus transcription. Cell 23: 477–484

Jiang T & Zhou C (2015) The past, present and future of immunotherapy against tumor. Translational lung cancer research 4: 253–264

Johnson JE, Nasar F, Coleman JW, Price RE, Javadian A, Draper K, Lee M, Reilly PA, Clarke DK, Hendry RM & Udem SA (2007) Neurovirulence properties of recombinant vesicular stomatitis virus vectors in non-human primates. Virology 360: 36–49

Johnson PR, Schnepp BC, Zhang J, Connell MJ, Greene SM, Yuste E, Desrosiers RC & Clark KR (2009) Vector-mediated gene transfer engenders long-lived neutralizing activity and protection against SIV infection in monkeys. Nat Med 15: 901–906

Kantoff PW, Higano CS, Shore ND, Berger ER, Small EJ, Penson DF, Redfern CH, Ferrari AC, Dreicer R, Sims RB, Xu Y, Frohlich MW & Schellhammer PF (2010) Sipuleucel-T immunotherapy for castration-resistant prostate cancer. N Engl J Med 363: 411–422

Kärber G (1931) Beitrag zur kollektiven Behandlung pharmakologischer Reihenversuche. Archiv f. experiment. Pathol. u. Pharmakol 162: 480–483

Kaufman HL, Kohlhapp FJ & Zloza A (2015) Oncolytic viruses: a new class of immunotherapy drugs. Nat Rev Drug Discov 14: 642–662

Kaufman HL, Ruby CE, Hughes T & Slingluff CL Jr (2014) Current status of granulocyte-macrophage colony-stimulating factor in the immunotherapy of melanoma. J Immunother Cancer 2: 11

Keir ME, Butte MJ, Freeman GJ & Sharpe AH (2008) PD-1 and its ligands in tolerance and immunity. Annual review of immunology 26: 677–704

Kern A, Schmidt K, Leder C, Müller OJ, Wobus CE, Bettinger K, Von der Lieth, CW, King JA & Kleinschmidt JA (2003) Identification of a heparin-binding motif on adeno-associated virus type 2 capsids. J Virol 77: 11072–11081

Kim ES (2017) Avelumab: First Global Approval. Drugs 77: 929–937

Kim K, Skora AD, Li Z, Liu Q, Tam AJ, Blosser RL, Diaz LA, Papadopoulos N, Kinzler KW, Vogelstein B & Zhou S (2014) Eradication of metastatic mouse cancers resistant to immune checkpoint blockade by suppression of myeloid-derived cells. Proceedings of the National Academy of Sciences of the United States of America 111: 11774–11779

King GD, Muhammad AKMG, Curtin JF, Barcia C, Puntel M, Liu C, Honig SB, Candolfi M, Mondkar S, Lowenstein PR & Castro MG (2008) Flt3L and TK gene therapy eradicate multifocal glioma in a syngeneic glioblastoma model. Neuro Oncol 10: 19–31

King JA, Dubielzig R, Grimm D & Kleinschmidt JA (2001) DNA helicase-mediated packaging of adeno-associated virus type 2 genomes into preformed capsids. EMBO J 20: 3282–3291

Kirn D, Martuza RL & Zwiebel J (2001) Replication-selective virotherapy for cancer: Biological principles, risk management and future directions. Nat Med 7: 781–787

Klapper LN, Kirschbaum MH, Sela M & Yarden Y (2000) Biochemical and clinical implications of the ErbB/HER signaling network of growth factor receptors. Advances in cancer research 77: 25–79

Korbelin J, Dogbevia G, Michelfelder S, Ridder DA, Hunger A, Wenzel J, Seismann H, Lampe M, Bannach J, Pasparakis M, Kleinschmidt JA, Schwaninger M & Trepel M (2016) A brain microvasculature endothelial cell-specific viral vector with the potential to treat neurovascular and neurological diseases. EMBO molecular medicine 8: 609–625

Kotin RM, Siniscalco M, Samulski RJ, Zhu XD, Hunter L, Laughlin CA, McLaughlin S, Muzyczka N, Rocchi M & Berns KI (1990) Site-specific integration by adeno-associated virus. Proc Natl Acad Sci U S A 87: 2211–2215

Kotterman MA, Chalberg TW & Schaffer DV (2015) Viral Vectors for Gene Therapy: Translational and Clinical Outlook. Annu Rev Biomed Eng 17: 63–89

Kotterman MA & Schaffer DV (2014) Engineering adeno-associated viruses for clinical gene therapy. Nat Rev Genet. 15: 445–451

Kottke T, Diaz RM, Kaluza K, Pulido J, Galivo F, Wongthida P, Thompson J, Willmon C, Barber GN, Chester J, Selby P, Strome S, Harrington K, Melcher A & Vile RG (2008) Use of biological therapy to enhance both virotherapy and adoptive T-cell therapy for cancer. Mol Ther 16: 1910–1918

Larkin J, Chiarion-Sileni V, Gonzalez R, Grob JJ, Cowey CL, Lao CD, Schadendorf D, Dummer R, Smylie M, Rutkowski P, Ferrucci PF, Hill A, Wagstaff J, Carlino MS, Haanen JB, Maio M, Marquez-Rodas I, McArthur GA, Ascierto PA & Long GV et al (2015) Combined Nivolumab and Ipilimumab or Monotherapy in Untreated Melanoma. N Engl J Med 373: 23–34

Larocca C & Schlom J (2011) Viral vector-based therapeutic cancer vaccines. Cancer journal (Sudbury, Mass.) 17: 359–371

Latchman Y, Wood CR, Chernova T, Chaudhary D, Borde M, Chernova I, Iwai Y, Long AJ, Brown JA, Nunes R, Greenfield EA, Bourque K, Boussiotis VA, Carter LL, Carreno BM, Malenkovich N, Nishimura

H, Okazaki T, Honjo T, Sharpe AH & Freeman GJ (2001) PD-L2 is a second ligand for PD-1 and inhibits T cell activation. Nat Immunol 2: 261–268

Lawson ND, Stillman EA, Whitt MA & Rose JK (1995) Recombinant vesicular stomatitis viruses from DNA. Proc Natl Acad Sci U S A 92: 4477–4481

Le Boeuf F, Diallo J-S, McCart JA, Thorne S, Falls T, Stanford M, Kanji F, Auer R, Brown CW, Lichty BD, Parato K, Atkins H, Kirn D & Bell JC (2010) Synergistic interaction between oncolytic viruses augments tumor killing. Mol Ther 18: 888–895

Lee KM, Chuang E, Griffin M, Khattri R, Hong DK, Zhang W, Straus D, Samelson LE, Thompson CB & Bluestone JA (1998) Molecular basis of T cell inactivation by CTLA-4. Science 282: 2263–2266

Lee S & Margolin K (2011) Cytokines in cancer immunotherapy. Cancers 3: 3856–3893

Lee Y-S, Kim J-H, Choi K-J, Choi I-K, Kim H, Cho S, Cho BC & Yun C-O (2006) Enhanced Antitumor Effect of Oncolytic Adenovirus Expressing Interleukin-12 and B7-1 in an Immunocompetent Murine Model. Clinical Cancer Research 12: 5859–5868

Lemay CG, Rintoul JL, Kus A, Paterson JM, Garcia V, Falls TJ, Ferreira L, Bridle BW, Conrad DP, Tang VA, Diallo J-S, Arulanandam R, Le Boeuf F, Garson K, Vanderhyden BC, Stojdl DF, Lichty BD, Atkins HL, Parato KA, Bell JC & Auer JC (2012) Harnessing oncolytic virus-mediated antitumor immunity in an infected cell vaccine. Mol Ther 20: 1791–1799

Leveille S, Goulet M-L, Lichty BD & Hiscott J (2011) Vesicular stomatitis virus oncolytic treatment interferes with tumor-associated dendritic cell functions and abrogates tumor antigen presentation. J Virol 85: 12160–12169

Lewis AD, Chen R, Montefiori DC, Johnson PR & Clark KR (2002) Generation of neutralizing activity against human immunodeficiency virus type 1 in serum by antibody gene transfer. J Virol 76: 8769–8775

Li Q & Tainsky MA (2011) Epigenetic silencing of IRF7 and/or IRF5 in lung cancer cells leads to increased sensitivity to oncolytic viruses. PLoS ONE 6: e28683

Li Y, Fang M, Zhang J, Wang J, Song Y, Shi J, Li W, Wu G, Ren J, Wang Z, Zou W & Wang L (2015) Hydrogel dual delivered celecoxib and anti-PD-1 synergistically improve antitumor immunity. Oncoimmunology 5: e1074374

Lichty BD, Breitbach CJ, Stojdl DF & Bell JC (2014) Going viral with cancer immunotherapy. Nat Rev Cancer 14: 559–567

Lichty BD, Power AT, Stojdl DF & Bell JC (2004) Vesicular stomatitis virus: Re-inventing the bullet. Trends in Molecular Medicine 10: 210–216

Lindsten T, Lee KP, Harris ES, Petryniak B, Craighead N, Reynolds PJ, Lombard DB, Freeman GJ, Nadler LM & Gray GS (1993) Characterization of CTLA-4 structure and expression on human T cells. J Immunol 151: 3489–3499

Liu BL, Robinson M, Han Z-Q, Branston RH, English C, Reay P, McGrath Y, Thomas SK, Thornton M, Bullock P, Love CA & Coffin RS (2003) ICP34.5 deleted herpes simplex virus with enhanced oncolytic, immune stimulating, and anti-tumour properties. Gene Ther 10: 292–303

Liu Y-P, Suksanpaisan L, Steele MB, Russell SJ & Peng K-W (2013) Induction of antiviral genes by the tumor microenvironment confers resistance to virotherapy. Sci Rep 3: 2375

Lv F, Qiu Y, Zhang Y, Liu S, Shi J, Liu Y & Zheng D (2011) Adeno-associated virus-mediated anti-DR5 chimeric antibody expression suppresses human tumor growth in nude mice. Cancer Lett. 302: 119–127

Lynch DH, Andreasen A, Maraskovsky E, Whitmore J, Miller RE & Schuh JC (1997) Flt3 ligand induces tumor regression and antitumor immune responses in vivo. Nat Med 3: 625–631

Mach N, Gillessen S, Wilson SB, Sheehan C, Mihm M & Dranoff G (2000) Differences in dendritic cells stimulated in vivo by tumors engineered to secrete granulocyte-macrophage colony-stimulating factor or Flt3-ligand. Cancer Res 60: 3239–3246

Maraskovsky E, Brasel K, Teepe M, Roux ER, Lyman SD, Shortman K & McKenna HJ (1996) Dramatic increase in the numbers of functionally mature dendritic cells in Flt3 ligand-treated mice: Multiple dendritic cell subpopulations identified. J Exp Med 184: 1953–1962

Marchini A, Scott EM & Rommelaere J (2016) Overcoming Barriers in Oncolytic Virotherapy with HDAC Inhibitors and Immune Checkpoint Blockade. Viruses 8

Marcus A, Gowen BG, Thompson TW, Iannello A, Ardolino M, Deng W, Wang L, Shifrin N & Raulet DH (2014) Recognition of tumors by the innate immune system and natural killer cells. Advances in immunology 122: 91–128

Martinez I, Rodriguez LL, Jimenez C, Pauszek SJ & Wertz GW (2003) Vesicular stomatitis virus glycoprotein is a determinant of pathogenesis in swine, a natural host. J Virol 77: 8039–8047

Maurer-Gebhard M, Schmidt M, Azemar M, Altenschmidt U, Stöcklin E, Wels W & Groner B (1998) Systemic Treatment with a Recombinant erbB-2 Receptor-specific Tumor Toxin Efficiently Reduces Pulmonary Metastases in Mice Injected with Genetically Modified Carcinoma Cells. Cancer Res. 58:2661–2666

McCarty DM (2008) Self-complementary AAV vectors; advances and applications. Mol Ther 16: 1648–1656

McCarty DM, Fu H, Monahan PE, Toulson CE, Naik P & Samulski RJ (2003) Adeno-associated virus terminal repeat (TR) mutant generates self-complementary vectors to overcome the rate-limiting step to transduction in vivo. Gene Ther 10: 2112–2118

McCarty DM, Monahan PE & Samulski RJ (2001) Self-complementary recombinant adeno-associated virus (scAAV) vectors promote efficient transduction independently of DNA synthesis. Gene Ther 8: 1248–1254

McDermott DF, Drake CG, Sznol M, Choueiri TK, Powderly JD, Smith DC, Brahmer JR, Carvajal RD, Hammers HJ, Puzanov I, Hodi FS, Kluger HM, Topalian SL, Pardoll DM, Wigginton JM, Kollia GD, Gupta A, McDonald D, Sankar V, Sosman JA & Atkins MB (2015) Survival, Durable Response, and Long-Term Safety in Patients With Previously Treated Advanced Renal Cell Carcinoma Receiving Nivolumab. J Clin Oncol 33: 2013–2020

McGeoch DJ (1979) Structure of the gene N: Gene NS intercistronic junction in the genome of vesicular stomatitis virus. Cell 17: 673–681

McLaughlin SK, Collis P, Hermonat PL & Muzyczka N (1988) Adeno-associated virus general transduction vectors: Analysis of proviral structures. J Virol 62: 1963–1973

Melero I, Gaudernack G, Gerritsen W, Huber C, Parmiani G, Scholl S, Thatcher N, Wagstaff J, Zielinski C, Faulkner I & Mellstedt H (2014) Therapeutic vaccines for cancer: An overview of clinical trials. Nat Rev Clin Oncol 11: 509–524

Melief CJM (2008) Cancer immunotherapy by dendritic cells. Immunity 29: 372–383

Mellman I, Coukos G & Dranoff G (2011) Cancer immunotherapy comes of age. Nature 480: 480–489

Melzer MK, Lopez-Martinez A & Altomonte J (2017) Oncolytic Vesicular Stomatitis Virus as a Viro-Immunotherapy: Defeating Cancer with a "Hammer" and "Anvil". Biomedicines 5

Michot JM, Bigenwald C, Champiat S, Collins M, Carbonnel F, Postel-Vinay S, Berdelou A, Varga A, Bahleda R, Hollebecque A, Massard C, Fuerea A, Ribrag V, Gazzah A, Armand JP, Amellal N, Angevin E, Noel N, Boutros C & Mateus C et al (2016) Immune-related adverse events with immune checkpoint blockade: a comprehensive review. European journal of cancer (Oxford, England: 1990) 54: 139–148

Miyajima A, Otsu K, Schreurs J, Bond MW, Abrams JS & Arai K (1986) Expression of murine and human granulocyte-macrophage colony-stimulating factors in S. cerevisiae: Mutagenesis of the potential glycosylation sites. EMBO J 5: 1193–1197

Mohr I, Sternberg D, Ward S, Leib D, Mulvey M & Gluzman Y (2001) A herpes simplex virus type 1 gamma34.5 second-site suppressor mutant that exhibits enhanced growth in cultured glioblastoma cells is severely attenuated in animals. J Virol 75: 5189–5196

Motylewska E & Melen-Mucha G (2009) Estrone and progesterone inhibit the growth of murine MC38 colon cancer line. The Journal of steroid biochemistry and molecular biology 113: 75–79

Mueller C, Gernoux G, Gruntman AM, Borel F, Reeves EP, Calcedo R, Rouhani FN, Yachnis A, Humphries M, Campbell-Thompson M, Messina L, Chulay JD, Trapnell B, Wilson JM, McElvaney NG & Flotte TR (2017) 5 Year Expression and Neutrophil Defect Repair after Gene Therapy in Alpha-1 Antitrypsin Deficiency. Mol Ther 25: 1387–1394

Muik A, Dold C, Geiß Y, Volk A, Werbizki M, Dietrich U & Laer D von (2012) Semireplication-competent vesicular stomatitis virus as a novel platform for oncolytic virotherapy. J Mol Med 90: 959–970

Muik A, Kneiske I, Werbizki M, Wilflingseder D, Giroglou T, Ebert O, Kraft A, Dietrich U, Zimmer G, Momma S & Laer D von (2011) Pseudotyping vesicular stomatitis virus with lymphocytic choriomeningitis virus glycoproteins enhances infectivity for glioma cells and minimizes neurotropism. J Virol 85: 5679–5684

Muik A, Stubbert LJ, Jahedi RZ, Geiß Y, Kimpel J, Dold C, Tober R, Volk A, Klein S, Dietrich U, Yadollahi B, Falls T, Miletic H, Stojdl D, Bell JC & Laer D von (2014) Re-engineering vesicular stomatitis virus to abrogate neurotoxicity, circumvent humoral immunity, and enhance oncolytic potency. Cancer research 74: 3567–3578

Münch RC, Janicki H, Völker I, Rasbach A, Hallek M, Büning H & Buchholz CJ (2013) Displaying high-affinity ligands on adeno-associated viral vectors enables tumor cell-specific and safe gene transfer. Mol Ther 21: 109–118

Münch RC, Muth A, Muik A, Friedel T, Schmatz J, Dreier B, Trkola A, Plückthun A, Büning H & Buchholz CJ (2015) Off-target-free gene delivery by affinity-purified receptor-targeted viral vectors. Nature communications 6: 6246

Nagaraj S & Gabrilovich DI (2008) Tumor escape mechanism governed by myeloid-derived suppressor cells. Cancer Res 68: 2561–2563

Nagata Y, Furugen R, Hiasa A, Ikeda H, Ohta N, Furukawa K, Nakamura H, Kanematsu T & Shiku H (1997) Peptides derived from a wild-type murine proto-oncogene c-erbB-2/HER2/neu can induce CTL and tumor suppression in syngeneic hosts. J Immunol 159: 1336–1343

Nagato T, Lee Y-R, Harabuchi Y & Celis E (2014) Combinatorial immunotherapy of polyinosinic-polycytidylic acid and blockade of programmed death-ligand 1 induce effective CD8 T-cell responses against established tumors. Clin Cancer Res 20: 1223–1234

Naidoo J, Page DB, Li BT, Connell LC, Schindler K, Lacouture ME, Postow MA & Wolchok JD (2016) Toxicities of the anti-PD-1 and anti-PD-L1 immune checkpoint antibodies. Ann Oncol. 27: 1362

Nakai H, Herzog RW, Hagstrom JN, Walter J, Kung SH, Yang EY, Tai SJ, Iwaki Y, Kurtzman GJ, Fisher KJ, Colosi P, Couto LB & High KA (1998) Adeno-associated viral vector-mediated gene transfer of human blood coagulation factor IX into mouse liver. Blood 91: 4600–4607

Natarajan A, Mayer AT, Xu L, Reeves RE, Gano J & Gambhir SS (2015) Novel Radiotracer for ImmunoPET Imaging of PD-1 Checkpoint Expression on Tumor Infiltrating Lymphocytes. Bioconjug Chem 26: 2062–2069

Natkunarajah M, Trittibach P, McIntosh J, Duran Y, Barker SE, Smith AJ, Nathwani AC & Ali RR (2008) Assessment of ocular transduction using single-stranded and self-complementary recombinant adeno-associated virus serotype 2/8. Gene therapy 15: 463–467

Nettelbeck DM, Jérôme V & Müller R (2000) Gene therapy: Designer promoters for tumour targeting. Trends Genet. 16: 174–181

Noser JA, Mael AA, Sakuma R, Ohmine S, Marcato P, Lee PW & Ikeda Y (2007) The RAS/Raf1/MEK/ERK signaling pathway facilitates VSV-mediated oncolysis: Implication for the defective interferon response in cancer cells. Mol Ther 15: 1531–1536

Obuchi M, Fernandez M & Barber GN (2003) Development of recombinant vesicular stomatitis viruses that exploit defects in host defense to augment specific oncolytic activity. J Virol 77: 8843–8856

Ohigashi Y, Sho M, Yamada Y, Tsurui Y, Hamada K, Ikeda N, Mizuno T, Yoriki R, Kashizuka H, Yane K, Tsushima F, Otsuki N, Yagita H, Azuma M & Nakajima Y (2005) Clinical significance of programmed death-1 ligand-1 and programmed death-1 ligand-2 expression in human esophageal cancer. Clin Cancer Res 11: 2947–2953

Oluwole OO & Davila ML (2016) At The Bedside: Clinical review of chimeric antigen receptor (CAR) T cell therapy for B cell malignancies. Journal of leukocyte biology 100: 1265-1272

Opie SR, Warrington KH, Agbandje-McKenna M, Zolotukhin S & Muzyczka N (2003) Identification of Amino Acid Residues in the Capsid Proteins of Adeno-Associated Virus Type 2 That Contribute to Heparan Sulfate Proteoglycan Binding. J Virol 77: 6995–7006

Palucka K & Banchereau J (2013) Dendritic-cell-based therapeutic cancer vaccines. Immunity 39: 38–48

Pan P-Y, Li Y, Li Q, Gu P, Martinet O, Thung S & Chen S-H (2004) In situ recruitment of antigen-presenting cells by intratumoral GM-CSF gene delivery. Cancer Immunol Immunother. 53: 17–25

Panda D, Dinh PX, Beura LK & Pattnaik AK (2010) Induction of interferon and interferon signaling pathways by replication of defective interfering particle RNA in cells constitutively expressing vesicular stomatitis virus replication proteins. J Virol. 84: 4826–4831

Pardoll D (2002) T cells take aim at cancer. Proc Natl Acad Sci U S A 99: 15840–15842

Pardoll DM (2012) The blockade of immune checkpoints in cancer immunotherapy. Nat Rev Cancer 12: 252–264

Park J-J, Omiya R, Matsumura Y, Sakoda Y, Kuramasu A, Augustine MM, Yao S, Tsushima F, Narazaki H, Anand S, Liu Y, Strome SE, Chen L & Tamada K (2010) B7-H1/CD80 interaction is required for the induction and maintenance of peripheral T-cell tolerance. Blood 116: 1291–1298

Peggs KS, Quezada SA, Chambers CA, Korman AJ & Allison JP (2009) Blockade of CTLA-4 on both effector and regulatory T cell compartments contributes to the antitumor activity of anti-CTLA-4 antibodies. J Exp Med. 206: 1717–1725

Pereira DJ, McCarty DM & Muzyczka N (1997) The adeno-associated virus (AAV) Rep protein acts as both a repressor and an activator to regulate AAV transcription during a productive infection. J Virol 71: 1079–1088

Péron JM, Esche C, Subbotin VM, Maliszewski C, Lotze MT & Shurin MR (1998) FLT3-ligand administration inhibits liver metastases: Role of NK cells. J Immunol 161: 6164–6170

Petersen JM, Her LS, Varvel V, Lund E & Dahlberg JE (2000) The matrix protein of vesicular stomatitis virus inhibits nucleocytoplasmic transport when it is in the nucleus and associated with nuclear pore complexes. Mol Cell Biol 20: 8590–8601

Philpott NJ, Gomos J, Berns KI & Falck-Pedersen E (2002) A p5 integration efficiency element mediates Rep-dependent integration into AAVS1 at chromosome 19. Proc Natl Acad Sci U S A 99: 12381–12385

Pillay S, Meyer NL, Puschnik AS, Davulcu O, Diep J, Ishikawa Y, Jae LT, Wosen JE, Nagamine CM, Chapman MS & Carette JE (2016) An essential receptor for adeno-associated virus infection. Nature 530: 108–112

Pinschewer DD, Perez M, Jeetendra E, Bächi T, Horvath E, Hengartner H, Whitt MA, La Torre JC de & Zinkernagel RM (2004) Kinetics of protective antibodies are determined by the viral surface antigen. J Clin Invest. 114: 988–993

Prestwich RJ, Harrington KJ, Pandha HS, Vile RG, Melcher AA & Errington F (2008) Oncolytic viruses: a novel form of immunotherapy. Expert Rev Anticancer Ther 8: 1581–1588

Principe M, Ceruti P, Shih N-Y, Chattaragada MS, Rolla S, Conti L, Bestagno M, Zentilin L, Yang S-H, Migliorini P, Cappello P, Burrone O & Novelli F (2015) Targeting of surface alpha-enolase inhibits the invasiveness of pancreatic cancer cells. Oncotarget 6: 11098–11113

Pulido J, Kottke T, Thompson J, Galivo F, Wongthida P, Diaz RM, Rommelfanger D, Ilett E, Pease L, Pandha H, Harrington K, Selby P, Melcher A & Vile R (2012) Using virally expressed melanoma cDNA libraries to identify tumor-associated antigens that cure melanoma. Nat Biotechnol 30: 337–343

Qing K, Mah C, Hansen J, Zhou S, Dwarki V & Srivastava A (1999) Human fibroblast growth factor receptor 1 is a co-receptor for infection by adeno-associated virus 2. Nat Med 5: 71–77

Quiroz E, Moreno N, Peralta PH & Tesh RB (1988) A human case of encephalitis associated with vesicular stomatitis virus (Indiana serotype) infection. Am J Trop Med Hyg 39: 312–314

Qureshi OS, Zheng Y, Nakamura K, Attridge K, Manzotti C, Schmidt EM, Baker J, Jeffery LE, Kaur S, Briggs Z, Hou TZ, Futter CE, Anderson G, Walker LS & Sansom DM (2011) Trans-endocytosis of CD80 and CD86: A molecular basis for the cell-extrinsic function of CTLA-4. Science (New York, N.Y.) 332: 600–603

Rahimian S, Fransen MF, Kleinovink JW, Amidi M, Ossendorp F & Hennink WE (2015) Polymeric microparticles for sustained and local delivery of antiCD40 and antiCTLA-4 in immunotherapy of cancer. Biomaterials 61: 33–40

Rehman H, Silk AW, Kane MP & Kaufman HL (2016) Into the clinic: Talimogene laherparepvec (T-VEC), a first-in-class intratumoral oncolytic viral therapy. J Immunother Cancer 4: 53

Rivera VM, Gao G-p, Grant RL, Schnell MA, Zoltick PW, Rozamus LW, Clackson T & Wilson JM (2005) Long-term pharmacologically regulated expression of erythropoietin in primates following AAV-mediated gene transfer. Blood 105: 1424–1430

Robert C, Long GV, Brady B, Dutriaux C, Maio M, Mortier L, Hassel JC, Rutkowski P, McNeil C, Kalinka-Warzocha E, Savage KJ, Hernberg MM, Lebbé C, Charles J, Mihalcioiu C, Chiarion-Sileni V, Mauch C, Cognetti F, Arance A & Schmidt H et al (2015a) Nivolumab in previously untreated melanoma without BRAF mutation. N Engl J Med. 372: 320–330

Robert C, Ribas A, Wolchok JD, Hodi FS, Hamid O, Kefford R, Weber JS, Joshua AM, Hwu W-J, Gangadhar TC, Patnaik A, Dronca R, Zarour H, Joseph RW, Boasberg P, Chmielowski B, Mateus C, Postow MA, Gergich K & Elassaiss-Schaap J et al (2014) Anti-programmed-death-receptor-1 treatment with pembrolizumab in ipilimumab-refractory advanced melanoma: A randomised dose-comparison cohort of a phase 1 trial. Lancet 384: 1109–1117

Robert C, Schachter J, Long GV, Arance A, Grob JJ, Mortier L, Daud A, Carlino MS, McNeil C, Lotem M, Larkin J, Lorigan P, Neyns B, Blank CU, Hamid O, Mateus C, Shapira-Frommer R, Kosh M, Zhou H, Ibrahim N, Ebbinghaus S & Ribas A (2015b) Pembrolizumab versus Ipilimumab in Advanced Melanoma. N Engl J Med. 372: 2521-2532

Rohrbach F, Weth R, Kursar M, Sloots A, Mittrucker H-W & Wels WS (2005) Targeted delivery of the ErbB2/HER2 tumor antigen to professional APCs results in effective antitumor immunity. J Immunol 174: 5481–5489

Rose JK (1980) Complete intergenic and flanking gene sequences from the genome of vesicular stomatitis virus. Cell 19: 415–421

Rosenberg JE, Hoffman-Censits J, Powles T, van der Heijden MS, Balar AV, Necchi A, Dawson N, O'Donnell PH, Balmanoukian A, Loriot Y, Srinivas S, Retz MM, Grivas P, Joseph RW, Galsky MD, Fleming MT, Petrylak DP, Perez-Gracia JL, Burris HA & Castellano D et al (2016) Atezolizumab in patients with locally advanced and metastatic urothelial carcinoma who have progressed following treatment with platinum-based chemotherapy: A single-arm, multicentre, phase 2 trial. Lancet 387: 1909–1920

Rosenberg SA & Restifo NP (2015) Adoptive cell transfer as personalized immunotherapy for human cancer. Science (New York, N.Y.) 348: 62–68

Rosenberg SA, Yang JC, Sherry RM, Kammula US, Hughes MS, Phan GQ, Citrin DE, Restifo NP, Robbins PF, Wunderlich JR, Morton KE, Laurencot CM, Steinberg SM, White DE & Dudley ME (2011) Durable complete responses in heavily pretreated patients with metastatic melanoma using T-cell transfer immunotherapy. Clin Cancer Res. 17: 4550–4557

Roth A, Rohrbach F, Weth R, Frisch B, Schuber F & Wels WS (2005) Induction of effective and antigen-specific antitumour immunity by a liposomal ErbB2/HER2 peptide-based vaccination construct. Br J Cancer 92: 1421–1429

Russell SJ, Peng K-W & Bell JC (2012) Oncolytic virotherapy. Nat Biotechnol 30: 658–670

Samulski RJ & Muzyczka N (2014) AAV-Mediated Gene Therapy for Research and Therapeutic Purposes. Annual Review of Virology 1: 427–451

Samulski RJ, Zhu X, Xiao X, Brook JD, Housman DE, Epstein N & Hunter LA (1991) Targeted integration of adeno-associated virus (AAV) into human chromosome 19. EMBO J 10: 3941–3950

Sarinella F, Calistri A, Sette P, Palù G & Parolin C (2006) Oncolysis of pancreatic tumour cells by a gamma34.5-deleted HSV-1 does not rely upon Ras-activation, but on the PI 3-kinase pathway. Gene Ther 13: 1080–1087

Schadendorf D, Hodi FS, Robert C, Weber JS, Margolin K, Hamid O, Patt D, Chen T-T, Berman DM & Wolchok JD (2015) Pooled Analysis of Long-Term Survival Data From Phase II and Phase III Trials of Ipilimumab in Unresectable or Metastatic Melanoma. J Clin Oncol. 33: 1889–1894

Schneider H, Downey J, Smith A, Zinselmeyer BH, Rush C, Brewer JM, Wei B, Hogg N, Garside P & Rudd CE (2006) Reversal of the TCR stop signal by CTLA-4. Science (New York, N.Y.) 313: 1972–1975

Schnell MJ, Buonocore L, Whitt MA & Rose JK (1996) The minimal conserved transcription stop-start signal promotes stable expression of a foreign gene in vesicular stomatitis virus. J Virol 70: 2318–2323

Schnell MJ, Mebatsion T & Conzelmann KK (1994) Infectious rabies viruses from cloned cDNA. EMBO J 13: 4195–4203

Schnepp BC, Chulay JD, Ye G-J, Flotte TR, Trapnell BC & Johnson PR (2016) Recombinant Adeno-Associated Virus Vector Genomes Take the Form of Long-Lived, Transcriptionally Competent Episomes in Human Muscle. Hum Gene Ther. 27: 32–42

Schnepp BC, Clark KR, Klemanski DL, Pacak CA & Johnson PR (2003) Genetic fate of recombinant adeno-associated virus vector genomes in muscle. J Virol 77: 3495–3504

Schnepp BC & Johnson PR (2014) Adeno-associated virus delivery of broadly neutralizing antibodies. Current opinion in HIV and AIDS 9: 250–256

Senapathy P, Tratschin JD & Carter BJ (1984) Replication of adeno-associated virus DNA. Complementation of naturally occurring rep- mutants by a wild-type genome or an ori- mutant and correction of terminal palindrome deletions. J Mol Biol 179: 1–20

Sfanos KS, Bruno TC, Meeker AK, Marzo AM de, Isaacs WB & Drake CG (2009) Human prostate-infiltrating CD8+ T lymphocytes are oligoclonal and PD-1+. Prostate 69: 1694–1703

Sharma P, Wagner K, Wolchok JD & Allison JP (2011) Novel cancer immunotherapy agents with survival benefit: recent successes and next steps. Nat Rev Cancer 11: 805–812

Shaw SG, Maung AA, Steptoe RJ, Thomson AW & Vujanovic NL (1998) Expansion of functional NK cells in multiple tissue compartments of mice treated with Flt3-ligand: Implications for anti-cancer and anti-viral therapy. J Immunol 161: 2817–2824

Shimada M, Abe S, Takahashi T, Shiozaki K, Okuda M, Mizukami H, Klinman DM, Ozawa K & Okuda K (2013) Prophylaxis and treatment of Alzheimer's disease by delivery of an adeno-associated virus encoding a monoclonal antibody targeting the amyloid Beta protein. PLoS ONE 8: e57606

Shin EJ, Wanna GB, Choi B, Aguila D, Ebert O, Genden EM & Woo SL (2007) Interleukin-12 expression enhances vesicular stomatitis virus oncolytic therapy in murine squamous cell carcinoma. Laryngoscope 117: 210–214

Shinozaki K, Ebert O, Suriawinata A, Thung SN & Woo SLC (2005) Prophylactic alpha interferon treatment increases the therapeutic index of oncolytic vesicular stomatitis virus virotherapy for advanced hepatocellular carcinoma in immune-competent rats. Journal of Virology 79: 13705–13713

Shortman K, Sathe P, Vremec D, Naik S & O'Keeffe M (2013) Plasmacytoid dendritic cell development. Advances in immunology 120: 105–126

Shurin MR, Pandharipande PP, Zorina TD, Haluszczak C, Subbotin VM, Hunter O, Brumfield A, Storkus WJ, Maraskovsky E & Lotze MT (1997) FLT3 ligand induces the generation of functionally active dendritic cells in mice. Cell Immunol 179: 174–184

Sikora AG, Jaffarzad N, Hailemichael Y, Gelbard A, Stonier SW, Schluns KS, Frasca L, Lou Y, Liu C, Andersson HA, Hwu P & Overwijk WW (2009) IFN-alpha enhances peptide vaccine-induced CD8+ T cell numbers, effector function, and antitumor activity. J Immunol 182: 7398–7407

Simmons AD, Moskalenko M, Creson J, Fang J, Yi S, VanRoey MJ, Allison JP & Jooss K (2008) Local secretion of anti-CTLA-4 enhances the therapeutic efficacy of a cancer immunotherapy with reduced evidence of systemic autoimmunity. Cancer Immunol Immunother. 57: 1263–1270

Simpson TR, Li F, Montalvo-Ortiz W, Sepulveda MA, Bergerhoff K, Arce F, Roddie C, Henry JY, Yagita H, Wolchok JD, Peggs KS, Ravetch JV, Allison JP & Quezada SA (2013) Fc-dependent depletion of tumor-infiltrating regulatory T cells co-defines the efficacy of anti-CTLA-4 therapy against melanoma. The Journal of experimental medicine 210: 1695–1710

Sisirak V, Vey N, Goutagny N, Renaudineau S, Malfroy M, Thys S, Treilleux I, Labidi-Galy SI, Bachelot T, Dezutter-Dambuyant C, Ménétrier-Caux C, Blay J-Y, Caux C & Bendriss-Vermare N (2013) Breast cancer-derived transforming growth factor-β and tumor necrosis factor-α compromise interferon-α production by tumor-associated plasmacytoid dendritic cells. Int J Cancer 133: 771–778

Skaricic D, Traube C, De B, Joh J, Boyer J, Crystal RG & Worgall S (2008) Genetic delivery of an anti-RSV antibody to protect against pulmonary infection with RSV. Virology 378: 79–85

Skrombolas D & Frelinger JG (2014) Challenges and developing solutions for increasing the benefits of IL-2 treatment in tumor therapy. Expert review of clinical immunology 10: 207–217

Slamon DJ, Godolphin W, Jones LA, Holt JA, Wong SG, Keith DE, Levin WJ, Stuart SG, Udove J & Ullrich A (1989) Studies of the HER-2/neu proto-oncogene in human breast and ovarian cancer. Science 244: 707–712

Sloots A, Mastini C, Rohrbach F, Weth R, Curcio C, Burkhardt U, Jäger E, Forni G, Cavallo F & Wels WS (2008) DNA vaccines targeting tumor antigens to B7 molecules on antigen-presenting cells induce protective antitumor immunity and delay onset of HER-2/Neu-driven mammary carcinoma. Clin Cancer Res. 14: 6933–6943

Smith RH & Kotin RM (1998) The Rep52 gene product of adeno-associated virus is a DNA helicase with 3'-to-5' polarity. J Virol 72: 4874–4881

Smyth MJ, Cretney E, Kershaw MH & Hayakawa Y (2004) Cytokines in cancer immunity and immunotherapy. Immunological reviews 202: 275–293

So T, Takenoyama M, Mizukami M, Ichiki Y, Sugaya M, Hanagiri T, Sugio K & Yasumoto K (2005) Haplotype loss of HLA class I antigen as an escape mechanism from immune attack in lung cancer. Cancer Res. 65: 5945–5952

Sonntag F, Schmidt K & Kleinschmidt JA (2010) A viral assembly factor promotes AAV2 capsid formation in the nucleolus. Proc Natl Acad Sci U S A 107: 10220–10225

Spain L, Diem S & Larkin J (2016) Management of toxicities of immune checkpoint inhibitors. Cancer treatment reviews 44: 51–60

Srivastava A, Lusby EW & Berns KI (1983) Nucleotide sequence and organization of the adeno-associated virus 2 genome. J Virol 45: 555–564

Srivastava MK, Zhu L, Harris-White M, Kar UK, Huang M, Johnson MF, Lee JM, Elashoff D, Strieter R, Dubinett S & Sharma S (2012) Myeloid suppressor cell depletion augments antitumor activity in lung cancer. PLoS ONE 7: e40677

Stojdl DF, Lichty B, Knowles S, Marius R, Atkins H, Sonenberg N & Bell JC (2000) Exploiting tumor-specific defects in the interferon pathway with a previously unknown oncolytic virus. Nat Med 6: 821–825

Stojdl DF, Lichty BD, tenOever BR, Paterson JM, Power AT, Knowles S, Marius R, Reynard J, Poliquin L, Atkins H, Brown EG, Durbin RK, Durbin JE, Hiscott J & Bell JC (2003) VSV strains with defects in their ability to shutdown innate immunity are potent systemic anti-cancer agents. Cancer Cell 4: 263–275

Sturmhoefel K, Lee K, Gray GS, Thomas J, Zollner R, O'Toole M, Swiniarski H, Dorner A & Wolf SF (1999) Potent activity of soluble B7-IgG fusion proteins in therapy of established tumors and as vaccine adjuvant. Cancer Res. 59: 4964–4972

Summerford C, Bartlett JS & Samulski RJ (1999) AlphaVbeta5 integrin: a co-receptor for adeno-associated virus type 2 infection. Nat Med 5: 78–82

Summerford C & Samulski RJ (1998) Membrane-associated heparan sulfate proteoglycan is a receptor for adeno-associated virus type 2 virions. J Virol 72: 1438–1445

Sun X, Roth SL, Bialecki MA & Whittaker GR (2010) Internalization and fusion mechanism of vesicular stomatitis virus and related rhabdoviruses. Future Virology 5: 85–96

Sun X, Yau VK, Briggs BJ & Whittaker GR (2005) Role of clathrin-mediated endocytosis during vesicular stomatitis virus entry into host cells. Virology 338: 53–60

Sutter G, Ohlmann M & Erfle V (1995) Non-replicating vaccinia vector efficiently expresses bacteriophage T7 RNA polymerase. FEBS Lett. 371: 9–12

Tagliamonte M, Petrizzo A, Tornesello ML, Buonaguro FM & Buonaguro L (2014) Antigen-specific vaccines for cancer treatment. Human vaccines & immunotherapeutics 10: 3332–3346

Thomas DA & Massagué J (2005) TGF-beta directly targets cytotoxic T cell functions during tumor evasion of immune surveillance. Cancer Cell 8: 369–380

Thomas L (1982) On immunosurveillance in human cancer. The Yale journal of biology and medicine 55: 329–333

Thompson RH, Dong H, Lohse CM, Leibovich BC, Blute ML, Cheville JC & Kwon ED (2007) PD-1 is expressed by tumor-infiltrating immune cells and is associated with poor outcome for patients with renal cell carcinoma. Clin Cancer Res. 13: 1757–1761

Thompson RH, Gillett MD, Cheville JC, Lohse CM, Dong H, Webster WS, Krejci KG, Lobo JR, Sengupta S, Chen L, Zincke H, Blute ML, Strome SE, Leibovich BC & Kwon ED (2004) Costimulatory B7-H1 in renal cell carcinoma patients: Indicator of tumor aggressiveness and potential therapeutic target. Proc Natl Acad Sci U S A 101: 17174–17179

Todo T, Martuza RL, Dallman MJ & Rabkin SD (2001) In situ expression of soluble B7-1 in the context of oncolytic herpes simplex virus induces potent antitumor immunity. Cancer Res. 61: 153–161

Toes RE, Ossendorp F, Offringa R & Melief CJ (1999) CD4 T cells and their role in antitumor immune responses. J Exp Med 189: 753–756

Topalian SL, Drake CG & Pardoll DM (2015) Immune checkpoint blockade: A common denominator approach to cancer therapy. Cancer Cell 27: 450–461

Topalian SL, Sznol M, McDermott DF, Kluger HM, Carvajal RD, Sharfman WH, Brahmer JR, Lawrence DP, Atkins MB, Powderly JD, Leming PD, Lipson EJ, Puzanov I, Smith DC, Taube JM, Wigginton JM, Kollia GD, Gupta A, Pardoll DM, Sosman JA & Hodi FS (2014) Survival, durable tumor remission, and long-term safety in patients with advanced melanoma receiving nivolumab. J Clin Oncol. 32: 1020–1030

van der Burg SH, Bijker MS, Welters MJP, Offringa R & Melief CJM (2006) Improved peptide vaccine strategies, creating synthetic artificial infections to maximize immune efficacy. Adv Drug Deliv Rev. 58: 916–930

Vigil A, Martinez O, Chua MA & García-Sastre A (2008) Recombinant Newcastle Disease Virus as a Vaccine Vector for Cancer Therapy. Mol Ther 16: 1883–1890

Viguier M, Lemaitre F, Verola O, Cho M-S, Gorochov G, Dubertret L, Bachelez H, Kourilsky P & Ferradini L (2004) Foxp3 expressing CD4+CD25(high) regulatory T cells are overrepresented in human metastatic melanoma lymph nodes and inhibit the function of infiltrating T cells. J Immunol 173: 1444–1453

Villarreal LP, Breindl M & Holland JJ (1976) Determination of molar ratios of vesicular stomatitis virus induced RNA species in BHK21 cells. Biochemistry 15: 1663–1667

Wang A, Braun SE, Sonpavde G & Cornetta K (2000) Antileukemic activity of Flt3 ligand in murine leukemia. Cancer Res 60: 1895–1900

Wang C, Sun W, Ye Y, Hu Q, Bomba HN & Gu Z (2017) In situ activation of platelets with checkpoint inhibitors for post-surgical cancer immunotherapy. Nat. biomed. eng. 1: 11

Wang C, Ye Y, Hochu GM, Sadeghifar H & Gu Z (2016) Enhanced Cancer Immunotherapy by Microneedle Patch-Assisted Delivery of Anti-PD1 Antibody. Nano letters 16: 2334–2340

Wang Z, Ma H-I, Li J, Sun L, Zhang J & Xiao X (2003) Rapid and highly efficient transduction by double-stranded adeno-associated virus vectors in vitro and in vivo. Gene Ther 10: 2105–2111

Weber JS, D'Angelo SP, Minor D, Hodi FS, Gutzmer R, Neyns B, Hoeller C, Khushalani NI, Miller WH, Lao CD, Linette GP, Thomas L, Lorigan P, Grossmann KF, Hassel JC, Maio M, Sznol M, Ascierto PA, Mohr P & Chmielowski B et al (2015) Nivolumab versus chemotherapy in patients with advanced melanoma who progressed after anti-CTLA-4 treatment (CheckMate 037): A randomised, controlled, open-label, phase 3 trial. The Lancet. Oncology 16: 375–384

Weitzman MD, Kyöstiö SR, Kotin RM & Owens RA (1994) Adeno-associated virus (AAV) Rep proteins mediate complex formation between AAV DNA and its integration site in human DNA. Proc Natl Acad Sci U S A 91: 5808–5812

Whelan SP, Ball LA, Barr JN & Wertz GT (1995) Efficient recovery of infectious vesicular stomatitis virus entirely from cDNA clones. Proc Natl Acad Sci U S A 92: 8388–8392

White J, Matlin K & Helenius A (1981) Cell fusion by Semliki Forest, influenza, and vesicular stomatitis viruses. J Cell Biol. 89: 674–679

Wing K, Onishi Y, Prieto-Martin P, Yamaguchi T, Miyara M, Fehervari Z, Nomura T & Sakaguchi S (2008) CTLA-4 control over Foxp3+ regulatory T cell function. Science (New York, N.Y.) 322: 271–275

Wu J, Zhao W, Zhong L, Han Z, Li B, Ma W, Weigel-Kelley KA, Warrington KH & Srivastava A (2007) Self-complementary recombinant adeno-associated viral vectors: packaging capacity and the role of rep proteins in vector purity. Hum Gene Ther 18: 171–182

Wu P, Xiao W, Conlon T, Hughes J, Agbandje-McKenna M, Ferkol T, Flotte T & Muzyczka N (2000) Mutational analysis of the adeno-associated virus type 2 (AAV2) capsid gene and construction of AAV2 vectors with altered tropism. J Virol 74: 8635–8647

Wu Z, Asokan A & Samulski RJ (2006) Adeno-associated virus serotypes: vector toolkit for human gene therapy. Mol Ther 14: 316–327

Xiao X, Li J & Samulski RJ (1998) Production of high-titer recombinant adeno-associated virus vectors in the absence of helper adenovirus. J Virol 72: 2224–2232

Xie Q, Bu W, Bhatia S, Hare J, Somasundaram T, Azzi A & Chapman MS (2002) The atomic structure of adeno-associated virus (AAV-2), a vector for human gene therapy. Proc Natl Acad Sci U S A 99: 10405–10410

Xie Y, Hicks MJ, Kaminsky SM, Moore MAS, Crystal RG & Rafii A (2014) AAV-mediated persistent bevacizumab therapy suppresses tumor growth of ovarian cancer. Gynecol Oncol. 135: 325–332

York IA, Roop C, Andrews DW, Riddell SR, Graham FL & Johnson DC (1994) A cytosolic herpes simplex virus protein inhibits antigen presentation to CD8+ T lymphocytes. Cell 77: 525–535

Zang X & Allison JP (2007) The B7 family and cancer therapy: costimulation and coinhibition. Clin Cancer Res 13: 5271–5279

Zhang K-x, Matsui Y, Hadaschik BA, Lee C, Jia W, Bell JC, Fazli L, So AI & Rennie PS (2010) Down-regulation of type I interferon receptor sensitizes bladder cancer cells to vesicular stomatitis virus-induced cell death. Int J Cancer 127: 830–838

Zhang Y-L, Chen S-S, Yang K-G, Su L, Deng Y-C & Liu C-Z (2005) Functional expression, purification, and characterization of human Flt3 ligand in the Pichia pastoris system. Protein Expr Purif 42: 246–254

Zhou ZF, Peretz Y, Chang Y, Miao DS, Li X & Prud'homme GJ (2003) Intramuscular gene transfer of soluble B7.1/IgG(1) fusion cDNA induces potent antitumor immunity as an adjuvant for DNA vaccination. Cancer Gene Ther 10: 491–499

Zitvogel L, Tesniere A & Kroemer G (2006) Cancer despite immunosurveillance: immunoselection and immunosubversion. Nat Rev Immunol. 6: 715–727

Zou W (2005) Immunosuppressive networks in the tumour environment and their therapeutic relevance. Nat Rev Cancer 5: 263–274

Zufferey R, Dull T, Mandel RJ, Bukovsky A, Quiroz D, Naldini L & Trono D (1998) Self-inactivating lentivirus vector for safe and efficient in vivo gene delivery. J Virol 72: 9873–9880

6 Abbreviations

°C	degree celsius
µ	micro
µl	microliter
µm	micrometer
A	ampere
AAP	assembly-activating protein
AAV	adeno-associated virus
ACT	adoptive cell transfer
APC	antigen-presenting cell
APS	ammonium persulfate
ATCC	American Type Culture Collection
ATP	adenosine triphosphate
AUC	area under the curve
BGH	bovine growth hormone
bp	base pair
cap	capsid protein
CAR	chimeric antigen receptor
CD	cluster of differentiation
cDC	conventional dendritic cell
cDNA	complementary DNA
c_H	constant region of the heavy chain
cm	centimeter
cm^2	square centimeter
cm^3	cubic centimeter
CMV	cytomegalovirus
ConA	Concanavalin A
CTLA-4	cytotoxic T-lymphocyte-associated antigen
CV	column volumes
DAMP	danger-associated molecular pattern
DARPin	designed ankyrin repeat protein
DC	dendritic cell
DMEM	Dulbecco's Modified Eagle Medium
DMSO	dimethyl sulfoxide
DNA	deoxyribonucleic acid
dNTP	deoxyribonucleotide triphosphate
dsRed	Discosoma red fluorescent protein
E. coli	*Escherichia coli*
EDTA	ethylenediaminetetraacetic acid
EF1α	elongation factor-1α
ELISA	enzyme-linked immunosorbent assay
ELISpot	enzyme-linked immune spot assay
EMCV	Encephalomyocarditis virus
EpCAM	epithelial cell adhesion molecule
et al.	and others

F2A	2A self-cleaving sequence from foot-and-mouth disease virus
Fc	fragment crystallizable
FCS	fetal calf serum
FDA	Food and Drug Administration
FITC	fluorescein isothiocyanate
Flt3L	FMS-like tyrosine kinase 3 ligand
for	forward
G	glycoprotein
g	gram or gravity force
GFP	green fluorescent protein
GM-CSF	granulocyte-macrophage colony-stimulating factor
GOI	genome containing particles per cell
Gy	gray
h	hour
HA	hemagglutinin
HDV	Hepatitis Delta Virus
Her2/neu	human epidermal growth factor 2
His_6	hexa-histidine motif
HIV	human immunodeficiency virus
HLA	human leukocyte antigen
HRP	horseradish peroxidase
HSPG	heparin sulfate proteoglycan
HSV	herpes simplex virus
HSV-1	herpes simplex virus-1
ICD	immunogenic cell death
IEE	integration efficiency element
IFN	interferon
IFN receptor	IFNAR
IgG	immunoglobulin G
IL	interleukin
irAE	immune-related adverse events
IRES	internal ribosomal entry site
ITR	inverted terminal repeat
JAK/STAT	Janus kinase/signal transducer and activator of transcription
kb	kilobase
kDa	kilo Dalton
L	large polymerase
l	liter
LB	Luria-Bertani
LCMV	lymphocytic choriomeningitis virus
LDL	low density lipoprotein
LPL	lipoprotein lipase
luc	luciferase
LV	lentiviral vector
M	matrix protein or molar
m	meter
mAb	monoclonal antibody
MHC	major histocompatibility complex

min	minutes
ml	milliliter
mM	millimolar
mm^3	cubic millimeter
MCC	Merkel cell carcinoma
MN	microneedle
MOI	multiplicity of infection
mRNA	messenger RNA
MVA	modified vaccinia virus Ankara
N	nucleoprotein
n.s.	not significant
nAb	neutralizing antibody
NCBI	National Center for Biotechnology Information
ng	nanogram
NK cell	natural killer cell
NSCLC	non-small cell lung cancer
NSG	NOD.Cg-Prkdc^{scid} Il2rg^{tm1Wjl}/SzJ
ORF	open reading frame
P	phosphoprotein
p/sec/cm^2/sr	photons/seconds/square centimeter/steradian
PAMP	pathogen-associated molecular pattern
PAP	prostatic acid phosphatase
PBMC	peripheral blood mononuclear cells
PBS	phosphate-buffered saline
pBSII	pBluescriptII
PCR	polymerase chain reaction
PD-1	programmed cell death protein-1
PDB	Protein Data Bank
pDC	plasmacytoid DC
PDGFR	platelet-derived growth factor receptor
PD-L1	programmed cell death ligand-1
PE	phycoerythrin
PEI	polyethleneimine
PET	positron emission tomography
PMA	phorbol 12-myristate 13-acetate
poly A	polyadenylation signal
qPCR	quantitative PCR
RCC	renal cell carcinoma
rep	viral regulatory proteins
rev	reverse
RNA	ribonucleic acid
RNP	ribonucleoprotein
rpm	rounds per minute
RPMI	Roswell Park Memorial Institute
rVSV	recombinant vesicular stomatitis virus
s	seconds
scAAV	self-complementary AAV
scFv	single chain Fragment variable

SD	standard deviation
SDS	sodium dodecyl sulfate
SDS-PAGE	sodium dodecyl sulfate-polyacrylamide gel electrophoresis
SFFV	spleen focus forming virus
SIV	simian immunodeficiency virus
srVSV	semireplication-competent vesicular stomatitis virus
ss	single-stranded
ssAAV	single-stranded AAV
SV40	simian virus 40
TAA	tumor-associated antigen
$TCID_{50}$	50 % tissue culture infective dose
TCR	T cell receptor
TEMED	tetramethylethylenediamine
TGF-β	transforming growth factor β
TILs	tumor infiltrating lymphocytes
TMB	3,3′,5,5′-Tetramethylbenzidine
TME	tumor microenvironment
T_{reg} cells	regulatory T cells
Tris	tris(hydroxymethyl)aminomethane
U	unit
UV	ultraviolet
V	volt
v/v	volume per volume
v_H	variable region of the heavy chain
v_L	variable region of the light chain
VP	viral protein
VSV	vesicular stomatitis virus
w/v	weight per volume
α	alpha or anti
β	beta
γ	gamma
Δ	delta
κ	kappa

7 Curriculum Vitae

Persönliche Informationen

Name	Johanna Reul
Gerburtsdatum	30.08.1987
Geburtsort	Mainz

Wissenschaftlicher Werdegang

seit 05/2013	Promotionsstudentin in der Abteilung "Molekulare Biotechnologie und Gentherapie" geleitetet von Prof. Dr. Christian Buchholz am Paul-Ehrlich-Institut in Langen
05/2016 - 12/2016	Stipendium des Zell- und Gentherapie Zentrums der Landesoffensive zur Entwicklung Wissenschaftlich-Ökonomischer Exzellenz (LOEWE)
05/2013 - 04/2016	Promotionsstipendium finanziert durch das Deutsche Konsortium für Translationale Krebsforschung (DKTK), Standort Deutsches Krebsforschungszentrum (DKFZ) in Heidelberg
10/2007 - 01/2013	Studium der Biochemie an der Goethe-Universität in Frankfurt am Main Studienabschluss: Diplom-Biochemikerin (Note: 1,0)
09/1998 - 06/2007	Allgemeine Hochschulreife am Max-Planck-Gymnasium in Rüsselsheim (Note: 1,4)

8 Publications

Muik A, **Reul J**, Friedel T, Muth A, Hartmann KP, Schneider IC, Münch RC & Buchholz CJ (2017). Covalent coupling of high-affinity ligands to the surface of viral vector particles by protein trans-splicing mediates cell type-specific gene transfer. Biomaterials 144: 84–94

Hanauer JDS, Rengstl B, Kleinlützum D, **Reul J**, Pfeiffer A, Friedel T, Schneider IC, Newrzela S, Hansman ML, Buchholz CJ & Muik A (2018). CD30-targeted oncolytic viruses as novel therapeutic approach against classical Hodgkin lymphoma. Oncotarget 9: 12971-12981

Parts of this thesis have been submitted for publication:

Reul J*, Frisch J*, Engeland CE, Thalheimer FB, Hartmann J, Ungerechts G & Buchholz CJ. Tumor-specific delivery of immune checkpoint inhibitors by engineered AAV vectors. Frontiers in Oncology, in revision January 2019

*shared first author

Presentations at scientific conferences

Johanna Reul, Christian J. Buchholz, Alexander Muik. Modulation of the antitumor immune response using semireplication-competent VSV armed with immunostimulatory transgenes. (Poster presentation)
American Society of Gene & Cell Therapy (ASGCT) 19th Annual Meeting, May 4 – 7, 2016 in Washington D.C., USA

Johanna Reul, Robert Münch, Christine Engeland, Guy Ungerechts, Christian J. Buchholz. Towards tumor-specific delivery of immune checkpoint inhibitors. (Poster presentation)
XXII Annual Meeting of the German Society of Gene Therapy (DG-GT), September 14 – 16, 2016 in Heidelberg, Germany

Johanna Reul, Robert Münch, Christine Engeland, Guy Ungerechts, Christian J. Buchholz. Towards tumor-specific delivery of immune checkpoint inhibitors. (Poster presentation)
7th UCT Science Day, October 7, 2016 in Frankfurt am Main, Germany

Johanna Reul, Robert Münch, Christine Engeland, Guy Ungerechts, Christian J. Buchholz. Towards tumor-specific delivery of immune checkpoint inhibitors. (Poster presentation)
XXIVth Annual Congress, Collaborative Meeting of the European Society of Gene & Cell Therapy (ESCGT) and the International Society for Stem Cell Research (ISSCR), October 18 – 21, 2016 in Florence, Italy

Johanna Reul, Janina Frisch, Robert Münch, Christine Engeland, Guy Ungerechts, Christian J. Buchholz. Tumor-specific delivery of αPD-1 checkpoint inhibitor by receptor-targeted AAV. (Poster presentation)
Third CRI-CIMT-EATI-AACR International Cancer Immunotherapy Conference, September 6 – 9, 2017 in Mainz, Germany

9 Danksagung

Ich bedanke mich herzlich bei Prof. Dr. Christian Buchholz für die Möglichkeit meine Doktorarbeit in seiner Arbeitsgruppe am Paul-Ehrlich-Institut anzufertigen sowie für das sehr interessante Thema meiner Arbeit. Seine wissenschaftliche Anleitung und ständige Diskussionsbereitschaft haben wesentlich zur Entstehung dieser Arbeit beigetragen.

Frau Prof. Dr. Beatrix Süß danke ich für die freundliche und unkomplizierte Betreuung seitens der TU Darmstadt. Ein weiterer Dank geht an Prof. Dr. Gerhard Thiel für seine Bereitschaft, die Aufgabe des Zweitgutachters an der TU Darmstadt zu übernehmen.

Ganz besonders möchte ich mich bei meinen jetzigen und ehemaligen Kollegen Julia, Ruben, Robert, Anke, Tobias, Irene, Jessica, Anett, Annika, Laura, Frederic, Janina, Thorsten, Sarah, Qi, Patricia, Alexander, Dina, Ruth, Tatjana, Gundula, Julia B. und Manuela aus der Arbeitsgruppe molekulare Biotechnologie und Gentherapie bedanken. Ihr habt mich mit eurer unermüdlichen Hilfsbereitschaft, den unzähligen fachlichen Diskussionen und der fantastischen Arbeitsatmosphäre während meiner Doktorarbeit sehr unterstützt und habt damit maßgeblich zur Entstehung dieser Arbeit beigetragen. Es hat Spaß gemacht mit euch zusammen zu arbeiten und auch außerhalb des Labors mit euch Zeit zu verbringen.

Ich danke auch den Mitarbeitern der ehemaligen Pr2 Jan, Vivian, Anna und Bianca. Ihr habt mir während meiner Doktorarbeit immer mit Rat und Tat zur Seite gestanden und mich sehr unterstützt.

Meinen Freunden möchte ich für ihre Unterstützung fernab des Labors sowie für ihr Verständnis, das sie mir in den letzten Jahren entgegengebracht haben, danken.

Mein besonderer Dank gilt meiner Familie Christa, Bernhard und Katrin sowie meinem Mann Andreas, dass sie immer für mich da waren, mich moralisch unterstützt haben und mir zu jeder Zeit den Rücken freigehalten haben.

10 Ehrenwörtliche Erklärung

Ich erkläre hiermit ehrenwörtlich, dass ich die vorliegende Arbeit entsprechend den Regeln guter wissenschaftlicher Praxis selbstständig und ohne unzulässige Hilfe Dritter angefertigt habe.

Sämtliche aus fremden Quellen direkt oder indirekt übernommenen Gedanken sowie sämtliche von Anderen direkt oder indirekt übernommenen Daten, Techniken und Materialien sind als solche kenntlich gemacht. Die Arbeit wurde bisher bei keiner anderen Hochschule zu Prüfungszwecken eingereicht.

Darmstadt, den

.....

(Johanna Reul)